

QE439.M5t  
no. 3-75  
1975

US-CE-C  
PROPERTY OF THE U.S. GOVERNMENT

AD

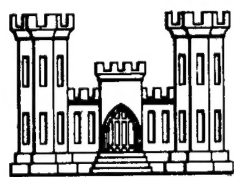
TECHNICAL REPORT MRD-3-75

TUNNEL SUPPORT LOADING  
CAUSED BY ROCK FAILURE

by

JAAK JOSEPH K. DAEMEN

MAY 1975



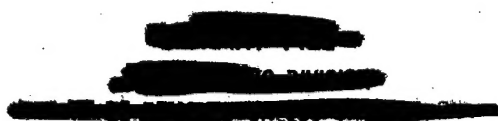
MISSOURI RIVER DIVISION, CORPS OF ENGINEERS  
OMAHA, NEBRASKA 68101

THIS RESEARCH WAS FUNDED BY OFFICE,  
CHIEF OF ENGINEERS, DEPARTMENT OF THE ARMY

19990525 040

PREPARED UNDER CONTRACT DACW 45-74-C-0066  
WITH UNIVERSITY OF MINNESOTA, MINNEAPOLIS MINN.

This document has been approved for public  
release and sale: its distribution is unlimited



RATIONAL DESIGN OF TUNNEL SUPPORTS:

TUNNEL SUPPORT LOADING

CAUSED BY ROCK FAILURE

Final Report

Department of the Army Contract No. DACW 45-74-C-0066

Prepared for

Geology, Soils, and Materials Branch

Missouri River Division, Corps of Engineers

Omaha, Nebraska

by

Jaak Joseph K. Daemen

University of Minnesota

Minneapolis, Minnesota

May 1975

## PREFACE

This investigation was accomplished and report prepared by Jaak Joseph K. Daemen in the Graduate School of the University of Minnesota, Minneapolis under Contract No. DACW 45-74-C-0066 with the Missouri River Division, Corps of Engineers.

The report is the thesis submitted by Dr. Daemen to the faculty in partial fulfillment of the requirements for the degree of Doctor of Philosophy in Civil Engineering in the Graduate School of the University of Minnesota. The work was accomplished under the direct supervision of Professor Charles Fairhurst, Chairman of the Department of Civil and Mineral Engineering of the University of Minnesota.

The contract was monitored by L. B. Underwood and Dennis J. Lachel of the Geology, Soils and Materials Branch of the Missouri River Division. Mr. J. F. Redlinger was Chief of the Geology, Soils and Materials Branch and L. A. Duscha was Chief of the Engineering Division of the Missouri River Division, Corps of Engineers, during the investigation.

Funds were provided by the Office, Chief of Engineers, Department of the Army under Civil Works Investigational Program CWIS 31214, Rational Design of Tunnel Supports.

TUNNEL SUPPORT LOADING CAUSED BY ROCK FAILURE

A THESIS  
SUBMITTED TO THE FACULTY OF THE GRADUATE SCHOOL  
OF THE UNIVERSITY OF MINNESOTA

By

Jaak Joseph K. Daemen

IN PARTIAL FULFILLMENT OF THE REQUIREMENTS  
FOR THE DEGREE OF  
DOCTOR OF PHILOSOPHY

March 1975

## ACKNOWLEDGMENTS

I wish to thank the many people who have helped me, in so many ways, during the preparation of this thesis, and especially:

Professor C. Fairhurst, my advisor, for his suggestions and continued support, for his help, and for the free and open research atmosphere he has created.

Dr. Thomas P. Bligh for his careful review and helpful criticism of major sections of this thesis, and for his valiant attempts at improving my command of the English language.

Professor Steven L. Crouch for making available his computer programs as well as his extensive personal notes on the development thereof.

Professors D. H. Yardley and C. R. Nelson for giving me the opportunity to be associated with some real life tunneling problems.

Dr. Francois H. Cornet for very valuable discussions on the mechanics of rock fracture, on the inadequacy of pseudo-elastic continuum models and on many related and unrelated subjects.

Dr. Bahawani Singh, Dr. Suradej Chuntranuluck,

Mr. Philippe Jamet and Mr. Dominique Rey for fruitful discussions of finite element analysis.

Dr. W. D. Lacabanne for his help with experimental work and for his continued encouragement.

Mrs. Marcy Scherbel and Ms. Suzanne Swain for typing much of the first draft. Mrs. Corinne Dickey for her careful typing of the final draft.

The National Science Foundation, RANN program, and the Missouri River Division, Omaha, of the U.S. Army Corps of Engineers for financial support, and in particular Mr. L. B. Underwood for his personal interest and for his valuable contributions to the author's understanding of practical tunnel support problems.

## ABSTRACT

Two methods are presented for the analysis of tunnel support loading caused by rock failure. In the first part of this thesis closed-form solutions are used, in the second part numerical techniques. Emphasis is put upon the statical indeterminacy of the problem and upon the necessity for considering the relative displacements between ground and support. From this follows the need for a realistic calculation of the stiffness of ground and support, as well as the need to consider the sequential development of the interaction between these two elements. It is assumed that the rock mass behavior during failure is softening and dilatant. Interface problems between ground and support that can strongly influence the effective support stiffness are discussed.

The closed-form solutions obtained in the first part are expressed in terms of ground and support characteristics. The derivations are based upon the assumption that the problem is radially symmetric. Bounds for the ground reaction can be derived by accounting for the intact and the

residual rock strength. Within the thus defined domain the ground behavior is determined by the rate of strength loss with increasing strain. The ground reaction curve can have fundamentally different shapes depending upon the post-failure rock behavior. Corresponding to failing or yielding sections of the ground reaction will be the desirability of stiff or soft supporting methods. The increased trend towards the use of stiffer supports as well as the emphasis on the need for early installation manifested by the combined use of reinforced shotcrete, grouted bolts and steel sets confirms the likelihood that optimum support conditions can be approached when only limited convergence is allowed. The optimum equilibrium state depends on the brittleness or the relative instability of the failing rock. The optimum displacement will be affected by rock loosening, but loosening will have a dominant effect only when the tunnel is shallow, the residual friction very low and when pronounced differences exist between support pressures required on the roof and on the floor.

Strength of material formulas are used to calculate the support stiffness or characteristic.

The significance of the ground-support interface is illustrated with examples of the influence of wood blocking on steel set characteristics and of the influence of end bonds and longitudinal shear bonds on the behavior of grouted bolts. The wide range of theoretically possible behavior modes indicates the need for pertinent field evaluation of the true support action provided by such systems.

The sensitivity of some support system characteristics to ostensibly secondary structural elements suggests that practical problems must exist in obtaining a consistent utilization of the full support capacity of such systems. It also indicates the serious difficulties likely to be encountered in the design and implementation of representative in-situ observation programs.

In the second part of this thesis the ground behavior is modeled by the finite element method. The elastic parameters that determine the rock behavior are changed progressively in order to simulate softening and volume increase of the failing rock mass.

This method is used in an axisymmetric analysis of failure patterns near the face and to study the influence of face behavior on support

loading. Initial support loading strongly depends on the stiffness of the rock ahead of the face relative to the rock stiffness behind the face, and can depend strongly on the face distance at the time of support erection.

A simple equivalent mining method is used to simulate progressive excavation in a plane strain analysis. The support model consists of beam and spring elements. At least for some support systems the latter must be chosen with care if the model is to be realistic.

## TABLE OF CONTENTS

	<u>Page</u>
ACKNOWLEDGMENTS . . . . .	ii
ABSTRACT . . . . .	iv
 <u>Chapter</u>	
I      INTRODUCTION . . . . .	I-1
II     CONTINUUM ANALYSIS OF TUNNEL SUPPORT LOADING CAUSED BY ROCK FAILURE . . . . .	II-1
1. Introduction . . . . .	II-1
2. Literature Survey . . . . .	II-6
3. Stress Changes Caused by Rock Failure . . . . .	II-14
1. Introduction . . . . .	II-14
2. Constant strength broken rock . .	II-15
3. Broken zone characterized by residual strength . . . . .	II-17
4. Gravity effects . . . . .	II-18
4. Tunnel Convergence Caused by Rock Failure Propagation . . . . .	II-31
1. Introduction . . . . .	II-31
2. Constant Volume expansion and minimum tunnel convergence . . .	II-33
3. Elastic Relaxation of the broken zone . . . . .	II-35
4. Influence of a progressive strain dependent strength decrease during rock failure . .	II-44

<u>Chapter</u>	<u>Page</u>
5. Numerical Generalization of the Ground Reaction Calculation . . . . .	II-53
1. Introduction . . . . .	II-53
2. Numerical generalization of ground reaction calculations . . .	II-54
6. Tunnel Support Characteristics . . .	II-60
1. Introduction . . . . .	II-60
2. Tunnel support characteristic . .	II-60
3. Characteristics of common tunnel support system . . . . .	II-62
1. Shotcrete liners . . . . .	II-63
2. Steel sets with wooden blocking . . . . .	II-63
3. Rock bolts . . . . .	II-69
4. Backfilled concrete segments	II-71
5. Composite support structures . . . . .	II-73
7. Extending the Ground Reaction Curve Derivations . . . . .	II-75
1. Introduction . . . . .	II-75
2. Time-dependent variations in support pressures . . . . .	II-76
3. Influence of discontinuities and inhomogeneities on tunnel sup- port requirements . . . . .	II-81
4. Influence of tunnel size on the required support pressure . . . .	II-87
8. Applications of the Continuum Analysis of Rock-Support Interaction . . . . .	II-89

<u>Chapter</u>	<u>Page</u>
1. Tunnel support design . . . . .	II-89
2. Optimum support stiffness . . . .	II-91
3. Tunnel support instrumentation	II-97
III STIFFNESS ANALYSIS OF TUNNEL SUPPORT LOADING CAUSED BY ROCK FAILURE . . . . .	III-1
1. Introduction . . . . .	III-1
2. Finite element analysis of rock failure . . . . .	III-5
1. Introduction . . . . .	III-5
2. Characteristics of (compres- sive) rock failure . . . . .	III-7
3. Finite element simulation of rock failure . . . . .	III-9
1. Introduction . . . . .	III-9
2. Literature survey . . . . .	III-11
3. Finite element simulation of compressive rock failure . . . . .	III-17
1. Introduction . . . . .	III-17
2. Isotropic rock failure model . . . . .	III-18
3. Orthotropic rock fail- ure model . . . . .	III-32
3. Stiffness Analysis of Tunnel Supports . . . . .	III-41
1. Introduction . . . . .	III-41
2. Stiffness model of tunnel supports . . . . .	III-44
3. Stiffness model of the rock support interface . . . . .	III-51

<u>Chapter</u>		<u>Page</u>
1.	Introduction . . . . .	III-51
2.	Stiffness model of a blocked steel set . . . . .	III-53
3.	Stiffness model of shotcrete support . . . . .	III-58
4.	Cast-in-place concrete . . .	III-59
5.	Rock bolt model . . . . .	III-60
6.	Concluding remarks on the support-rock interface model . . . . .	III-61
4.	Stiffness Analysis of Tunnel Support Loading Caused by Rock Failure . . . . .	III-62
1.	Introduction . . . . .	III-62
2.	Influence of the face distance upon support loading and rock failure . . . . .	III-63
1.	Introduction . . . . .	III-63
2.	Axisymmetric finite element analysis of rock failure near the face . . . . .	III-65
3.	Implications of axisymmetric face influence analysis for support loading . . . . .	III-69
4.	Face influence in non-homo- geneous rock masses . . . . .	III-84
3.	Plane strain stiffness analysis of support loading caused by rock failure . . . . .	III-100
1.	Introduction . . . . .	III-100
2.	Support loading during face advance . . . . .	III-102

<u>Chapter</u>		<u>Page</u>
3.	Examples of ground and support behavior analysis performed in plane strain .	III-107
IV	SUMMARY, CONCLUSIONS AND POSSIBLE FURTHER DEVELOPMENTS . . . . .	IV-1
1.	Summary . . . . .	IV-1
2.	Conclusions . . . . .	IV-6
3.	Further Development and Research .	IV-9
1.	Introduction . . . . .	IV-9
2.	Further development of presented analyses . . . . .	IV-10
3.	Evaluation of the validity and the practical significance of the presented analysis methods . . . . .	IV-18
REFERENCES	. . . . .	R-1

Appendix

A	DETAILED CALCULATIONS FOR THE CONTINUUM ANALYSIS OR ROCK-SUPPORT INTERACTION .	A-1
1.	Stress Distribution . . . . .	A-1
2.	Displacements . . . . .	A-10
1.	Constant volume increase throughout the broken zone .	A-10
2.	Displacements caused by elastic relaxation . . . . .	A-11
3.	Computer Programs for the Calculation of the Ground Reaction Curve .	A-18
1.	Introduction . . . . .	A-18
2.	Input . . . . .	A-20

<u>Appendix</u>		<u>Page</u>
	1. PROGRAM GRCSZE . . . . .	A-20
	2. PROGRAM GRCEXPD . . . . .	A-21
	3. Output . . . . .	A-22
	1. PROGRAM GRCSZE . . . . .	A-23
	2. PROGRAM GRCEXPD . . . . .	A-25
	4. Support Stiffness Calculation . . .	A-34
	1. Shotcrete cylinder . . . . .	A-34
	2. Blocked steel set . . . . .	A-34
	3. Rock Bolts . . . . .	A-37
	1. Point anchored bolts . . . .	A-39
	2. Full friction bolts . . . .	A-40
B	DETERMINATION OF THE PSEUDO-ELASTIC CONSTANTS IN THE FINITE ELEMENT ROCK FAILURE MODEL . . . . .	B-1
	1. Introduction . . . . .	B-1
	2. Plane Strain Isotropic Model . . . .	B-1
	3. Transversally Isotropic Model . . . .	B-2
	4. Orthotropic Rock Failure Model . . . .	B-20
	5. Orthotropic Cylinder with Cylindrical Anisotropy . . . . .	B-23
C	COMPUTER PROGRAM TUNSUP FOR THE PLANE STRAIN ANALYSIS OF TUNNEL SUPPORT LOADING CAUSED BY ROCK FAILURE . . . .	C-1
	1. Introduction . . . . .	C-1
	2. Input . . . . .	C-4
	3. Output . . . . .	C-13
	4. Computational Scheme . . . . .	C-14

## Chapter I

### INTRODUCTION

Driving a tunnel disturbs the equilibrium of the penetrated rock mass. The disturbed rock mass will search and find a new state of equilibrium. If the tunnel were left unsupported, the new state of equilibrium frequently would be reached through collapse of the tunnel. Installing a support system is the method commonly used to prevent such an undesirable occurrence. The function of tunnel support then is to permit the rock mass to reach a post-tunneling equilibrium state in which a safe usable tunnel is guaranteed.

The goal of tunnel support selection and design is to arrive at a support system that will function satisfactorily while minimizing the cost of the total tunnel construction. Both criteria must be satisfied simultaneously if an optimum is to be achieved. The overall economics of a tunneling operation depend on a number of factors that

frequently conflict to a considerable extent. The purpose of tunnel support design, therefore, cannot be limited to a narrow optimization of the support system *per se*. But neither can one minimize the total tunnel cost by treating the support requirements as a variable with little or no constraints. This consideration is particularly significant since the complex interaction between ground and support makes it a non-trivial matter to determine the consequences of support system variations and modifications. A more straightforward example is that when support requirements are averaged along tunnels or tunnel sections, it can suffice that the minimum required support function is not met at one or a few locations along the section to completely negate all potential gain that was expected from standardizing the construction operations along that section.

In order to optimize the support selection and design within the framework of the total tunnel cost, it is thus necessary first to determine the (minimum) required support function, and second to determine what available support techniques can be used most efficiently to fulfill that minimum requirement. "Minimum support requirement" does

not refer to minimum support "strength" but rather to a combination of factors such as bending and ring stiffness, strength and time of installation.

To ascertain the minimum support requirement one needs an understanding of the mechanics that determine the pre- and post-tunneling equilibrium states as well as the transition process from one to the other. This does not imply that the design of supports nor, more generally, the construction of tunnels requires an explicit understanding of the mechanics involved. Indeed, tunnels have been driven and supported, more or less safely, for many centuries. And only in the last decades has mechanics entered the field of support design with serious pretensions.

The variety of methods that have been developed for the design of tunnel supports is extremely great. Moreover, they have been developed in a number of different fields, and often have been published in journals of limited circulation with main interests ranging from railroad construction to coal mining to water supply, and many others. As a consequence, it would be a difficult and major undertaking, although an interesting one, to present a comprehensive survey of the existing design methods as

they developed over the last century. It is possible, nevertheless, to distinguish some broad classes of approach to the problem.

In what is likely to be the oldest method, one proceeds by trial and error, or full-scale in situ modeling. This approach is still used quite commonly, particularly in mining, or in those urban areas where numerous tunnels have been driven without excessive difficulties. When sufficient experience can be gained under a fairly fixed set of conditions, and when the possibility for experimentation with various systems exists, such a method can lead to an adequate and efficient support. Errors, however, tend to be very costly. And it is not easy with such an approach to assess the influence of significant variations in either encountered ground conditions or applied support methods from previously experienced ones.

The earlier design methods, i.e., methods in which an effort was made to quantify the support requirements, were based upon estimates of the amount of rock likely to fall out of the roof. It was then postulated that the support's function is the safe carrying of the loads that would result from such a fall-out. Numerous methods of this

type were further developed on the basis of various assumptions about the development of possible failure planes, arching action and beam action in the roof. In the meantime, increased attention was being paid to the possibility of applying elastic and later plastic analysis to the rock behavior around tunnels. As the realization of the full complexity of the problem grew, two very different schools of thought developed.

The first one attempted to simplify the problem of support determination to the greatest possible extent. This goal was approached by correlating information about the rock, and preferably a bare minimum of information, with corresponding support requirements. This minimum of information would hopefully be sufficient to narrow down the range of support requirements for a particular situation to a fairly precise point on a scale of support requirements determined empirically for a wide range of conditions. This approach has led to a large number of rock classification systems for support determination purposes. The most recent methods of this type are computerized statistical correlations between parameters characterizing the rock mass and support requirements.

The second school of thought strives towards a more complete and precise understanding of tunnel support mechanics. This approach led to more comprehensive continuum analyses of rock behavior, studies of arching and instability along joints, as well as advanced structural analysis of the supports. The most recent methods of this type are computerized numerical analyses of the mechanics of rock-support interaction.

In this thesis a two-fold approach is made towards a clarification of the problem of rock-support interaction, or the mechanics of tunnel supports. In the first part a combination of simple continuum and structural mechanics methods is used for the study of the interaction about a circular tunnel in a highly idealized rock mass. In the second part of the thesis use is made of the finite element method to develop a more general analysis technique.

For both approaches emphasis is put on the necessity to include a sufficient degree of realism in the model. This requires the use of a truthful description of both rock and support behavior, as well as a correct description of the problem posed by the interaction between these two basic elements.

of the structure.

The problem considered is that of the role played by the support system during the transition from the pre-tunneling rock mass equilibrium to the post-tunneling equilibrium. The support is installed near the face. As excavation progresses, the tunnel walls converge, and the support is compressed. The reaction forces developed by the support induce a stressfield in the rock mass, and constitute a new "external" factor in the post-tunneling equilibrium state. The problem, even in its most simplified form, is a statically indeterminate one. Therefore the rock mass stiffness and the support stiffness must be incorporated into the analysis. Through an analysis of the deformation and force changes during the sequence of support loading the final state of equilibrium can be determined.

The analysis of the rock mass displacements requires a realistic estimate of the rock mass properties prior to tunneling and of the behavioral changes induced by tunneling. Throughout this thesis, except for some minor and usually qualitative comments, the rock mass is treated as a continuous medium that reacts instantaneously. Both of these assumptions imply a severe idealization

of the real behavior, and allow great simplifications in the analysis. Whether or not one is willing to accept the one in order to accomplish the other will depend upon one's basic approach to rock mechanics problems, as can be attested more or less by the fact that the disagreement between proponents of the use of "continuum" or "discontinuum" approaches is longstanding, continuing and unresolved (but for die-hard proponents of either school). Conceptual as well as practical arguments can be invoked to justify the continuum simplification. Of the first type are the arguments that lead to the definition of equivalent continuum models, i.e., models that under certain boundary and geometrical conditions will lead to an adequate description of rock mass behavior. More specifically for tunnels, it can be argued that one of the frequently essential functions of an efficient support is the elimination or at least the restriction of the detrimental influence exerted by the discontinuities. A "continuum" representation is then helpful in studying conditions under which discontinuities are likely to become a dominating factor. Finally, only under very unusual circumstances are tunnels driven through a rock mass in

which the discontinuity locations and their mechanical properties are known, and with few exceptions, an analysis of their influence must be fully three-dimensional with all the complications this entails.

The analysis of rock-support interaction usually will have to be based upon a significant amount of idealization and generalization, and it is felt that the analysis presented here includes several basic characteristics of rock mass behavior that have not been included previously. Particular attention is paid to the consequences of strain-softening, i.e., the fact that a reduced but significant strength remains in rock that has been deformed beyond its peak strength, as well as to the associated inelastic volume increase.<sup>1</sup> Whether these effects are due to the influence of newly-created or pre-existing discontinuities is assumed here to be of secondary importance. What is not of

---

<sup>1</sup>The term "dilatancy" is avoided here because it appears to have a different meaning in several related fields of mechanics. Whereas in plasticity theory and soil mechanics the term is reserved specifically for volume increases associated with changes in shear stress, such a restriction is not commonly observed in the rock mechanics literature.

only secondary importance is the extent to which these strength and stiffness reductions, as well as eventual volume changes, continue with time, because this will influence the long-term stability and support requirements. Certainly in some rock types, because of weathering, swelling, alterations, wash-outs, drying or wetting, etc. a time-dependent decrease in strength and in stiffness does occur. When such effects can be predicted quantitatively, their incorporation into the presented analysis techniques is straightforward.

It is a common and widely accepted statement that "the ground is unknown," or certainly not well-known. A frequently implied association is that the support system is a well-defined structural unit and that the analysis of the support is, therefore, straightforward. Even though some elements of the support structure are usually well-defined, e.g., a steel set, a steel rod, a ring of concrete elements, most support systems contain additional elements that are frequently very variable, and unknown prior to construction, such as blocking, anchors, backfill. As a consequence, neither the stiffness nor the strength of the support system, as a rule, can be considered as immutable constants

imposed once and for all at the design stage. Too many construction imponderables can affect the in-situ support behavior to permit such an assumption without at least a critical evaluation of its validity.

Two methods of attack have been used in this thesis to study the loading of tunnel supports caused by rock failure. While both methods have advantages and disadvantages, they tend to be complementary.

In the first part, closed-form solutions have been derived for the case of a circular tunnel in a radially symmetric rock mass and with radially symmetric supports. Although the problem is simplified greatly compared to some tunneling situations, it is not an unrealistic approximation to many tunnels. A more fundamental justification for this approach is that it allows the quantification of some general concepts. It is possible, within this simplified framework, to evaluate the influence of most significant variables that determine rock and support behavior, particularly by incorporating such effects in the derivation of the ground and support load-deflection curves. Visualization of the dominating factors and of their respective

contributions follows then immediately.

The finite element analysis complements the study in the first part quite logically because, while some of the generality of the conclusions is lost when a case-by-case study becomes necessary, some problems are exceedingly difficult to handle with closed-form solutions. Many of these, in principle at least, should not present fundamental problems when a numerical analysis technique is used. Difficulties such as complicated geometrical boundaries and boundary conditions, gravity effects, inhomogeneity and non-isotropy can be handled easily with the finite element method. The use of the finite element method was oriented towards the development of a strain-softening dilatant rock model that would permit a heuristic analysis of the influence of such effects upon tunnel support loading. Particular attention was paid to support loading near the face, where a three-dimensional configuration was approximated by an axi-symmetric model and by a sequential plane strain analysis corresponding to progressive excavation and tunnel support loading.

## Chapter II

### CONTINUUM ANALYSIS OF TUNNEL SUPPORT LOADING CAUSED BY ROCK FAILURE

#### II-1. Introduction

The use of continuum mechanics for the analysis of tunnel stability and the design of tunnel supports has been suggested frequently, and in a variety of forms. In the most common methods the problem is discussed by analyzing the stress distribution around an opening (usually circular) in an infinite medium with given constitutive properties. In an attempt to improve the realism with which the model approximated the real situation, the material models that were used became increasingly complex. They evolved from isotropic into orthotropic elastic solutions, and various elasto-plastic, visco-elastic and visco-plastic calculations were considered. While a progressively better understanding of tunnel support loading might have developed, it does not appear that a fundamental influence on support or construction procedures has been exercised by these methods.

The usual procedure for estimating support requirements from such calculations was based on the potential development of fracture or failure zones. This, then, was complemented by calculating the support pressures required to prevent failure or by determining support strengths required to prevent collapse of the tunnel when certain failure modes were assumed to occur.<sup>1</sup>

The applicability of continuum analysis to tunnel support design has been disputed from two opposite points of view:

- The methods involve too many assumptions regarding material behavior, require much more knowledge about the material properties and the state of stress than is usually available, and are, therefore, only of theoretical interest. They do not offer a practical alternative to conventional rule of thumb design.

- The methods involve too many simplifying assumptions regarding material behavior and problem geometry. These restrictions, due to the insurmountable mathematical difficulties associated with

---

<sup>1</sup>Most older design methods are similar with regard to this final step. They were usually based upon assumptions and observations of possible roof fall-outs rather than upon explicit stress distribution calculations.

solving all but the very simplest problems make it unlikely that these simplistic methods are still useful when compared to the flexibility and potential of computerized numerical methods.

Both types of criticism, stated here in a somewhat extreme form, have validity under certain circumstances. They imply, however, that the use of continuum mechanics is threatened from two directions, by the simple pseudo-empirical design methods and by the sophisticated modern numerical analysis techniques. The potential use or significance of continuum mechanics solutions compared with the two classes of methods listed above can be based upon the following arguments:

- Continuum analysis attempts to explain the mechanics of tunnel support loading. This requires an explicit evaluation of the factors needed to make an analysis. It reduces the likelihood of unconsciously hiding assumptions under a cover of empirical parameters.

- Continuum analysis provides guidelines as to what type of factors or results must be considered or expected when various support types are loaded by various rock failure mechanisms. This facilitates narrowing down the range of effective

influence factors. It reduces the likelihood of having to consider a near-infinite number of possible case studies.

Continuum mechanics steers a middle course between the simplest and the most complicated analysis procedures. The former, with a nearly exclusive interest in the final goal, the determination of support requirements, might never reach it by neglecting potentially valuable information. The latter, with an extreme interest in determining the optimum path to the goal might never reach it by becoming enmeshed in a wealth of potentially valuable information.

The analysis of support loading in this chapter incorporates a comprehensive (if greatly simplified) model of rock failure characteristics and of support characteristics within a continuum mechanics framework.

A survey is given of the literature on the analysis of tunnel support loading caused by rock failure. This survey is limited strictly to methods of the continuum type<sup>2</sup> that have been published with

---

<sup>2</sup>Frequently referred to as "plasticity" solutions in the tunneling literature, i.e., excluding elastic, visco-elastic, and other continuum mechanics solutions.

explicit reference to support design.<sup>3</sup> The survey aims to indicate in which way a growing awareness of rock failure characteristics was appreciated and applied to the study of tunnel support loading. Only publications that present a significant additional feature over earlier ones are included, but they are neither fully summarized nor critically discussed.

In the subsequent sections the basic phenomena associated with rock failure are used in calculations of the stress redistribution and the tunnel convergence caused by progressive failure. Considered are the (gradual) strength, stiffness and volume changes. As relaxation advances, it becomes necessary to include the influence of gravity forces. More comprehensive or detailed calculations can be done by one-dimensional numerical generalizations.

The problem of rock-support interaction is a statically indeterminate one. For this reason the stiffness of the support plays a critical role in the establishment of the final equilibrium position.

---

<sup>3</sup>The numerous plasticity solutions to such problems as holes in plates, hollow cylinders, etc. that could be used either directly or after some modification are not reviewed.

The significant influence of construction "details" is shown with simple but realistic methods. This obviates the need for qualitative comparisons between support systems.

The results are summarized in the form of typical ground and support characteristics. Such graphs illustrate the principal examples of possible equilibrium modes. Included are suggestions for a simplified analysis of time-dependent changes as well as a discussion of the influence of discontinuities and of tunnel size upon support requirements.

The applicability of the derived methods depends directly on a sufficient knowledge of the rock mass behavior. It is unlikely that sweeping generalizations regarding "ideal" tunnel support characteristics can be realistic in view of the wide range of possible rock types and properties. Differences in the latter can cause fundamental differences in the ground reaction. A final appreciation of the discussed hypotheses must await in-situ confirmation of calculated predictions.

## II-2. Literature Survey

One of the first calculations of an elasto-

plastic stress distribution around a cylindrical underground opening was performed by Terzaghi (1919, 1925, 1943). This solution was presented in a slightly different form by Westergaard (1940). The resulting stress distribution was used by these authors to explain the stability of small bore-holes, stability that could be obtained with minimal support in cohesionless sand and without support in a cohesive clay. Terzaghi (1925) suggested that these calculations might lead to a semi-empirical evaluation of a plastic load bearing zone around a tunnel, but he did not consider or discuss the application of these calculations for the design of tunnel supports. Moreover, he did not accept these calculations as a valid method for calculating support pressures on shaft liners, although it was implied clearly that this rejection was based on the observations of failures near a shaft mouth.

An attempt to use elastoplastic stress calculations for determining the support pressures required in cylindrical underground excavations was first made by Fenner (1938). Because the cohesion is always included in his calculations they lead to the conclusion that stability of the opening is always possible without support. In order to

circumvent this contradiction with practical experience in shafts and tunnels Fenner imposes some arbitrary limits upon the depth to which plastic zones can be allowed to propagate. This he justifies with the argument that the plastic zones required to eliminate the need of any support pressure are very large. It, therefore, takes a long time before they are developed fully, and supports are usually installed long before the "natural equilibrium state" has been attained. Moreover, the development of the plastic zone is associated with a rock volume increase, and in order for the natural equilibrium to be reached, large displacements should be allowed or large amounts of rock should be removed.<sup>4</sup> Fenner assumed that the volume increase of the plastic region would equal the elastic volume increase following a total destressing of the plastic region from a hydrostatic pressure equivalent to the overburden pressure at the tunnel center. The plastic zones required to guarantee

---

<sup>4</sup>This is probably the origin (or at least a theoretical justification) of the "stress-relief" technique that has been suggested occasionally for stabilizing tunnels at reduced support pressures by removing some of the rock behind the supports.

unsupported stability that resulted from his numerical examples were extremely large (several orders of magnitude larger than the tunnel radius). Fenner, therefore, concluded that the volume of rock to be removed was excessive and that it was preferable in practice to install supports.

Goguel (1947) derived the stress distribution by using the second stress invariant as a criterion for plastic flow. He pointed out some of the difficulties associated with including in the analysis the stress component parallel to the tunnel axis. To negate the conclusion that support is not required, he suggested that the process of deformation is not finished with the development of the plastic zone but that deformations continue, particularly within this plastic zone. The function of the support then is to provide a boundary, which makes it possible for the surrounding material to regain a hydrostatic state of stress (at a velocity that might be extremely small). Goguel suggested that it might be necessary to use reduced cohesion and friction values in the calculations.

Labasse (1949) derived essentially the same stress distributions. He proposed several possible alternative calculations to approach the problem

for the case where the pre-tunneling stressfield is not hydrostatic. Labasse's essential contribution was to consider the interaction between rock and support: support cannot be characterized by a "support pressure," nor can rock be characterized by a "rock load." The equilibrium state between rock and support will determine the contact pressure between the two structural elements. This indicates that the relative displacements are a significant factor. It is, therefore, necessary to consider the influence of volume increases associated with rock failure.

Kastner (in a series of papers, 1947-1952, incorporated and extended in his 1962 book) presented a stress distribution similar to the one derived by the above-mentioned authors. His solution for the non-hydrostatic case is based on the potential fracture zones calculated from an elastic stress distribution. The support design application is derived by imposing some fairly arbitrary limits upon the depth to which such "plastic zones" can be allowed to propagate. Kastner characterizes the support by a required support pressure and strength, and gives minimal attention to the statically indeterminate nature of the problem.

Morrison and Coates (1955) discussed in great detail the paper by Fenner (1938) and corrected many of the numerous errors in the original. They presented a graphical estimate of the stress distribution around a tunnel based upon the assumption that the "broken" material in the plastic zone should be characterized by a failure envelope with a smaller cohesion than the initial envelope. A comprehensive calculation of the stress distribution based on such a "bilinear" approach was given by Krech (1966).

Mandel (1959) strongly criticized the use of continuum type plasticity calculations for analyzing rock failure around underground openings. He emphasized that rock crushing or breaking was neglected in such analyses. Mandel postulated that the only reasonable conclusion to be retained from such an elasto-plastic analysis is that a maximum stress concentration develops somewhere within the rock mass.

Rabczewicz (1963) suggested that the "ground unloading curve" could be determined by measurements of pressure and deformation on shotcrete liners with a known "loading curve."

Pacher (1964) emphasized the necessity of an

empirical approach to the determination of the rock-support equilibrium state. He presented a comprehensive qualitative discussion of the interaction between rock and support in terms of their respective "characteristics," pointing out the importance of the time of support installation and the necessity to avoid the development of "loosening" pressure.

Sirieys (1964) suggested that a "broken" zone might develop inside the plastic zone, and so did Serata (1964) who suggested a series of various material models around the opening.

Hobbs (1966) calculated the stress distribution for a circular roadway surrounded by a broken zone in which a nonlinear failure criterion is satisfied. The nonlinear relation between the largest and the smallest principal stresses was derived from the results of compressive strength tests. He complemented the solution with an approximate calculation of the roadway closure and of the possible displacement patterns.

Richter (1966) characterized the zone around a failing tunnel as a succession of an annulus with reduced elastic modulus, an annulus with increased modulus and the outside region with the unchanged original modulus.

DeBeer and Buttiens (1966) calculated the tunnel closure assuming a constant volume deformation in the plastic region, and found fairly good agreement with the volume of surface settlement.

Lombardi (1966) subdivided the ground characteristic by two limiting points: the transition from elastic to plastic, and the point where rupture occurs.

Bray (1967) calculated the displacements by considering slip along fracture planes.

Luetgendorf (1968) emphasized the significance of gravity effects in the broken rock as well as the reduced strength properties of the broken zone, while Lecian (1968) in his similar discussion underscored the need to include a time factor in such an analysis.

Lombardi (1970) pointed out that the volume increase due to failure does not merely increase the displacements but can also have a significant stabilizing effect.

Daemen and Fairhurst (1970), Wagner (1970) and Egger (1972, 1973) discuss the strength reduction in the broken zone and the resulting changes in support pressure requirements in terms of the complete stress-strain curve.

II-3. Stress Redistribution Caused by Rock Failure Around a Tunnel

II-3.1. Introduction. When the stresses around a newly-excavated tunnel exceed the rock strength, failure occurs. Tunnel supports usually are not sufficiently stiff and strong, and generally they cannot be installed early enough to maintain a stress state in which the rock remains intact. Even if it were possible to construct such a support, it would not necessarily be the most economical one, because it would not allow the mobilization of the significant residual strength of the surrounding rock. Optimizing a support system will require this mobilization. It is necessary, therefore, to analyze the consequences of rock failure on the stress distribution around a tunnel. Failed rock has a reduced strength, and the propagation of failure causes stress relaxation. Pronounced relaxation can lead to a situation where local gravity effects around the tunnel can no longer be ignored.

The following analysis starts along the same lines as the derivations presented by most of the aforementioned authors, and specific references are, therefore, omitted.

The problem considered is that of a circular opening being driven through a rock mass under hydrostatic stress. The problem is statically determinate so that stresses can be calculated without regard to displacements or strains (assumed small enough so that no significant changes in the geometry occur).

Prior to tunneling the rock is assumed to be homogeneous, isotropic and linearly elastic. The stress concentration induced by the excavation exceeds the rock strength, and a homogeneous isotropic cylindrical broken zone develops.

### II-3.2. Constant Strength Broken Rock.

Failure around the opening is initiated when the stress state reaches a failure condition. The condition accepted here is that failure occurs when the circle representing the stress state in an elastic rock intersects the failure envelope in a Mohr diagram. A preliminary calculation of the stress distribution can be made assuming that the stresses throughout the plastic zone satisfy the condition of incipient failure (i.e., the stress circle touches the failure envelope). The solution can then be obtained from the following conditions:

## i) Equilibrium

$$\frac{\sigma_\theta - \sigma_r}{r} - \frac{d\sigma_r}{dr} = 0 \quad (\text{II-3.1})$$

## ii) Boundary conditions

$$\sigma_r = \sigma_\theta = P \quad \text{at } r = \infty$$

$$\sigma_r^e = \sigma_r^b \quad \text{at } r = b$$

$$\sigma_r = P_i \quad \text{at } r = a$$

$$\sigma_\theta^e (1 - \sin \phi) = \sigma_r^e (1 + \sin \phi) +$$

$$2 c \cos \phi \quad \text{at } r = b$$

## iii) Constitutive equations

$$\sigma_\theta^b (1 - \sin \phi) = \sigma_r^b (1 + \sin \phi) +$$

$$2 c \cos \phi \quad \text{for } a \leq r \leq b$$

$$\sigma_r^e + \sigma_\theta^e = 2 P$$

where:

$\sigma_r$ ,  $\sigma_r^e$ ,  $\sigma_r^b$  = radial stress, in the elastic region, in the broken zone.

$\sigma_\theta$ ,  $\sigma_\theta^e$ ,  $\sigma_\theta^b$  = tangential stress, in the elastic region, in the broken zone.

$r$ ,  $\theta$ : polar coordinates

$P$ : hydrostatic stressfield

$c$ ,  $\phi$ : cohesion and angle of internal friction

$a$ ,  $b$ : tunnel radius and radius of the broken zone.

The resulting relation between the radius  $b$  of the plastic zone and the support pressure  $P_i$  is given by:

$$P_i = \frac{1}{\sin \phi} [(P \sin \phi + c \cos \phi)(1 - \sin \phi) \left( \frac{a}{b} \alpha - c \cos \phi \right)] \quad (\text{II-3.2})$$

$$\text{where } \alpha = \frac{2 \sin \phi}{1 - \sin \phi}$$

(Details of all calculations summarized in this chapter are given in Appendix A).

The support pressure required to maintain equilibrium decreases monotonically with increasing radius of the plastic zone. For all rock types with cohesion, i.e., with at least some uniaxial strength, equilibrium can be reached without support if the broken zone is allowed to propagate deep enough.

III-3.3. Broken Zone Characterized by Residual Strength. When rock is strained beyond its peak strength, the residual strength tends to decrease more or less rapidly. As a first approximation, this effect can be accounted for by specifying a constant residual strength throughout the broken zone. The only change from the basic equations in the preceding section is in the constitutive

equation describing the behavior of the rock in the broken zone. This equation now becomes:

$$\sigma_e^b (1 - \sin \phi_r) = \sigma_r^b (1 + \sin \phi_r) +$$

$$2 c_r \cos \phi_r$$

$$\text{for } a \leq r < b$$

where  $c_r$  and  $\phi_r$  are the residual cohesion and the residual angle of internal friction, properties of the broken rock.

The resulting relationship between the radius  $b$  of the broken zone and the support pressure  $P_i$  can be written as:

$$P_i = [P(1 - \sin \phi) - c \cos \phi + c_r \cot \phi_r] \frac{(\frac{a}{b})^{\alpha_r} - c_r \cot \phi_r}{(II-3.3)}$$

$$\text{where } \alpha_r = \frac{2 \sin \phi_r}{1 - \sin \phi_r}$$

The required support pressure decreases monotonically with increasing radius of the broken zone. For all materials with some residual cohesion, i.e., some residual uniaxial strength, equilibrium is possible without support pressure.

**II-3.4. Gravity Effects.** In the preceding sections the state of stress around the tunnel was assumed to be generated by a hydrostatic stressfield

maintained at a great distance from the tunnel.

When gravity forces are taken into account, the radial and tangential stresses are no longer principal stresses, and the equilibrium equation in the radial and in the tangential directions can be written as:

$$\sigma_\theta - \sigma_r - r \frac{\partial \sigma_r}{\partial r} - \frac{\partial \tau}{\partial \theta} + rw \cos \theta = 0$$

$$\frac{\partial \sigma_\theta}{\partial \theta} + 2\tau + \frac{\partial \tau}{\partial r} r - rw \sin \theta = 0$$

where  $w$  is the specific weight of the rock,  $\tau$  is the shear stress.

Because of the symmetry about the vertical axis, the radial and tangential stresses are principal stresses along that axis. The equilibrium conditions along that axis can be reduced to:

$$\sigma_\theta - \sigma_r - r \frac{d\sigma_r}{dr} \pm rw = 0 \quad (\text{II-3.4})$$

(+: floor; -: roof)

Comparing this equation with (II-3.1) it can be seen that the gravity term was neglected in the previous sections. It is justifiable to neglect that term when it is small compared with the difference between the others. The other terms are a positive one, the stress difference, and a negative one, the radial stress increase into the rock mass.

Both of these terms decrease rapidly in absolute value with the development of a plastic or stress-relieved zone around the tunnel. This decrease is accelerated when residual properties are assigned to the broken zone, and both terms decrease particularly rapidly with a decreasing angle of internal friction. The error introduced by neglecting the gravity field will, therefore, become larger under such conditions. In particular, when the broken zone becomes so large that little or no support is required the stress distribution near the opening can be so small and equalized that neglecting the gravity term in this region can no longer be justified.

The problem can now only be solved when severe simplifications are introduced. Neglecting the gravity forces in the elastic region, and assuming the same boundary conditions as in Section 3.2, the relation between the support pressure  $P_i$  and the radius  $b$  of the broken zone can now be written as:

$$\begin{aligned}
 P_i &= [P(1 - \sin \phi) - c \cos \phi + c_r \cot \phi_r] \\
 &\quad \frac{2 \sin \phi_r}{\frac{a}{b} \frac{1 - \sin \phi_r}{1 - \sin \phi_r - c_r \cot \phi_r + aw \frac{1 - \sin \phi_r}{1 - 3 \sin \phi_r}} \\
 &\quad \frac{3 \sin \phi_r - 1}{[\frac{a}{b} \frac{1 - \sin \phi_r}{1 - \sin \phi_r} - 1]} \quad (II-3.5a)
 \end{aligned}$$

Two special cases have to be considered.

When  $\sin \phi_r = 1/3$ ,

$$P_i = [P(1 - \sin \phi) - c \cos \phi + 2\sqrt{2} c_r] \frac{a}{b} - 2\sqrt{2} c_r$$

$$+ w a \ln \frac{b}{a} \quad (\text{II-3.5.b})$$

When  $\phi_r = 0$ ,

$$P_i = P(1 - \sin \phi) - c \cos \phi - 2 c_r \ln \frac{b}{a} + w(b - a)$$

$$(\text{II-3.5.c})$$

The derivation of these equations is given in Appendix A.1. The preceding equations contain two unknowns, the radius  $b$  of the broken zone and the support pressure  $P_i$ . Application of these equations to tunnel support loading requires consideration of rock-support interaction, and therefore of the displacements. The determination of the displacements necessitates even more simplifying assumptions regarding rock failure behavior than does the determination of the stress distribution. It seems reasonable, therefore, to discuss the above results in somewhat more detail by illustrating the various factors included in the analysis up to now.

Figure II.1 shows the material strength model representation used in this analysis. The rock around the tunnel is in a state of incipient failure when the stress reaches a state represented by a

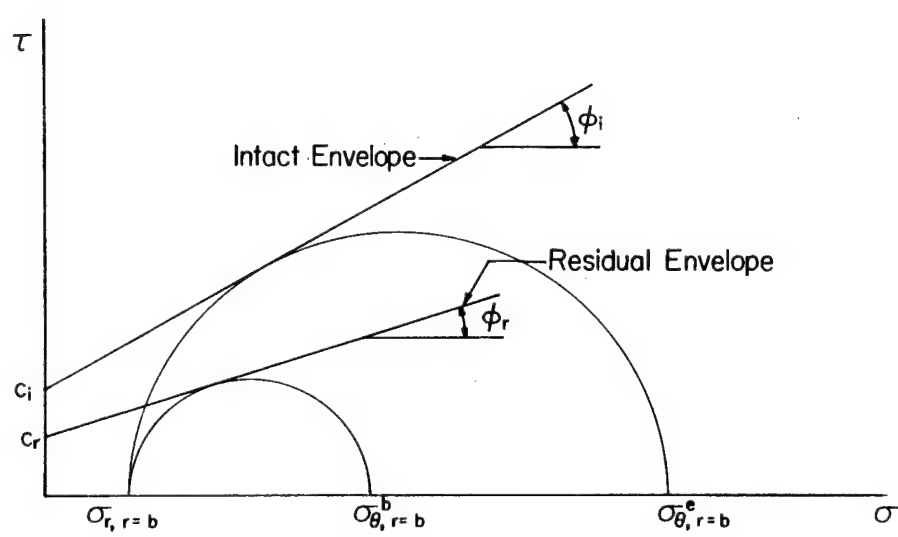


Figure II.1. Failed Rock Description Used in the Broken Zone

circle touching the intact rock failure envelope.

It is assumed that the circles corresponding to the stress states throughout the failed zone touch the residual envelope.

A reduction in internal friction and in cohesion, associated with rock failure, can have a significant bearing upon the support pressure requirements. This is illustrated in Figures II.2 and II.3.

Taking into account the gravity forces acting on the stress-relieved or loosened rock can introduce basic modifications of the results. The support requirements in the roof and on the floor can differ significantly (Figures II. 4, 5). This conclusion is not likely to be considered a major revelation by tunnel engineers. When the difference between roof and floor support is significant, it also will depend strongly upon the tunnel size (Figure II.5). For a tunnel of given size, the gravity term is determined mainly by the residual friction (Figure II.6), because the specific weight usually will not change greatly. The relative significance of the gravity term with respect to the total support requirements decreases with increasing pre-tunneling pressure (Figure II.7),

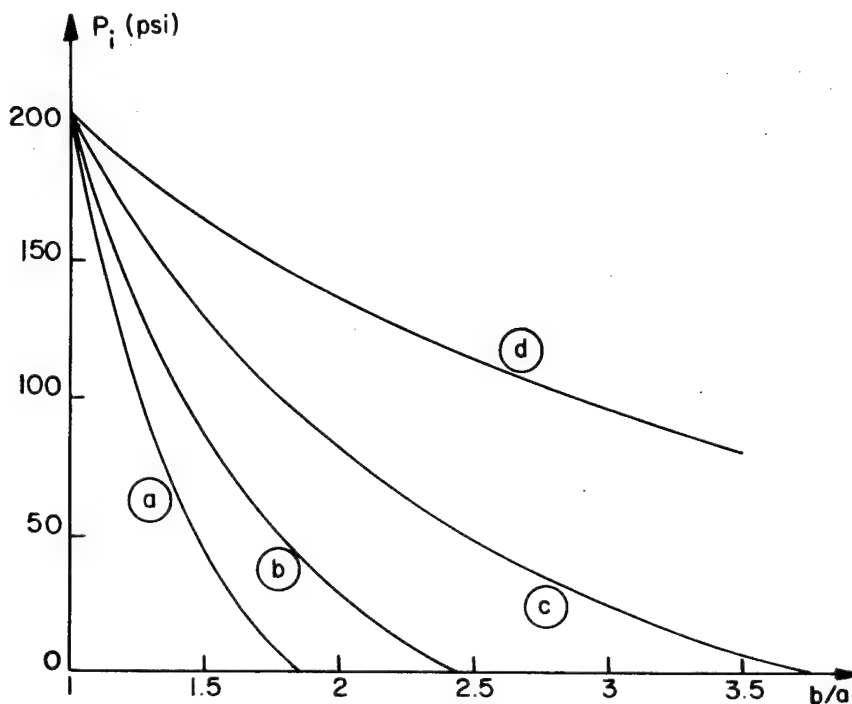


Figure II.2. Support Pressure  $P_i$  Required to Limit Failure Propagation to a Radius  $b$  for Various Values of the Residual Internal Friction. Gravity Terms are Neglected. Hydrostatic Pressure  $P = 500$  psi

Intact Cohesion  $c =$  Residual Cohesion = 50 psi

$\phi =$  Intact Friction =  $30^\circ$

$\phi_r =$  Residual Friction

Graphs: a:  $\phi_r = 30^\circ$       b:  $\phi_r = 20^\circ$   
 c:  $\phi_r = 10^\circ$       d:  $\phi_r = 0^\circ$

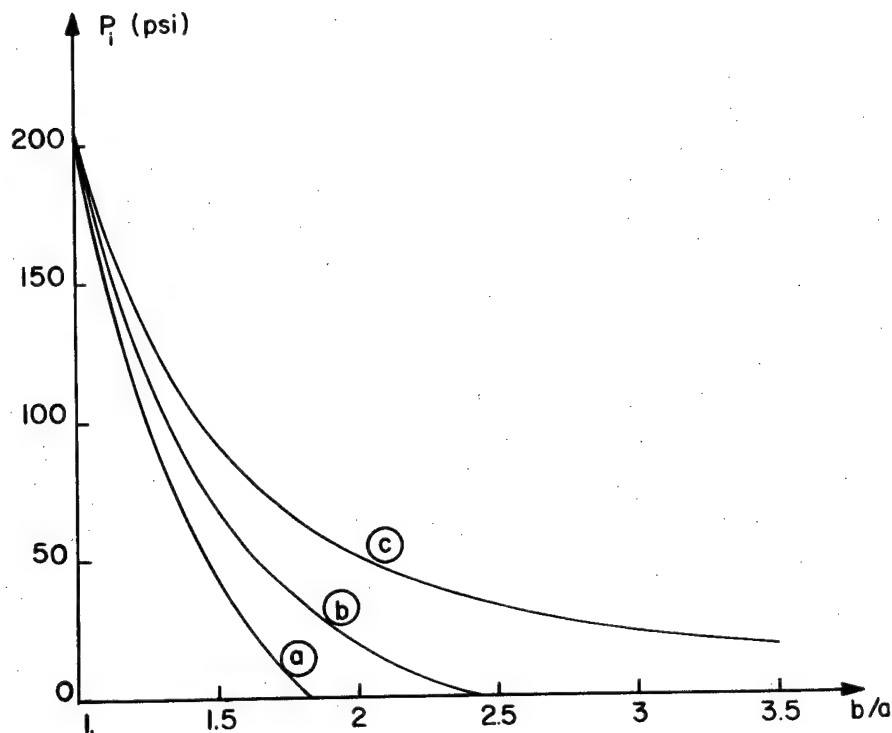


Figure II.3. Support Pressure  $P_i$  Required to Limit Failure Propagation to a Radius  $b$  for Various Values of the Residual Cohesion.

Hydrostatic Pressure  $P = 500$  psi

Intact Cohesion  $c = 50$  psi

$c_r$  = Residual Cohesion

Intact Friction  $\phi$  = Residual Friction

$\phi_r = 30^\circ$

Graphs: a:  $c_r = 50$  psi b:  $c_r = 25$  psi

c:  $c_r = 0$  psi

Gravity is neglected;  $w = 0$  lbs/in<sup>3</sup>.

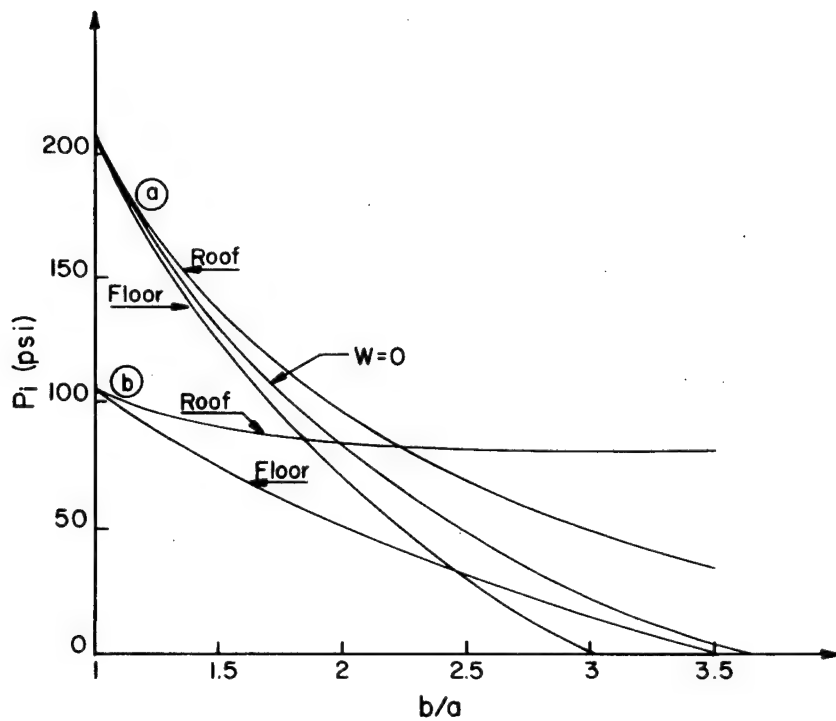


Figure II.4. Support Pressure  $P_i$  Required at the Roof and at the Floor to Prevent Failure Propagation Beyond a Radius  $b$ .

Specific Weight  $w = 0.09 \text{ lbs/in}^3 = 155.5 \text{ lbs/ft}^3$

Graphs a:  $c = c_r = 50 \text{ psi}$   $\phi = 30^\circ$

$\phi_r = 10^\circ$

Tunnel Radius  $a = 10 \text{ feet}$

Hydrostatic stress  $P = 500 \text{ psi}$

Graphs b:  $c = c_r = 25 \text{ psi}$   $\phi = 30^\circ$

$\phi_r = 0^\circ$

Tunnel Radius  $a = 15 \text{ feet}$

Hydrostatic stress  $P = 250 \text{ psi}$

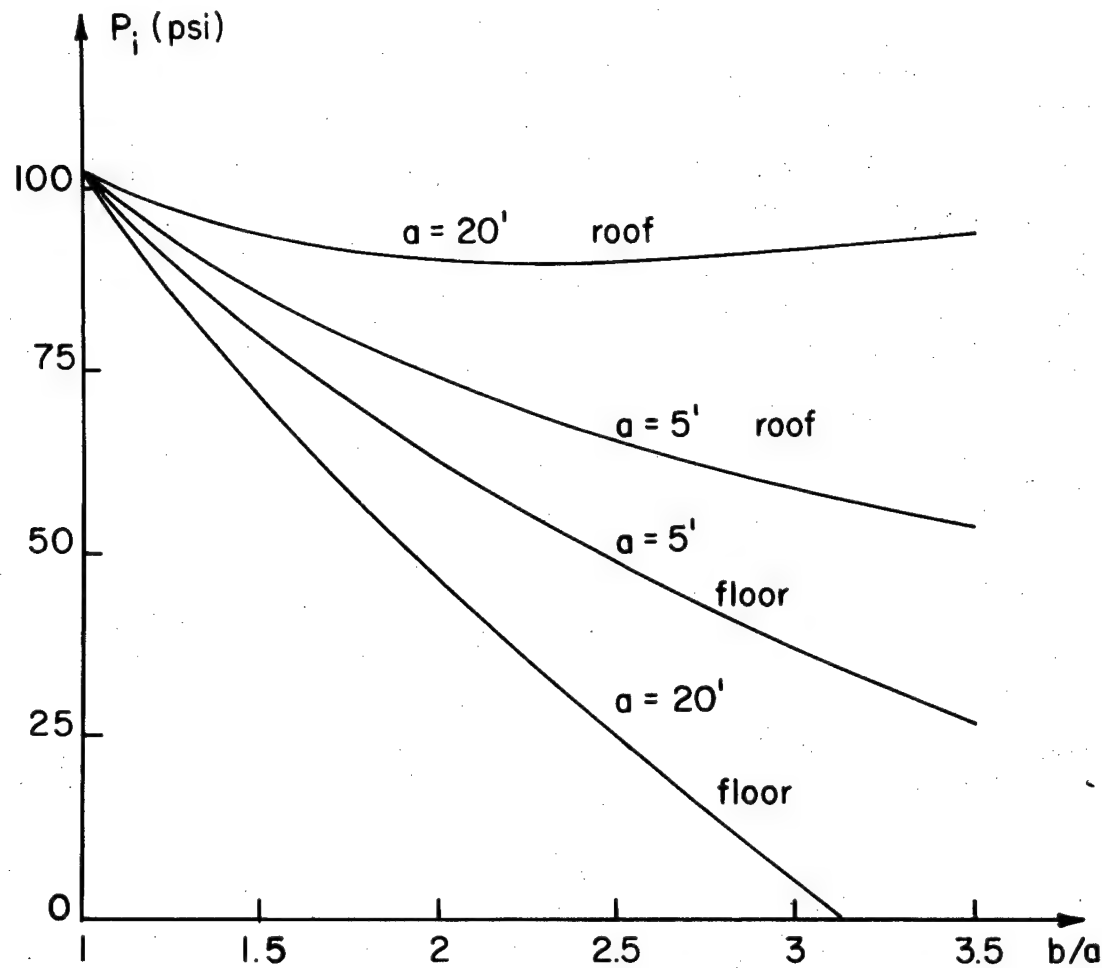


Figure II.5. Influence of the Tunnel Size Upon  
the Required Support Pressure.

$a$  = Tunnel Radius

$P$  = 250 psi

$c = c_r = 25$  psi

$\phi = 30^\circ$        $\phi_r = 0^\circ$

$w = 0.09$  lbs/in<sup>3</sup>

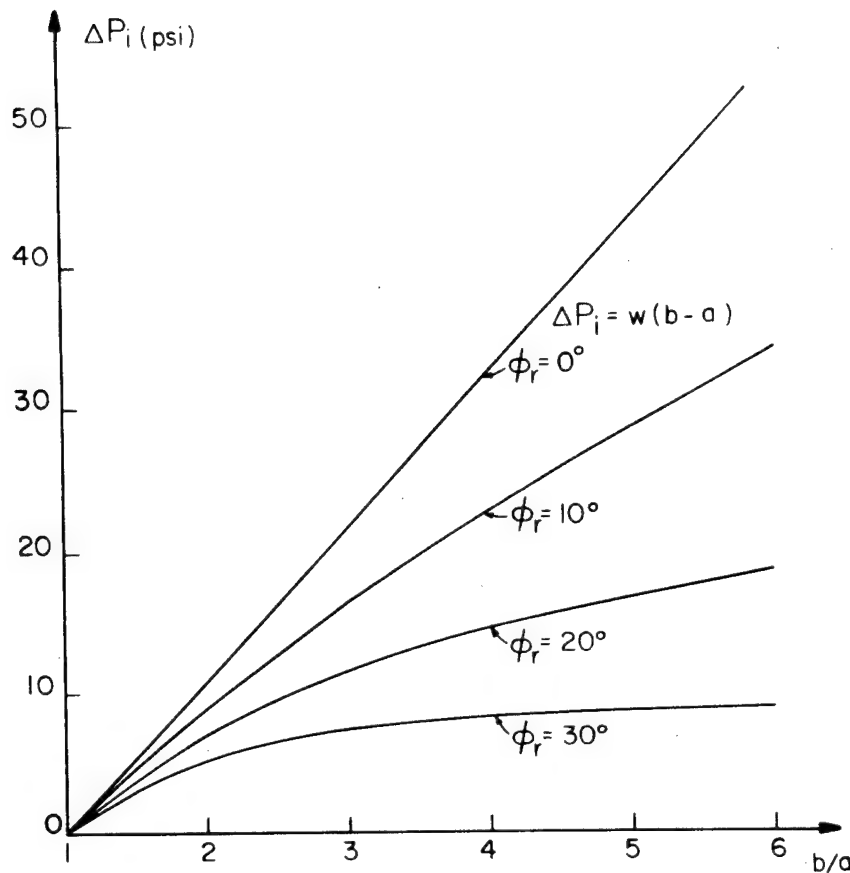


Figure II.6. Gravity Term  $\Delta P_i$  for an Increasing Broken Zone Radius  $b$  and for Various Residual Angles of Internal Friction  $\phi_r$ . The Term  $\Delta P_i$  Must be Added to or Subtracted from the "Weightless" Support Pressure to Obtain the Roof or Floor Support Pressure.

Tunnel Radius  $a = 10$  ft.

Specific Weight  $w = 0.09$  lbs/in<sup>3</sup> =  
155.5 lbs/ft<sup>3</sup>.

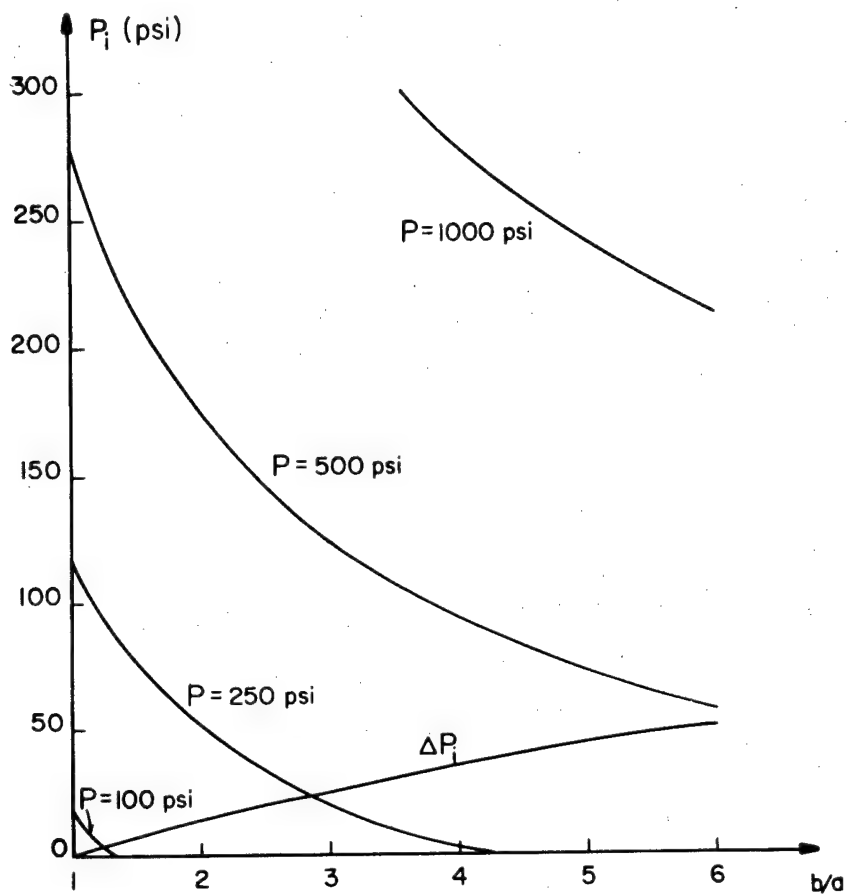


Figure II.7. Relative Significance of the Gravity Term  $\Delta P_i$  Compared to the "Weightless" Support Pressure  $P_i$  Required in Four Hydrostatic Stressfields  $P$  ( $\sim$  Depths).

Tunnel Radius  $a = 15$  feet

Intact Cohesion  $c = 50$  psi

Intact Friction  $\phi = 20^\circ$

Specific Weight  $w = 0.09 \text{ lbs/in}^3$

Residual Cohesion  $c_r = 25$  psi

Residual Friction  $\phi_r = 10^\circ$

or in general with increasing depth. When the friction drops to zero in the broken zone the full weight of this zone has to be supported in the roof, as can be seen from the last term in equation II-3.5c.

The terms in equations II-3.5 which are independent of the specific weight can be written as  $f(b/a, c, c_r, \phi, \phi_r)$ . The broken zone radius  $b$  enters the relation only relative to the tunnel radius, through the ratio  $b/a$ . The resulting graphs of the required support vs. the relative radius of the broken zone therefore can be used for any tunnel size provided the rock properties are identical.

The terms in equations II-3.5 which are dependent upon the specific weight can be written as  $aw \cdot f(b/a, \phi_r)$ . Graphs of the gravity terms versus the relative value of the broken zone radius  $b/a$  can be used for a tunnel of any size with the same residual friction, provided they are scaled appropriately for size and specific weight. The gravity term for a residual friction angle  $\phi_r = 0^\circ, 10^\circ, 20^\circ, 30^\circ$  can be derived from the  $\Delta P_i$  value in Figure II.6. If the actual tunnel radius differs from ten feet, the value read from Figure II.6 must be multiplied by the tunnel radius divided by ten. If the specific weight differs from  $0.09 \text{ lbs/in}^3$ , the gravity term  $P_i$

read from Figure II.6 must be multiplied by the actual value and divided by 0.09.

#### II-4. Tunnel Convergence Caused by Rock Failure Propagation

II-4.1. Introduction. The load build-up on a (passive) tunnel support system results from the interaction between the support and the converging rock. As the problem is statically indeterminate, the determination of the displacements is a prerequisite for the calculation of the support requirements.

An analytical solution is possible only for relatively simple material models. Nevertheless, these can be made sufficiently comprehensive to include, at least qualitatively, the principal deformational characteristics of rock failure. It is then possible to evaluate the potential significance of such characteristics on tunnel stability and support requirements.

Several additional assumptions beyond the ones involved for the stress distribution have to be made in order to derive displacement results. Several additional rock properties have to be known as well. One of the principal requirements is a more comprehensive definition of the stressfield. In

the previous section, during the derivation of the stress distribution, it was tacitly assumed that the (principal) stress parallel to the tunnel axis is always intermediate between the radial and the tangential stress, and has no influence upon the rock behavior in the broken zone. Such an implicit understanding is not sufficient when the displacements are calculated because the axial stress enters the results explicitly.

General assumptions regarding the axial stress are somewhat more difficult to make than similar hypotheses for in-plane stressfields. The axial stress, in a way similar to the horizontal in-plane stress, undoubtedly will depend strongly upon the site conditions for a particular tunnel. This can be illustrated best by two extreme but realistic examples:

- i. Consider a short tunnel through a long narrow ridge and well above the average level of the surrounding terrain. Both tunnel portals are in vertical or near-vertical cliffs. Certainly near the portals the axial stress will be close to zero. If the axial stress is larger near the center of the ridge then it is not a principal stress, at least along some sections of the tunnel.

This can be seen from the equilibrium equation for a direction  $z$  parallel to the tunnel axis:

$$\frac{\partial \sigma_z}{\partial z} + \frac{\partial \tau_{xz}}{\partial x} + \frac{\partial \tau_{yz}}{\partial y} = 0$$

In a situation such as this, for example near a tunnel portal, the failure mode will bear little resemblance to what is suggested by a two-dimensional analysis of the type discussed in the preceding sections. In such a case, unless the horizontal and vertical stress are very different, the axial stress is the smallest (principal) stress throughout the rock surrounding these tunnel sections.

ii. Consider a tunnel well below the average (and lowest) terrain level. A reasonable first assumption is that prior to tunneling all stresses are equal to the overburden pressure. A plane strain condition can be imposed along the tunnel for the stress and displacement changes induced by tunneling.

In this thesis only the second situation is considered in more detail.

II-4.2. Constant Volume Expansion and Minimum Tunnel Convergence. A first assumption that

can be made regarding the deformational characteristics of breaking rock is that the entire broken zone experiences an equal and constant volume increase (Labasse, 1949). The tunnel wall displacement can then be written as:

$$u_a = a - [a^2(1 + K) - b^2K - 2bu_b + u_b^2]^{1/2} \quad (\text{II-4.1})$$

where:

$K$  = constant volume expansion factor

$a, b$  = radius of tunnel and of broken zone

$u_a, u_b$  = radial displacements at  $r = a$  and  $r = b$

The radial displacement  $u_b$  is given by:

$$u_b = \frac{(1 + \nu)b}{E} [P \sin \phi + c \cos \phi] \quad (\text{II-4.2})$$

where:

$E, \nu$  = Young's modulus and Poisson's ratio

$c, \phi$  = cohesion and angle of internal friction

$P$  = hydrostatic stress

When  $K = 0$  in (II-4.1) it is assumed that no volume change occurs in the broken zone, and this results in a lower bound for the displacement or tunnel convergence. When the displacements are small in comparison with the tunnel radius one can simplify equation (II-4.1) to:

$$u_a = \frac{b}{a} u_b + \frac{K(b^2 - a^2)}{2a} \quad (\text{II-4.3})$$

**II-4.3. Elastic Relaxation of the Broken Zone.** The lower bound displacement calculation of the previous section implies that a substantial change in the stress and stress deviation invariants can take place (stress relaxation around the tunnel) without an associated volume change. This is incompatible with the assumed failure criterion (at least when the angle of internal friction is not zero). The assumption of a constant volume change, independent of strain and stress is obviously an extreme simplification, although it can be used with benefit in some circumstances.

A reasonable basic assumption for the displacement calculations is to regard the volume changes or displacements induced by the progressive unloading during the propagation of the broken zone as elastic. Prior to tunneling the rock has been compressed, and the volume change due to that compression, in a plane perpendicular to the tunnel axis, is given by:

$$\frac{dv}{v} = \frac{du}{dr} + \frac{u}{r} = \frac{\sigma_r - \nu(\sigma_\theta + \sigma_z) + \sigma_\theta - \nu(\sigma_r + \sigma_z)}{E} = \frac{2P(1 - 2\nu)}{E} \quad (\text{II-4.4})$$

where  $\sigma_r$ ,  $\sigma_\theta$  and  $\sigma_z$ , the radial, tangential and axial stresses are assumed to equal the hydrostatic stress  $P$ .

If the rock remains elastic after excavation of the tunnel and a plane strain condition is imposed for changes induced by tunneling the axial stress will remain constant. This can be seen from:

$$\Delta\sigma_z = \nu[\Delta\sigma_r + \Delta\sigma_\theta] = \nu[\sigma_r - P + \sigma_\theta - P] = 0 \quad (\text{II-4.5})$$

where  $\Delta\sigma_z$ ,  $\Delta\sigma_r$  and  $\Delta\sigma_\theta$  are stress changes induced by tunneling. It follows that no rock volume change occurs around an elastic tunnel, as can be seen directly by substituting  $\Delta\sigma_z$ ,  $\Delta\sigma_r$  and  $\Delta\sigma_\theta$  in equation (II-4.4).

Assuming that the elastic plane strain condition remains valid for the broken rock, the axial stress in the broken zone can be derived from:

$$\Delta\sigma_z = \nu(\Delta\sigma_r + \Delta\sigma_\theta) = \nu(\sigma_r^{\text{br}} + \sigma_\theta^{\text{br}} - 2P) \quad (\text{II-4.6})$$

where  $\Delta\sigma_z = \sigma_z^{\text{br}} - \sigma_z^{\text{el}} = \sigma_z^{\text{br}} - P$ ,  $\Delta\sigma_\theta = \sigma_\theta^{\text{br}} - \sigma_\theta^{\text{el}}$  and  $\Delta\sigma_r = \sigma_r^{\text{br}} - \sigma_r^{\text{el}}$  are the stress changes induced by failure. The axial stress in the broken zone is then given by:

$$\sigma_z^{br} = (1 - 2\nu)P + \nu(\sigma_r^{br} + \sigma_\theta^{br}) \quad (II-4.7)$$

Assuming elastic stress-strain relations, the volume increase caused by the stress relaxation in the broken zone can be written as:

$$\frac{dv}{v} = \frac{du}{dr} + \frac{u}{r} = \frac{\sigma_r^{br} - \nu(\sigma_\theta^{br} + \sigma_z^{br}) + \sigma_\theta^{br} - \nu(\sigma_r^{br} + \sigma_z^{br})}{E}$$

The tunnel wall displacement can then be calculated by equating the final volume of the rock within the broken zone to the original volume augmented with the expansion caused by the stress relaxation during the propagation of the broken zone. Assuming that the displacements (or strains) are small compared to the tunnel radius, this results in:

$$u_a = \frac{b}{a} u_b + \frac{(1+\nu)(1-2\nu)}{aE} [P(b^2 - a^2) - \int_a^b (\sigma_r^{br} + \sigma_\theta^{br}) r dr] \quad (II-4.8)$$

where:  $u_b$  is the radial displacement at the outer boundary of the broken zone, given by

$$(II-4.2)$$

$u_a$  is the radial displacement on the tunnel periphery,  $r = a$   
 $E, \nu$  are the Young's modulus and Poisson's ratio

P is the hydrostatic stressfield

$\sigma_r^{br}$ ,  $\sigma_\theta^{br}$  are the radial and tangential stress in the broken zone.

Equation (II-4.8) can be rewritten in terms of residual and intact elastic properties:

$$u_a = \frac{b}{a} \frac{1+\nu}{E} (P \sin \phi + c \cos \phi) + \frac{(1+\nu_r)}{3aK_r} [P(b^2-a^2) - \int_a^b (\sigma_r^{br} + \sigma_\theta^{br}) r dr] \quad (II-4.8a)$$

where  $\nu_r$  and  $K_r = \frac{E_r}{3(1-2\nu_r)}$  are the Poisson's ratio and the bulk modulus of the broken rock,  $E_r$  the Young's modulus.

It is clear from equation (II-4.8a) that an inelastic volume increase due to failure in the broken zone, expressed as an increase in the Poisson's ratio, a decrease in the bulk modulus, or both, will lead to an increase of the tunnel convergence beyond the value resulting from purely elastic relaxation.

It is illustrative to rewrite (II-4.8) for the assumption that the axial stress  $\sigma_z$  remains equal to P during failure. The displacement is then given by:

$$u_a = \frac{b^2}{a} \frac{(P \sin \phi + c \cos \phi)}{2G} + \frac{1}{2G_r} [P(b^2-a^2) - \int_a^b (\sigma_\theta^{br} + \sigma_r^{br}) r dr] \quad (II-4.8b)$$

where  $G$  and  $G_r$  are the shear moduli of the intact and of the broken rock. This shows that a decrease in the rock shear stiffness caused by rock failure will increase the tunnel convergence.

When failure propagates into the rock the tangential stress near the tunnel periphery decreases (as does the radial stress). For both of the preceding  $\sigma_z$  assumptions a situation can develop where the tangential stress in a region  $(a, r)$  with  $a \leq r \leq b$ , drops below the axial stress  $\sigma_z$ . Failure is then most likely in between the  $(z, r)$  directions. This type of failure induces stress relief in the axial direction. A third reasonable  $\sigma_z$  assumption can be made, and it eliminates the problem of  $\sigma_z$  becoming the largest principal stress. One can impose as a condition for  $\sigma_z$  that the stress state in the broken zone must satisfy the generalized three-dimensional Mohr-Coulomb failure criterion (Drucker and Prager, 1952). Combining this with the plane strain condition leads to:

$$\sigma_z^{\text{br}} = \frac{\sigma_\theta^{\text{br}} + \sigma_r^{\text{br}}}{2} - \sin \phi_r \frac{\sigma_\theta^{\text{br}} - \sigma_r^{\text{br}}}{2} \quad (\text{II-4.9})$$

The displacement at the tunnel wall is then given by:

$$u_a = \frac{b}{a} u_b + \frac{P(1-2\nu)(b^2-a^2)}{aE} - \frac{1-2\nu}{aE} \int_a^b (\sigma_{\theta}^{br} + \sigma_r^{br}) r dr$$

$$- \frac{\nu \sin \phi}{aE} \int_a^b (\sigma_{\theta}^{br} - \sigma_r^{br}) r dr \quad (II-4.8c)$$

The full derivation of the preceding equations leads to rather lengthy expressions and is given in Appendix A where a Fortran program for the numerical evaluation of the ground reaction curve is included.

Examples of the relation between displacements and corresponding support pressures as calculated from the preceding expressions are shown in Figure II.8. The straight line in this figure comprises the elastic section of the ground reaction curve (full line) as well as the ground reaction that would result if the rock were to remain elastic after complete removal of all internal confinement (dotted line). The "minimum displacement" ground characteristic is based on the assumption that no volume change occurs when the failure zone develops, i.e.,  $K = 0$  in equation II-4.1. The same equation was used to calculate the displacements when a constant 0.1% ( $K = 0.001$ ) volume increase accompanies failure throughout the broken zone. Two sets of "elastic relaxation" ground reaction curves are

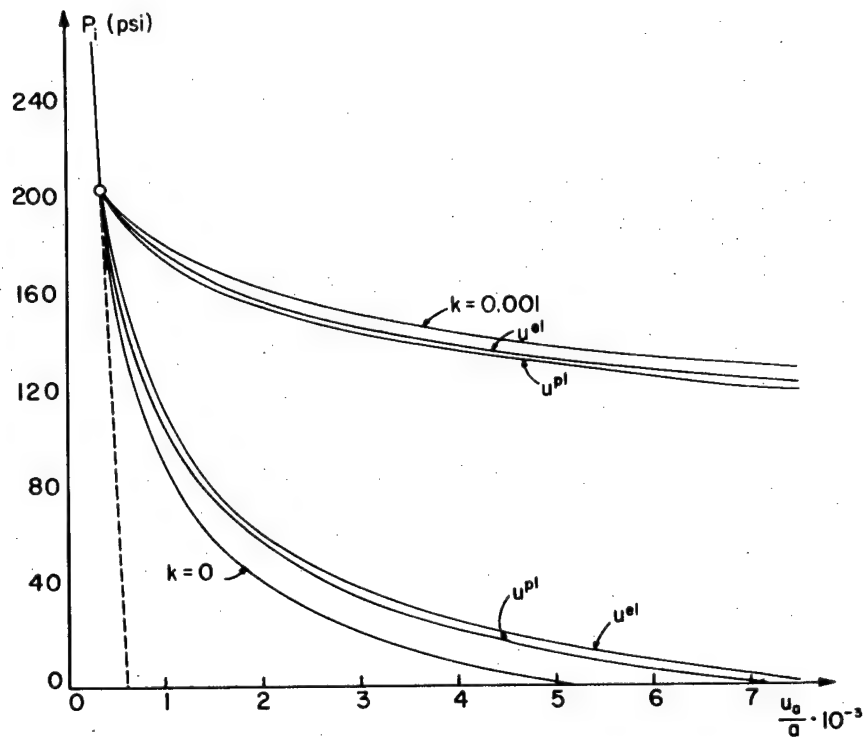


Figure II.8. Influence of Variations in Residual Properties on Ground Reaction Curves Calculated for Different Assumptions

Common data:  $P = 500$  psi;  $E = 10^6$  psi;  
 $\nu = 0.2$ ;  $c = 50$  psi;  $\phi = 30^\circ$ ;  $w = 0$   
---Ground reaction curve when rock  
remains elastic, i.e., when  $\sigma_z > 2P$

$u_z^{\text{el}}$ : displacement when  $\sigma_z$  is calculated from an elastic plane strain assumption (equation II-4.7)

$u_z^{\text{pl}}$ : displacement when  $\sigma_z$  is calculated from a plastic plane strain assumption (equation II-4.9)

Lower  $u_z^{\text{el}}, u_z^{\text{pl}}$ :  $c_r = 25$  psi;  $\phi_r = 20^\circ$ ;

Upper  $u_z^{\text{el}}, u_z^{\text{pl}}$ :  $c_r = 0$  psi;  $\phi_r = 10^\circ$ ;  
 $E_r = 0.6E$

$k = 0$ : minimum displacement ground reaction curve

included, for two different sets of residual (broken rock) properties. One graph of each set was calculated for an axial stress  $\sigma_z$  calculated from the elastic plane strain assumption (II-4.7), the other graph results from the plastic  $\sigma_z$  definition (II-4.9). No gravity effects were included in the results of Figure II.8.

Three fundamentally different types of "roof" ground reaction curves are illustrated in Figure II.9. When the rock strength drops very steeply once the ultimate strength has been exceeded, the support pressure required in the roof increases rapidly with deeper failure propagation (curve 1). For a rock type that can be subjected to large inelastic strains without significant strength loss the increased "arching" in the larger tangential compression zone more than compensates for the combined contribution of the (limited) strength loss and increased broken rock weight (curve 2). Finally, and possibly most realistic or common, when a gradual strength loss occurs (or a fairly steep one but only well beyond the peak strength) the support pressure required in the roof can decline during the initial stage of nonelastic deformation but will increase beyond the point where the

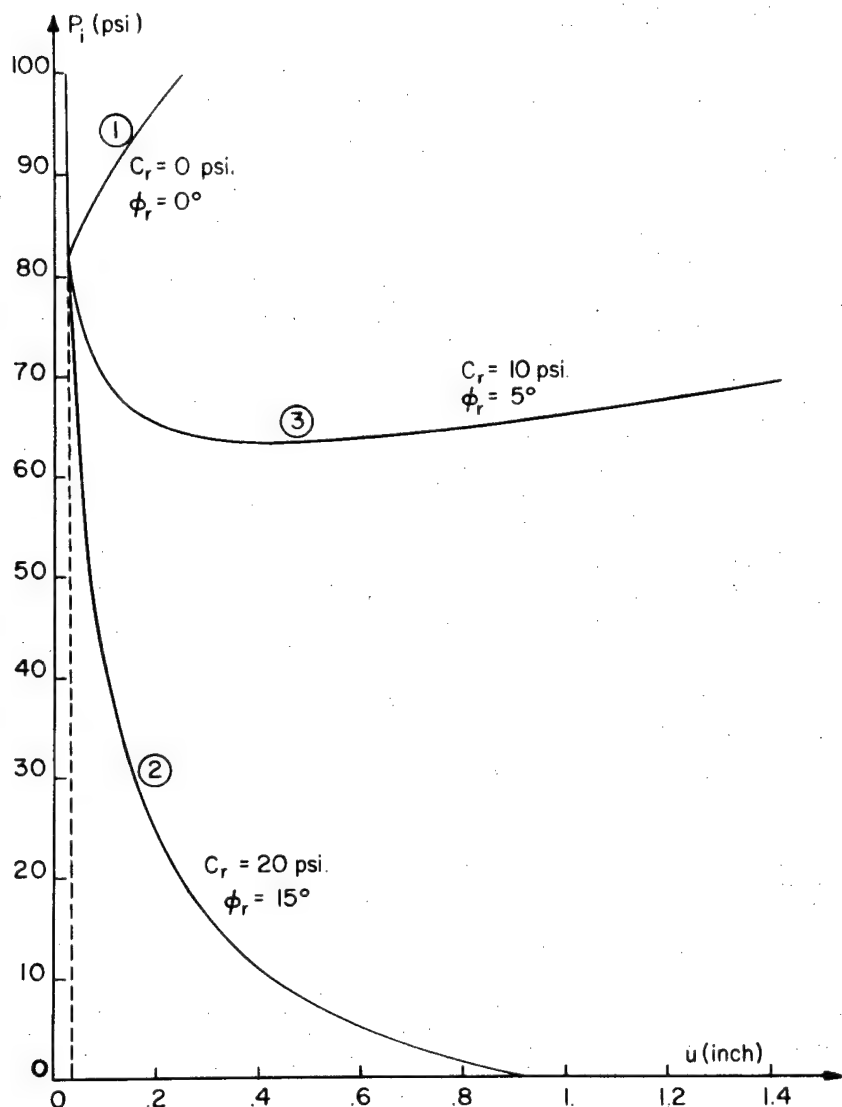


Figure II.9. Fundamental Types of "Roof" Ground Reaction Curves

- (1) Failing ground
- (2) Yielding ground
- (3) Transition from yielding to failing ground

Data:  $P = 250 \text{ psi}$ ;  $E_r = E = 10^6 \text{ psi}$ ;

$\gamma = 0.25$ ;  $a = 10 \text{ ft}$ .  $c = 50 \text{ psi}$ ;

$\phi = 30^\circ$ ;  $w = 155.5 \text{ lbs/ft}^3$

combined effects of strength loss and increased broken rock weight preponderate (curve 3). This is the shape of the ground reaction originally suggested by Pacher (1964) in his discussion of the influence of "genuine rock pressure" and of "loosening pressure" upon support requirements.

#### II-4.4. Influence of a Progressive Strain

##### Dependent Strength Decrease During Rock Failure.

The analysis of the preceding section, where residual properties have been assigned to the broken zone, implies that an abrupt change in material behavior occurs across the broken zone boundary. It also implies that all residual properties are strain-independent. Stress-strain diagrams for such a material are shown in Figure II.10, dotted lines. Such a material is characterized by a sudden lowering of the failure envelope from its original level to the residual level, at the instant the strength is exceeded. When the strength properties are changed according to this model a discontinuity in the tangential stress and in the radial stress gradient across the broken-intact boundary is introduced. A similar discontinuity is added in the displacement behavior if deformational

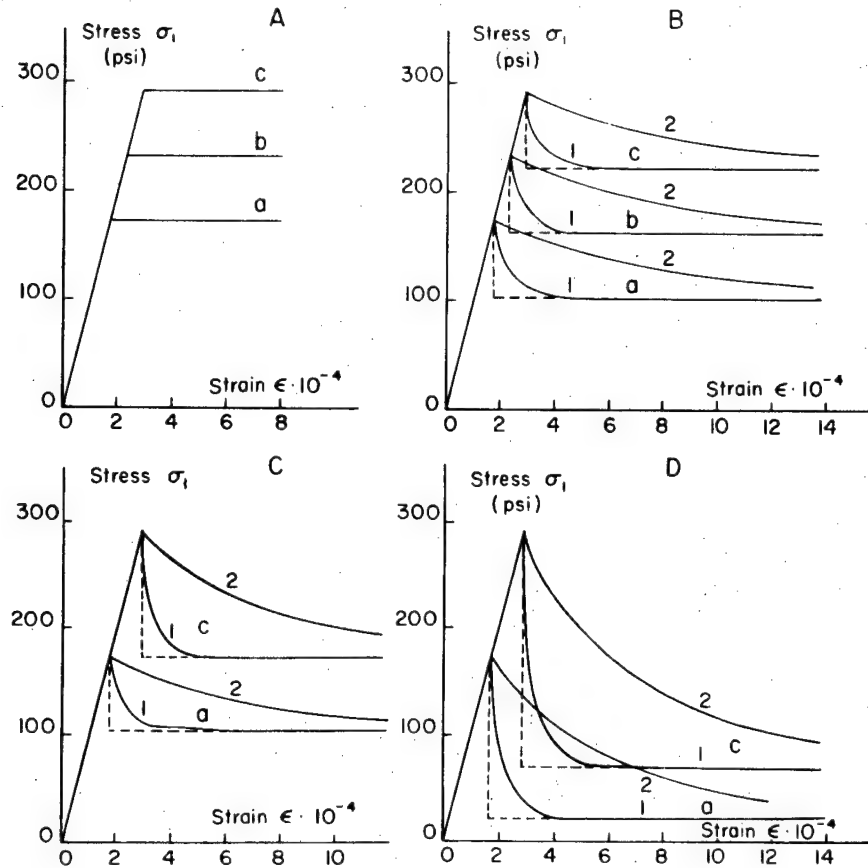


Figure II.10. Calculated Stress-Strain Curves

----: sudden strength loss beyond peak

—: exponential strength decrease beyond peak (equations II-4.16 and II-4.17)

Data:  $E = 10^6$  psi;  $c = 50$  psi;  $\phi = 30^\circ$

$$1: \frac{k^p}{P_t} = \frac{l^p}{P_t} = 0.01 \quad a: \sigma_3 = 0 \text{ psi} \quad b: \sigma_3 = 20 \text{ psi}$$

$$c: \sigma_3 = 40 \text{ psi} \quad A: c_r = 50 \text{ psi};$$

$$2: \frac{k^p}{P_t} = \frac{l^p}{P_t} = 0.001 \quad \phi_r = 30^\circ \quad B: c_r = 30 \text{ psi};$$

$$\phi_r = 30^\circ \quad C: c_r = 40 \text{ psi}$$

$$\phi_r = 15^\circ \quad D: c_r = 10 \text{ psi} \quad \phi_r = 5^\circ$$

properties such as the moduli are changed abruptly once failure does occur. The brusqueness of the changes is revealed particularly well when the drastic changes are considered that occur when failure is initiated on the tunnel periphery. At least these sudden changes at the rock surface can be eliminated by incorporating a rock failure model with a gradual change in properties, the change being related to the increasing inelastic straining of the rock.

An easy inclusion of such a modification into the closed form solutions is possible by considering the residual cohesion  $c_r$  as a function of the maximum inelastic strain, while maintaining  $c_r$  constant throughout the broken zone.<sup>5</sup> This can be achieved by letting:

$$c_r = c \exp \left\{ -k \left[ \left( \frac{b}{a} \right)^2 - 1 \right] \right\} \quad (\text{II-4.10})$$

where the constant  $k (> 0)$  determines the rate of decrease of the residual cohesion  $c_r$  for increasing broken zone radius  $b$  and  $a$  is the tunnel radius.

---

<sup>5</sup> The strength for every specific  $b$ -value remains then strain independent. Incorporating a truly strain-dependent strength variation leads to integrations that cannot be solved in closed form.

The relationship between  $c_r$  and the maximum strain can be derived explicitly in a simple form for the special case of the small displacement solution without volume increase. Applying equation (II-4.3) twice, with  $K = 0$ , once for  $b = a$ , resulting in  $u_a^{el}$ , once for  $b > a$ , and subtracting the results after substitution of (II-4.2), one obtains:

$$\frac{u_a - u_a^{el}}{a} = \left[ \left( \frac{b}{a} \right)^2 - 1 \right] \frac{(1 + \nu)(P \sin \phi + c \cos \phi)}{E} \quad (II-4.11)$$

$$= Q \left[ \left( \frac{b}{a} \right)^2 - 1 \right] \quad (II-4.12)$$

The relation between the maximum strain and the cohesion decrease results from the substitution of (II-4.12) into (II-4.10), giving:

$$c_r = c \exp \left[ -k \frac{u_a - u_a^{el}}{a} \cdot \frac{1}{Q} \right] \quad (II-4.13)$$

$Q$  is a constant for a given problem, but depends on the stressfield  $P$ , and thus is not a material constant. By translating the problem to an equivalent one in an applied stressfield  $P_t = P - \sigma_c/2 = P - c \cos \phi / (1 - \sin \phi)$  for a rock with strength parameters  $c_t = 0$ ,  $\phi_t = \phi$  equation (II-4.11) can be rewritten as:

$$\frac{u_a - u_a^{el}}{a} = \left[ \left( \frac{b}{a} \right)^2 - 1 \right] \frac{(1 + \nu) \sin \phi_t}{E} P_t = \left[ \left( \frac{b}{a} \right)^2 - 1 \right] Q_t P_t \quad (II-4.14)$$

Substitution of (II-4.14) into (II-4.10)

results in:

$$c_r = c \exp [-k^P \cdot \frac{u_a - u_a^{el}}{a} \cdot \frac{1}{Q_T} \cdot \frac{1}{P_T}]$$

(II-4.15)

 $Q_T$  is thus reduced to a material constant.An appropriate  $k^1$  factor can be selected for  $P_T = 1$ .

The same material behavior, i.e., strain dependent

 $c_r$  reduction can then be obtained in an arbitrary  
<sup>6</sup> stressfield by letting  $k^P = P_T \cdot k^1$ .

It follows from equation (II-4.10) that the residual cohesion will approach asymptotically a zero value for increasing broken zone radius  $b$ . If it is desired that the residual cohesion tend to a constant value  $c_r^{\min}$  one can generalize equation (II-4.10) in the form:

$$c_r = c_r^{\min} + (c_r - c_r^{\min}) \exp \left\{ -k \left[ \left( \frac{b}{a} \right)^2 - 1 \right] \right\} \quad (II-4.16)$$

---

<sup>6</sup> The preceding translation is unnecessary when either the angle of internal friction  $\phi$  or the cohesion  $c$  equal zero. For these cases  $\sigma_c = 0$ , and equations (II-4.11) and (II-4.12) reduce to:

i)  $\phi = 0 \quad \frac{u_a - u_a^{el}}{a} = Q \left[ \left( \frac{b}{a} \right)^2 - 1 \right]$

ii)  $c = 0 \quad \frac{u_a - u_a^{el}}{a} = P \cdot Q \cdot \left[ \left( \frac{b}{a} \right)^2 - 1 \right]$

Similar relations can be written down for other residual properties:

$$\phi_r = \phi_r^{\min} + (\phi - \phi_r^{\min}) \exp \left\{ -1 \left[ \left( \frac{b}{a} \right)^2 - 1 \right] \right\} \quad (\text{II-4.17})$$

$$E_r = E_r^{\min} + (E - E_r^{\min}) \exp \left\{ -m \left[ \left( \frac{b}{a} \right)^2 - 1 \right] \right\} \quad (\text{II-4.18})$$

The direct substitution of these equations into the expressions used for calculations of the support pressures and the displacements leads to very lengthy equations, and therefore the substitutions are made numerically within a computer program (Appendix A-3.2).

Figure II.10 shows four sets of stress-strain curves. The post peak section of this curve was calculated from equations (II-4.16) and (II-4.17) after substitution of (II-4.14). Four different values  $c_r^{\min}$  and  $\phi_r^{\min}$  defining the residual strength, have been used, as well as two values of the factors  $k^p$  and  $l^p$  that define the rate of exponential decrease.

The influence on the resulting ground characteristic of variations in the rate of decrease of the strength and deformational properties is illustrated in Figures II.11a,b,c. These three figures are calculated for different values of the

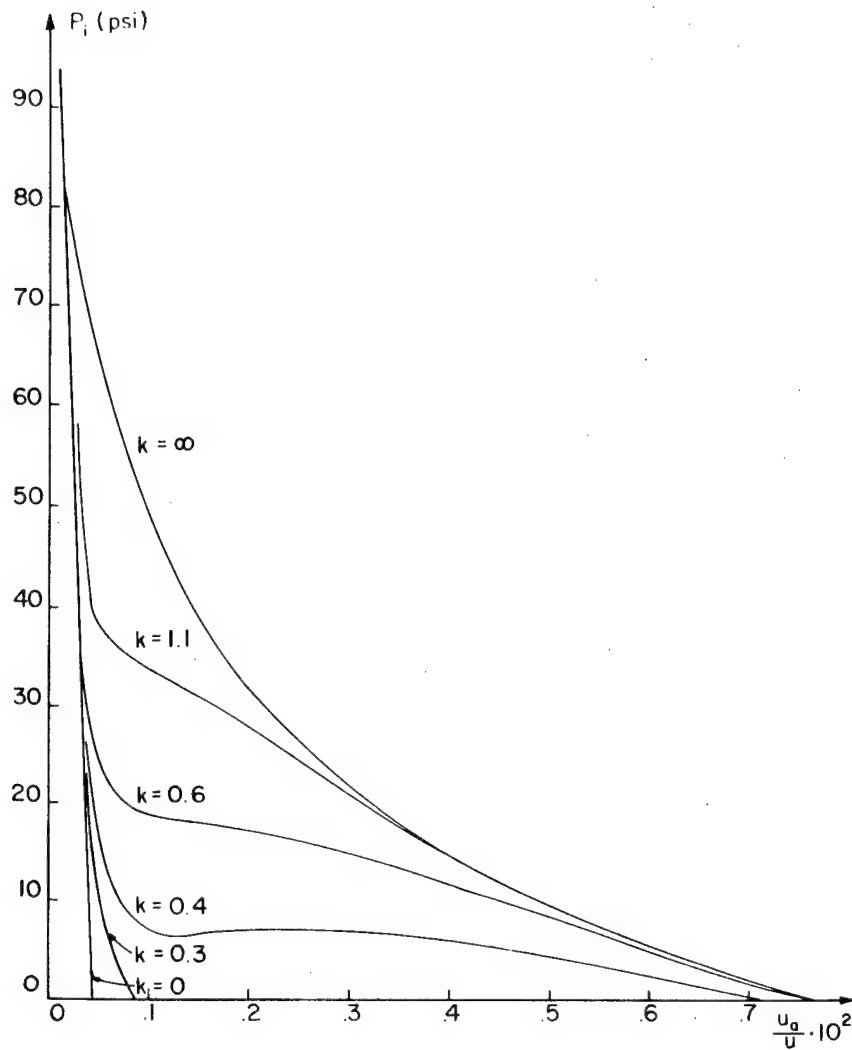


Figure II.11a. Ground Reaction Curve for a Rock with a Gradual (Exponential) Strength Decrease

Data:  $P = 250$  psi;  $E = 10^6$  psi;

$\gamma = 0.25$ ;  $c = 50$  psi;  $\phi = 30^\circ$

$c_r^{\min} = 20$  psi;  $\phi_r^{\min} = 10^\circ$ ;

$E_r^{\min} = 0.2E$ ;  $w = 0$ ;  $k = 1 = m$

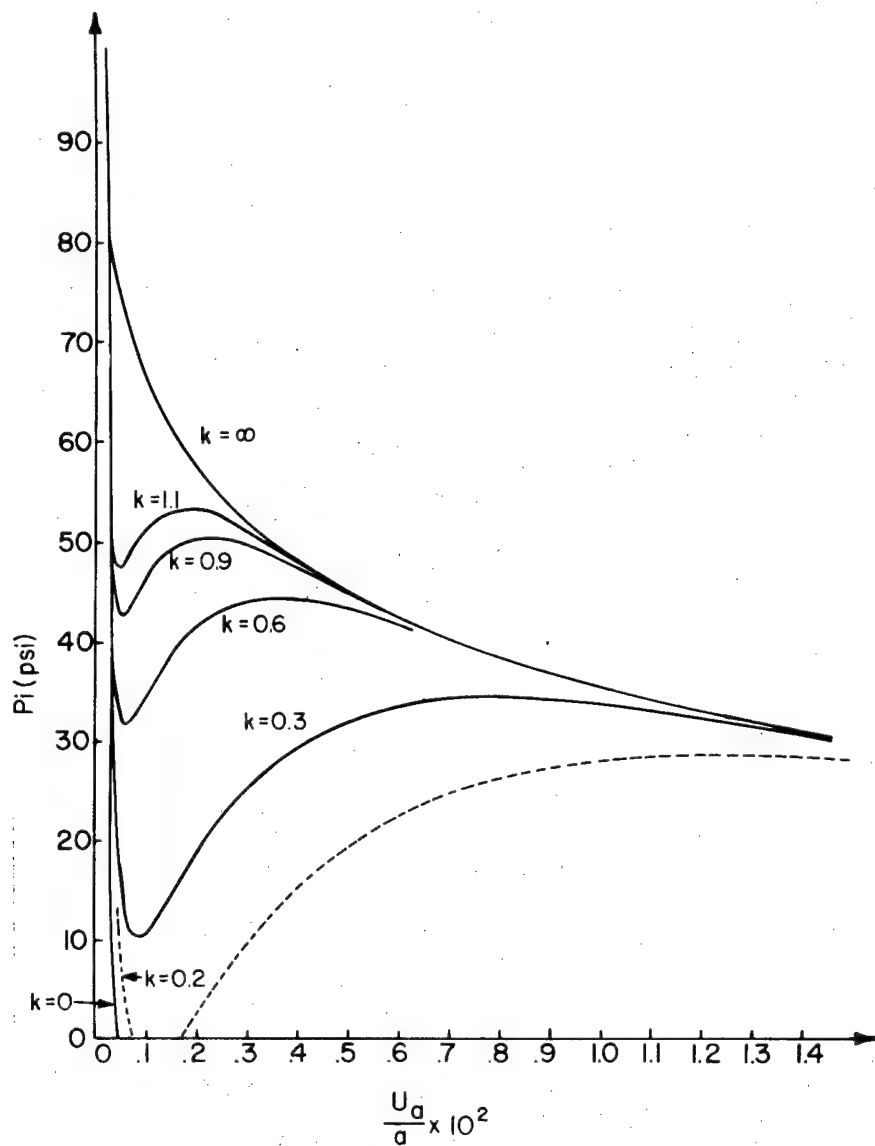


Figure II.11b. Ground Reaction Curve for a Rock with a Gradual (Exponential) Strength Decrease

Data:  $P = 250$  psi;  $E = 10^6$  psi;

$\nu = 0.25$ ;  $c = 50$  psi;

$\phi = 30^\circ$

$c_r^{\min} = 10$  psi;  $\phi_r^{\min} = 5^\circ$ ;

$E_r^{\min} = 0.2E$ ;  $w = 0$ ;  $k = 1 = m$

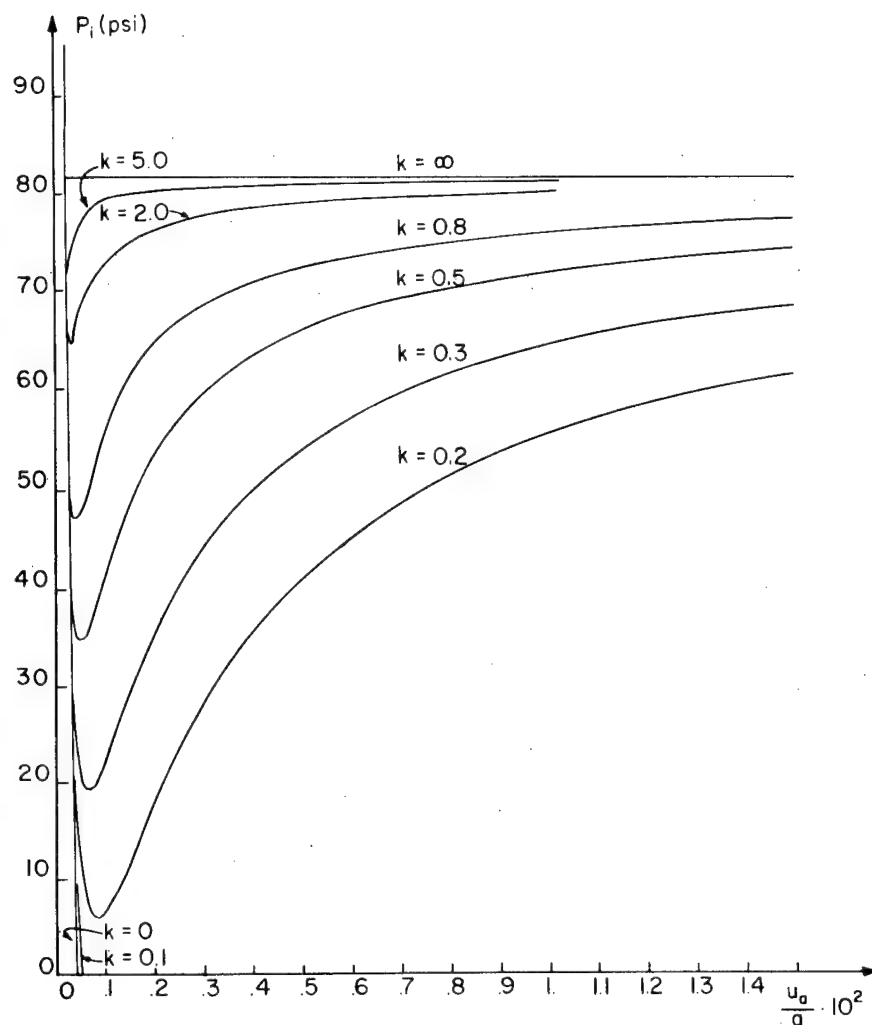


Figure II.llc. Ground Reaction Curve for a Rock with a Gradual (Exponential) Strength Decrease

Data:  $P = 250$  psi;  $E = 10^6$  psi;

$\nu = 0.25$ ;  $c = 50$  psi;

$\phi = 30^\circ$

$c_r^{\min} = 0$  psi;  $\phi_r^{\min} = 0^\circ$ ;

$E_r^{\min} = 0$  psi

$w = 0$  lbs/in<sup>3</sup>

$k = l = m$

minimum residual properties. The resulting ground reaction curves are within the domain bound by the extreme cases where the intact properties are maintained ( $k = l = m = 0$ ) or where the residual properties are attained instantaneously ( $k = l = m = \infty$ ). However, the path along which the residual properties are approached has a decisive influence upon the shape of the ground reaction curve. The gravity forces in the broken zone were neglected in all graphs of Figures 11 ( $w = 0$ ).

### III-5. Numerical Generalization of the Ground Reaction Calculation

III-5.1. Introduction. The closed form determination of the ground reaction curve developed in the preceding sections permits inclusion of the principal features that characterize rock failure. Nevertheless numerous approximations and assumptions are made that could be considered too restrictive. Some of the factors that might have to be included in a more comprehensive or detailed analysis are the nonlinearity of the failure envelope, particularly for low confining pressures, and a strain-dependent decrease, along an arbitrary and more complicated path, of the strength and deformational properties characterizing the rock behavior once the peak

strength has been exceeded. Incorporating such effects into the analysis, at least in a generalized form, requires the use of numerical methods.

II-5.2. Numerical Generalization of Ground Reaction Calculations. In the preceding sections the entire rock mass around a tunnel is subdivided in two regions: a broken zone surrounded by an elastic rock mass. Both regions are homogeneous and isotropic. For the broken zone particularly, it would appear reasonable to relax these restrictions at least partially.<sup>7</sup>

A simple approach to the generalization of the problem, suggested by the assumption of complete radial symmetry, is to subdivide the region around the tunnel in a series of concentric zones. Each zone is characterized by a set of rock properties.<sup>8</sup> These properties are constant for a given

---

<sup>7</sup> This not only complicates the mathematics, an objection only prior to the derivation of the solution, but it tends to increase rapidly the number of required material properties. Even for the simplest of methods discussed in this thesis the determination of realistic material properties poses difficult problems.

<sup>8</sup> An extreme example of such a zone would be a superficial rock layer with a strength and stiffness significantly reduced by blasting.

radius of the broken zone, but can change when failure propagates deeper. This provides a direct physical picture for a mathematical model that can be used to calculate the relationship between the support pressure and the tunnel wall displacement for cases where the rock behavior cannot be represented adequately by the simple laws used in earlier sections.

In the numerical analysis the rock around the tunnel is subdivided into a number ( $n$ ) of concentric regions. The rock behavior within each cylindrical zone  $j$  is characterized by properties  $c_j$ ,  $\phi_j$ ,  $E_j$ ,  $\nu_j$ . At the internal ( $r_j$ ) and external ( $r_{j+1}$ ) boundaries of each zone the equilibrium condition (equality of radial stresses on both sides of the boundary) as well as continuity in the (radial) displacement must always be satisfied. The external radius  $r_{n+1}$  of the thus subdivided zone is equal to the broken zone boundary  $b$  (or falls within the elastic region, although this increases the number of calculations unnecessarily). The internal radius  $r_1$  equals the tunnel radius  $a$ .

An iterative procedure is used to calculate the stresses, displacements and strains throughout the broken zone for increasing radius of that zone.

The properties of each particular subzone  $j$  are changed after each iteration so that a prescribed correspondence is satisfied between the desired material behavior and the results from the last iteration.

Results obtained from a simplified calculation of this type are shown in Figures II.12 and II.13b. Figure II.12 shows the decrease in required support pressure for an increasing broken zone radius. A stepwise approximation to the (linear) cohesion decrease was used. It was assumed that no volume change occurred in the broken zone. Three rates of cohesion decrease are considered, and the (variable) cohesion was taken constant throughout the broken zone.

Figure II.13b illustrates the potential significance of nonlinearities in the failure envelope. The intact and residual failure envelopes (I, II, III, IV) used for this calculation are shown in Figure II.13a. The iteration consisted in deciding which of the straight line segments was the appropriate tangent to a stress circle. Only stress distributions were considered, so that the strength parameters fully define the problem. The results corroborate the expectation that in low stressfields

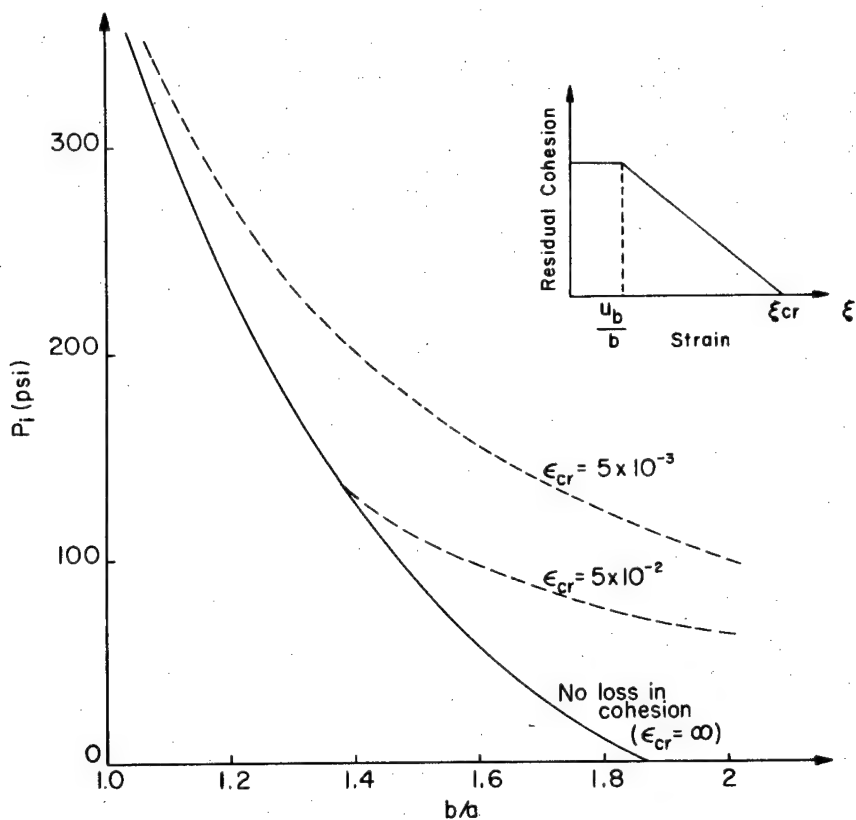


Figure II.12. Required Support Pressure Versus Radius of Broken Zone. Linear Decrease of Residual Cohesion for Increasing Inelastic Strain

$$\frac{u_b}{b} = \text{elastic strain at boundary } b$$

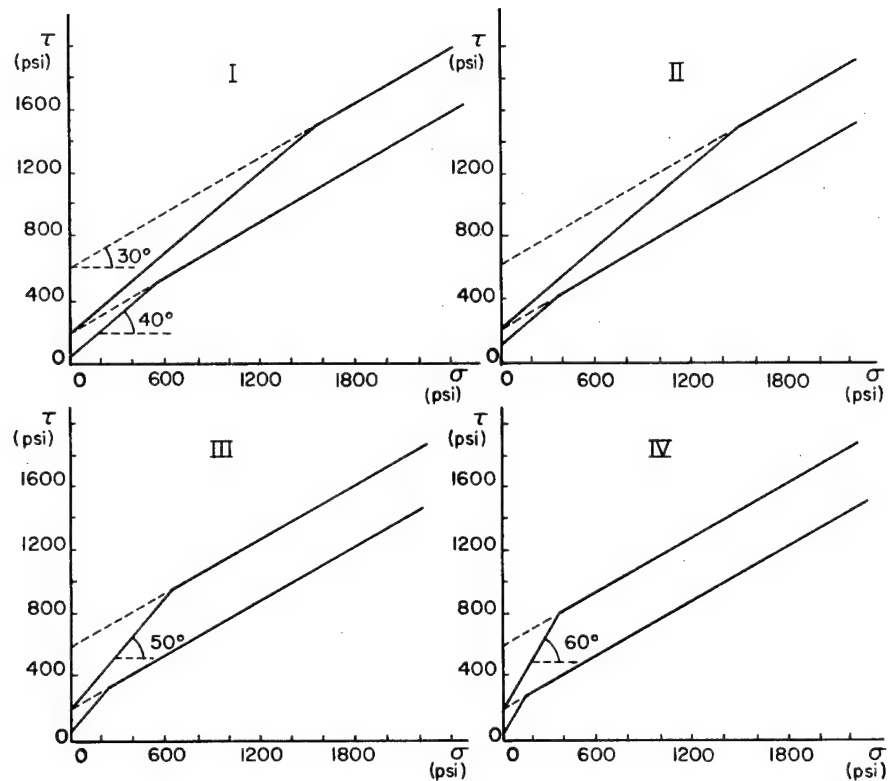


Figure II.13a. Four Sets of Bilinear Intact and Residual Failure Envelopes Used for the Calculation of the Support Pressures in Figure II.13b

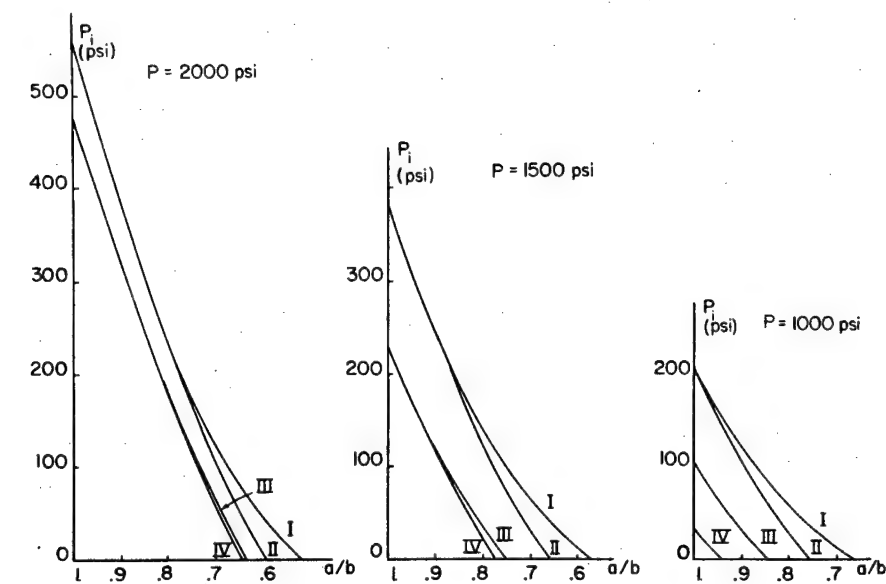


Figure II.13b. Required Support Pressure  $P_i$  vs. the Broken Zone Radius  $b$  in Three Different Pre-tunneling Stress-fields  $P$ . Roman numerals correspond to the sets of failure envelopes in Figure II.13a

there is a greater chance that the initial high-friction part of the failure envelope will dominate the results. It will depend on all factors that determine the stress state, i.e., on the original stressfield, the support pressure and the rock strength whether or not bilinearities in the failure envelopes have a significant influence upon the ground reaction.

The numerical method proposed here has not been developed beyond this fairly elementary stage, and will not be discussed in any greater detail.

### II-6. Tunnel Support Characteristics

II-6.1. Introduction. The ground reaction characteristic determines one-half of the statically indeterminate problem posed in the analysis of tunnel support loading. The other half can be described by the load deflection curve of the support system. The point where the two characteristics intersect defines the equilibrium state, and thus, in the absence of time-dependent stiffness changes, the final tunnel support loading and tunnel convergence.

II-6.2. Tunnel Support Characteristic. Common support systems can be considered as being

built up of two elements: on the one hand the support "strictu sensu", e.g., a steel set, a concrete liner, and on the other hand the elements connecting the support to the rock, e.g., wooden blocks, gravel backfill, a bolt anchor. It is convenient to describe the support behavior in terms of the "support ring stiffness,"<sup>9</sup> defined as the slope of the curve representing the support pressure  $P_i$  versus the radial deformation  $u_a$ . The "support pressure" as used here is not necessarily the contact pressure between the support and the rock, but is rather the contact pressure averaged over the area to be stabilized by a particular support element (for a steel set, a wooden block, a rock bolt, this would depend upon the spacing).

It will be assumed that the support system stiffness ( $K_s$ ) can be derived from the stiffness of the support "strictu sensu" ( $K_{ss}$ ) and the

---

<sup>9</sup> The rather neutral term "support stiffness" is avoided here in order to emphasize that it is necessary to differentiate between bending and compression stiffness. The latter is the significant factor under the highly restrictive assumption of radially symmetric convergence used here. Any generalizations regarding "support stiffness" conclusions for real tunnels have to be tempered by an evaluation of what the support behavior will be when the tunnel convergence is not uniform all around.

stiffness of the connection between rock and support ( $K_c$ ). The two components of the support system are considered to be springs in series, and the overall support stiffness is then given by:

$$\frac{1}{K_s} = \frac{1}{K_{ss}} + \frac{1}{K_c} \quad (\text{II-6.1})$$

### II-6.3. Characteristics of Common Tunnel

Support Systems. The determination of the support characteristic requires an evaluation of the two stiffness components in the preceding equation. For most support systems a realistic determination of the second term requires a reasonably good assessment of the actual in-situ support conditions. Alternatively a range of installation conditions corresponding to practical possibilities can be considered, and the significance of construction "details" can thus be evaluated. A comprehensive summary of stiffness expressions for various support systems is given in Appendix A-4. The results are presented here graphically, in a form similar to the ground characteristics shown on Figures II.11 in order to facilitate a comparison between the various support systems as well as an evaluation of the rock-support equilibrium mode.

II-6.3.1. Shotcrete liner. The stiffness of a shotcrete liner ( $K_{ss}$  in equation II-6.1) is calculated as the stiffness of a plane strain cylinder (thick or thin wall) with constant (i.e., time independent) properties. It is assumed that the shotcrete liner is in intimate contact with the rock ( $K_c = \infty$  in equation II-6.1). Several methods could be used to account for the lower stiffness during the initial hardening period near the face. The simplest way of doing so is to include a pre-installation displacement, or offset from the displacement at installation along the displacement axis. Alternatively one could calculate cylinder stiffnesses for various curing steps and modify the elastic modulus according to a time-displacement relation corresponding approximately to the sequence of face advance (see III-4.2). Several examples of (linear) shotcrete characteristics are included in Figures II.14 and II.15.

#### II-6.3.2. Steel set with wooden blocking.

The stiffness of the steel set ( $K_{ss}$  in equation II-6.1) was calculated for a steel ring with equally spaced loads (corresponding to the blocking points). The calculation of the block stiffness ( $K_c$ ) was

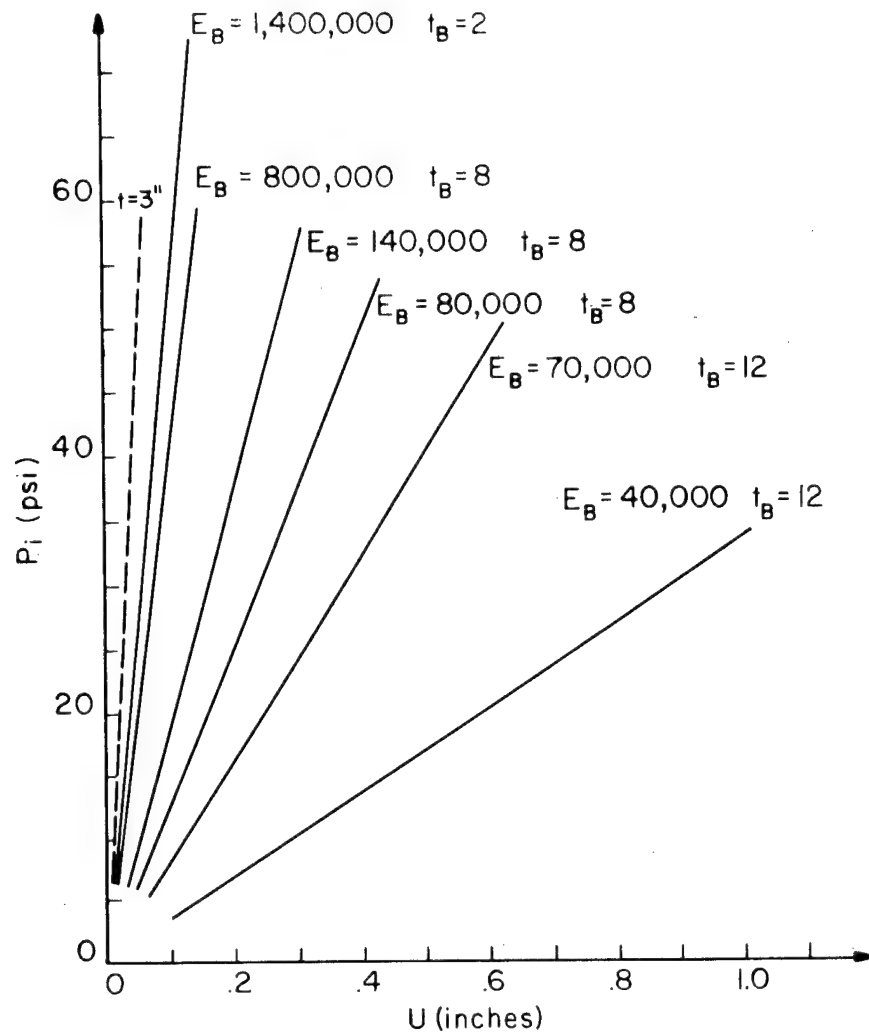


Figure II.14. Support Characteristics of a Blocked Steel Set for a Range of Blocking Parameters

Tunnel diameter = 16.7 feet  
 Steel set: 6" x 4" light beam,  
 16 lbs/ft, 2' spacing  
 Block spacing = 41.9 inches  
 $E_B$  = elastic modulus of block, in psi  
 $t_B$  = block thickness, in inches

Dotted line is characteristic of a  
 3 inch thick shotcrete liner, with  
 Young's modulus  $E = 3,000,000$  psi

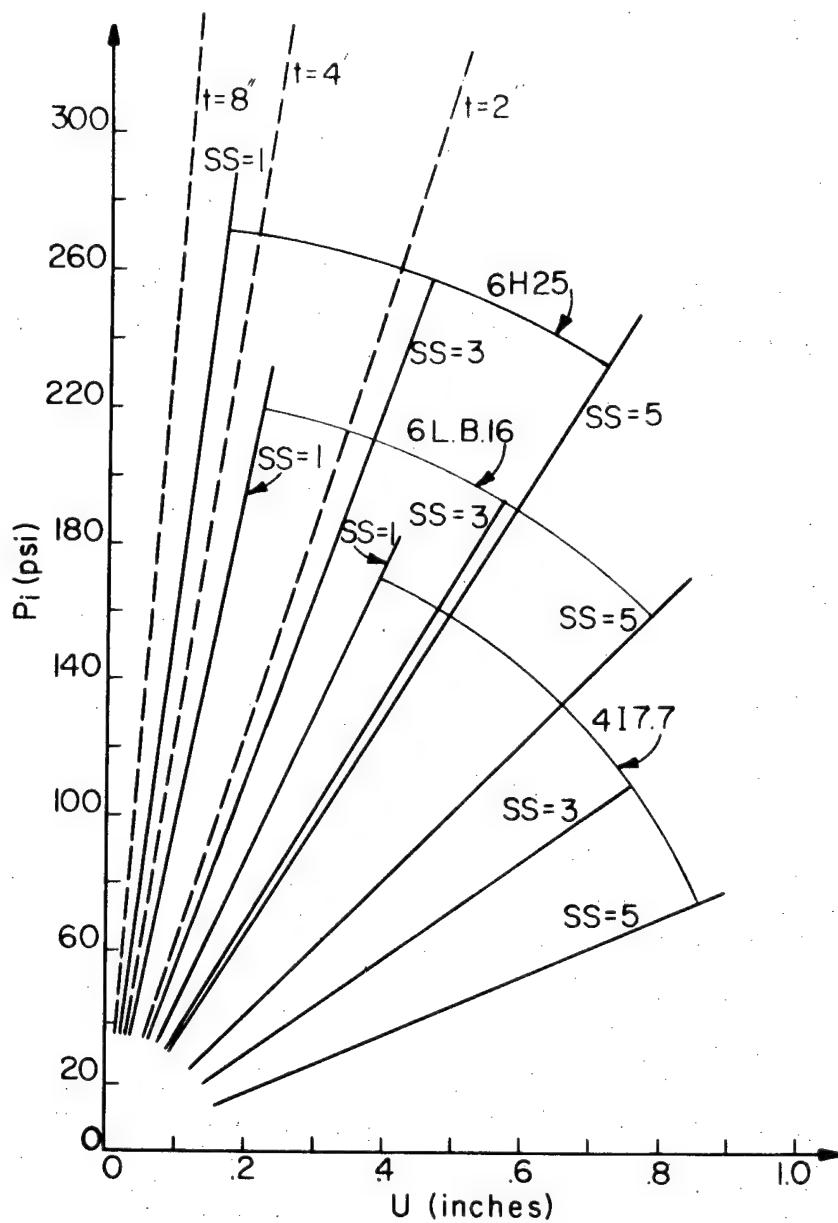


Figure II.15. Support Characteristics of Blocked Light, Intermediate and Heavy Steel Sets. Support Characteristics of Thin (2"), Intermediate (4") and Thick (8") Shotcrete Liners

Tunnel diameter = 16.7 feet

Block modulus  $E_B$  = 1,400,000 psi;

block thickness

$t_B$  = 4 inches, block spacing = 41.9"

SS = Set spacing in feet

based on the assumption that the blocks function as linear springs.

Major variables of practical significance that have to be considered are the set spacing, block spacing and block stiffness. The stiffness of the wooden blocks, as well as the block spacing, depends greatly on construction details. The dominating role of the block stiffness can be established by evaluating the overall blocked steel set stiffness for a realistic range of block stiffnesses. A precise determination of the support stiffness does require an in-situ evaluation of the block behavior (or, alternatively, imposing certain blocking procedures in order to guarantee a particular stiffness level).

Factors that affect the block stiffness are:

i. Overbreak

It might appear at first that the block (spring) stiffness is simply inversely proportional to the distance between steel set and rock. Such an assumption is likely to lead to a significant underestimate of the loss in stiffness caused by increased overbreak. Indeed, a larger gap between steel set and rock complicates the composite of wooden blocks composing a blocking point, which

requires progressively more careful workmanship if gaps and "soft spots" are to be avoided.

ii. Block construction

Although it is common practice to draw blocking points as a single wood block, actual blocking points, particularly in situations where the overbreak is large, have to be build up of a number of blocks, boards, wedges, etc. The true stiffness of such a blocking point, constructed under difficult if not dangerous conditions in between the steel set and the rock, might bear little resemblance to the stiffness of an ideal "one block" blocking point.

iii. Wood properties

Even under optimum conditions the stiffness of wooden blocks will vary greatly, because wood is strongly anisotropic so that the orientation of the block is important, and because all wood properties change markedly with changes in humidity and temperature as well as with the duration of loading (Wood Handbook, 1955).

It is clear that wooden blocking introduces a significant uncertainty factor in the determination of the stiffness of a blocked steel set.

Only when the blocking is done with unusual care

will the stiffness of this support system depend mainly on the stiffness of the steel set.

The overall stiffness of blocked steel sets in a 16.7 ft. diameter tunnel is illustrated in Figures II.14 and II.15. Figure II.14 illustrates stiffness variations of an average steel set selected for this tunnel (Proctor and White, 1968) under a variety of blocking conditions. Steel set type is 6" x 4" Light Beam, 16 lbs. per foot, set spacing 2 ft., block spacing 42 inches, and the wood modulus ranges from 1,400,000 psi (upper range for softwood parallel to the grain) down to 40,000 psi (lower range for softwood perpendicular to grain and parallel to ring). Blocking thicknesses range from 2 inches up to 12 inches. In the same figure the load deflection curve of a 3 inch shotcrete liner is included.

The load deflection curves of light (4I7.7), intermediate (6LB16) and heavy (6H25) blocked steel sets at set spacings of 1, 3 and 5 ft are shown on Figure II.15 for a 16.7 ft. diameter tunnel. The blocking point spacing is the recommended maximum 42", block thickness is 4" and the block modulus is 1,400,000 psi. Included for a comparison with these very stiffly blocked steel sets are the

corresponding lines for shotcrete thicknesses of 2", 4" and 8".

II-6.3.3. Rock bolts. Because the resultant compressive (reinforcing) stresses induced in-between the bolt ends are limited to that region, and because of the tensile stresses induced behind the anchor, it can be argued justifiably that rock bolts are not truly a support system, and in particular that a support characteristic or support stiffness concept as used here does not provide a meaningful tool for the analysis of rock bolt mechanics. This general idea being accepted, there are nonetheless conditions under which an array of rock bolts can be considered as a support system. This is true in particular for point anchored bolts with an anchor section well within the elastic or intact rock. Under these conditions it can be assumed that the compressive force applied at the tunnel periphery does reinforce the rock in a similar way to blocking forces at steel set blocking points, while the tensile stresses induced behind the anchor are rather small relative to the existing (compressive) stresses and do not significantly affect the displacements

nor impair the opening stability by propagating deeper fracturing.

The stress distribution induced by deformation and tensioning of fully grouted bolts is more complicated, and particularly during the initial stages of deformation will correspond to a reinforcement mechanism rather than to an external support. Once plastic yield of a friction bolt is induced, the stress distribution will approach the one induced by a point anchored bolt, certainly when optimum boundary requirements (sufficiently stiff and strong anchor and bearing plate) are satisfied (Appendix A-4). Under the latter conditions, plastic yield in a fully grouted bolt is likely to be initiated for a smaller convergence than in a point anchored bolt.

The stiffness of an array of bolts presented here is calculated for steel only, i.e., the contact term  $K_c$  is assumed equal to infinity. Whether this is a reasonable assumption or not will depend on the stiffness of the connections between rock and bolt. It certainly will require a sufficiently large bearing plate as well as a "good" anchor, i.e., a thin grout over a sufficiently large area in order to minimize shear deformations of the

grout and in order to prevent local overstressing of either rock or grout (resin or cement). A good tensile bond between hole bottom and anchor end, although probably difficult to achieve, would be desirable.

It is assumed in the stiffness calculation that the force exerted at the bearing plate is distributed evenly throughout the rock. A representative set of support pressure versus convergence graphs, ranging from a very dense pattern (1' spacing) of short (4') thick (1.25" diameter) bolts up to a set of widely spaced (5') long and thin bolts is given in Figure II.16, on the same scale as Figures II.11 and II.14. Accounting for an installation tension can be done by raising the ordinate at the point of zero bolt displacement to the support pressure applied by the pre-tension.

II-6.3.4. Backfilled concrete segments. As a first approximation concrete liners composed of precast segments can be treated as hollow cylinders loaded externally. When the segments are jacked in place so that intimate contact between ground and support is assured the stiffness of the support system will equal the stiffness of the concrete

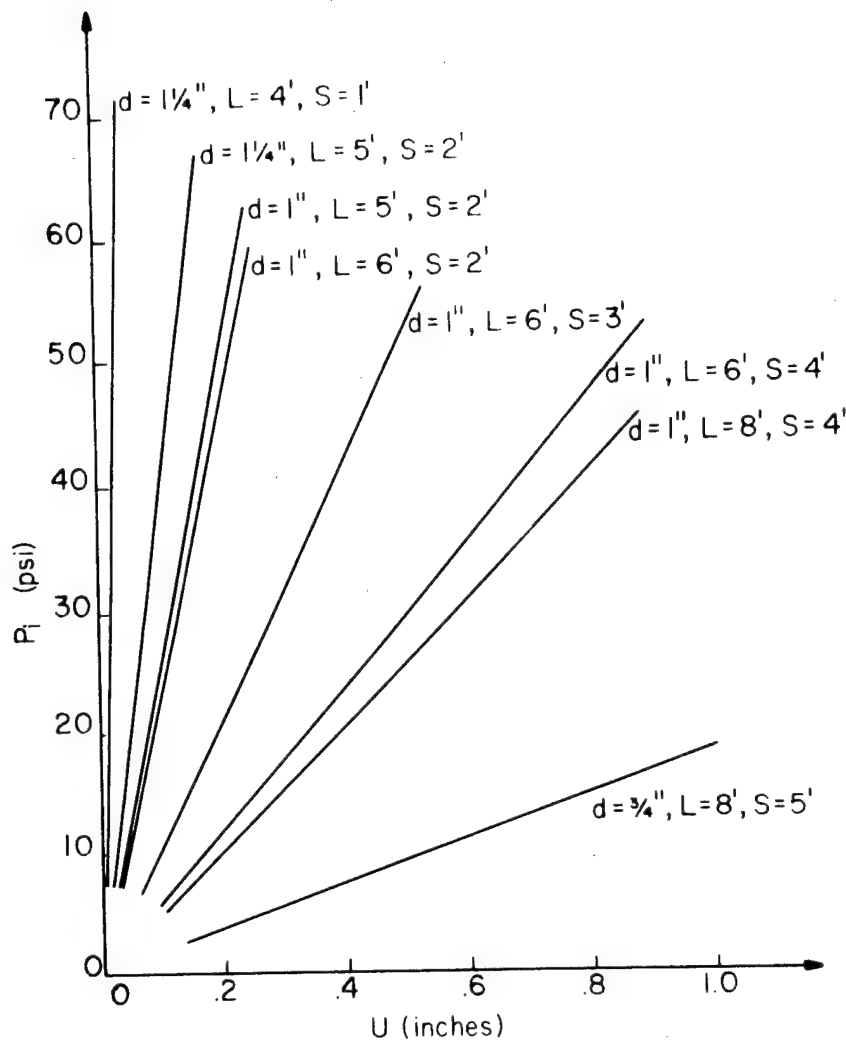


Figure II.16. Support Characteristics of Various Patterns of Bolts Anchored Within the Elastic Region.

Tunnel diameter = 200 inches (16.7 feet)

$d$  = bolt diameter (inches)

$L$  = bolt length (feet)

$S$  = bolt spacing (feet)

ring ( $K_c = \infty$ ). When the segmented ring is back-filled, the situation becomes more complicated because then the support stiffness will depend on the type of backfill and on the care with which the backfilling operation is performed. In the case where a high quality backfill or grout is injected carefully the combined support stiffness can approach that of a two-material cylinder, or the support system stiffness can be considered equal to that of two parallel springs. At the other extreme, for loosely blown in gravel it is more appropriate to consider two springs in series, and the overall stiffness, certainly during the initial convergence or gravel compaction would be dominated by the rather low gravel stiffness.

III-6.3.5. Composite support systems. When two or more support methods are used simultaneously, the overall support stiffness can be obtained by a combination of the stiffnesses of the individual support elements. The type of combination to be used will depend on the distribution of the generated reaction forces over the various support elements. The combination of bolts with either shotcrete or steel sets is a clear case where the

supports are acting in parallel, and the composite stiffness is obtained as the sum of the individual stiffnesses. The situation is less obvious for a combination of shotcrete and steel sets. The simplest and not altogether unreasonable approach is to postulate that the combined stiffness corresponds to the sum of the two unit stiffnesses. As discussed in the above section on shotcrete, the gradual hardening of shotcrete can be accounted for by a stepwise stiffness increase corresponding to the displacement increments associated with the face advance cycle. If the shotcrete thickness within the external periphery of the steel ring constitutes a significant fraction of the total shotcrete thickness, the shotcrete stiffness could be separated into two parts, the first one corresponding to the ring outside the steel set, the second one to the ring within the steel set. The total (final) stiffness would be the sum of three terms, and the same as before. However, the outside shotcrete ring is the vehicle through which the equilibrium pressure between rock and steel must be transmitted. If it is assumed that the initial shotcrete stiffness and strength are very low, then this is also a limiting factor on its

stress transmission capacity. If, during initial convergence, the shotcrete remains sufficiently soft to flow plastically between the steel set and the rock the combined support action becomes one of springs in series, rather similar to that of a blocked steel set.

The individual stiffnesses are used to calculate the composite stiffness of the support. Once the equilibrium support pressure is determined, the decomposition of this total pressure in accordance with the respective individual stiffnesses allows the determination of the pressures exerted by and on the separate support components. This, combined with the strength of the various components, makes it possible to judge the effectiveness with which the support pressure is distributed over the components.

### III-7. Extending the Ground Reaction Derivations

III-7.1. Introduction. In the preceding sections the ground characteristic and the support characteristic have been derived. They can be considered as essential tools for the analysis of rock-support interaction. An attempt was made to incorporate as many significant parameters as

possible in order to derive a realistic model of that interaction, while maintaining the simplicity of a closed form solution. Nevertheless, numerous simplifying assumptions were made, some of them sweeping generalizations that could put severe restrictions on the range of conditions for which the results remain meaningful. The influence of at least some of these simplifications can be assessed by comparing observed behavior of tunnel supports as described in the literature with conclusions that would be reached from the preceding analysis. Such a comparison can point out basic shortcomings of the analysis, and one can then proceed by making appropriate changes in order that a better approximation to the true solution might be achieved. The extensions that will be suggested here are mostly rather simple and qualitative in nature, although, if appropriate data were available, a quantitative generalization would be straightforward.

III-7.2. Time-dependent Variations in Support Pressures. Numerous measurements of pressures on a variety of support systems installed in a wide range of ground conditions have shown that changes

in support pressures can continue for prolonged periods of time following the support erection. The changes can be quite regular and monotonic or they can be very erratic. Measurements of tunnel convergence similarly indicate that shifts in the equilibrium position are not uncommon.

Within a short distance from the face, changes in tunnel support loads can be explained by convergence increments caused by face advances (Daemen and Fairhurst, 1972). In homogeneous ground such geometric effects will be reduced to negligible values within at most two or three tunnel diameters behind the face (see III-4.2). In rock interspersed by discontinuities the effects are likely to be limited to an even shorter distance from the face. As pointed out by Lombardi (1974), the extent to which convergence behind the face is controlled by the stiffness of the rock in the face depends on the competence of the rock behind the face, and in particular on its ability to transmit shear stresses. The convergence postponement also depends on the stiffness of the rock in the face, stiffness that is more likely to be significantly decreased by blasting, mucking, etc. in a jointed rock than in a homogeneous one. A more precise

evaluation of the geometric effects on tunnel support load changes should be possible with three-dimensional finite element methods (e.g., Isenberg, 1973) or with "discontinuity analysis" (Crouch and Fairhurst, 1973).

Assuming that an initial "equilibrium" state<sup>10</sup> is reached near the face, subsequent displacement and support pressure changes (around a single tunnel not affected by extraneous excavations) can be explained by the following mechanisms:

- a decrease in support stiffness
- a decrease in rock stiffness
- a decrease in rock strength (it is assumed that the rock throughout the broken zone is working at its strength limit)
- a change in temperature (Burke 1957, Lane, 1957).

These factors cannot be considered as being truly independent because mutual interaction effects are likely to occur.

Once equilibrium has been reached an increase in the support stiffness (for example, with continued

---

<sup>10</sup> It is not strictly necessary that an equilibrium state must be reached. The listed factors can also influence the behavior for example during the pre-equilibrium support stage.

shotcrete hardening) will not change the equilibrium position.

Many mechanisms can cause a decrease in the support stiffness, the most obvious and extreme one being support failure. Support stiffness decreases are to be expected for steel sets with wood blocks. This is particularly true in wet tunnels, because the elastic moduli of wood decrease rapidly with increasing moisture content, but it is generally true because the wood stiffness decreases under continuous loading (Wood Handbook, 1955). Creep is also common in mechanical bolts and in shotcrete, for the latter certainly during initial curing. Whether a decreasing support stiffness will cause an increase or a decrease of the support pressure depends on whether a "dynamic" equilibrium is being approached along an ascending or a descending branch of the ground reaction characteristic (Figures II.11).

A decrease in rock stiffness and in rock strength will initiate renewed convergence and will cause a support load increase. A variety of closed-form visco-elastic and visco-plastic solutions to the problem of a (reinforced) circular hole in an infinite medium can be used to illustrate

such conclusions. Besides rock materials that behave inherently according to the mentioned rheological models, there are a number of mechanisms that can cause an (apparently time-dependent) reduction in the rock properties. Several of these mechanisms can be related to the presence, and particularly to the flow of water. Notable examples of this are volume increases or decreases of minerals in the rock or in the joint fillings caused by hydration, dehydration or changes in crystal structure. Along similar lines effects such as weathering, decomposition and washing out of rock particles can contribute significantly to rock mass strength losses. Also to be considered is the possibility of a gradual strength and stiffness reduction of rock or of discontinuities within it when both are loaded at or around their peak strength for prolonged periods of times.

A simple and at least qualitative model of time-dependent variations can be obtained by replacing the material constants in the expressions for the ground reaction characteristic (II.4) by appropriate time-dependent functions, e.g.,

$$E = E_0 \times f(t) = E_0 \cdot e^{\alpha t} = E_0 (1 - e^{-\beta/t})$$

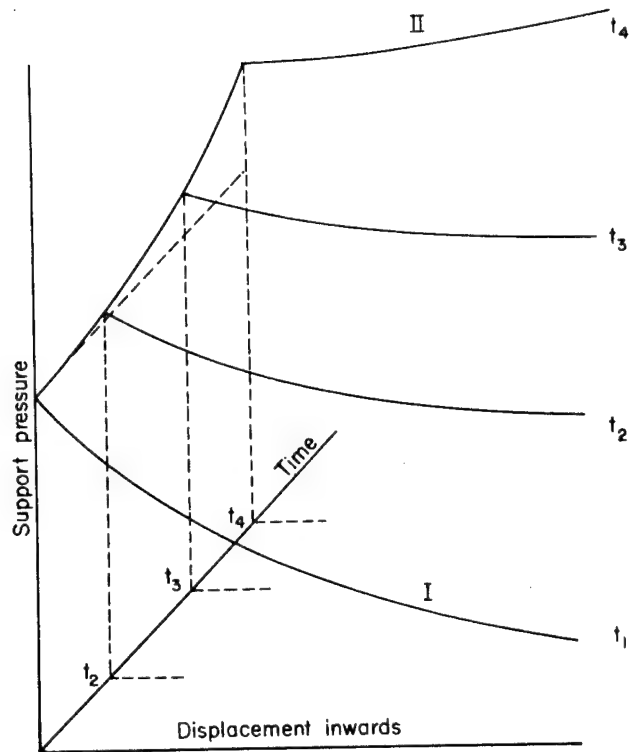
$$c = c_0 \times f(t)$$

A possible hypothetical result from a calculation of this type is illustrated in Figure II.17a, and a resulting support load graph is shown on Figure II.17b.

### II-7.3. Influence of Discontinuities and Inhomogeneities on Tunnel Support Requirements.

The entire analysis of the interaction between tunnel support and rock as presented here is based on the assumption that the rock mass can be described as a homogeneous isotropic continuum. It has been assumed that this holds true prior to tunneling as well as after tunneling, and in the latter case whether or not failure occurs.

The rock mass characteristics that can cause deviations from such an idealized model are numerous and exist in many, if not most, rock formations. Their combined effect will be that the rock mass tends to behave as an inhomogeneous non-isotropic discontinuum. Factors that can be significant contributions to such effects on a scale influencing most tunnels are variations in rock type (e.g., in bedded deposits, near intrusive contacts, etc.), preferred orientations within rock types (e.g., in



Decrease in peak and post-peak strength as rock is subjected to load for prolonged time...  $t_4 > \dots > t_1$

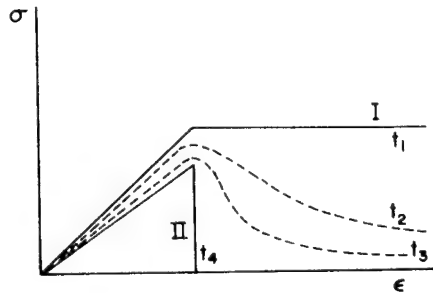


Figure II.17a. Support Pressure-Deformation-Time Ground Characteristic for a Tunnel in a Rock Mass That Has a Decreasing Strength and Stiffness When it is Loaded for Extended Periods of Time

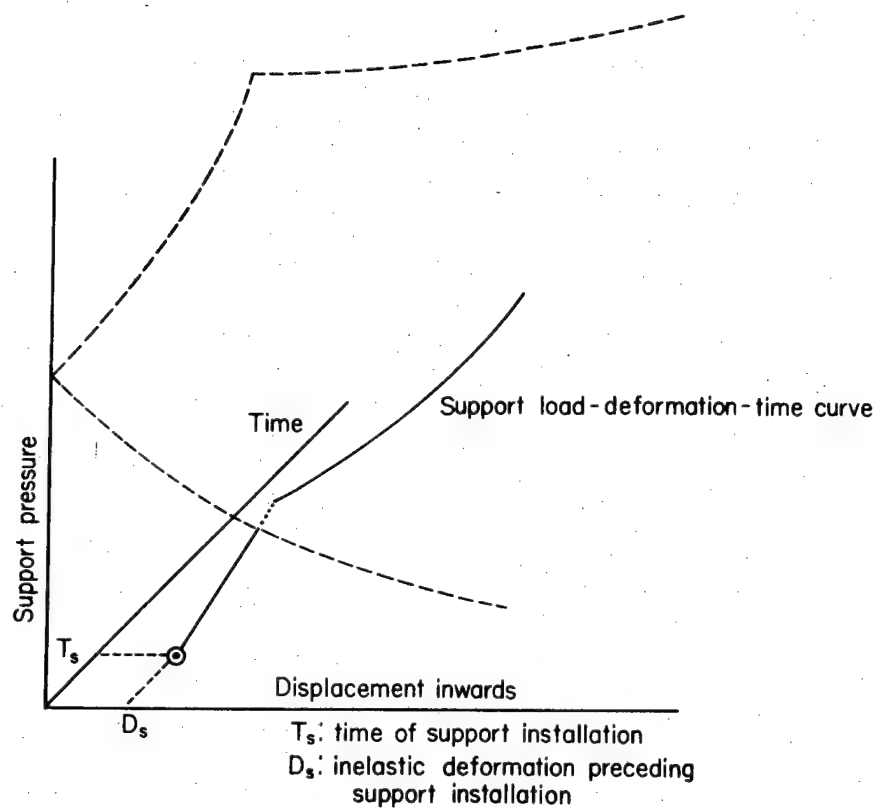


Figure II.17b. Progressive Tunnel Support Loading  
Caused by Continued Rock  
Deterioration

shale, gneiss, etc.) and sections through the rock mass with very different strength and stiffness (e.g., joints, bedding planes, dykes, new fracture planes, etc.)

Rock mass characteristics of the type listed affect the tunnel-support interaction on two different scales. Firstly, they modify the effective parameters that are to be used to describe the overall rock mass behavior, whether or not a tunnel is being driven through the rock. To the extent that the needed parameters are known they can be taken into account when adequate numerical analysis techniques are used (Singh, 1973). The problem nearly always will be a truly three-dimensional one.

A second consequence of the presence of the above-listed rock mass characteristics is that they modify the changes induced by tunneling from the ones predicted by the simple continuum analysis methods used here. Specifically, it is possible that low strength discontinuities have a dominating role in the development of failure around an advancing tunnel (Cording, et al., 1971). Discontinuities will determine the failure mode when the stress changes caused by slip along the discontinuity planes disturb the stress field to such

an extent that the results as calculated in II.3 become meaningless. When the circumferential stress is thus reduced or eliminated, it follows from the equilibrium condition that the gravity force becomes a dominating factor. The problem nearly always will be a truly three-dimensional one.

A simplified and at least qualitative representation of the effect of slip along discontinuities on the ground reaction curve is shown in Figure II.18. For the "calculation" of this graph it was assumed that no stress deviations from the ideal (continuum) solution occur until sudden slip (corresponding to a vertical jump in the characteristic) causes complete relaxation of a "ring." The weight of the ring (= pressure jump) is then added to the required support pressure, and it is assumed that further convergence of the rock without the relaxed ring is possible and reduces the support pressure to be provided there until renewed slip is initiated. It is likely that Figures II.11 correspond to smoothed-out versions of this ground reaction type curve, whether the discontinuous stress changes are caused by slip along pre-existing discontinuities or by slip along freshly created

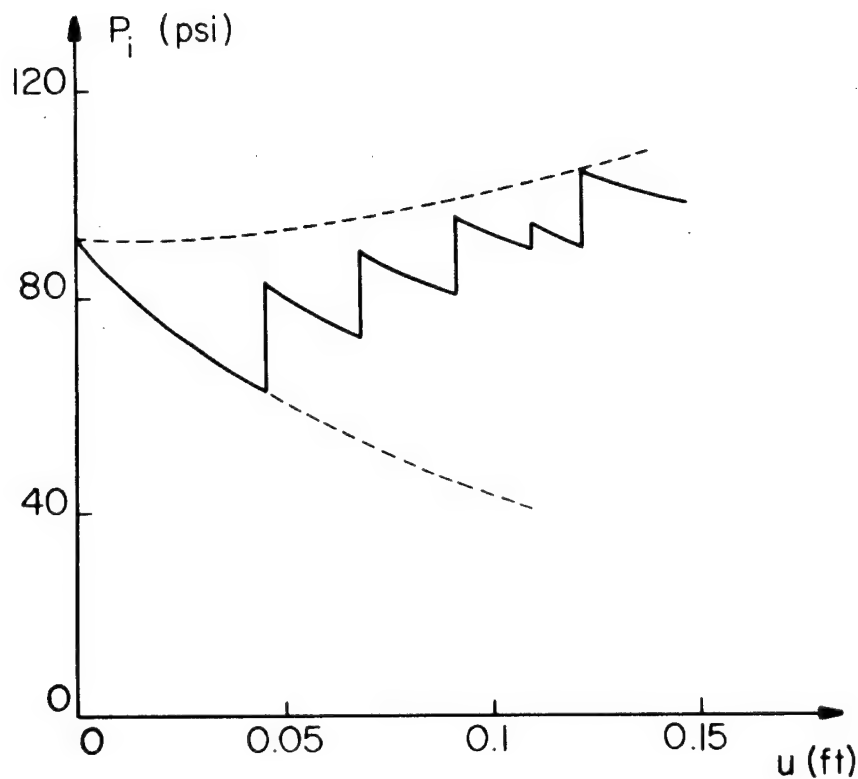


Figure II.18. Hypothetical Discontinuous Ground Reaction Curve. Jumps in the required support pressure are due to the sudden relaxation of a "rock ring" caused by slip along discontinuities

$$P = 200 \text{ psi} \quad c = 10 \text{ psi} \quad \phi = 30^\circ$$

Tunnel radius  $a = 12 \text{ feet}$

fracture surfaces.

II-7.4. Influence of Tunnel Size on the Required Support Pressure. It is axiomatic to many writers discussing the subject of tunnel supports that larger support pressures are required in larger tunnels. Neglecting gravity forces, it follows from the continuum analysis that the required support pressure is independent of the tunnel size. However, this does necessitate heavier supports in a larger tunnel. For a (thin wall) shotcrete liner the thickness required to provide the same support pressure at the same relative displacement ( $u_a/a$ ) is approximately proportional to the tunnel size. If the same absolute displacement is allowed, the required thickness is proportional to the square of the tunnel size (Equation A-28b). For a steel ring with widely spaced blocking, so that only bending displacements are significant, the required moment of inertia of the steel section is proportional to the fourth power of the tunnel radius when the same set spacing and the same number of blocks are used (Equation A-29, middle term).<sup>11</sup> For steel sections

---

<sup>11</sup> The imposed blocking criterion is usually the maximum allowed block point spacing. Although

of the same shape it follows that the cross-sectional area and the weight of the sets are proportional to the square of the tunnel radius.

(Proportional to  $a^{1.5}$  if the relative rather than the absolute displacement is used). The fact that heavier supports are needed in larger tunnels is not in itself an indication of increased support pressures.

Support pressure requirements are likely to increase with tunnel size in rock masses with an average joint spacing much smaller than the tunnel dimensions because of the increased number of possible displacement modes (Daemen and Fairhurst, 1974). A direct method for including a rock strength reduction, causing increased support pressure, with larger tunnel size could proceed along similar lines as the methods used for the design of mine pillars. A variety of such methods (Jaeger and Cook, 1969; Obert and Duvall, 1967) postulate that the rock strength ( $\sigma_c$ ) decreases with increasing pillar height ( $t$ ), the rate of decrease being determined

---

not directly proportional to the tunnel size, as is assumed here, it does increase markedly with size (Proctor and White, 1968, pp. 238, 240). Observations in tunnels would be required to determine what is common practice.

by an empirical parameter  $\alpha$ :

$$\sigma_c \sim t^{-\alpha}$$

By analogy one could include similar relations for the rock characteristics in the calculations of the ground reaction curve, with the tunnel diameter ( $d$ ) relative to a reference diameter ( $d_o$ ) as parameter, e.g.,

$$c = c_o \left(\frac{d}{d_o}\right)^{-\alpha} \quad \phi = \phi_o \left(\frac{d}{d_o}\right)^{-\beta} \quad E = E_o \left(\frac{d}{d_o}\right)^{-\gamma}$$

### III-8. Applications of the Continuum Analysis of Rock-support Interaction

III-8.1. Tunnel Support Design. Continuum approaches to the problem of rock-support interaction of the type discussed here can be considered as intermediate level methods of analysis. These are bounded on the one side by empirical or pseudo-empirical methods, on the other side by sophisticated and all-inclusive numerical techniques.

The very simple methods base the determination of support requirements on a correlation between one or a small number of parameters describing the rock mass and the necessary support. Ideally they are based on a sufficiently large amount of data obtained under a variety of conditions representative of those for which the methods are to be used.

As a general rule, these methods are based on an extremely simple mechanistic model of the tunnel support loading mode.

The highly sophisticated numerical analysis methods, at present mainly finite element methods, make it possible, at least in principle, to study the support loading mechanism in detail, by incorporating in the analysis an extremely wide range of possible material behavior models. Ideally, they are based upon a sufficiently large number of data about at least one particular location, so that the soundness of the analysis method and the validity of the used properties is confirmed by a match between predicted and observed behavior.

As can be expected from its relative position inbetween these two extremes, continuum analysis of tunnel supports combines some of the advantages and some of the disadvantages of both. It requires more information than the simple empirical methods. The information required is of a different nature, namely specific mechanical properties rather than descriptive rock mass characterizations. On the other hand, the needed mechanical properties are average values, and less precise detail is necessary, whether factual or assumed, than for numerical methods.

The information needed for the direct design of tunnel supports by means of continuum analysis must be sufficient to allow a reasonably accurate description of the two structural components, the support system and the rock mass. Within limits one can impose a range of permissible values for the support characteristic by means of construction specifications. But construction problems in rock frequently cannot be predicted to the point where very narrow limits on the amount of overbreak can be imposed, or where it can be assumed that it is a trivial problem to make a reasonable estimate of such factors as blocking stiffness, footing stiffness and strength, rock bolt anchor stiffness. Regarding the rock mass behavior, one needs reasonably accurate values for the average strength and displacement properties, particularly for the residual properties. Factors that might reduce these properties under prolonged loading must be considered. Also needed is an estimate of the stressfield at tunnel level.

III-8.2. Optimum Support Stiffness. The parameters needed for a direct tunnel support design by means of continuum analysis are numerous

and difficult to measure. It, therefore, is appropriate to ask whether the results from the analysis might suggest some general guidelines that would be helpful in optimizing support design and construction.

In general, a ground reaction curve can have descending and ascending sections. Ideally the support stiffness and the time of support erection should be selected in such a way that equilibrium is attained at the lowest minimum of the ground characteristic. Ideals not easily being attained, the more general question to be answered is whether it is preferable to install stiff supports early or to install soft supports late. Figures II.11a, b, c indicate that the ground reaction curve is characterized by a steeply descending initial part followed by a more gradually ascending section when the post-failure strength drop is significant, i.e., when the residual strength is markedly lower than the intact strength and is reached quickly. This general demeanor of the ground reaction is amplified when gravity forces are included.

A stiff support, installed close to the face and in intimate contact with the rock, can be extremely efficient under such conditions whenever

equilibrium is reached at or before the initial minimum. This is consistent with the numerous practical observations of the effectiveness of shotcrete and rock bolt supports. The justification of this effectiveness frequently has been explained on the basis of the traditional elastoplastic ground reaction curve as derived by Fenner, Goguel, Labasse and Kastner. Explanations of this type have been used since the early successful use of such supports (Rabczewicz, 1957) up to very recently (Egger, 1973). It would seem more reasonable that the logical conclusion from the elastoplastic derivation is that the use of yielding supports (Labasse, 1949) and delayed installation following substantial deformation (Fenner, 1938) would be the most efficient method of supporting tunnels. It is probably not incidental that these conclusions were accepted fully by these authors, both of whom were associated with (European) coal mining during the time when yielding steel roadway and face supports were introduced with great success. The support mechanics along a longwall face are clearly entirely different from tunnel support mechanics. But so are the mechanics of roadway supports, because the overwhelming

majority of mine roadways are repeatedly subjected to the influence of nearby large-scale mining excavations.

The contradiction between the logical conclusion from the traditional elastoplastic analysis and shotcrete practice becomes particularly striking when one considers the great emphasis put on the necessity to use appropriate hardening accelerators.

While shotcrete and rock bolts will be activated rapidly for small displacements, they also maintain some flexibility, certainly very shortly after installation during initial hardening. This flexibility allows the minor displacements required to approach optimal support conditions without detrimental effects.

There exists, moreover, an unmistakable general trend towards the use of stiffer supports. This is illustrated by several typical examples:

- the replacement of timber sets by blocked steel sets
- the replacement of blocked steel sets by a combination of bolts, shotcrete and light steel members
- the replacement of blocked steel sets by

## shotcreted steel sets

- the replacement of mechanical anchor bolts by grouted bolts
- the use of jacked-in-place concrete segments<sup>12</sup>

A critical factor determining the shape of the ground reaction curve, as illustrated in Figures II.11, is the rate of change from the intact to the residual strength. This effectively corresponds to the sequence or rate of stress relaxation around the tunnel. Two other factors can complement such effects.

The first one is the "additional" load component that can be caused by the weight of the broken zone (Pacher, 1964). Prior discussion (II-3.4) has indicated that this factor is unlikely to be significant except for rather shallow tunnels surrounded by rock with an extremely low residual friction. Whenever these gravity loads are

---

<sup>12</sup>The use of unbolted segmented liners does not contradict this general trend, because it is aimed at reducing the bending stiffness of the support ring. Conditions where increased bending stiffness is advantageous would be most unusual. There is no doubt, however, that jacking precast segments is frequently done in order to minimize subsidence rather than to optimize the support loads.

significant one should expect a pronounced difference between roof and floor support requirements (Figures II.4,5). This is contradictory with recommended good practice in difficult tunneling conditions, where local gravity effects should be most likely to develop (because of a relatively low internal friction).

A second factor, and one generally more likely to contribute significantly to the aforementioned results is the influence of joints on tunnel support requirements. Slip along joints intersecting the tunnel will have a relaxation effect similar to that of the strength reduction previously treated as a continuous homogeneous phenomenon. Taking into account the gradual reduction of joint strength with excessive slip, a picture at least qualitatively similar to Figures II.11 can be expected.

There is no reason to expect a similar or even qualitatively the same behavior in all rock types. A specific example that is likely to constitute a different class of behavior is that of rock susceptible to large volume increases for reasons not associated with failure. In ground of this type there can be distinct disadvantages to

the use of unyielding supports. Displacements caused by such volume changes can be accounted for in a simplified way by a constant volume change factor, similar to the one used in equations II-4.1 and II-4.3. It is clear that whatever failure mode might occur in such rock, the support characteristic is likely to have a rather flattened or level appearance.

#### II-8.3. Tunnel Support Instrumentation.

Whether or not continuum analysis is a viable and practical proposition for studying tunnel support mechanics will depend on results from comparisons between in-situ measurements and calculated predictions. Conversely, the mechanics of support action must guide the design of measurement and instrumentation programs. Continuum analysis provides the simplest techniques that can be used for a reasonably comprehensive evaluation of support systems.

The ultimate answer as to what constitutes an optimum support system can be obtained only from actual support installations, and the ultimate criterion is a strictly economical one: what support system will perform all necessary functions

and minimize the total cost of the tunnel. Depending upon the circumstances the support cost can vary from a minor to a major fraction of the total tunnel cost. Because the latter case is not uncommon and because of the increasing volume of tunneling works an increased need for rational analysis of support structures is felt, and numerous methods and variations of analysis procedures are being developed. The assessment of the worth of such methods depends upon their validation by in-situ observations. This makes the interpretation of in-situ measurements an essential element in a comparative evaluation of various design and analysis methods.

The purpose of support instrumentation is to observe the equilibrium state reached between rock and support. The problem is highly statically indeterminate, and an infinite number of equilibrium positions are possible. The variables fully defining the equilibrium position of such an indeterminate problem are the displacement and the stressfields. An appropriate general instrumentation program, therefore, will be planned so that sufficient information about these two groups of values is obtained to allow an analysis of the

support loading. In order that an understanding of the sequence of events leading to the equilibrium state might be achieved, it is necessary to know the fundamental characteristics that define the problem, i.e., the rock and support properties.

Corresponding to the complexity or completeness of the methods of support-rock interaction analysis (II-8.1) must be an equivalent complexity or completeness of the data gathering and interpretation effort. For the simple semi-empirical methods an obvious need exists for expanding the available data basis. For design methods that correlate one rock mass parameter with one parameter defining the support requirements the most efficient method of providing a sounder design basis consists in increasing the number of instances where the two parameters have been observed and the reliability of the predictions evaluated. The simple empirical methods derive their value from the practical limitations that preclude a more comprehensive analysis in many situations. There are obvious limitations to the applicability of such simple methods.

As more complex conditions are encountered, the reliability of "correlation methods" not based

on the mechanics of the problem decreases. A two-fold reason for this lies in the selection of the correlated parameters and in the evaluation of the meaning of the resulting correlations. The selection of the parameters used in the correlations is quite independent from the method, and the adequacy of the choice can neither be vindicated nor refuted by the correlation results. A rather simple tool such as continuum analysis can provide valuable guidelines as to what parameters must be considered if a detailed explanation of the support loading mechanism is desired. The significance of the resulting correlations is notably dependent upon the assumed statistical model. From this point of view also continuum analysis provides insight into the type of mathematical relations that are likely to exist between a variety of parameters.

A complete and detailed analysis of support loading, as should in principle be possible with appropriate finite element methods, requires a very comprehensive body of information. The needed data input might be reduced by a combination of statistical and mechanical methods aimed at establishing a significance level for the possible variables. Such a reduction is likely to be

limited by a general lack of specific knowledge about the (wide) range of potential values of the potentially large number of significant parameters. The wide range of possible numbers facilitates the adjustment between observed and calculated results. By the same token, this complicates and reduces the predictive value of such methods.

The discussed principles probably can be clarified best by means of examples. A classical pseudo-empirical design method is the Terzaghi rock load theory (Proctor and White, 1968). An instrumentation program to solidify the foundation of the method would consist in obtaining more data of steel set loads and the corresponding rock classification. Other parameters needed are obtained very simply, as only steel set spacing and tunnel size are necessary. The raw data has been obtained in several tunnels, but appears to be unpublishable unless it has been sanitized by statistical manipulations sufficient to obfuscate any simple and direct meaning behind reams of computer output (e.g., Abel, 1967). A straightforward comparison between predicted and measured values for one of the most frequently used support design methods obviously would be of great value to the tunneling

community at large. It is doubtful that a significant additional contribution to the improvement of this method can be expected from more detailed observations or from very precise measurements. One can select a larger number of rock properties and make more detailed observations, and correlate the resulting data by means of increasingly sophisticated statistical techniques. If the selection of the parameters is not based on the mechanics of the problem, one is apt to exclude significant ones or to include trivial ones. An example of this would be a correlation between some rock characteristics and steel set loads (measured over prolonged periods of time) while neglecting significant stiffness factors such as set spacing, blocking point stiffness, temperature changes, time-dependent changes of the rock properties. As correlations become more complicated and the number of parameters more numerous, the amount of data required to guarantee a meaningful sample increases rapidly. While such methods can be of benefit in the back-analysis of the support loading in a particular tunnel, they cannot be used to predict support requirements in different ground for the same support type nor for different supports in the

same ground. Indeed, correlations do not provide information about the characteristics of either of the two interacting elements of the structure.

Anything more comprehensive than a simple empirical analysis must be based on the mechanics of tunnel supports in order that causal rather than coincidental relations might be established. Conversely, causal relations such as the ground characteristic have to be confirmed by experimental evidence. Such a confirmation has to show that it is possible to make a reliable estimate of tunnel support loading once the stiffness and the strength of rock and support are known. Completing the cycle, such experimental confirmations must indicate what significant parameters are needed and which simplifications are possible in order to derive a rational support design method.

## Chapter III

### STIFFNESS ANALYSIS OF TUNNEL SUPPORT LOADING CAUSED BY ROCK FAILURE

#### III-1. Introduction

Driving a tunnel through a rock mass disturbs the equilibrium of the rock mass. In order to maintain a safe opening it is frequently necessary to install a support system. The function of the support system is to assist the rock mass in finding a new state of equilibrium. This assistance is given through the reaction forces developed by the support system. These reaction forces are caused by the compression of the support system under increasing tunnel wall convergence. The stresses thus induced in the rock by the support system strongly depend upon the support system stiffness.

A simplified closed-form analysis of this rock-support interaction was given in the preceding chapter. It is clear that, given the complexity of the problem, any analysis intended to be more

than a basic model must invoke numerical methods.

In order to have a numerical model that is reasonably well balanced, it is necessary that it incorporates the two elements of the structure with a similar degree of realism. This requires that increasing accuracy or complexity of modeling the rock behavior be accompanied by an increased sophistication of the support analysis method.

If, on the other hand, a very simple rock load concept is acceptable, it is doubtful that a detailed analysis of support behavior is necessary or justified.

The tunnel wall convergence depends directly upon the rock displacements induced by the tunneling operations. In order to evaluate these displacements it is necessary to know the pre-tunneling equilibrium state as well as the changes caused by tunneling. Within the context of this thesis, the full emphasis is put on changes induced by tunneling, although it is well recognized that an accurate description of the pre-tunneling rock mass equilibrium state is a formidable problem in itself. The pre-tunneling rock mass will be assumed to be a homogeneous elastic continuum characterized by known properties and stress distribution. The

changes induced by tunneling will be studied by means of the displacement finite element method.

While the tunnel walls converge, the support system is activated. The reaction forces thus developed determine the final equilibrium around the tunnel. In order to clarify the support system behavior a distinction will be made between the support itself and the interface between rock and support, even though this interface or connection can justifiably be considered to be a part of the support. Such a distinction makes it possible, however, as was already shown in the simplified analysis of the preceding chapter, to illustrate the dominating role that can be played by seemingly minor construction details. These details are one of the principal reasons for the very wide range of possible support characteristics. They are at the basis of the variability and uncertainty regarding the support structure, and make the support behavior an "unknown quantity" in a manner not unlike the rock behavior, even though support behavior uncertainties can be reduced more easily through appropriate observations and specifications. The support system will be modeled by means of the stiffness method of structural analysis.

In this text the methods used for the analysis of the two structural components will consistently be referred to as the finite element method for the rock (continuum) analysis and as the stiffness method for the support analysis. The distinction between the two is rather arbitrary, but simplifies the terminology. The finite element method is "defined" here as the use of discrete triangular and quadrilateral elements to describe the mechanics of the (rock) continuum while in the stiffness method beam and spring elements are used to describe the support system. There is no generally accepted rigorous definition of these and similar methods that use matrix analysis for the study of structures. Depending upon one's point of view, one can consider the displacement finite element method as used here as a particular type of stiffness structural analysis (Przemieniecki, 1968), or one might consider the stiffness method as used here as a subsection of the finite element method (Desai and Abel, 1972).

The purpose of this chapter is not the development of a computer program that might automate the design of tunnel supports by substituting data manipulations for engineering judgment. The purpose

is the development of a tool that can assist in making an engineering judgment by quantifying and rationalizing the procedures for deriving such a judgment.

### III-2. Finite Element Analysis of Rock Failure

III-2.1. Introduction. Tunnel support loading is caused by the convergence of the tunnel walls that occurs after the support system has been installed. The support pressures thus developed must be sufficient to guarantee the stability of the opening. As an extreme condition the stability can be guaranteed by maintaining a stress state that assures elastic rock behavior. Even neglecting practical problems caused by the very early installation and the intimate contact necessary to allow the development of such a stress state, it remains an excessively conservative proposition and an inefficient method to try to recreate an equilibrium state equal to or even approximating the pre-tunneling state.

Frequently it is unavoidable (if not undesirable) that some failure does occur around the opening. An optimized support system is one that will allow failure to the extent that it helps

mobilizing the inherent rock strength and thus minimizes the support requirements. Once the optimum is exceeded rock failure can become a self-propagating phenomenon. This situation must be avoided.

The study of the failed rock behavior around the tunnel must be directed towards the determination of the mentioned optimum, and centered upon the analysis of the factors that influence the location of the optimum. These factors characterizing the broken rock zone can be determined, to a greater or lesser extent, from two sources: laboratory investigations of rock failure and *in-situ* observation of stability problems in tunnels.

The fundamental information must come from controlled investigations on a laboratory scale, and in-situ observations must confirm at least qualitatively the extrapolation from the one situation to the other. The extrapolation requires an analysis technique that makes it possible to calculate the consequences of the failure characteristics determined under a specific set of circumstances for a quite different set of conditions. The finite element method is a numerical analysis technique that might be sufficiently powerful and flexible to

make such an extension possible. The use of the finite element method in this context requires the definition of the basic phenomena that characterize rock failure and the formulation of a mathematical model that will adequately describe these characteristics under the various circumstances for which the model is to be used.

### III-2.2. Characteristics of (Compressive)

Rock Failure. The discussion (and the computer model) is limited to the failure of rock in purely compressive stressfields. To some extent this limitation can be justified by the argument that compressive stressfields are more likely around tunnels. Nevertheless this limitation remains somewhat artificial.

The discussion is limited to a phenomenological description, and no attempt is made to explain the mechanics of failure. Failure has some consequences for the requirements of rock behavior description that are significant for determining tunnel support requirements, but (hopefully) at a level well removed from the point where a detailed study of crack initiation and propagation becomes necessary. This presumption is basic for the here

included attempt at a large-scale numerical analysis of rock failure effects upon support loading.

Particularly during the last decade a great deal of work has been performed in the area of rock fracture mechanics. This has led, at least on the laboratory scale, to a fairly comprehensive description of the principal features that characterize rock fracture, from failure initiation down to final collapse. It will be assumed here that these features, studied mostly on small cylinders in triaxial compression, also characterize rock failure around tunnels, in polyaxial inhomogeneous stress-fields. The experimental work on which the following summary is based has been reported by Wawersik (1968), Wawersik and Fairhurst (1970), Wawersik and Brace (1971), Brace (1963), Brace, et al. (1966), Brace and Byerlee (1966), Wiebols, et al. (1968), Crouch (1970a,b; 1971), Bieniawski (1970), Rummel and Fairhurst (1970), Hudson, et al. (1971), Cornet and Fairhurst (1974), Cornet (1975).

Greatly simplified, the fracturing process can be described as the progressive but somewhat overlapping sequence of three main developments:

- i. Micro-fracturing, with opening of cracks, volume increase or dilatation and change in "elastic"

properties.

ii. Decrease in stiffness or strain softening and stable or unstable fracturing, i.e., energy must be added to or withdrawn from the failing rock as the final collapse state is approached.

iii. Development of a major throughgoing failure plane, characterized by extremely low shear stiffness.

Phenomena i and ii are pervasive properties of the failing rock, and on a scale substantially larger than that of the "fracture details" the failing rock remains homogeneous. This is no longer true in the final collapse stage.

The principal tool that has been used for quantifying the failure behavior is a set of complete stress-strain and volumetric strain-axial strain curves. For the application to the analysis of the long-term stability of underground openings it is necessary to have such curves for the rock mass while it remains subjected to prolonged loading.

### III-2.3. Finite Element Simulation of Rock Failure.

III-2.3.1. Introduction. The interaction between rock and supports is a complicated problem, and unless greatly simplifying assumptions are made

it is necessary to study it by means of numerical techniques. Presently the most popular of these techniques for the study of continuum mechanics is the finite element method. The method has been documented exhaustively in a large number of textbooks (e.g., Martin and Carey, 1973; Desai and Abel, 1972; Przemieniecki, 1968), conferences including review and state-of-the-art papers and innumerable publications on new developments of the method. A discussion of the fundamentals of the method seems therefore superfluous, and reference will be made only to publications discussing problems related to tunnel stability, rock failure, or both.

The finite element simulation of rock failure used in this thesis closely follows the procedure developed by Crouch (1970). In this approach failure propagation is assumed to be equivalent to a sequential development of a series of elastic states. Each state is characterized by an iterative derivation of appropriate elastic constants. The independent variables defining the elastic constants are the largest principal strain and the smallest principal stress. The "principal" elastic constants are defined as secant values from stress-strain and volumetric strain-axial

### III-11

strain curves. Because of the lack of numerical information about failed rock properties some "associated" constants are selected upon the basis of qualitative considerations.

III-2.3.2. Literature Survey. A number of methods have been used to study rock failure by means of finite element analysis. The earlier developments of this type were based upon the finite element methods formulated to study "stable" plasticity problems. Such calculations clearly are subject to the same kind of criticism as the conventional closed-form plasticity solutions used for the evaluation of tunnel support requirements that have been discussed in section II-2. The essential shortcoming of such methods is that they do not allow for the deterioration of rock properties with failure propagation.

Reyes (1966) and Reyes and Deere (1966) used the generalized Mohr-Coulomb criterion (Drucker and Prager, 1952) to study the development of plastic zones around circular tunnels during incremental unloading of the "confining" pressure on the tunnel walls. Kovári (1969) simplified the generalized Mohr-Coulomb criterion by eliminating

the intermediate principal stress in order to reduce computing time. Kovári imposed incompressible flow and used the "initial stress" technique (Zienkiewicz, 1971, pp. 372, 381) to solve the problem for several lined tunnels. Kovári included a numerical example of the influence of neglecting the construction sequence upon the stresses in the support. He used equivalent nodal point forces to simulate excavation of the tunnel. In a more recent version of the program (Grob, 1973) the fully generalized Drucker and Prager yield surface seems to be used.

Dahl (1969) and Dahl and Voight (1969) used an anisotropic generalization of the Mohr-Coulomb yield function to study the plastic zone propagation around a circular opening subjected to incremental external loading. Dahl (1969) compared results for incremental external loading with results for incremental unloading of the walls of a hole in a stressed medium and found the final results to be quite insensitive to the used approach.

Baker, et al. (1969) used the same generalized Mohr-Coulomb criterion as Reyes (1966) with an improved method for the "plastic displacement" corrections to study stresses and displacements

around a deep circular tunnel. Chang, et al. (1972) compared results from an analysis based upon Reyes' (1966) derivation with published experimental results and obtained a qualitatively similar behavior. Baudendistel (1972, 1973) apparently used a simple Mohr criterion and some type of initial strain technique developed by Malina (1970). Desai and Reese (1970) used a simple Mohr failure criterion in combination with a non-linear stress-strain curve approximated by tangent moduli to study failure around an incrementally loaded deep borehole. Hayashi and Hibino (1970) incrementally unload the walls of a large underground cavity. They assign lower stiffness values to the superficial layer of blasted rock and use a parabolic two-dimensional Mohr envelope as well as a variable modulus and Poisson's ratio in combination with an initial stress analysis that includes a time increment. Ishijima and Suzuki (1970) combine the original Griffith criterion with a time-dependent decrease of the tensile strength included therein and a decreasing modulus as well as an increasing Poisson's ratio to study loading of a circular tunnel support.

of particular interest within the context of

this thesis, discussing the influence of rock failure on tunnel support requirements, are finite element analyses that incorporate techniques for simulating strain softening behavior. The incremental-iterative model with secant orthotropic elastic constants developed by Crouch (1970) is used in the following section and is discussed there in more detail. Hoyaux and Ladanyi (1970a, b) used a somewhat similar pseudo-elastic analysis but with isotropic strain-dependent elastic properties. These authors used a two-dimensional Tresca as well as a parabolic failure criterion to study plastic flow around shallow tunnels in a medium with reduced post-peak strength.

The isotropic secant modulus variation, based upon relations between octahedral stress and strain had been applied to plate loading tests of sand by Girija Vallabhan and Reese (1968) and to the analysis of a rock-soil interaction problem by Girija Vallabhan and Jain (1972). A combination of a variable "secant modulus"<sup>1</sup> with a stress transfer technique is proposed by Lo and Lee (1973).

---

<sup>1</sup>Although not defined as "secant" by the authors, who used the absolute value of the descending slope of the stress-strain curve in the post-peak region.

The amount of stress transfer is defined by the properties of a residual (linear, two-dimensional) Mohr-Coulomb envelope. A similar stress transfer analysis for a strain-dependent strength decrease has been used by Zienkiewicz, et al. (1970).

A somewhat extreme example of "secant" modulus variation was given by Barla (1972). At (compressive) fracture initiation, determined from the modified Griffith criterion (Jaeger and Cook, 1969, p. 95), the Poisson's ratio is increased to account for non-elastic volume increases. At "strength failure," i.e., when a (non-linear) failure envelope condition is reached, the strength and stiffness of the concerned element(s) are equated to zero. Around a circular opening in a hydrostatic stressfield this implies total collapse.

A straightforward extension of incremental nonlinear elastic solutions, including a negative shear stiffness in the post-peak region, was used by Perloff and Pombo (1969).

Models of rock failure based upon sequential variations of the secant stiffness properties can be closely associated with an elastic or pseudo-elastic approach. Some models are based more directly upon a plastic formulation of the strain-

softening problem. Prime examples of these are the models developed by Gates (1971, 1972), by Höeg (1972) and by Isenberg and Bagge (1972). The method proposed by Höeg involves an extension of the von Mises yield criterion, while Gates as well as Isenberg and Bagge use a similar extension of the generalized Drucker and Prager criterion. Gates formulates a sudden complete reduction to residual strength values and combines this with Reyes' (1966) stress-strain matrix. Höeg and also Isenberg & Bagge incorporate a negative strain-hardening term in the stiffness matrix in order to simulate a strain-softening material. This procedure had been suggested by Dahl (1969, Appendix B) in a discussion of the significance of strain softening for rock mechanics problems.

There is little doubt but that serious problems remain to be solved in the general area of simulating strain-softening behavior by means of finite element techniques. Neither for the pseudo-elastic nor for the pseudo-plastic approach have the questions of uniqueness, convergence or stability received a satisfactory final answer (Crouch, 1970, p. 98; Isenberg and Bagge, 1972, p. 1157; Desai, 1972, p. 36; Lo and Lee, 1972). Probably the best

argument for using such methods at present is the heuristic justification invoked by Zienkiewicz (1971, p. 370) for engineering applications of non-linear finite element analysis.

### III-2.3.3. Finite Element Simulation of Compressive Rock Failure.

III-2.3.3.1. Introduction. The finite element analysis of compressive rock failure used in this thesis follows an incremental-iterative path similar to the one developed by Crouch (1970). In this model it is assumed that propagating rock failure can be considered as being equivalent to a sequence of pseudo-elastic states, each one of these corresponding to the rock mass behavior after the last load increment or decrement. After each change in boundary conditions, corresponding either to a load increment on the structure or to an additional step in the sequential excavation of an opening in a stressed medium, iterations are performed to determine a set of elastic constants corresponding to the new stress and strain state in every element. The failed rock is thus treated at each increment as an inhomogeneous linearly elastic continuum build up of elements with properties

derived from the preceding stress and strain conditions to which they have been subjected.

The main practical problem with this approach, besides the previously-mentioned more fundamental difficulties of uniqueness, convergence and stability, is the determination of a sequence of pseudo-elastic constants that will guarantee a fair modeling of rock failure. In order to illustrate the combination of empirical data, mathematical derivations and heuristic arguments upon which such a selection of equivalent constants is based, the procedure will be detailed for a few elastic models. Starting with the assumption of isotropy, the models progress from the simplest one, one that is probably physically not very satisfactory, but that allows the most internally coherent and rational derivations.

#### III-2.3.3.2. Isotropic rock failure model.

Although rock failure causes the rock to lose its (presumed initial) isotropy, it is worthwhile to discuss the requirements that would be imposed upon a set of equivalent isotropic elastic constants used to model rock failure. The assumption of isotropy simplifies the mathematical expressions

while providing an easier insight into the physical nature of the problem and still illustrating the general requirements of a finite element rock failure model.

The principal failure characteristics as presented in the greatly simplified discussion of section III-2.2 are represented, in a linearized form that will be used throughout, in Figure III.1. These graphs show, for an idealized uniaxial compression test, the axial stress and the lateral strain or volume change as a function of the axial strain. The secant isotropic elastic constants at any strain level can be derived from:

$$\varepsilon_z = \frac{\sigma_z}{E} \quad \varepsilon_r + \varepsilon_\theta = -\frac{2\nu}{E} \sigma_z = -2\nu \varepsilon_z \quad (\text{III-2.1})$$

The equivalent secant elastic modulus  $E$  decreases as soon as fracture is initiated, while the equivalent Poisson's ratio starts increasing at that point. The changes accelerate in the post-peak region, until the residual plateau is reached, and the changes slow down rapidly. In the finite element model of the uniaxial compression test the elastic constants  $E^j$  and  $\nu^j$ , after any applied strain increment  $j$ , are calculated from:

$$E^j = \frac{\sigma_z}{\varepsilon_z} \quad \nu^j = \left| \frac{\varepsilon_r + \varepsilon_\theta}{2\varepsilon_z} \right| \quad (\text{III-2.2})$$

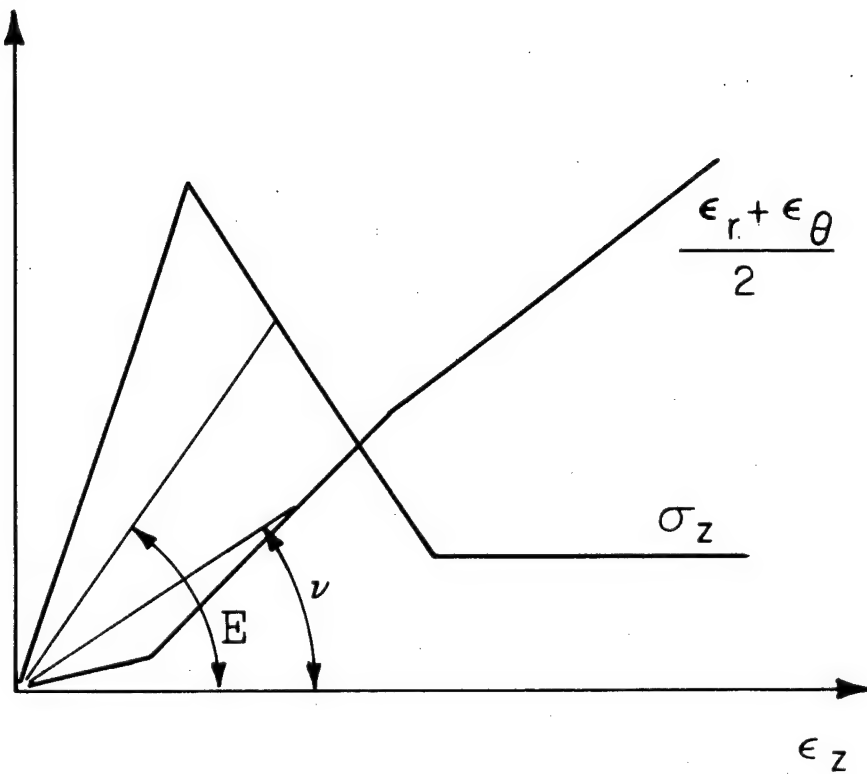


Figure III.1. Idealized Uniaxial Compression Stress-Strain Curve and Associated Lateral Expansion  $\epsilon_r + \epsilon_\theta$ . The Elastic Modulus  $E$  and the Poisson's Ratio  $\nu$  are Secants.

$\sigma_z$  and  $\epsilon_r + \epsilon_\theta$  are the total axial stress and lateral volumetric strain in any element with total largest principal strain  $\epsilon_z$  after the boundary condition increment  $j$  has been applied. The problem is solved again with the same boundary conditions, and if a significant strain change has occurred in one or more elements the elastic constants are adjusted so that they correspond to the new strain level. This procedure is iterated until no more changes take place. The next boundary load or displacement increment or decrement is then applied.

Rock failure is, even qualitatively, strongly dependent upon the confining pressure. For this reason it is necessary to specify the pseudo-elastic constants for a range of confining pressure levels. In the computer program it is assumed that the intermediate principal stress does not influence rock fracturing, and that the confining pressure equals the smallest principal stress. The requirements this entails for the finite element analysis can be derived by considering an (idealized) tri-axial compression test. In this case the stress-strain relations are given by:

$$\epsilon_z = \frac{\sigma_z - \nu(\sigma_r + \sigma_\theta)}{E} = \frac{\sigma_z - 2\nu \sigma_{con}}{E} \quad (III-2.3)$$

$$\epsilon_r + \epsilon_\theta = \frac{(1 - \nu)(\sigma_r + \sigma_\theta)}{E} - \frac{2\nu \sigma_z}{E} = \frac{2(1 - \nu) \sigma_{con} - 2\nu \sigma_z}{E}$$

The secant to the axial stress-strain curve is no longer the elastic modulus, and neither is the Poisson's ratio (half) the secant of the lateral volumetric strain versus axial strain diagram.

Both curves depend upon both elastic constants, and a straightforward derivation as "secants" is no longer possible. In order to find such a direct secant definition, one can rewrite equations

(III-2.3) in terms of the total volumetric strain:

$$\varepsilon_r + \varepsilon_\theta + \varepsilon_z = \frac{(\sigma_r + \sigma_\theta + \sigma_z)(1-2\nu)}{E} = \frac{\sigma_z + 2\sigma_{\text{con}}}{3K} \quad (\text{III-2.4})$$

It is thus possible, from a plot of the total volumetric strain versus the first stress invariant, to define the bulk modulus K as a pseudo-elastic constant. A second (independent) elastic constant that can be derived from a polyaxial test is the shear modulus G. Indeed, one can rewrite (III-2.3) in the form:

$$\varepsilon_z - \frac{\varepsilon_\theta + \varepsilon_r}{2} = \frac{(2\sigma_z - \sigma_r - \sigma_\theta)(1+\nu)}{2E} = \frac{\sigma_z - \sigma_{\text{con}}}{2G} \quad (\text{III-2.5})$$

Equations (III-2.4) and (III-2.5) permit the derivation of the two independent "secant" elastic constants K and G. It is then a trivial matter to calculate the corresponding values for the Poisson's

ratio  $\nu$  and for the elastic modulus  $E$  that are used in the stiffness matrix formulation.

Equations (III-2.4) and (III-2.5) indicate limiting necessary conditions that must be satisfied by the "experimental" volume-stress-strain relations in order that they might be represented by an equivalent secant isotropic model. From the conditions that bulk and shear modulus must be positive follow the requirements:

$$\varepsilon_r + \varepsilon_\theta + \varepsilon_z > 0 \quad 2\varepsilon_z - (\varepsilon_\theta + \varepsilon_r) > 0$$

Alternatively this can be expressed as:

$$E = \frac{9KG}{3K+G} > 0 \quad 0 < \nu = \frac{3K - 2G}{2(3K+G)} < \frac{1}{2}$$

The last of the latter conditions clearly indicates the restrictive character of the isotropic model. Indeed, numerous experiments have shown that frequently, and even well before the peak strength is reached, the tested rock could no longer be considered as an "equivalent isotropic" material, because such an assumption would violate the requirement that the Poisson's ratio should not exceed 0.5.

A somewhat arbitrarily selected set of complete stress-strain curves is shown in Figures III.2. Intact and residual strengths were selected so that

the intact and residual failure envelopes would be linear ( $\phi_i = 30^\circ$ ,  $\phi_r = 15^\circ$ ). In order to illustrate the restrictions imposed by the isotropy conditions, long-dashed lines on Figures b and c indicate the limits of the domain that can be covered by an isotropic model. These lines correspond to a residual Poisson's ratio equal to one-half. Because numerical instabilities in the solution of the stiffness equations are likely to occur well before this limit is reached, a bound of more practical significance is indicated by the solid lines, corresponding to a maximum residual Poisson's ratio of 0.45. As a consequence of this restriction the volume increase (Figure III.2c - K secant) ends when the peak strength is reached. The initial section of the graphs in III.2b corresponds to an idealized triaxial test in which the pressures are increased hydrostatically until the confining pressure is reached (solid lines) or in which the confining pressure is applied first (dotted lines).

Two possibilities exist for the use of the preceding derivations in the plane strain finite element analysis. It is possible to use a set of curves as shown in Figures III.2 as input data, and to consider the resulting largest principal

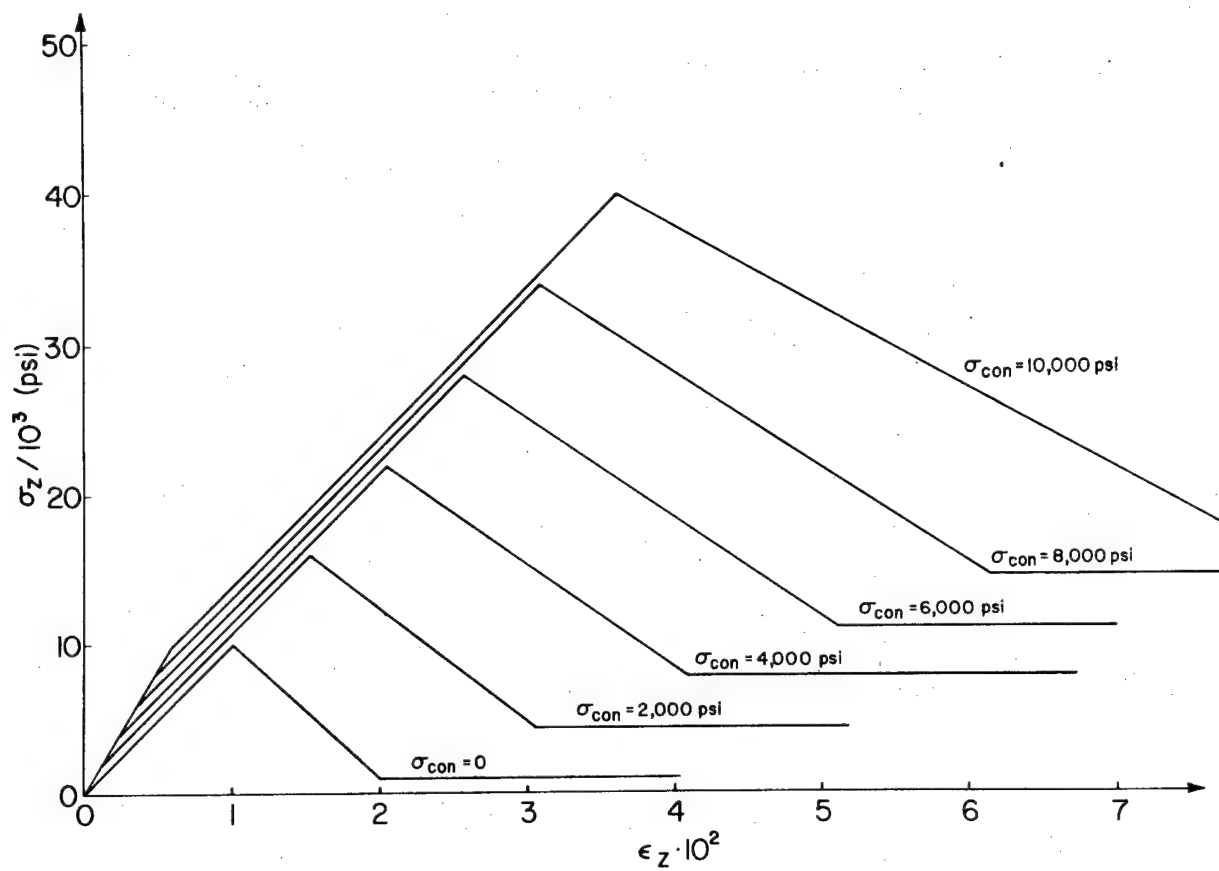


Figure III.2a. Set of Idealized Complete Stress-Strain Curves for Various Confining Pressures  $\sigma_{\text{con}}$  and for Linear Intact and Residual Failure Envelopes, with Angles of Internal Friction  $\phi_i = 30^\circ$  and  $\phi_r = 15^\circ$ , respectively.

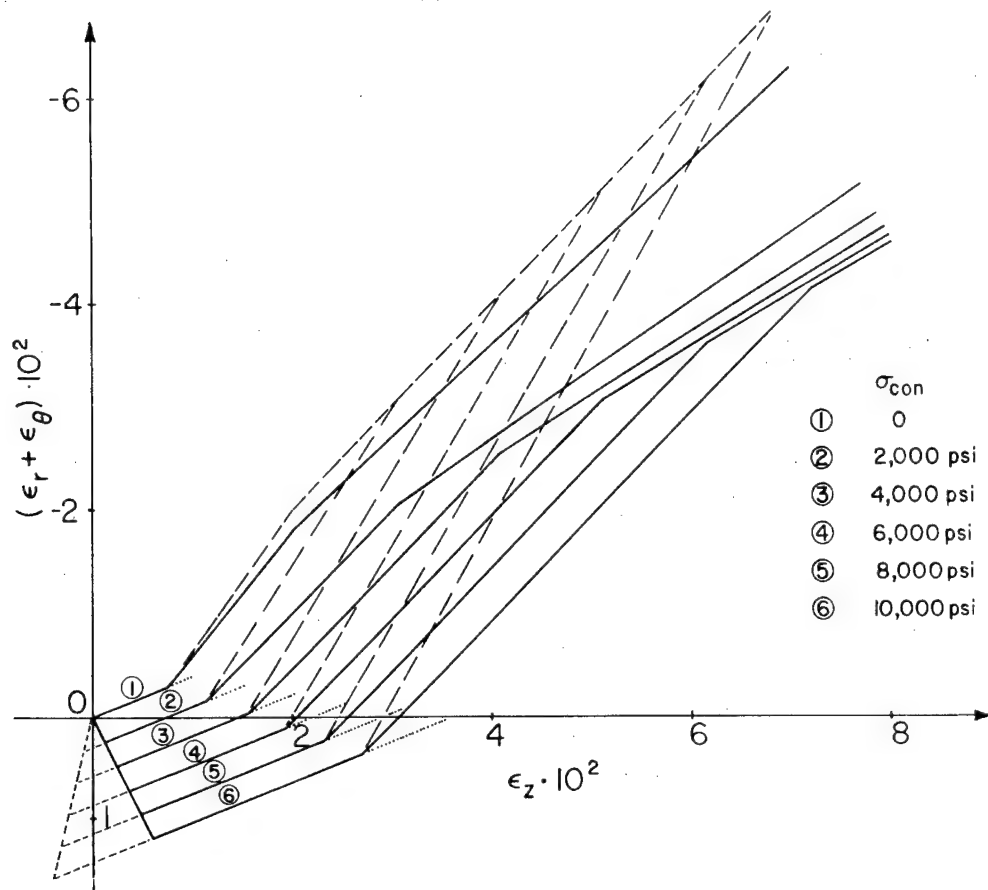


Figure III.2b. Set of Idealized Lateral Expansion

$(\epsilon_r + \epsilon_\theta)$  Curves Associated with  
Stress-Strain Curves of Figure

III.2a.

Solid lines are for a residual Poisson's ratio of 0.45, long-dashed lines for a residual Poisson's ratio of 0.5. The initial (at origin) loading path is for a test in which the pressures are increased hydrostatically until the confining pressure is reached (solid lines) or for a test in which the confining pressure is applied prior to any axial load (dotted lines).

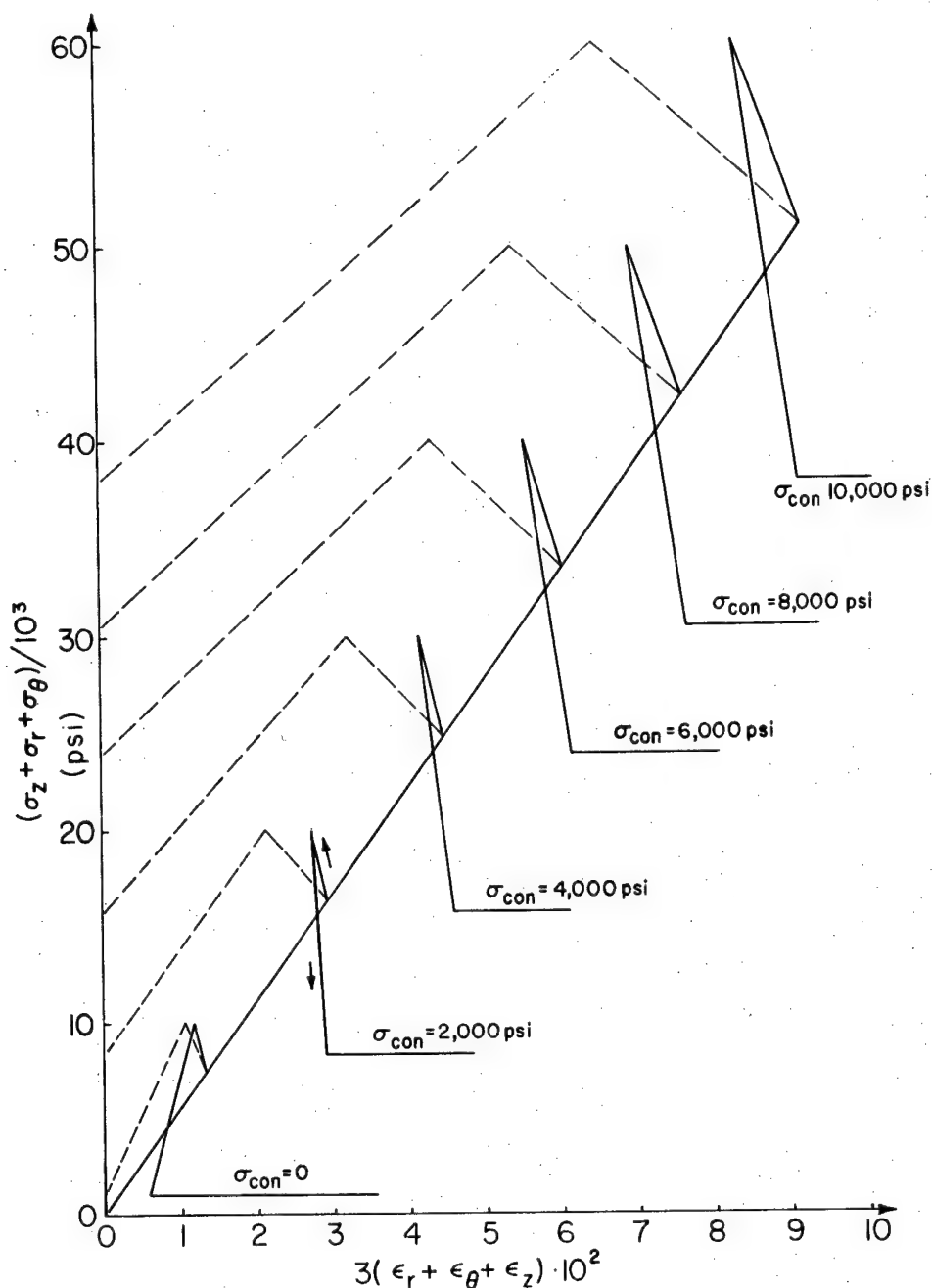


Figure III.2c. Mean Hydrostatic Stress or First Stress Invariant Versus Dilatation or First Strain Invariant Corresponding to the Stress-Strain-Volume Behavior of Figures III.2a and b. The bulk modulus  $K$  is secant. Solid lines correspond to a residual Poisson's ratio of 0.45, dashed lines to a residual Poisson's ratio 0.5.

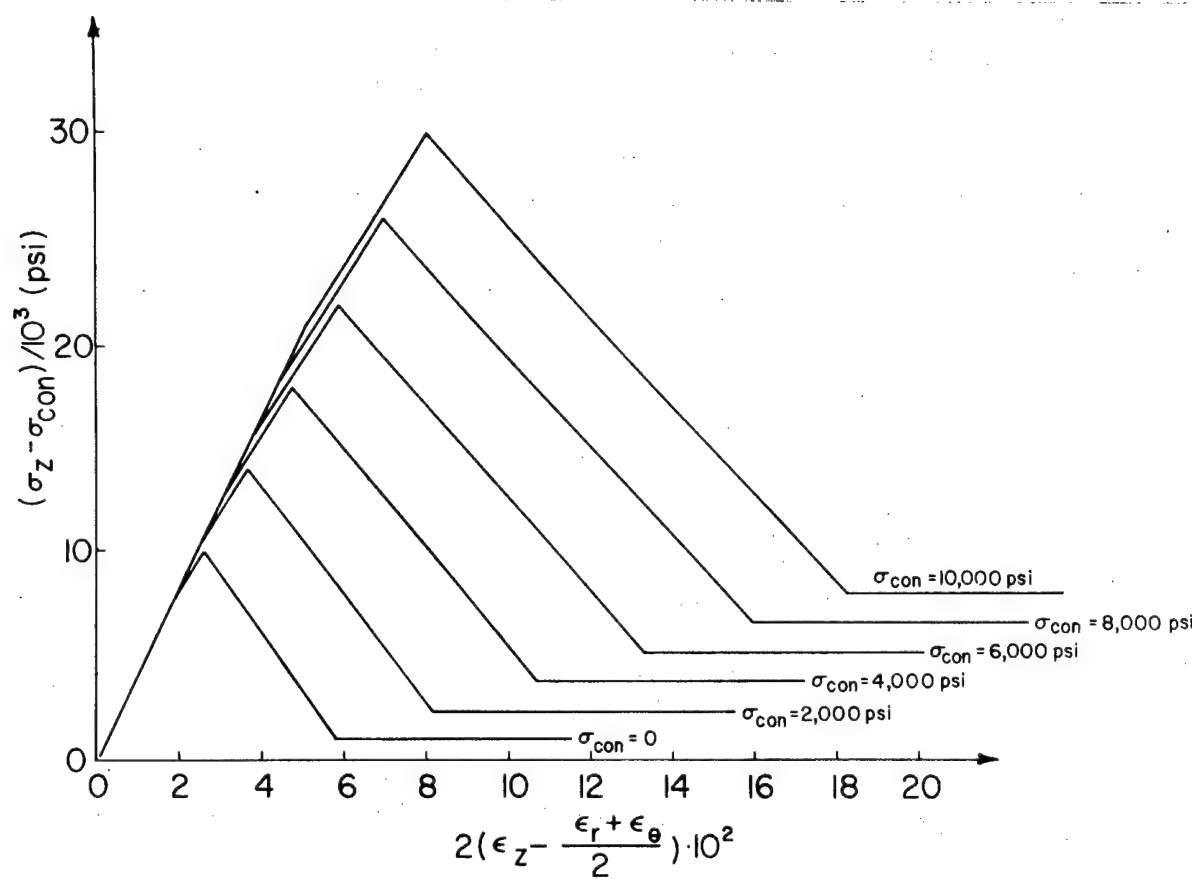


Figure III.2d. Stress Deviator Versus Strain Deviator Corresponding to the Stress-Strain-Volume Behavior of Figures III.2a and b.

The shear modulus  $G$  is secant.

strain and smallest principal stress in every (plane) element as equivalent to the axial strain and the confining pressure in polyaxial tests. One would then proceed by using equations (III-2.4) and (III-2.5) to calculate the equivalent elastic constants. The simplified results of such a translation from a triaxial to a plane strain domain performed (analytically) on the graphs on Figures III.2a and b are shown in Figures III.3a and b. These results are not strictly "linear" because of the simultaneous change of the Poisson's ratio and of the elastic modulus. (An indication of the simplification introduced here is given, in the ascending section only, by the dotted lines for the zero confining pressure curve).

An alternative approach was incorporated into the computer program included in Appendix C. It was assumed that a set of (idealized) results from a series of plane strain tests at different "confining" pressures were available, and that their appearance would be entirely similar to that of Figures III.3. The pseudo-elastic constants are calculated directly from the following expressions, the equivalents of (III-2.4) and (III-2.5) for the plane strain case:

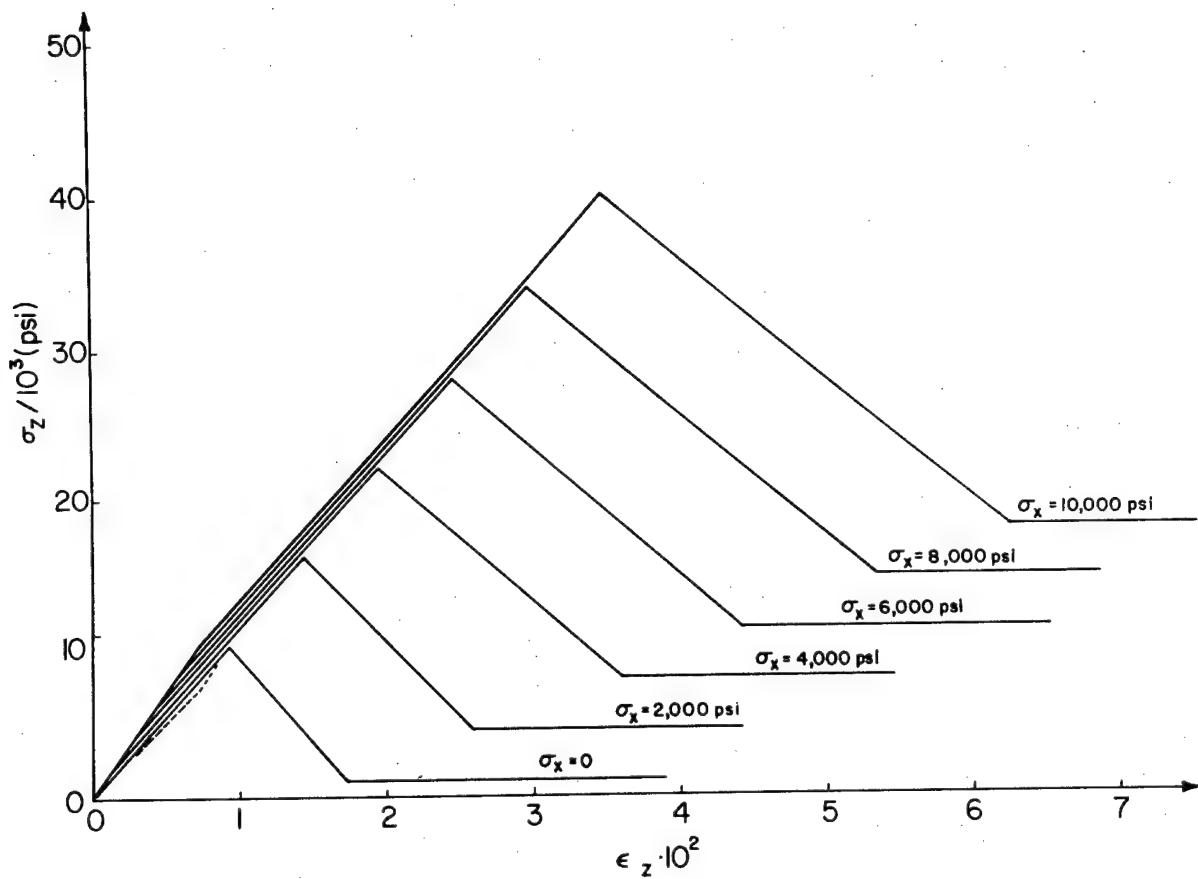


Figure III.3a. Idealized Plane Strain ( $\epsilon_y = 0$ )  
 Axial Stress-Strain Curves Derived  
 From Triaxial Curves of Figures  
 III.2a and b.

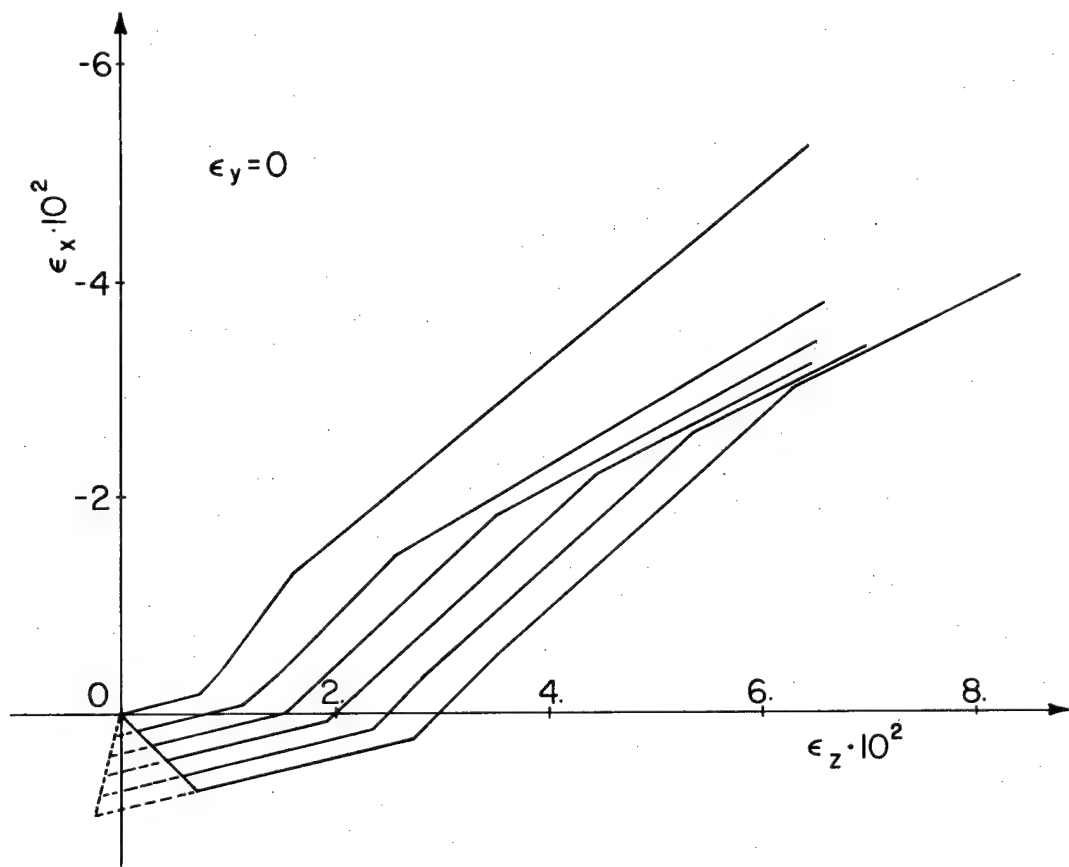


Figure III.3b. Idealized Plane Strain Curves of the Lateral Expansion Versus the Axial Strain Derived from Tri-axial Curves of Figures III.2a and b.

$$\nu = \frac{\epsilon_z \sigma_x - \epsilon_z \sigma_x}{(\sigma_x + \sigma_z) \epsilon_x - (\sigma_z + \sigma_x) \epsilon_z} \quad (\text{III-2.6})$$

$$E = \frac{(1+\nu) [(1-\nu) \sigma_z - \nu \sigma_x]}{\epsilon_z}$$

The derivation of these equations, in which the z-direction corresponds to the larger and the x-direction to the smaller in-plane directions, is given in Appendix B-1. The numerical approximations calculated according to this method, with a single square finite element, for a minimum principal stress equal to zero and for a minimum principal stress equal to 6,000 psi respectively are shown in Figures III.4a and b. The solid lines and squared points are input, while the dotted lines and circled points indicate the successive approximations under stepwise increased axial strain.

#### III-2.3.3.3. Orthotropic rock failure model.

Rock fracture initiation coincides with the development or propagation of cracks, usually in preferred directions, depending upon the three-dimensional stress state. Detailed study of the fracture mechanism (see authors listed in section III-2.2, particularly Wawersik) has clearly revealed this directional character of crack development and rock

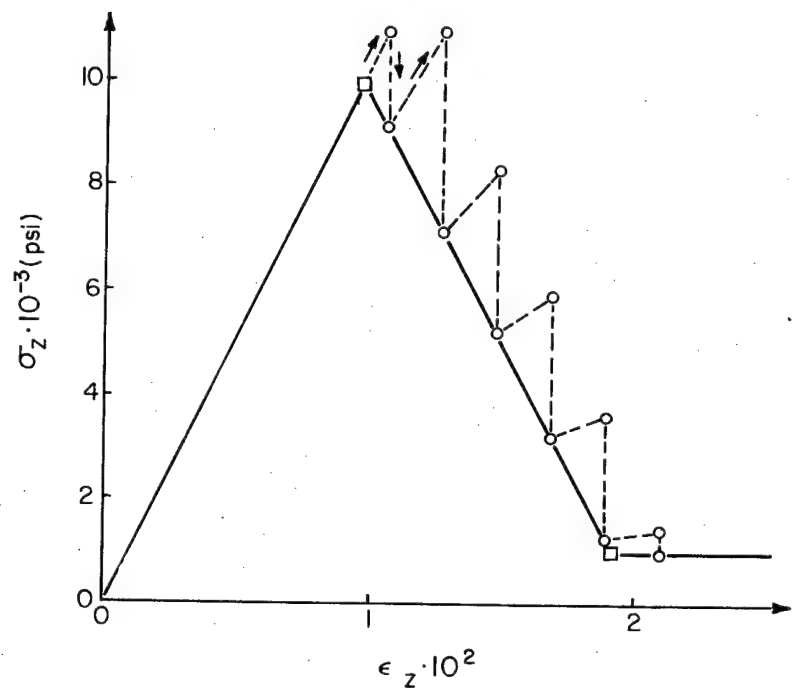
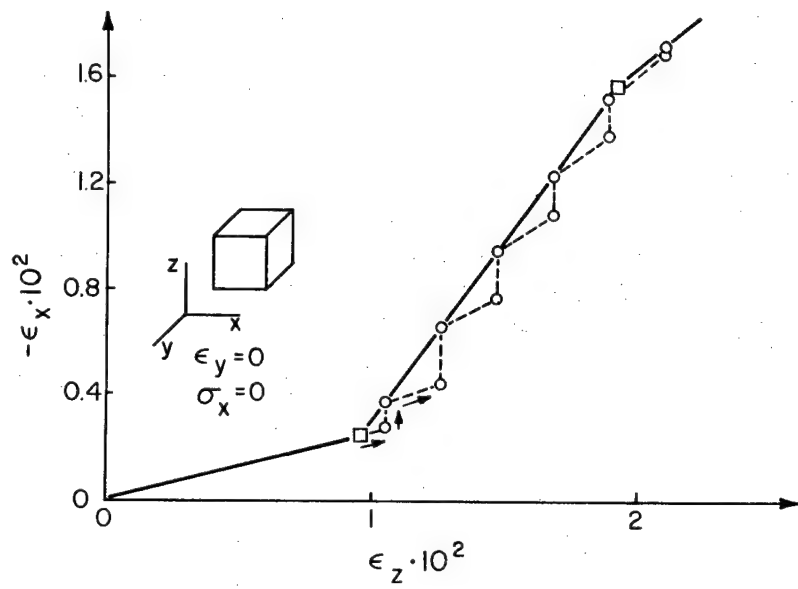


Figure III.4a. Numerical Approximation (dashed lines, circled points) to an Idealized Plane Strain Compression Input (solid lines, squared points) for Zero Minimum Principal Stress. Calculation with one square finite element and stepwise incremented largest principal strain  $\epsilon_z$ .

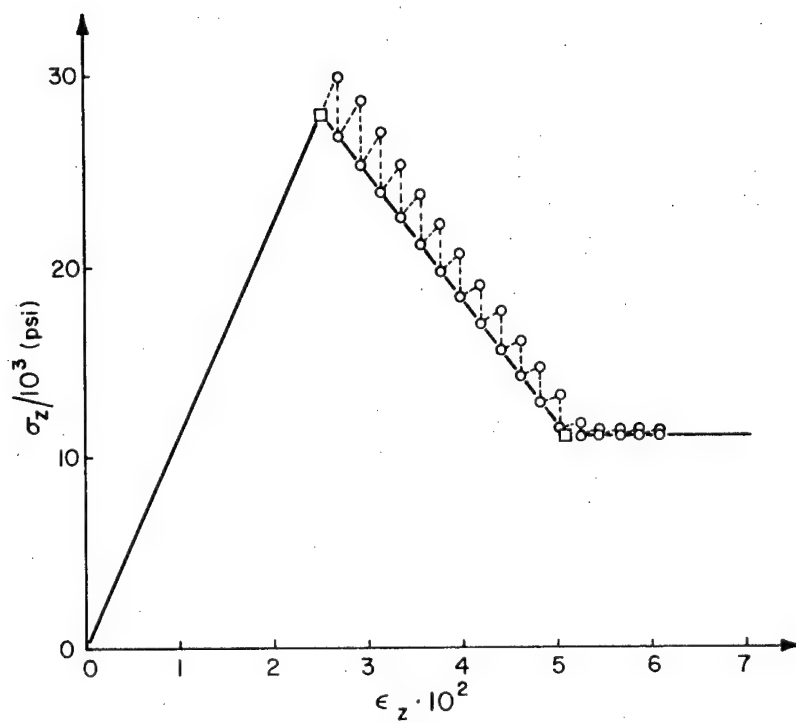
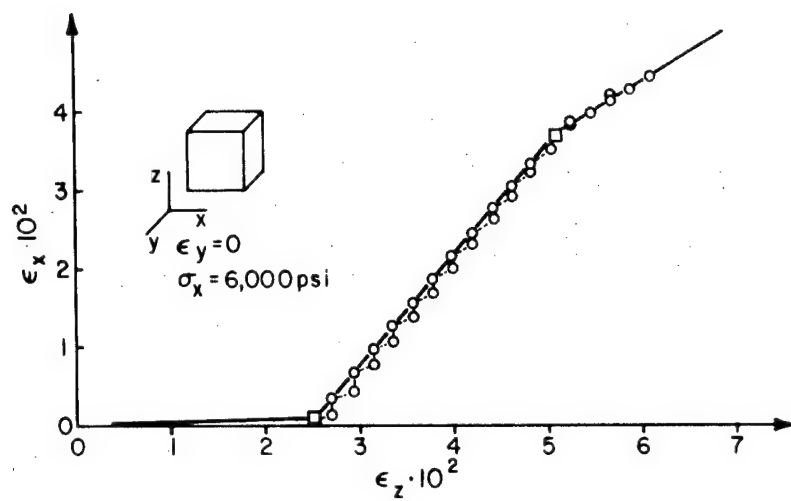


Figure III.4b. Numerical Approximation (dashed lines, circled points) to an Idealized Plane Strain Compression Input (solid lines, squared points) for a Minimum Principal Stress of 6,000 psi. Calculation with one square finite element and stepwise incremented largest principal strain  $\epsilon_z$ .

failure. This implies that an isotropic model is unlikely to be satisfactory for the description of rock failure.

The most reasonable three-dimensional generalization of the isotropic pseudo-elastic failure model would seem to be that of an orthotropic medium (orthogonally-anisotropic or orthorombic; Lekhnitskii, 1963, p. 19; Hearmon, 1961, p. 36), i.e., a material with three orthogonal planes of elastic symmetry.

The three planes of symmetry are assumed to correspond pointwise to the planes perpendicular to the principal stress directions. This is based on the assumption that the facility of crack development in a particular direction, and therefore the directional softening and dilatancy, is determined by and only by the principal stresses, their directions and relative values.

It is obvious that the determination of the nine independent elastic constants in this model is a major task, and a problem that requires, in the absence of experimental data, that several assumptions be made. In order to develop some guidelines for the selection of these constants it is worthwhile to look in some more detail at the triaxial compressive test, one of the most frequently performed

and therefore best documented rock tests. In an ideal triaxial test the radial and tangential directions are fully equivalent ( $\sigma_\theta = \sigma_r$  and  $\epsilon_\theta = \epsilon_r$ ). Assuming that this remains true during failure, the orthotropic model can be reduced to a transversally isotropic one, the number of independent elastic constants reduces to five, and the stress-strain relations can be written as:

$$\begin{aligned}\epsilon_r &= \frac{\sigma_r - \nu_1 \sigma_\theta}{E_1} - \frac{\nu_2}{E_2} \sigma_z \gamma_{rz} = \frac{t_{rz}}{G} \\ \epsilon_\theta &= \frac{\sigma_\theta - \nu_1 \sigma_r}{E_1} - \frac{\nu_2}{E_2} \sigma_z \quad \gamma_{\theta z} = \frac{t_{\theta z}}{G} \quad (\text{III-2.7}) \\ \epsilon_z &= \frac{\nu_2}{E_2} (\sigma_r + \sigma_\theta) + \frac{\sigma_z}{E_2} \quad \gamma_{\theta r} = \frac{2(1 + \nu_1) t_{\theta r}}{E_1}\end{aligned}$$

There is little or no information about values for the shear modulus during rock failure, and therefore its value is determined from the following combination:

$$\frac{1}{G} = \frac{1}{E_1} + \frac{1}{E_2} + \frac{2\nu}{E_2} \quad (\text{III-2.8})$$

This reduces to the correct expression for an isotropic material, and it is a special reduction from the more general formulation given in Appendix B-4.

It is possible to derive some information

about the secant elastic properties from a uniaxial compressive test on a cylindrical rock specimen, as equations (III-2.7) then reduce to:

$$\varepsilon_r + \varepsilon_\theta = - \frac{2\nu_2}{E_2} \sigma_z \quad \varepsilon_z = \frac{\sigma_z}{E_2} \quad (\text{III-2.9})$$

Complementing this with assumed relations for the remaining unknown constants  $\nu_1$  and  $E_1$  fully defines the pseudo-elastic sequence. The problem is somewhat more complicated in a conventional triaxial test, where, with  $\sigma_{\text{con}} = \sigma_r = \sigma_\theta$ , the following relations are measured:

$$\varepsilon_r + \varepsilon_\theta = \frac{2(1-\nu_1) \sigma_{\text{con}}}{E_1} - \frac{2\nu_2}{E_2} \sigma_z \quad (\text{III-2.10})$$

$$\varepsilon_z = - \frac{2\nu_2}{E_2} \sigma_{\text{con}} + \frac{\sigma_z}{E_2}$$

It does not appear feasible to reduce these equations into a form that permits a direct secant formulation of the type given by equations (III-2.4) and (III-2.5) for the isotropic material. The most direct approach to the determination of the elastic constants is then based upon the substitution of assumed relations for  $\nu_1$  and  $E_1$  in function of  $\nu_2$  and  $E_2$  into (III-2.10), followed by a point-wise calculation along the stress-strain curves of the appropriate elastic constants for various

confining pressures. The assumed relations between the elastic constants must, as a minimum condition, correspond to an assumption that is physically reasonable. One such relation was proposed and discussed in some detail by Crouch (1970, p. 90):

$$E_1 = \frac{E_0}{1 + \alpha \left( \frac{V_2}{V_0} - 1 \right)} \quad V_1 = \frac{V_0}{1 + \alpha \left( \frac{V_2}{V_0} - 1 \right)}$$

(III-2.11)

$E_0$  and  $V_0$  are the initial elastic modulus and Poisson's ratio of the unfailed (isotropic) rock,  $\alpha$  is an as yet undetermined parameter. These relations were based on the assumption that the stiffness perpendicular to the largest principal stress decreases with increasing (inelastic) lateral expansion. Substituting expressions (III-2.11) into the stress-strain relations (III-2.10) results in equations for all elastic constants in function of the stress-strain-volume input data. In order to ensure positive definiteness of the sequential elastic systems, it is necessary to impose conditions similar to the requirements that the isotropic modulus be positive and the Poisson's ratio less than one-half; the choice of the as yet undetermined parameter  $\alpha$  facilitates satisfying this requirement. Details and manipulations are

given in Appendix B-3, as well as a more comprehensive discussion of the problems involved in the calculations.

In order to apply a derivation similar to the preceding one for the analysis of a polyaxial test to the study of a plane strain problem, accepting the anisotropy assumption for which far less justification exists in this case, it is necessary to make several decisions. The first and most straightforward possibility at this stage is the one previously mentioned in the discussion of the isotropic model: analyze the plane strain problem, consider the largest principal strain and the smallest principal stress in each element and at every iteration as independent variables equivalent to the axial strain and the confining pressure in the triaxial test, and calculate the new elastic constants with the expressions derived in Appendix B-3, based upon the preceding discussion. The last decision that remains open then is whether to assign the plane strain direction constants equal to those in the direction of the largest principal strain or equal to those in the direction of the smallest principal stress.<sup>2</sup>

---

<sup>2</sup>Back-analysis of plane-strain experiments

An alternative method, again parallel to the isotropic discussion, is to start with the assumption of the availability of plane strain data input. The expressions used for the calculation of the sequence of elastic constants are then derived directly from the plane strain stress-strain formulations. It will then be necessary to start the derivation with the decision of whether the plane strain direction is equivalent to the largest strain or to the smallest stress direction. A more comprehensive discussion of this alternative is presented in Appendix B-3.

There is little doubt but that the physically most appealing model is the fully orthotropic one. Moreover, a fully consistent formulation of such a model would eliminate the need for a separate consideration of each particular boundary condition problem (e.g., plane strain versus triaxial), a particularly inelegant aspect of the preceding discussion. Unfortunately, the number of constants and the lack of experimental evidence create a situation where the derivation of equivalent elastic constants

---

on rock could provide an indication which is more appropriate, or whether the anisotropy assumption is a reasonable one altogether.

becomes increasingly arbitrary and artificial. Ideally, one should wish for a completely symmetric formulation of the derivation of the equivalent pseudo-elastic constants, in such a form that "special cases" such as plane strain or axisymmetric conditions could logically and simply be derived from it. Such a formulation has not been attempted here.

### III-3. Stiffness Analysis of Tunnel Supports

III-3.1. Introduction. Two basic requirements must be satisfied by a support model that is to be part of the numerical analysis of the rock-structure interaction. In the first place it must permit the generation of realistic reaction forces. This requires that the support model, compressed during tunnel convergence, induces accurate support stresses in the rock mass. In the second place it is necessary to obtain sufficient information about the stresses in the support, so that the safety as well as the efficiency of the system can be evaluated.

Several stiffness methods have been used to study support behavior and the influence of supports on tunnel stability. One of the simplest methods, and one that has some attractiveness when one has

access only to a very simple finite element program consists in using constant strain triangular or linear strain quadrilateral plane elements (e.g., Zienkiewicz, et al., 1968; Zienkiewicz, 1971, p. 389; Baudendistel, 1972, 1973). Part of the overall mesh is then used to represent the support system, and the elements in that part are given support (e.g., concrete) properties. In principle it should be possible to use such a method. But because of the poor characteristics of these "simple" elements under bending conditions it is necessary to use a large number of elements across the support section, or to limit these methods to problems where bending strains are comparatively small. It will be shown in the next section that the support models used by the aforementioned authors are inadequate for the types of support loading they considered.

A second very simple support model is obtained by representing the support action as a pressure applied to the tunnel walls (Heuzé and Goodman, 1972). As in the preceding case, its simplicity makes this model attractive. It does assume that the support behavior is known, rather than provide information about it. Nevertheless, under

appropriate conditions, such as the case of a failed support considered by Heuzé and Goodman (1972), it provides an approximation that could be improved only by going to a great deal of sophistication.

A more precise tool for modeling the support system is provided by stiffness structural analysis. Kovári (1969) derived a combination of one-dimensional bar elements, equivalent to a concrete liner. Dixon (1969, 1971, 1973) and Isenberg (1973) used beam elements to represent the support. This type of element will be used here, because it minimizes the number of equations needed for adequate support representation, while allowing an accurate stiffness model and providing full information about support moments, stresses and displacements.

A general discussion of the necessary requirements to be satisfied by a support model must be restricted by the great variability of support characteristics. Because this variability is mainly related to installation procedures and construction details, it is necessary to pay careful attention to the elements that determine the stiffness of the rock-support interface. The same

factors that were shown to have a dominating role on the support system stiffness in section II-6 must also be considered here, in addition to factors that can become significant in the general non-axisymmetric case. The requirements this poses for the numerical model will be discussed separately for a variety of support methods, as indeed different support systems tend to have very different interface structures.

### III-3.2. Stiffness Model of Tunnel Supports.

A very simple model for shotcrete and concrete supports has been used by Baudendistel (1972, 1973) and by Zienkiewicz (1968, 1971). Because it makes use of triangular and quadrilateral elements, its incorporation into a finite element analysis is of trivial facility and therefore very tempting. Such a method must raise serious doubts as to the accuracy of the results, because of the questionable value of the used element types when a single element must account for the entire strain variation associated with bending or for a large fraction thereof. Such situations do arise in most of the problems discussed by the above-mentioned authors. Indeed, because a relatively large number of

elements is already used to represent the rock mass, one tends to minimize the number of elements used to represent the support structure. Such a minimization can easily lead to large numerical inaccuracies in stress and displacement results. Although fairly large errors in some of these results might be acceptable, one should be aware of conditions where they can occur, as well as of the cumulative effect they can have. The latter consequence results from the fact that under non-homogeneous loading the models described by the preceding authors tend to be much stiffer than the actual supports they are supposed to represent, i.e., the external displacements of the support, at the rock-support contact, tend to be smaller than the true values. This obviously influences the results of iterative schemes used to approach non-linear rock mass behavior. By the same token it makes the use of such simple methods unreliable for the calculation of the stress distribution in the support, i.e., for evaluating the safety or the efficiency of a particular system.

The support models used by Zienkiewicz, et al. (1968) and by Baudendistel (1972, 1973) are shown in Figures III.5a and b, as well as the

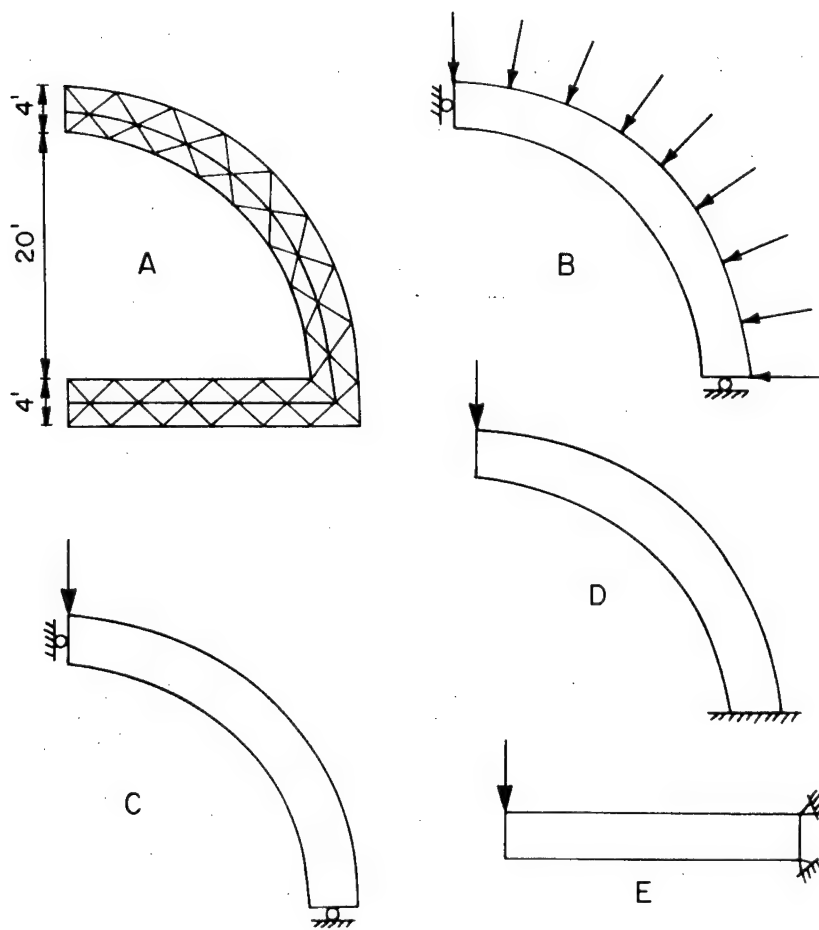


Figure III.5a. Tunnel Support Model (A) Used by Zienkiewicz, et al. (1968) and Loading Conditions (B-E) used to Evaluate the Adequacy of the Model.

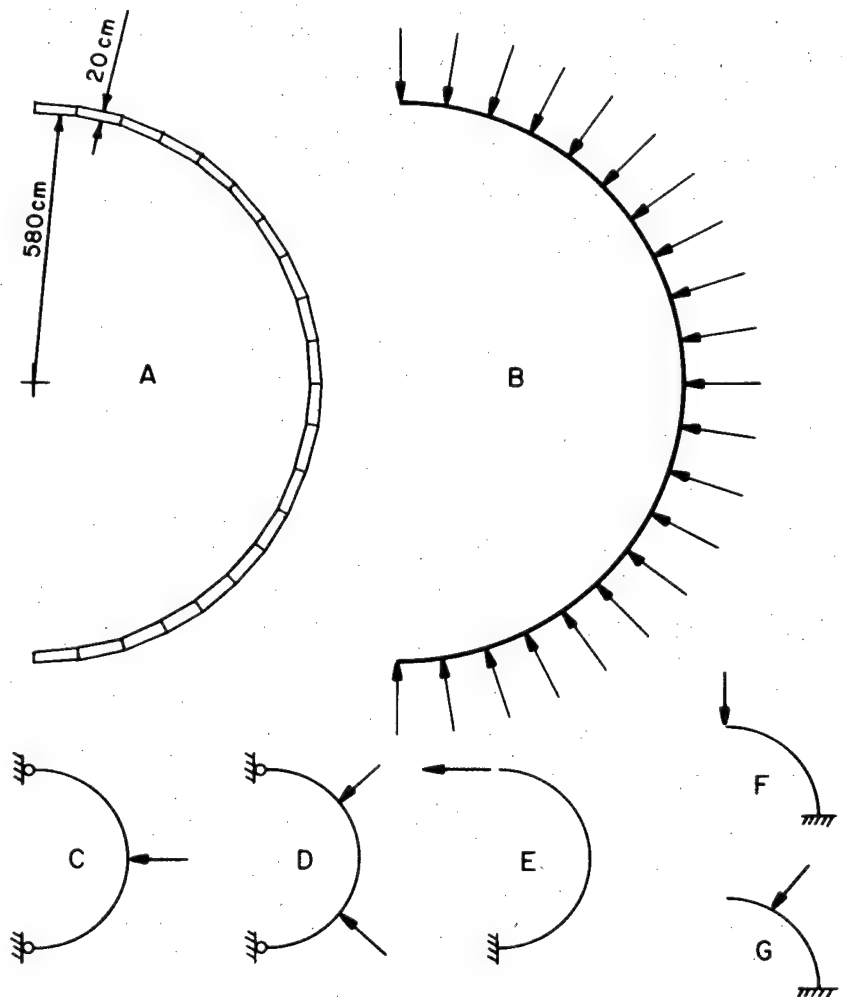


Figure III.5b. Tunnel Support Model (A) used by Baudendistel (1972, 1973) and Loading Conditions (B-G) used to Evaluate the Adequacy of the Model.

loading configurations that have been used to evaluate the adequacy of the models. The results of the evaluation are summarized in Table III-1. The first column of this table gives a problem designation, corresponding to Figure III.5a for Z and to Figure III.5b for B. The second letter indicates the loading case.<sup>3</sup>

Two types of stiffness models have been used, and the results under various loads compared with the theoretical results. For the in-plane plate element analysis either constant strain

---

<sup>3</sup> All calculations on which the results in this section are based were performed with FORTRAN programs in single precision arithmetic on a CDC 6600 computer (with about 14 significant decimal digits per word). This should minimize the errors compared to the ones resulting on most other computer types. Gaussian block elimination was used to solve the stiffness equations. The nodal point numbering system was always the same, and corresponded to a solution sequence away from the fixed nodes (e.g., ZB, BE, BF), towards the fixed nodes (e.g., ZE, BG), or a mixed sequence (e.g., BC). This type of analysis should correspond reasonably well to an analysis that might be performed under routine conditions, when no special attention is paid to error minimization. It is realized that the matrix population density is particularly low in these problems, lower than it would be if the supports were connected within a larger mesh, so that the errors are likely to be larger, at least if they contain an error component due to the equation solver (Melosh, 1969).

Table III-1. Relative Errors (%) for Support Stiffness Models Consisting of in-plane Elements and of Beam Elements. Loading cases and meshes are illustrated in Figure III.5a for problems Z and in Figure III.5b for problems B

Problem	Type	Plate Elements			Beam Elements		
		No. El.	No. NP	% Error	No. El.	No. NP	% Error
ZB	T	36	30	0.8			
ZC	T	36	30	165.	9	10	4.04
ZD	T	36	30	170.	9	10	0.24
ZE	T	25	21	94.6			
BB	Q	20	42	0.2			
BC	Q	20	42	1366.	20	21	0.73
BC	T	80	62	1370.			
BC	QS	20	42	23.1			
BD	Q	20	42	160.2	20	21	1.30
BD	QS	20	42	295.			
BE	Q	20	42	1358.	20	21	0.31
BE	QS	20	42	48.8			
BF	Q	10	22	1405.	10	11	0.52
BF	QS	10	22	91.7			
BG	Q	10	22	1380.	10	11	0.01
BG	QS	10	22	38.8			

triangular elements (T), quadrilateral (Q) elements with a stiffness matrix build up from four triangles and elimination of the central nodal point, or a higher order quadrilateral element (QS, Wilson, 1970) have been used. The number of elements and the number of nodal points is tabulated so that a quick comparison of the work necessary to calculate the stiffness matrix and of the number of equations to be solved is possible. The largest relative error in the nodal point displacements is given in the last column of each of the basic element type tabulations.

The relative errors that occur with the plate element model clearly indicate the existence of two very different types of problems. Very accurate displacement results are obtained for a thick wall cylinder under radially symmetric load (problems ZB and BB). Very large errors occur in all tested cases where bending displacements dominate. None such errors are observed in the models using (straight) beam elements. As would be expected in the displacement finite element method, the errors in the stresses at the element centers tend to be more erratic and generally larger than the displacement errors.

The very poor behavior of the "triangular" and the "quadrilateral" models under bending is very clear, and not unexpected (Zienkiewicz, 1971, p. 155; Wilson, 1970). More specifically for tunnel supports, Vouille (1974) used triangular elements with six nodal points, and justified this choice by mentioning the difficulty of obtaining adequate accuracy with simpler elements. Although the meshes of Figure III.5 would be adequate under some very special circumstances, e.g., hydrostatic loading and circular structure, and small variations thereof, it would appear that beam elements can usually be relied upon to provide better results with less computing time.

### III-3.3. Stiffness Model of the Rock-Support Interface.

III-3.3.1. Introduction. Incorporating the connection between rock and support into the analysis requires as much care as does the development of rock and support models. This could already be expected from the results in section II-6, where it was shown how dominant the influence of connecting elements can be upon the overall stiffness of the support in a circular tunnel. In the general case

of non-hydrostatic loading and non-circular problem geometry some additional factors will have to be considered.

A realistic discussion of the support-rock mass interaction must take into account the three-dimensional nature of the problem. This aspect of tunnel support loading will be taken up in more detail in section III-4.2.

The interface between rock and supports must be characterized by an appropriate combination of shear and normal stiffness. What constitutes an "appropriate combination" will depend on the support type, and also rather strongly on construction procedures. For these reasons the interface connections will be discussed separately for a number of common support systems. The type of interface stiffness also has an influence upon the requirements to be imposed on the support model itself. A complete separation of the two would be somewhat artificial and therefore this mutual influence also is discussed under this heading.

Although the principles of an interface model can be based on mechanical concepts, the numerical values can be obtained only from actual installed supports. For some support types it is possible to

combine visual observation with simple assumptions to obtain a reasonable estimate of the interface stiffness. For other support types this is a very questionable approach, although it is generally unavoidable. Indeed, the published information on the subject is widely scattered, usually more or less incidentally included in the presentation of case histories, and frequently incomplete and qualitative or descriptive. One of the few definite statements that can be made is that a wide range of stiffness values do occur. It is therefore worthwhile to consider the consequences of such variations for support requirements, and particularly their influence on the efficiency of various support systems.

III-3.3.2. Stiffness model of a blocked steel set. The analysis of a blocked steel set as a stiffness structural problem is of practical significance because of the continued widespread use of steel supports. In addition it allows an easy illustration of the problems that arise in the development of a realistic model for a rather simple support structure.

The basic model of the blocked steel set is shown in Figure III.6. The steel set itself is

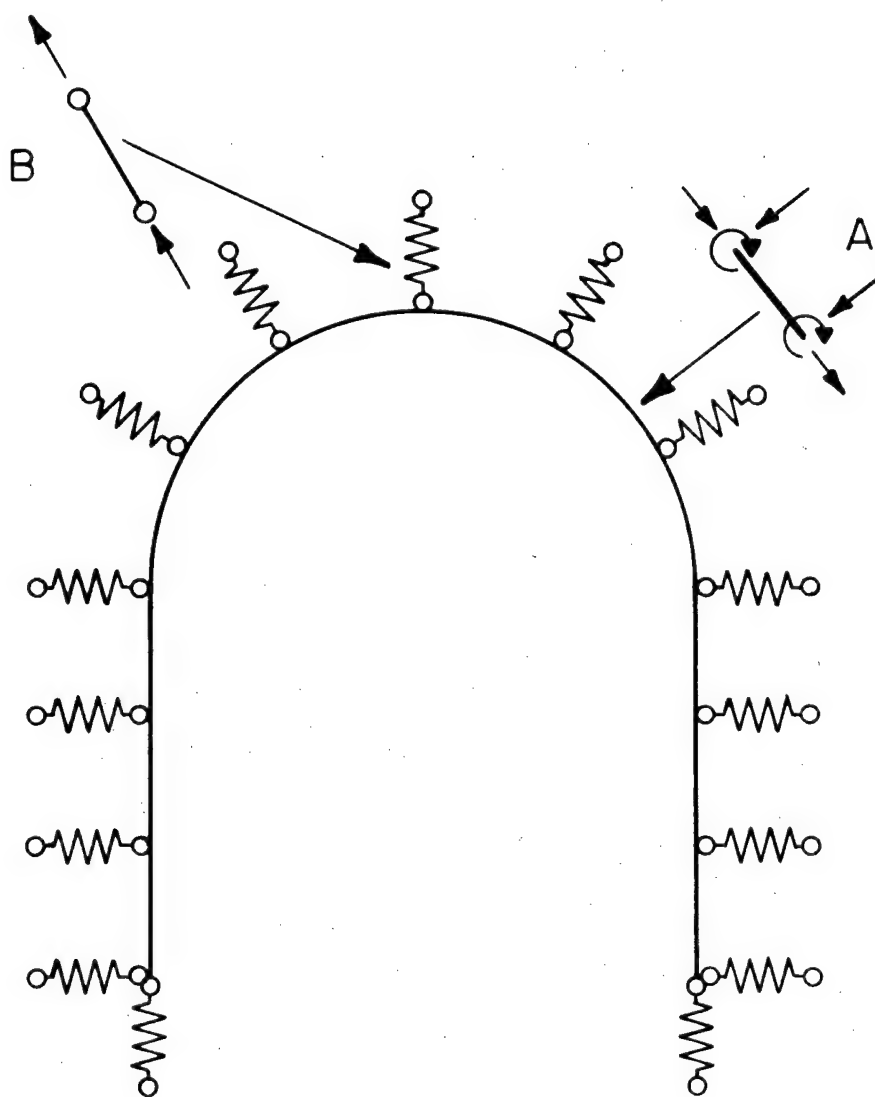


Figure III.6. Stiffness Model of a Blocked Steel Set.

A: Beam Element

B: Hinged Bar (Spring) Element

represented by a number of straight beam elements, and the wooden blocks by one-dimensional bar elements. These springs function in compression only. The external hinges on the spring element coincide with finite element mesh nodal points representing points on the tunnel circumference. The model implies that no shear stiffness exists between rock and steel. This can be justified by the very low combined shear strength of the wood-rock contact, the wood-wood contacts, the wood-steel contact and the wood shear stiffness (Proctor and White, 1968, pp. 208-209). This justification also implies that all set loads are in-plane loads, a conclusion that might be valid in clean-cut situations, with relatively large overbreak and consistent separation between rock and steel. Frequently this is not the case, particularly when the convergence is large and a soft ground embeds the steel set. In such situations there is no reason to presume that the rock displacement patterns are limited to two dimensions, and this is especially unlikely when the rock behavior is dominated by joints, shear zones or other discontinuities. The simplest evidence for out-of-plane loads is given by the turning over of steel sets.

The stiffness calculation will commonly be performed internally, and it is therefore necessary to adjust the input parameters in such a way that the pointwise, three-dimensional nature of the contact between rock and steel set is accounted for. The simplest way to make this adjustment for the steel set itself is by using the properties of the steel set as installed, and multiplying the stiffness matrix of the surrounding rock mass with a thickness factor equal to the set spacing. The stiffness of the wood blocking can be estimated from the (usually flimsy) available information about block spacing, amount of overbreak, type of block build-up, and care exerted in the blocking point construction. Maintaining a constant distance between rock and steel set facilitates data generation, and therefore stiffness variations of the blocking points can best be entered as variations in area and in elastic modulus. It is likely that a statistical variation of such parameters, based upon a sufficiently large number of observations of blocked steel sets, could produce a range of blocking point types and spacings that covers common practice.

Of particular significance in the analysis of

a horseshoe-shaped steel set as shown in Figure III.6 is the characterization of the footing spring. This footing spring is a very simple symbol for a complex structural component consisting of the connection between the steel set and the wall plate, the wall plate itself, what frequently amounts to not much more but a very wet layer of disintegrated rock, and finally the floor rock itself, more or less scattered depending upon the amount of explosives used to avoid tight corners. The footing stiffness can have a dominant influence upon the overall vertical stiffness of the support. This is particularly so because it is not uncommon that footings have less strength than the sets resting on them. Some examples of situations where this condition exists can be seen in Proctor and White (1968), pp. 84, 86, 126. A case of wall plate collapse is described by Hopper, et al. (1972). Numerous factors complicate a straightforward definition of the footing spring, but they all tend to indicate that this spring, unless its real equivalent is carefully designed and built, will be of lower strength, will be non-linear and will be of greatly reduced stiffness in comparison with the steel set resting on it.

III-3.3.3. Stiffness model of shotcrete support. The interface modeling problem for a shotcrete support is likely to be nonexistent in most situations where shotcrete can be applied successfully. In such situations the assumption of complete displacement continuity between rock and support is probably realistic. This eliminates the interface modeling problem, but by the same token greatly complicates the overall support modeling problem. Because shotcrete is usually sprayed as close to the face as possible, the problem of the initial loading sequence is generally three-dimensional. Because of the shear stiffness between rock and support tangential load components, in-plane as well as out-of-plane forces do exist. Moreover, the major three-dimensional effects coincide with the period of rapid change in stiffness of the shotcrete layer. An additional problem, of main but not exclusive interest in blasted tunnels, is posed by surface irregularities. It is next to impossible to model all irregularities in detail. But when they have a major effect upon the shotcrete behavior (e.g., Mahar, et al., 1972, p. 675) a model that entirely negates their influence is obviously inadequate.

III.3.3.4. Cast-in-place concrete. Pouring of concrete generally proceeds only after the stability of the tunnel has been guaranteed, at least temporarily. If the temporary support is left in place, unchanged, during the concreting operation, loading of the concrete liner will occur only when a stiffness change develops in any of the components of the statically indeterminate structural system. Concrete support loading is therefore essentially a time-dependent phenomenon.

The interface between cast-in-place concrete and rock will greatly depend upon the construction techniques employed during casting. In any event, a complete displacement continuity between rock and concrete (as assumed for example by Zienkiewicz, et al., 1968) is unlikely to exist. The most obvious reason for this is the almost unavoidable gap between rock and concrete in the roof following concrete settlement, and the all-around influence of shrinkage. With the growing tendency to avoid the labor costs associated with removing the wood blocks, and the use of longer telescoping concrete forms it becomes more difficult to assure a homogeneous distribution of concrete around the entire tunnel periphery.

For these reasons, and given the lack of published field information, the contact problem for a concrete liner remains largely an unknown quantity. Reasonable assumptions for a first approach to an analysis are that the shear stiffness of the contact will be very low, and that numerous gaps will cause a quite erratically variable normal stiffness distribution, with very low normal stiffness likely during the initial tunnel convergence following concreting.

III-3.3.5. Rock bolt model. The interaction between mechanical bolts and rock is determined by the strength of the anchor and of the bearing plate contacts. A realistic model must allow slip or crushing at an appropriate stress level.

The interaction between grouted bolts and rock is determined by the shear stiffness along the bolt of the grout-rock and grout-bolt contact as well as by the shear stiffness of the grout itself. The relative displacements allowed by these shear elements determine the induced stresses, and thus the stabilizing effect of the bolts. The relative displacements depend on the quality of the contacts, and this is likely to depend upon

rock type, precision of the drilled hole and workmanship quality.

A detailed stiffness model of a bolt would require a very large number of elements to represent the great stiffness variations between steel, grout and rock that occur over very short distances, and would have to be three-dimensional.

III-3.3.6. Concluding remarks on the support-rock interface model. The connecting elements, or the absence thereof, between rock and support can be considered as an integral part of the support system if so desired. They can certainly not be treated as a fully known quantity, however, but are more likely to be very variable and frequently unknown parameters. This obviously does not mean that their importance can be neglected, but requires that a reasonable assessment be made of what range of stiffness parameters might characterize the interface.

As more sophisticated and costly analysis techniques are used it becomes necessary to include such variations more precisely if the improved techniques are to be truly as realistic as they are assumed to be. The above discussion centered on

the problems this creates for some of the commonly used support systems. Stiffness analysis is a powerful tool, and in its most advanced forms can deal with the problems. This does not alleviate the problem of obtaining adequate information, in fact, as the model becomes more comprehensive and complicated the input information problem becomes more acute. This does not negate the value of the analysis method for studying the significance of the various parameters, but its efficient use as a design tool requires parametric analyses in order to determine what are the truly important parameters.

#### III-4. Stiffness Analysis of Tunnel Support Loading Caused by Rock Failure

III-4.1. Introduction. The progressive loading of tunnel supports during the face advance is studied in two ways. In the first approach the three-dimensional problem is reduced to a two-dimensional one by considering an axisymmetric case. Tunnel and support are circular (or at least the tunnel support stiffness can be reduced to an axisymmetric expression), the stressfield is hydrostatic, at least in the plane perpendicular to the tunnel axis, and gravity effects are neglected.

This model is a direct generalization of the analysis in Chapter II.

In the second approach a plane strain finite element model is used. The boundary conditions are changed sequentially so that an approximate simulation of the three-dimensional face-influence is made.

#### III-4.2. Influence of the Face Distance Upon Support Loading and Rock Failure.

III-4.2.1. Introduction. In most theoretical analyses of tunnel support loading the problem is treated as a two-dimensional one, in a plane perpendicular to the tunnel axis. Such an analysis is clearly inadequate to study the events near the face. When neither rock nor support undergo time-dependent stiffness changes, the final equilibrium state will be reached within a relatively short distance (corresponding to a few diameters at most) from the face. Even in the more general case where time-dependent stiffness changes do occur the initial loading can be influenced strongly by the three-dimensional nature of the problem.

Because of the nearness of the face (stiffness), the tunnel wall convergence, even in an

ideally elastic rock mass, approaches its full value only at some distance behind the face.

Terzaghi (1946, pp. 65-66) describes this support provided by the face in terms of a dome action, and visualizes a transition from a half-dome near the face to an arch at about one and a half times the advance length behind the face. Peck (1969, p. 249) suggests that the face influence can be taken into account by allowing for a fraction of the wall convergence to occur prior to the support installation, i.e., by giving the support load-deflection curve an offset from the origin. Lombardi (1972, pp. 373-374) assigns an independent support characteristic to the rock in the face, and includes it in the force-displacement diagram. Wagner (1970) and Daemen and Fairhurst (1970; 1972) use the results from axisymmetric finite element calculations to estimate the face influence on tunnel wall convergence along the tunnel, and the consequences for support loading. The geometry of the problem is entirely similar to that used by Desai and Reese (1970; also Desai and Abel, 1972, pp. 340-343) to study the development of plastic zones around deep boreholes.

analysis of rock failure near the face. Axisymmetric finite element analysis (Zienkiewicz, 1971, pp. 73-89) permits the study of the face influence in a circular tunnel with only minor modifications from plane two-dimensional analysis. A fully three-dimensional analysis, in contrast, requires a different order of magnitude in computer time and in programming effort.

The problem considered here is that of a circular cylindrical hole penetrating into a hydrostatically loaded cylindrical body, along its axis. The central part of the finite element mesh used for the analysis is shown in Figure III-7. The analysis was performed by incremental external loading of the cylinder. Two different types of material behavior during failure were used. These are illustrated in Figure III.8 by means of the corresponding sets of stress-strain-volume change curves. Data input for the finite element analysis was in the form of three straight line segments for each curve. All calculations of equivalent elastic constants were performed internally, according to the orthotropic cylindrical model described in Appendix B-5. An independent check on the positive definiteness was made prior to the

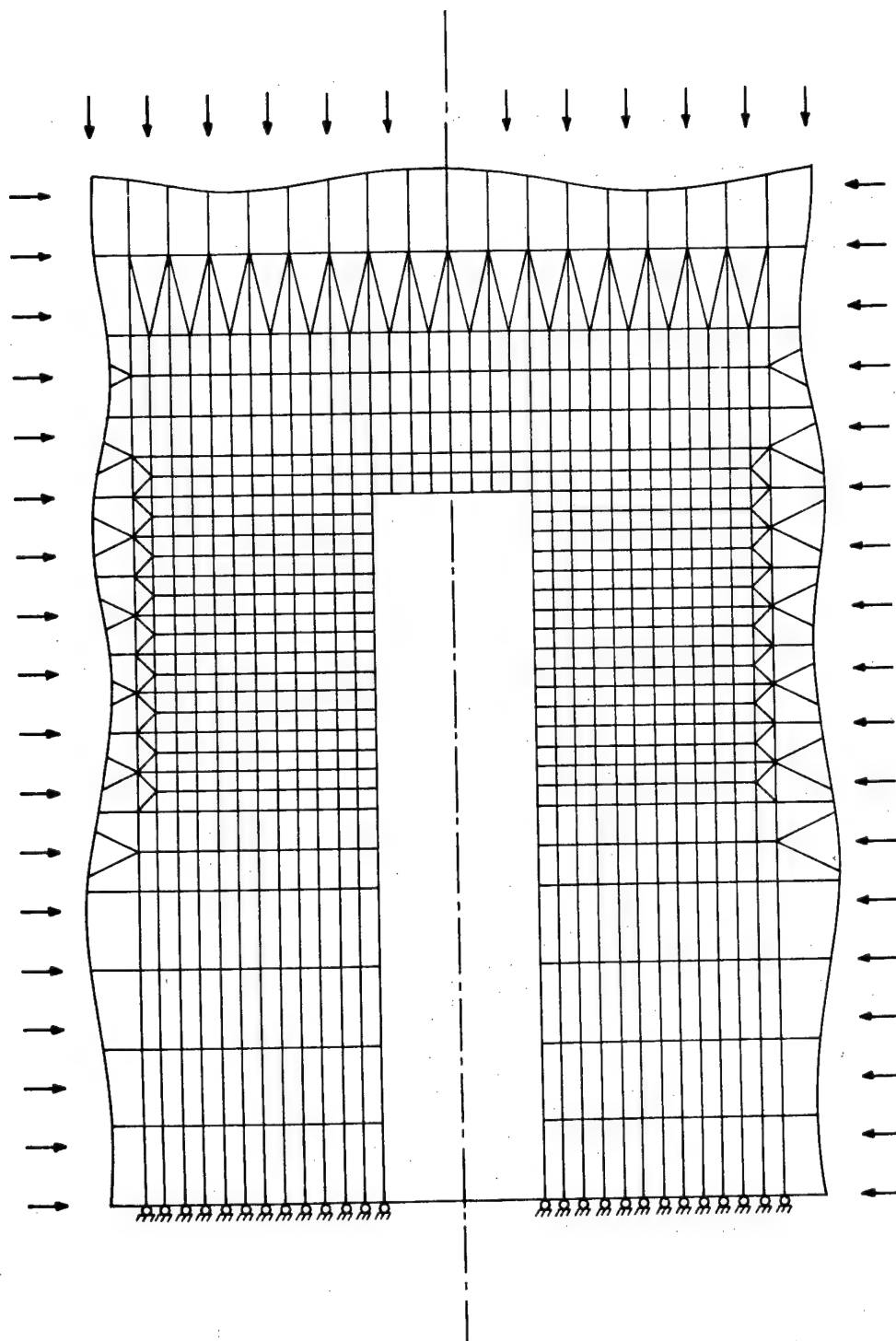


Figure III.7. Central Section of the Axisymmetric Finite Element Mesh used for Figures III.9 Through III.23.

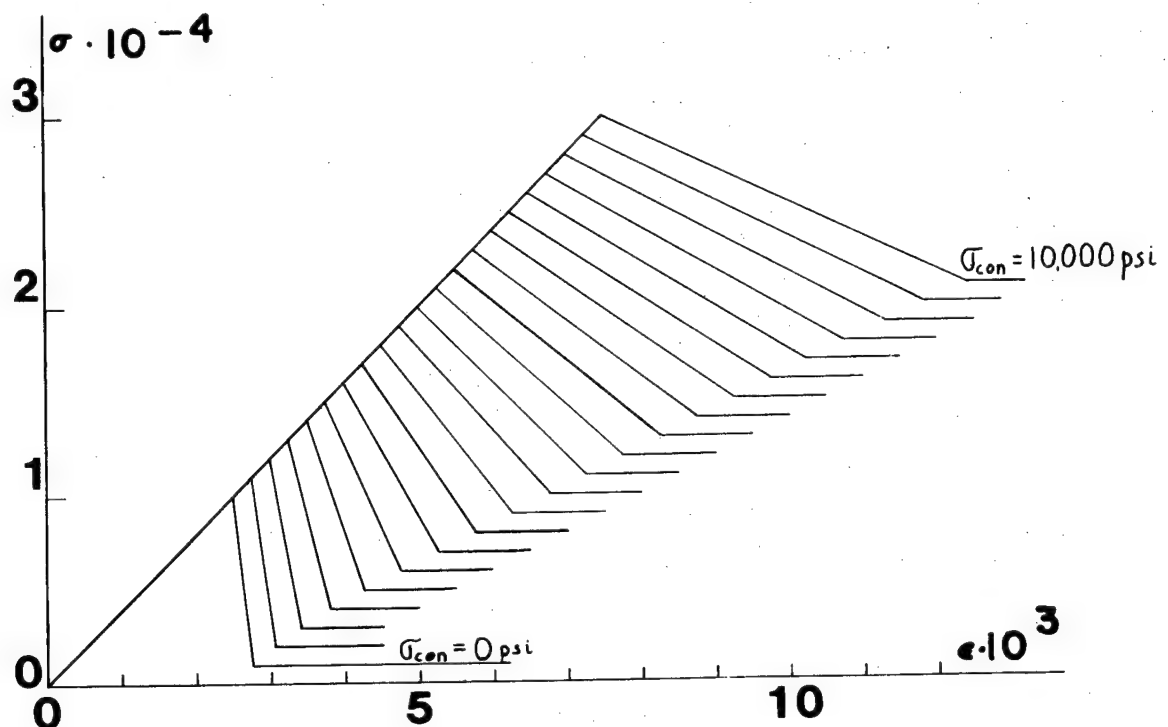


Figure III.8a. Axial Stress-Strain Curves used in the Rock Model for the Calculations of the "Brittle" Failure Patterns Plotted in Figure III.9, Lower Figure at each Loading Step. Confining Pressures Ranging from 0 psi up to 10,000 psi, in steps of 500 psi.

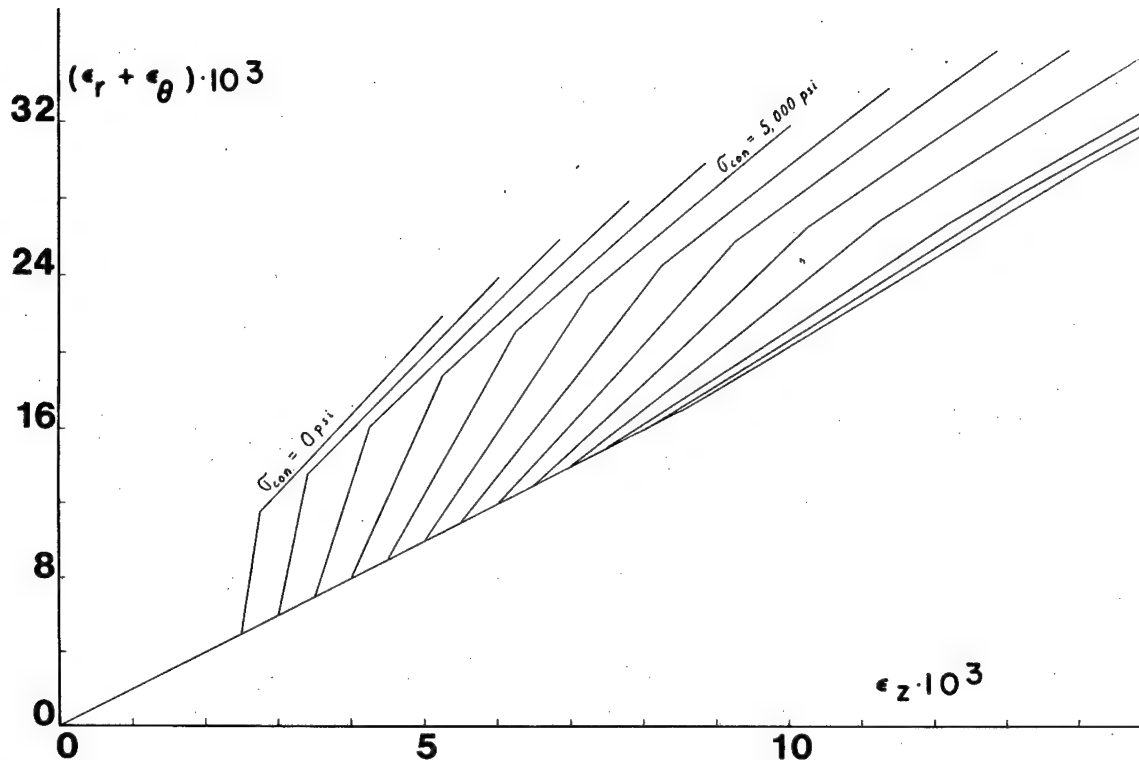
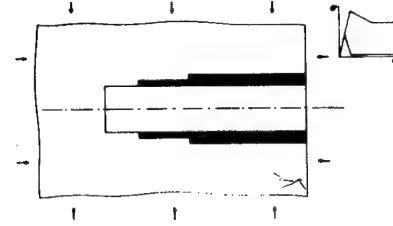
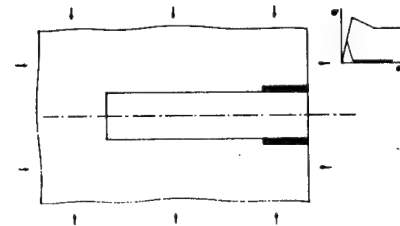
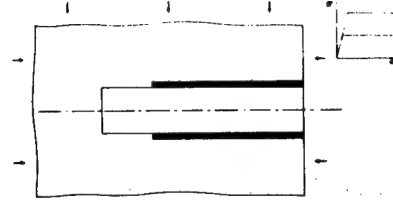
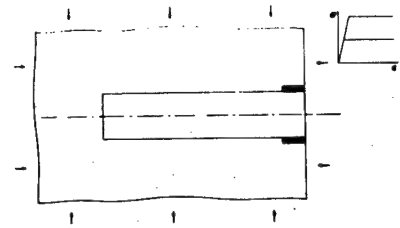


Figure III.8b. Lateral Strain Versus Axial Strain Curves used in the Rock Model for the calculations of the "Brittle" Failure Patterns Plotted in Figure III.9. Curves are associated with Figure III.8a, but for confining pressures from 0 psi up to 12,000 psi, increments of 1,000 psi.

finite element analysis, and it was found that satisfactory results were obtained by selecting parameters  $\alpha = 0$  and  $\gamma = 100$ .

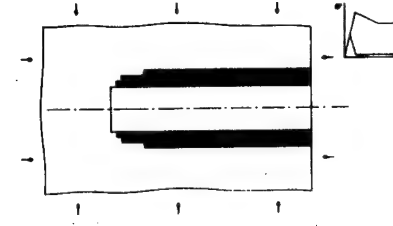
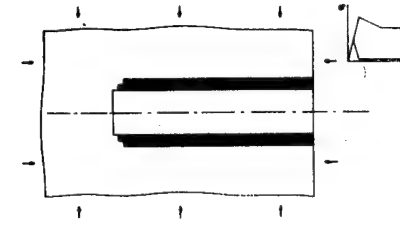
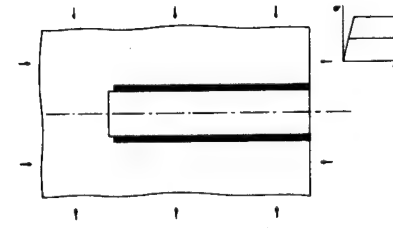
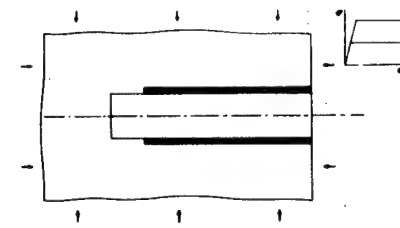
The progressive development of the failure zone during incrementally increasing external displacements is shown in Figure III.9. On Figure III.10 the tunnel wall displacement (equal to half the tunnel convergence) is shown along the tunnel axis, for identical external displacements, in the assumption that the rock remains elastic and in the assumption that the rock fails.

III-4.2.3. Implications of axisymmetric face influence analysis for support loading. A qualitative summary of the failure development near the face is given on Figure III.11. Two basically different types of behavior are shown. In the first type the integrity of the face is essentially maintained. The full development of the broken zone occurs then only well behind the face, because the stiffness of the face rock prevents the development of large stress differences in that area. On the other hand, when the face stiffness decreases substantially, e.g., because rock blocks in the face are permitted to slip out, a large fraction



Loading Step A

Loading Step B



Loading Step C

Loading Step D

Figure III.9. Failure Zone Near the Tunnel Face  
for Increasing Field Stress and  
for "Pseudo-Plastic" or for  
"Failing" Rock Behavior.

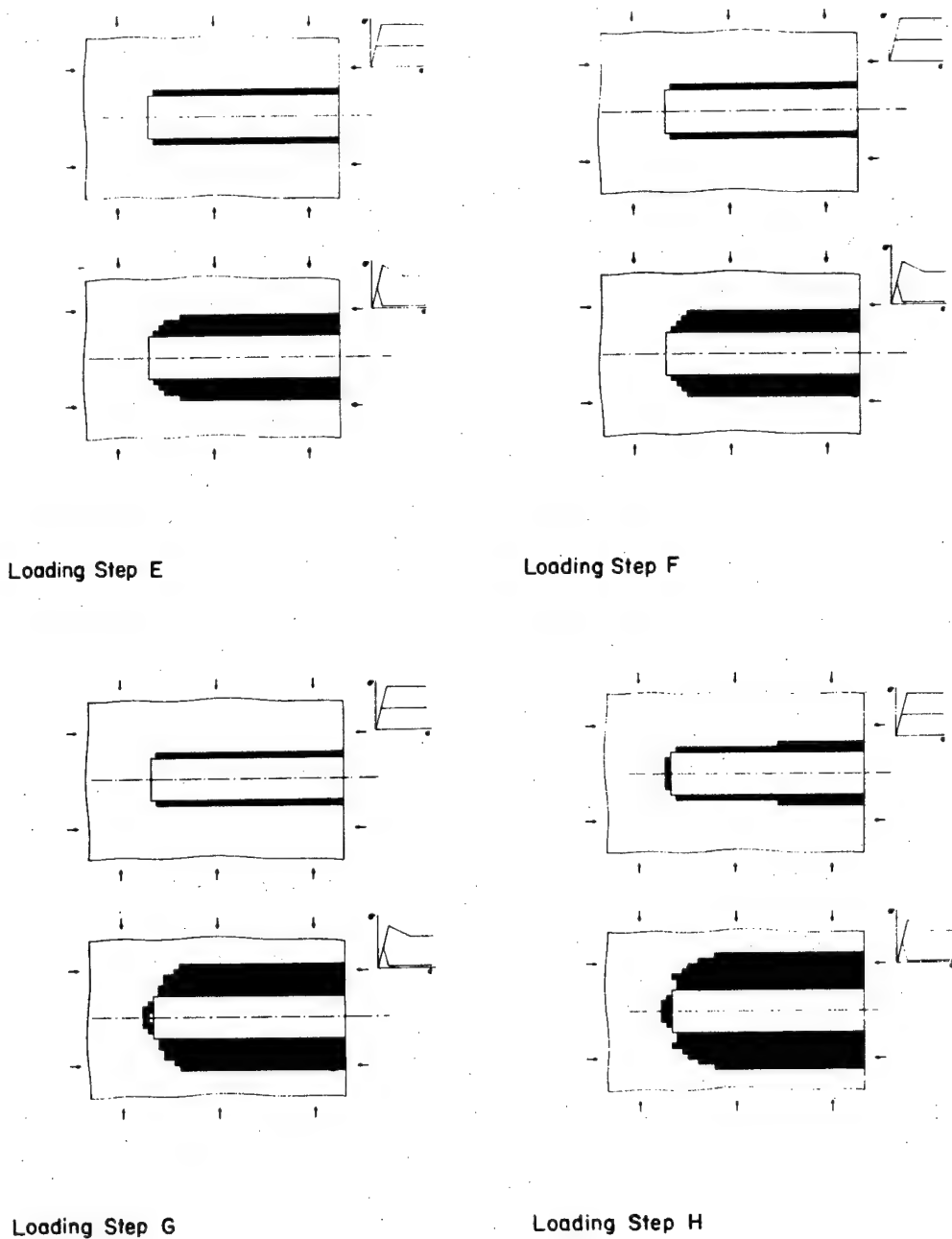


Figure III.9. Failure Zone Near the Tunnel Face  
(cont.) for Increasing Field Stress and for  
"Pseudo-Plastic" or for "Failing"  
Rock Behavior.

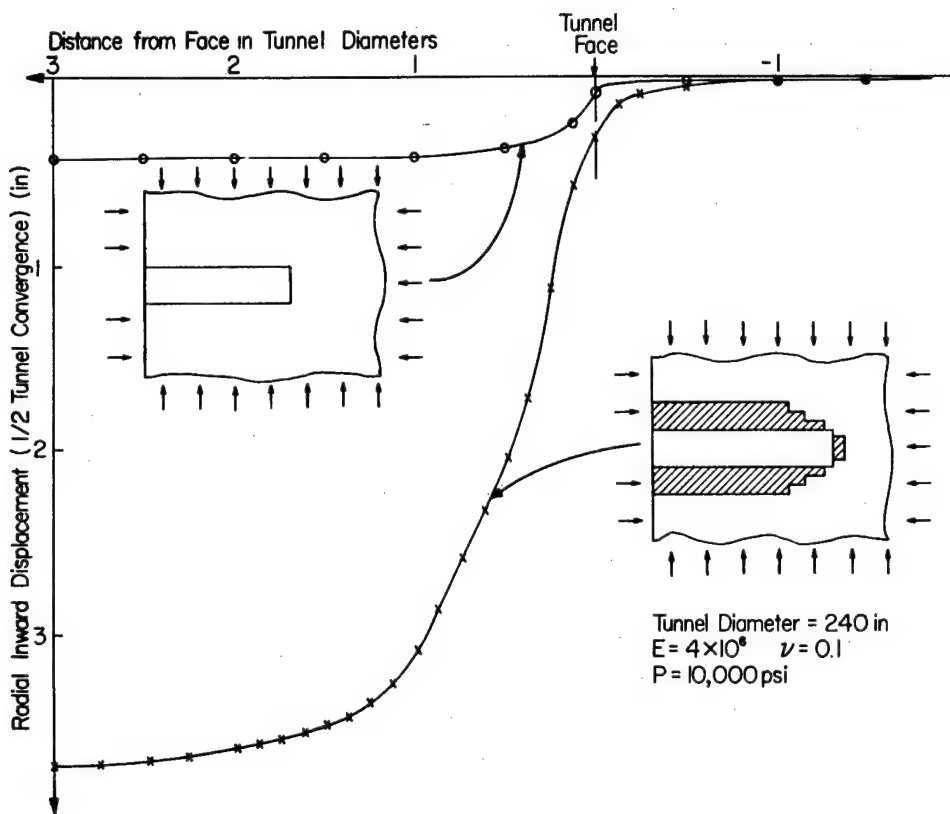


Figure III.10. Tunnel Wall Displacements Near the Face in Elastic Rock and in Failing Rock.

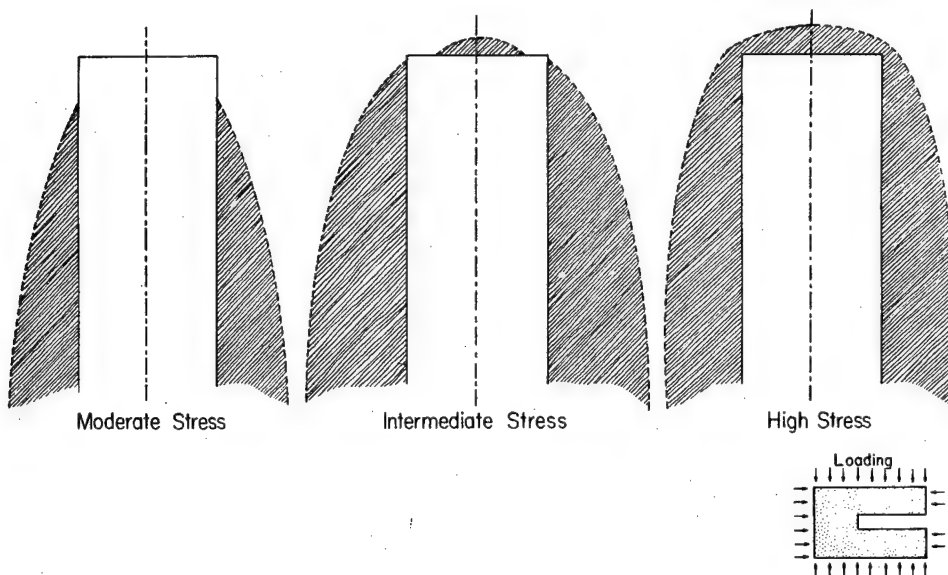


Figure III.11. Schematic Summary of Failure Zones Near a Tunnel Face for Increasing Ratios of the Field Stress to the Rock Strength.



Figure III.12. Typical Fracture Trace on Plane Through Tunnel Axis, Navajo Tunnel No. 3 (After Sperry and Heuer, 1972).

of the failure zone can develop ahead of the face. When this implies a strength reduction of the wall rock to low residual values it means that the support system will not function in optimum conditions.

It is clear from Figure III.10 that the convergence and therefore the support loading path near the face strongly depends upon the rock behavior. In elastic rock nearly one-fourth of the ultimate convergence occurs ahead of the face, well over half within one-fourth of a diameter and over ninety per cent within one diameter from the face. This behavior can be altered radically when the rock does not remain elastic, and the mode of change will be contingent upon the face rock behavior.

When the face remains quite stiff during failure propagation, as in the example of Figure III.10, and failure develops exclusively, or nearly so, behind the face a very steep displacement gradient exists for the first diameter along the tunnel axis. Only a small fraction of the convergence occurs ahead of the face. Convergence has nearly reached its final value within one to two diameters behind the face. Support loading (and

thus the exerted support pressure) will be very sensitive to the distance of installation from the face .

At the other extreme, when the face is allowed to disintegrate, a very large fraction of the total convergence can occur ahead of the face. Support loading will then be rather insensitive to the distance of erection.

A qualitative analysis of face influence on support loading is possible in a very simple form for the case where the rock remains elastic. The influence of support stiffness, and of the distance from the face at which support is installed on its effectiveness will be illustrated here for the idealized case of a circular lining installed in perfect contact with the tunnel wall.

The final displacement  $u_f$  induced by driving a tunnel of diameter D in an (elastic) rock mass under hydrostatic pressure P is given by:

$$u_f = \frac{PD(1 + \nu_r)}{2 E_r} \quad (\text{III-4.1})$$

where  $\nu_r$  and  $E_r$  are the Poisson's ratio and the elastic modulus of the rock.

At a distance d from the tunnel face a circular support of external diameter D and thickness

t is installed (Figure III.13). As the face advances the tunnel walls at this point, if unsupported, would move inwards a distance  $u_d$ . This displacement can be expressed as a fraction of the total displacement,

$$u_d = X u_f = X \frac{PD (1 + \frac{\nu}{r})}{2 E_r} \quad (\text{III-4.2})$$

where X is a proportionality factor that can be derived from the tunnel wall displacements along the tunnel, results obtained from an axisymmetric finite element analysis (Figure III.14). As the face advances a radial contact pressure  $P_s$  builds up between rock and support. Under this contact pressure the inwards displacement at the rock-support contact of the circular cylindrical support is equal to:

$$u_s = \frac{P_s R (1 + \frac{\nu_s}{r})}{E_s [R - (R-t)]^2} [R^2 (1 - 2 \frac{\nu_s}{r}) + (R-t)^2] \quad (\text{III-4.3})$$

where  $R = D/2$  and  $\nu_s$  and  $E_s$  are the Poisson's ratio and the elastic modulus of the support cylinder.

Under this contact pressure  $P_s$  the rock mass will displace outwards (or the inwards displacement will be reduced) by:

$$u_f = \frac{P_s D (1 + \frac{\nu}{r})}{2 E_r} \quad (\text{III-4.4})$$

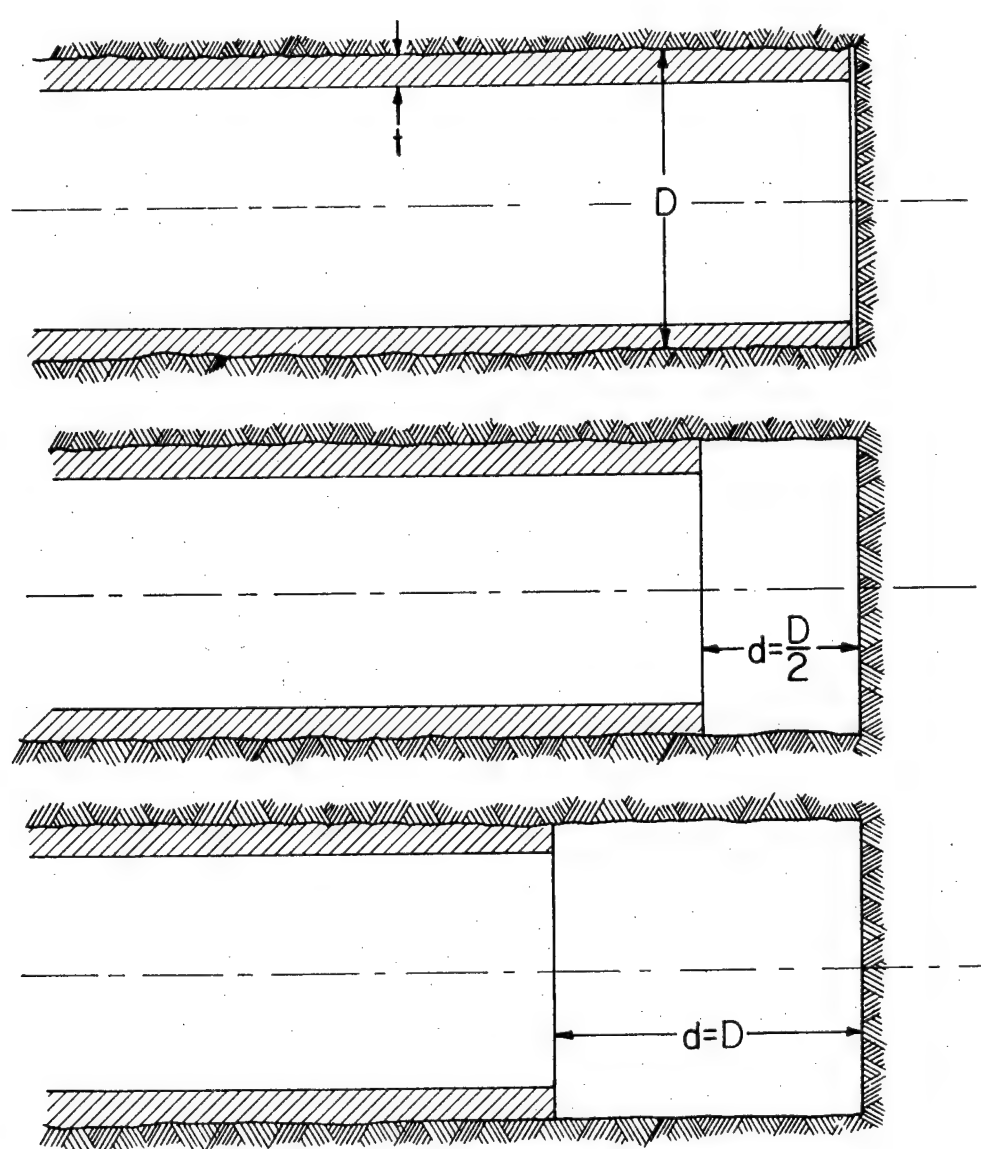


Figure III.13. Geometry of the Problem used to Study the Influence on Support Loading of the Support Stiffness and of the Distance from the Face at the Moment of Support Erection.

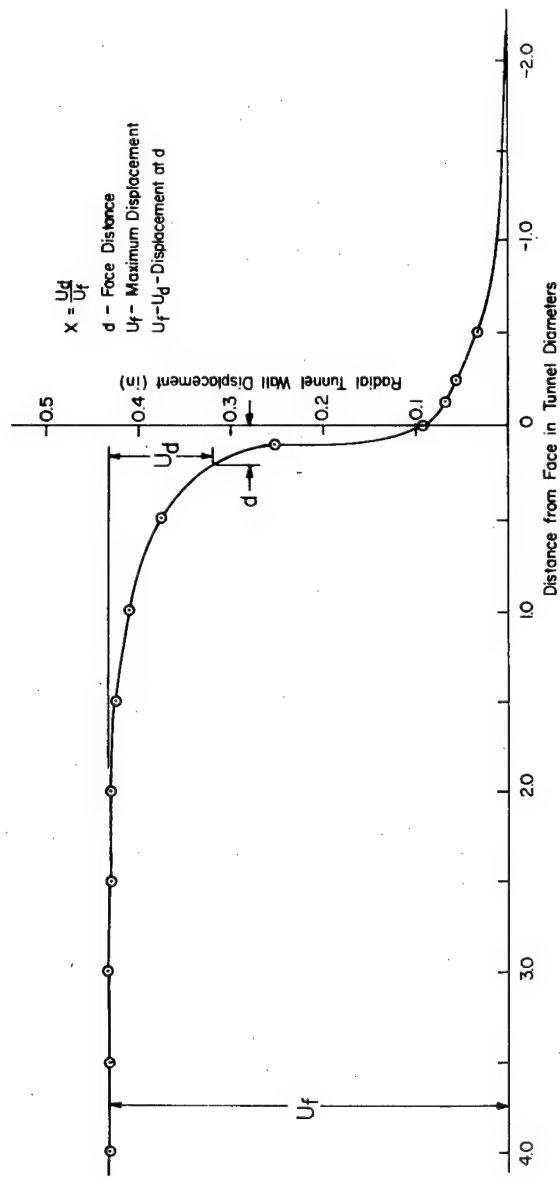


Figure III.14. Determination of the Proportionality Factor  $X$  used in the Calculation of the Influence on Support Loading of the Face Distance at the Point of Support Erection.

The total displacement that would occur, after the face has advanced to the point corresponding to support erection, if no support were installed, is equal to the sum of the displacement which does take place and the displacement which was prevented:

$$u_d = u_s + u_r \quad (\text{III-4.5})$$

Substitution in this equation of the expressions for the displacements results in the following relation for the support pressure  $P_s$  (relative to the virgin hydrostatic stress  $P$ ):

$$\frac{P_s}{P} = X \frac{1}{1 + \frac{\nu_s}{1 + \nu_r} \cdot \frac{E_r}{E_s} \cdot \frac{t}{R} \cdot \frac{(1 - 2\nu_s) + (1 - t/R)}{(2 - t/R)}}^2 \quad (\text{III-4.6})$$

This expression can be used to illustrate the influence of:

- i. Distance from the face of support erection.

The support pressure is directly proportional to  $X$ , and the rapid nonlinear decrease of this factor is obvious from Figure III.14. Although an extrapolation to a nonlinear situation is not straightforward, it would appear from Figure III.10 that for a situation in which most of the failure development takes place behind the face the support pressure would be even more sensitive to the face-

installation distance. The opposite would be true when large stiffness reductions are permitted within the face.

ii. Relative stiffness of rock and liner.

- a. Mechanical properties  $\nu$  and E.
- b. Liner thickness  $t/R$ .

In Figure III.15 the resulting pressure is plotted versus the distance from the face at which the support is installed. Figure III.16 shows the resulting support pressure and the maximum tangential stress in the support cylinder as a function of liner thickness. The vast majority of real support systems would fall in between  $t/R = 0.05$  and  $t/R = 0.25$ , more densely concentrated around  $t/R = 0.15$ .

Several conclusions can be drawn from these graphs. The extrapolation of these conclusions to real tunnel support problems must be tempered by an awareness of the idealizations implicit in the derivation of the results.

1. The same support pressure can be obtained with support systems of different stiffnesses (e.g., different thickness) when installed at different distances from the face.
2. The earlier a support is installed the higher support pressure it will provide (and the

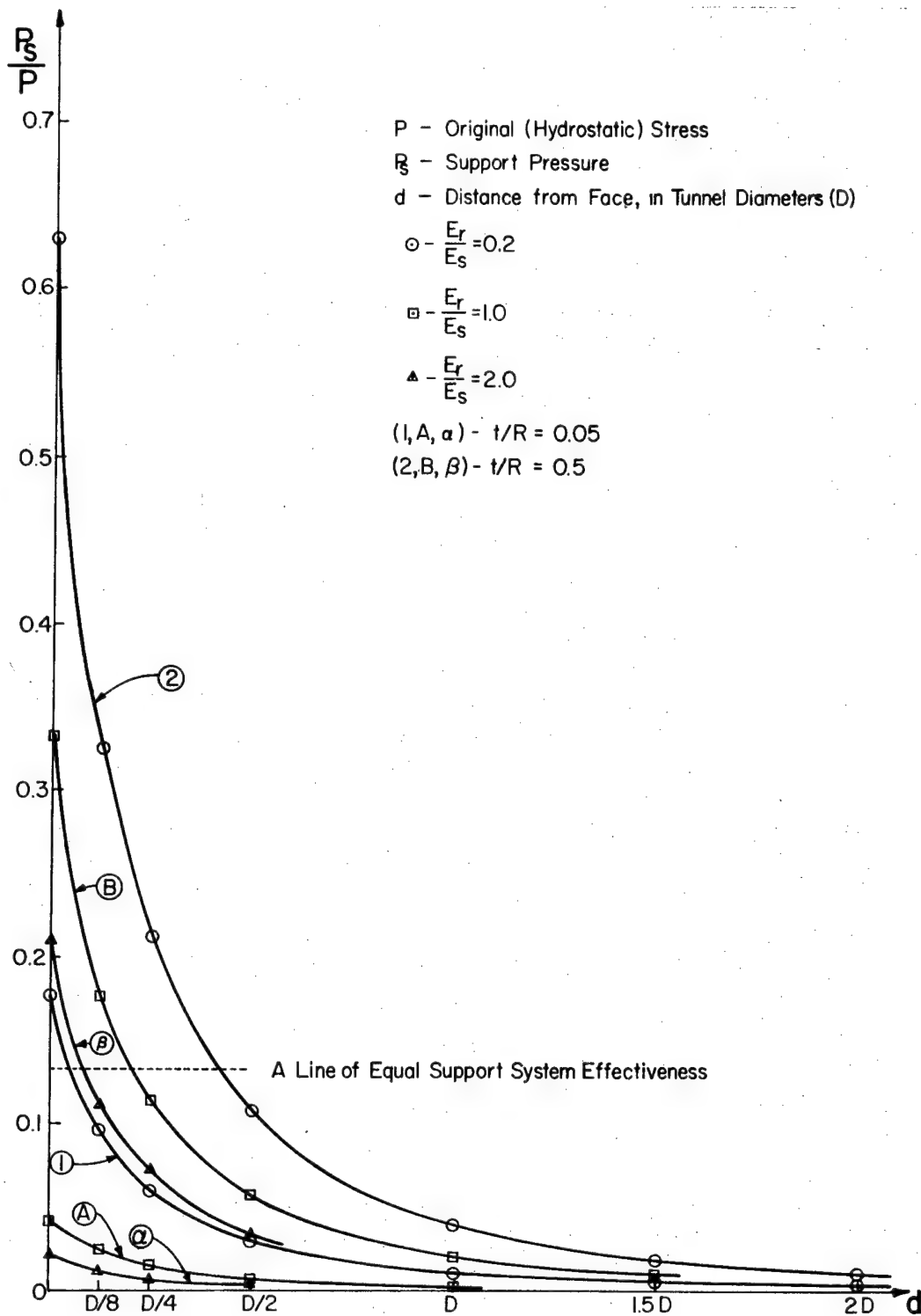


Figure III.15. Support Pressure (as a Fraction of the Pre-mining Hydrostatic Stress) Versus Distance from the Face at the Moment of Support Erection for Various Values of the Support Stiffness (Thickness  $t$  Relative to Tunnel Radius  $R$  and Support Modulus  $E_s$  Relative to Rock Modulus  $E_r$ ).

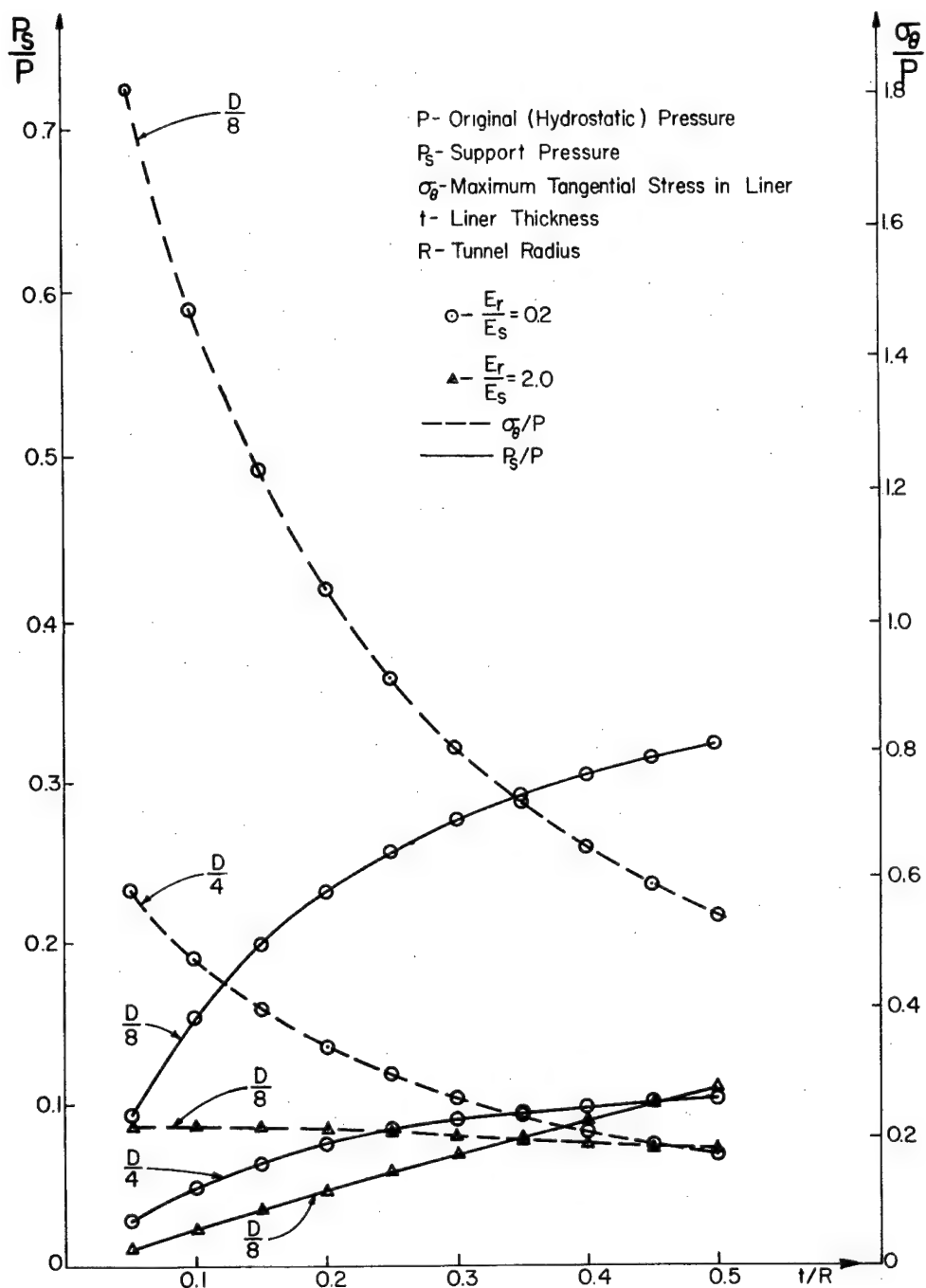


Figure III.16. Support Pressure and Maximum Tangential Stress in the Support Versus Support Thickness for Two Distances ( $D/4, D/8$ ) from the Face at the Point of Support Installation.  $D$  is the tunnel diameter.

higher the load it will be subjected to). Depending upon the type of rock mass behavior, i.e., the rate of strength loss of the rock with increasing inelastic strain, early installation of stiff supports will be good or poor practice.

3. The thicker a support installed at any particular location the smaller the maximum stress in it will be. This conclusion is true in this particular case where hydrostatic loading and perfect rock-support contact is assumed, so that no bending moments can develop.

4. The higher the stiffness of a support system relative to the rock mass stiffness the higher the developed support pressure will be. When the rock mass stiffness exceeds the support stiffness substantially (i.e.,  $E_r > 2 E_s$ ) the maximum stress in the liner cannot be reduced significantly by increasing the liner thickness.

The preceding analysis was made for a truly cylindrical support. By means of the axisymmetric support stiffness expressions derived in Appendix A-4 a generalization to and comparison of various support systems is straightforward.

The problem is less trivial when nonlinear behavior must be considered. It is then necessary

to simulate the actual mining sequence, i.e., to progressively eliminate elements from the central part of the mesh corresponding to the face advance and connect stiffness terms equivalent to (radially symmetric) support systems.

III-4.2.4. Face influence in non-homogeneous rock masses. In homogeneous rock masses the distance from the face at which a support is erected can have a major influence upon the exerted support pressure. It is pointed out by Lombardi (1974b) that the effectiveness of the face in providing "support" near the face depends upon the ability of the rock in that area to transmit shear stresses perpendicular to the tunnel axis. This ability is likely to be seriously impeded in fault zones and similar major inhomogeneities or discontinuities with low shear strength.

In the previous section it was emphasized that failure-induced face stiffness changes (or the absence thereof) will diminish (or amplify) the three-dimensional character of support loading. A similar influence can be expected when the tunnel face approaches and intersects rock formations of markedly different stiffnesses, e.g., dykes or shear zones.

These two modifications from the problem analyzed previously, due to variations in rock mass stiffness along the tunnel axis that are not induced by tunneling, can be analyzed with the elastic axisymmetric finite element method. To use this method it is necessary to limit the problems to the highly idealized situation where it is assumed that the tunnel is driven perpendicular to the rock formation contacts. A schematic representation of the problem as analyzed is given in Figures III.17a and b. The first figure illustrates the problem where the face approaches a rock formation of very different characteristics, while the second figure is an idealized case of a narrow stiff or soft zone intersecting an otherwise homogeneous region.

The (radial) displacements at the tunnel wall radius along the tunnel axis are plotted in Figure III.18 for two different boundary conditions. In the first one external stress boundary conditions ( $\sigma_r = 12,000$  psi;  $\sigma_z = 4,000$  psi) were imposed on the cylinder. In the second one external boundary displacements were imposed such that for a homogeneous solid cylinder ( $E_1 = E_2 = 10^6$  psi;  $\nu_1 = \nu_2 = 0.2$ ) a hydrostatic stress state ( $\sigma_r =$

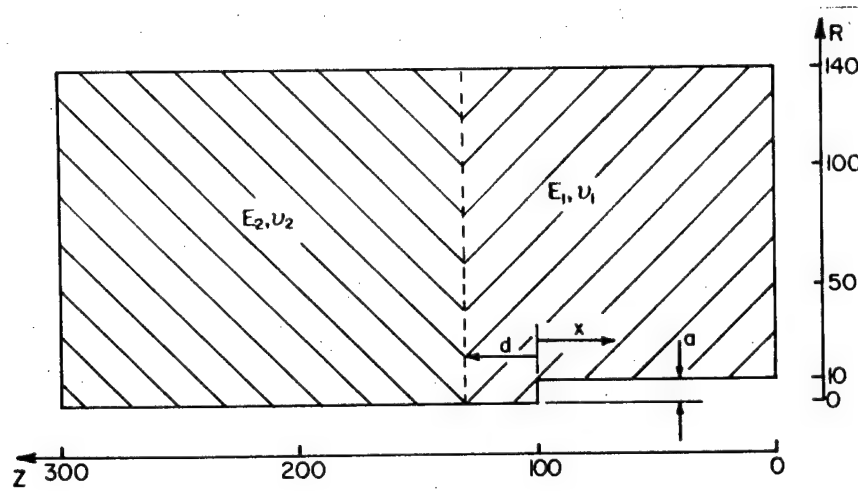


Figure III.17a. Geometry of the Problem Used to Study the Convergence Near the Face When a Tunnel Approaches a Contact Between Two Rock Zones with Different Stiffnesses.

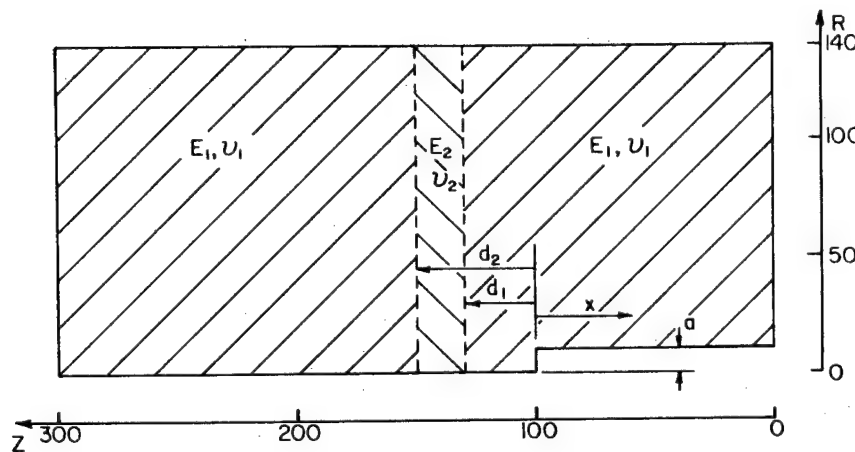


Figure III.17b. Axisymmetric Problem Used to Study the Influence of a Narrow Zone of Different Rock on the Tunnel Convergence Near the Face.

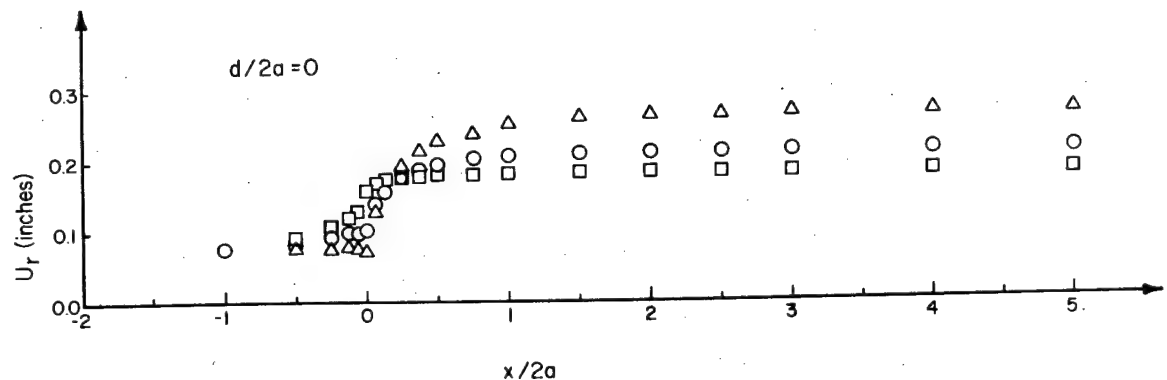
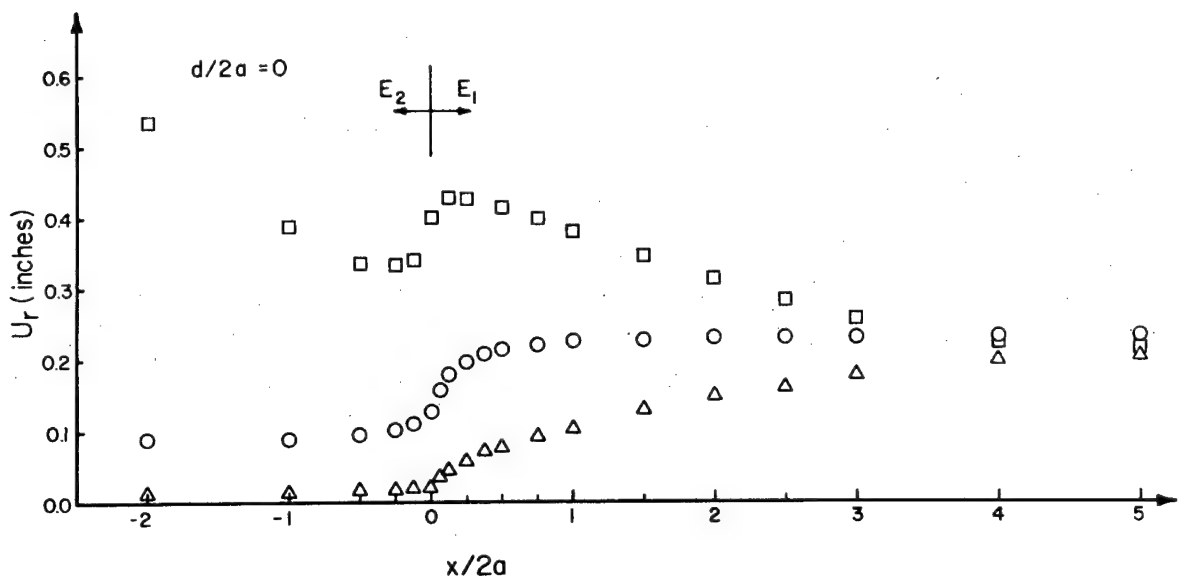


Figure III.18. Radial Displacement  $U_r$  at the Tunnel Periphery Versus the Distance from the Face  $x$ , when the Face is at the Contact Between Two Rock Masses of Different Stiffness ( $d = 0.$ )  
 Triangles:  $E_2 = 10 E_1$  Circles:  $E_2 = E_1$   
 Squares:  $E_2 = E_1/10$

Top: Hydrostatic pressure applied.

Bottom: Displacements imposed at external boundaries

$a$ : tunnel radius

$d$ : distance between rock contact and tunnel face

$\sigma_e = \sigma_z = 12,000$  psi) would result. For both these figures the face has just reached the contact area between two large zones of different stiffnesses ( $d = 0$ ). The corresponding result for a homogeneous rock mass is included to facilitate comparisons. As would be expected, a "stiff" face tends to delay convergence, while convergence runs ahead of the tunnel when the face is "soft." When the displacement distribution for the non-homogeneous cases is compared with that for the homogeneous problem it is clear, especially on the lower figure, that a large fraction of the final displacement occurs ahead of the tunnel when the face is very soft compared to the tunnel walls, while the opposite is true when the face is relatively stiff.

A recurring peculiarity of the results is the nonmonotonic displacement distribution observed in the top graph on Figure III.18. This suggests that at some points near the interface between the rock types an outwards radial displacement might be induced by further tunnel advance (as can also be seen on Figure III.19). Although such movements have been observed (Müller, et al., 1970; Lombardi, 1974), there is an element of the

unexpected in this result. It is at least somewhat influenced by the boundary conditions, but it is not obvious that it would be eliminated by modeling the mining sequence rather than loading a partly hollow cylinder, because that would not eliminate the necessity to decide upon either stress or displacement boundary conditions. The physical interpretation of the result is complicated by its three-dimensional nature and by the influence of the large shear stresses along the contact between the two rock types. Before making precise numerical conclusions from these results it would seem necessary to study in more detail the influence of such factors as boundary conditions and the sequence in which they are imposed as well as that of the mesh size along the contact area and possibly the method of solving the stiffness equations.

The next sets of Figures (III.19 and III.20) present a series of results for situations where the face is at various distances from the contact plane. Deviations from the homogeneous case are rather minor when the contact plane is more than one tunnel diameter ahead of the face or once the tunnel has advanced more than two diameters beyond

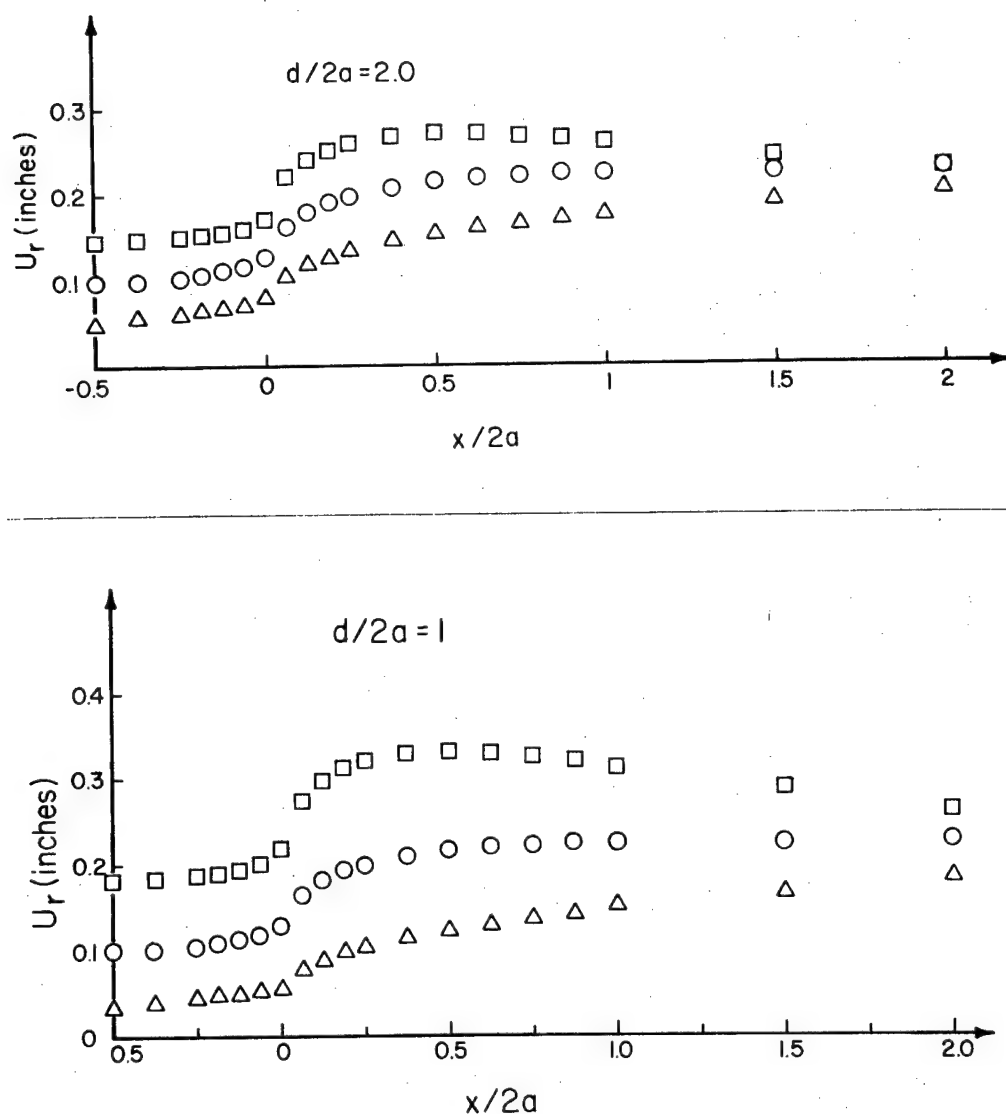


Figure III.19. Radial Displacement  $U_r$  at the Tunnel Periphery Versus the Distance  $x$  from the Face for Various Values of the Distance  $d$  from the Face to the Contact Between Two Rock Zones. A hydrostatic pressure is applied at the external boundaries.

Triangles:  $E_2 = 10 E_1$  Circles:  $E_2 = E_1$   
 Squares:  $E_2 = E_1/10$

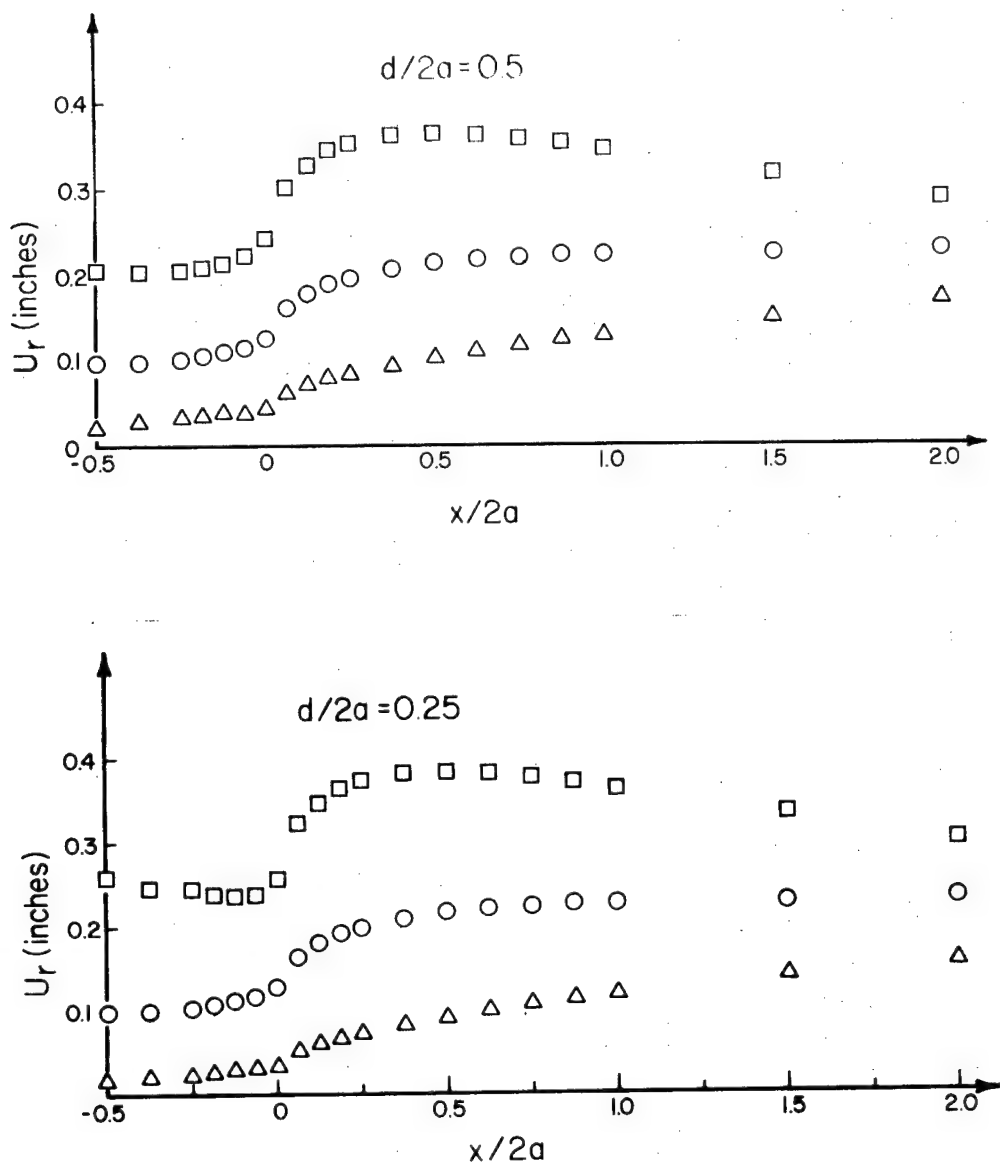


Figure III.19. Radial Displacement  $U_r$  at the Tunnel Periphery Versus the Distance  $x$  from the Face for Various Values of the Distance  $d$  Between the Face and the Contact of Two Rock Formations.

A hydrostatic pressure is applied at the external boundaries.

Triangles:  $E_2 = 10 E_1$  Circles:  $E_2 = E_1$

Squares:  $E_2 = E_1/10$

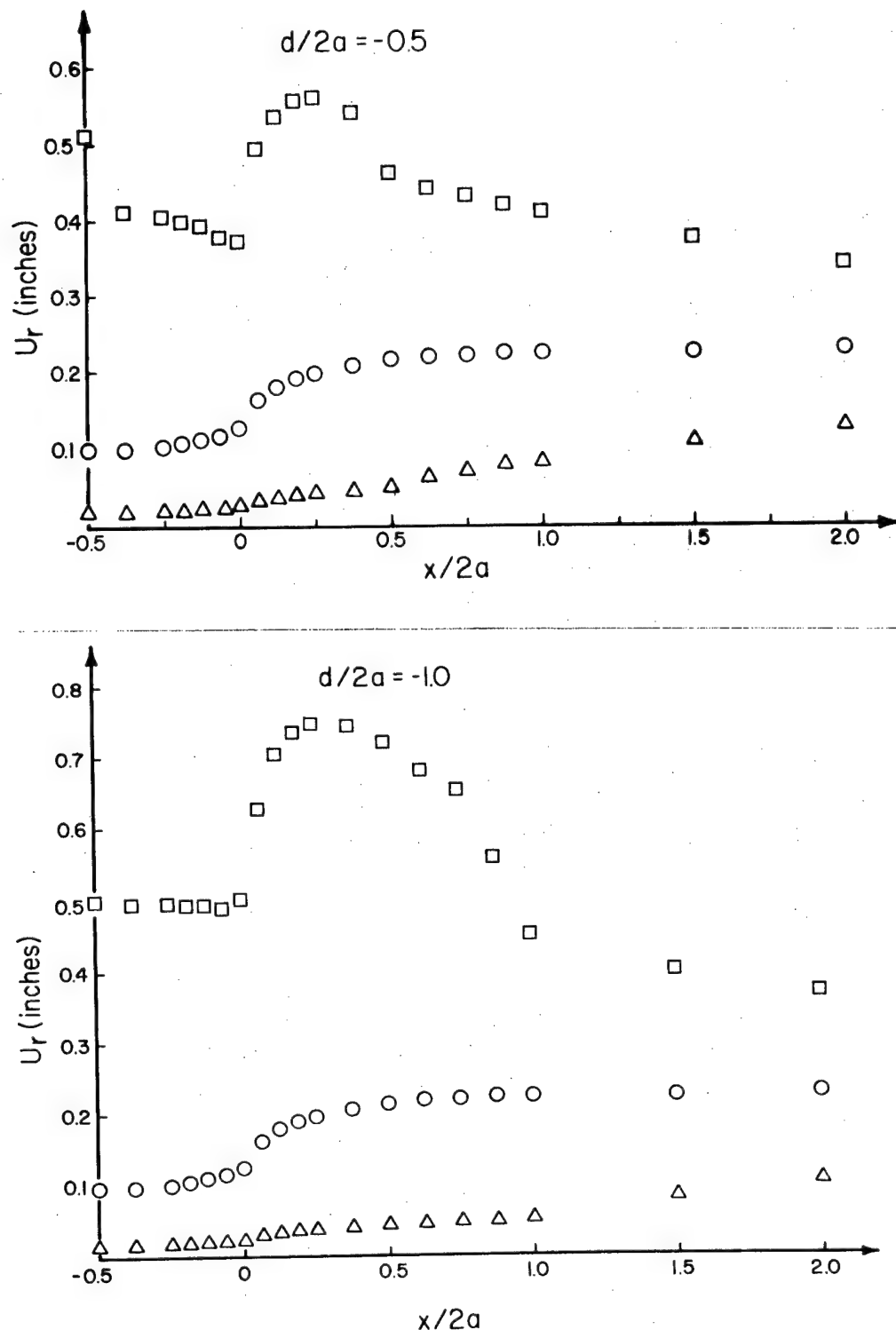


Figure III.19. Radial Displacement of the Tunnel Periphery Along the Tunnel for Different Distances Between the Face and the Rock Formation Contact. Applied hydrostatic pressure.

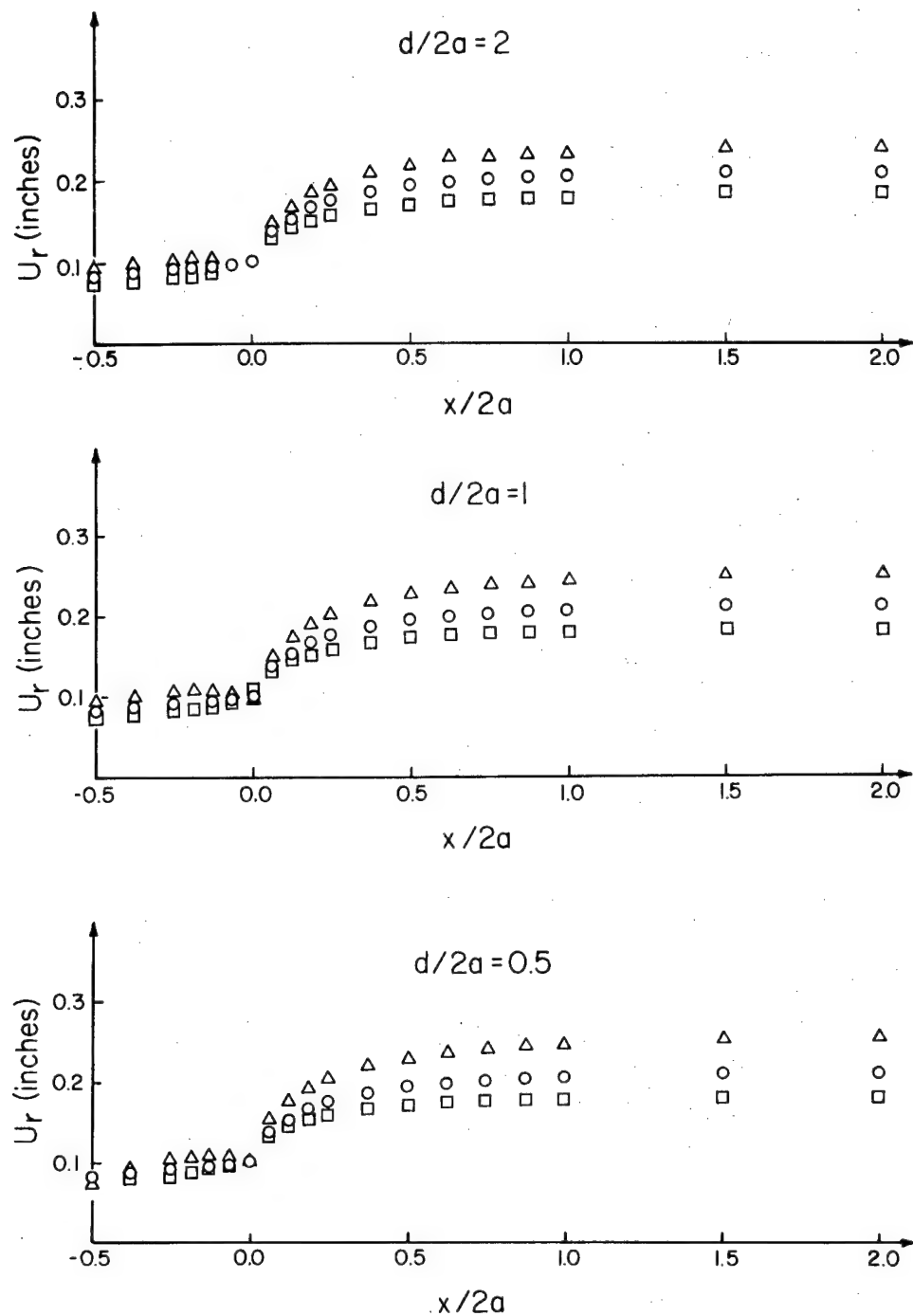
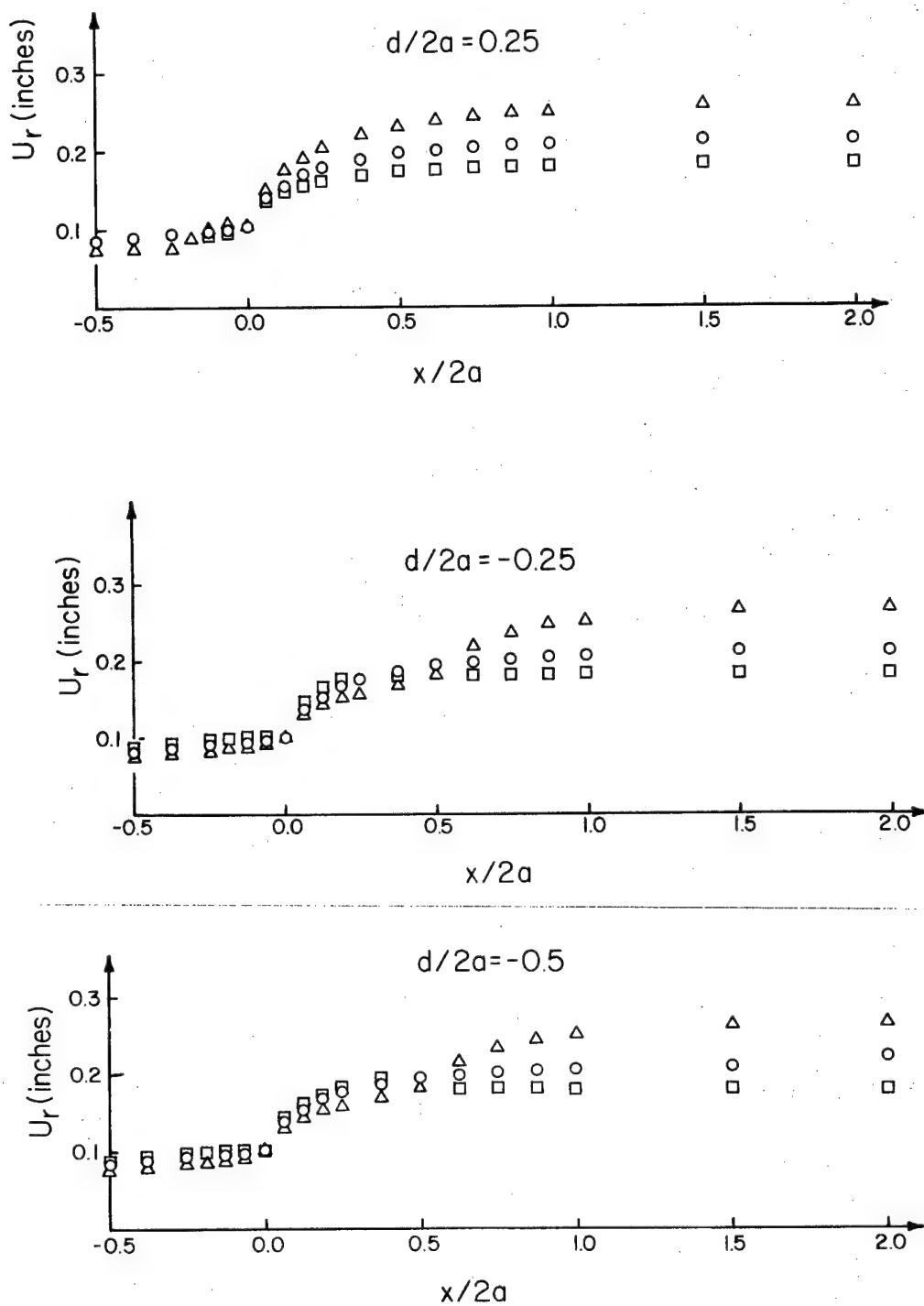


Figure III.20. Radial Displacement of the Tunnel Periphery Along the Tunnel for Different Distances from the Face to the Rock Formation Contact. Displacements imposed at the external boundaries.



**Figure III.20.** Radial Displacement of the Tunnel Periphery Along the Tunnel for Different Distances from the Face to the Rock Formation Contact. Displacements imposed at the external boundaries.

the contact plane. Because no limits are imposed in any of these calculations upon the shear stresses that can be transmitted along the contact plane it is likely that this represents somewhat of an upper bound upon the spatial extent of the influence from inhomogeneities. This is confirmed by the results from the analysis of a narrow zone of very different stiffness. These results are shown on Figure III.23. The displacement pattern near the face is markedly different from the one in homogeneous rock when the face is close to the soft or stiff zone. A soft zone in the face enhances convergence ahead of the tunnel. The difference drops off rather rapidly when the face is more than a few diameters away from the soft (or stiff) band.

Figure III.22 gives the radial displacement for a point on the contact plane and for two points on either side of it as a function of the face distance, i.e., as the face approaches and passes by the points. This kind of a plot could be used to study support loading in a similar way as the analysis given in section III-4.2.3 for the homogeneous problem. It is obvious that support loading will be much more sensitive to the face distance

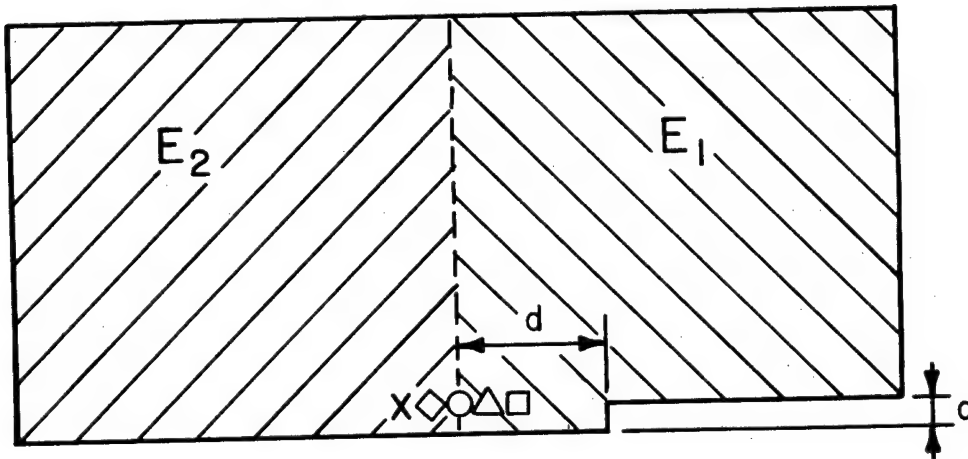


Figure III.21. Geometry of the Problem Used for the Convergence Calculations Plotted in Figure III.22.

III-96

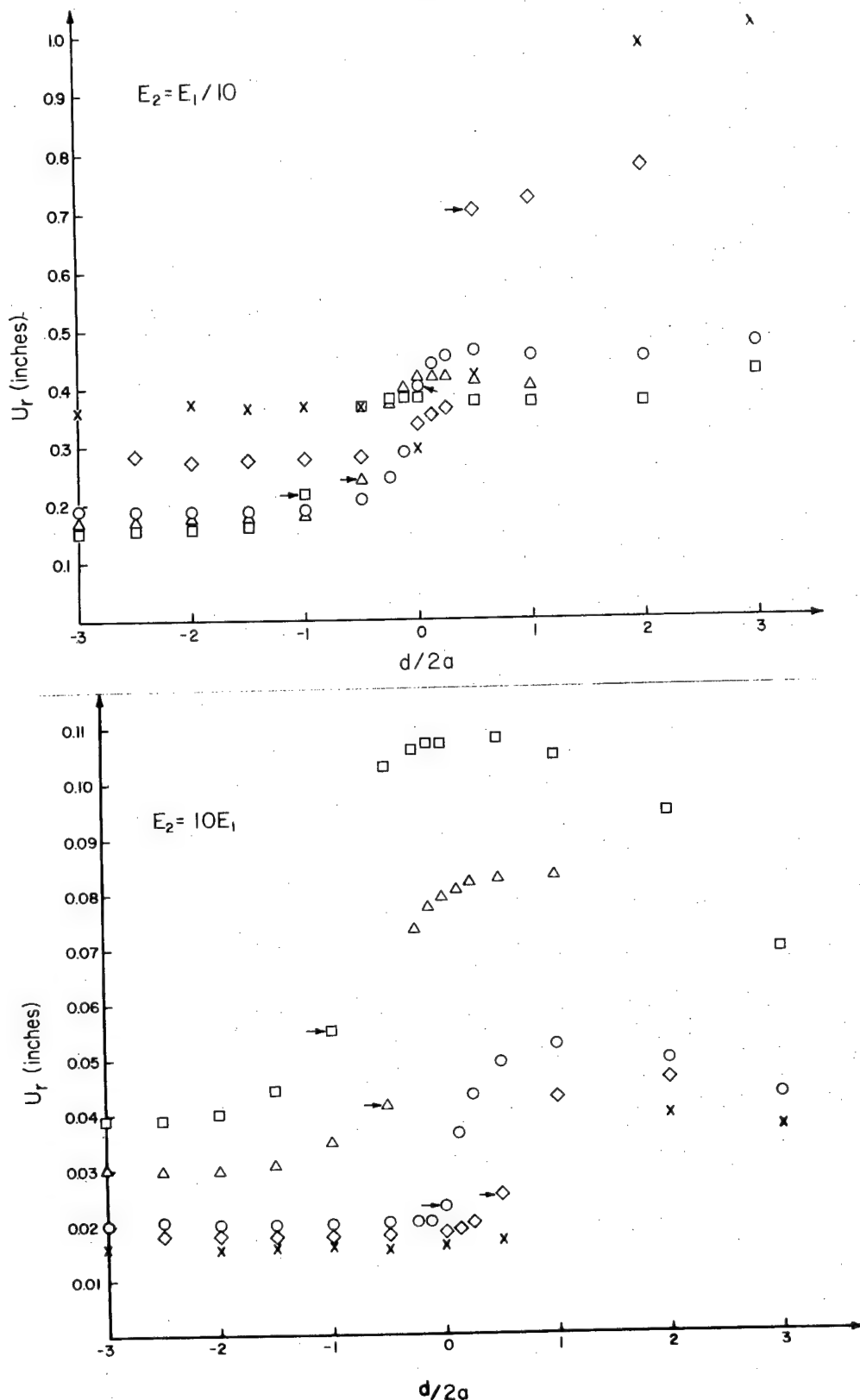


Figure III.22. Radial Displacement Versus the Distance from the Face to the Contact Between Two Rock Zones for Five Points on and Near the Contact.

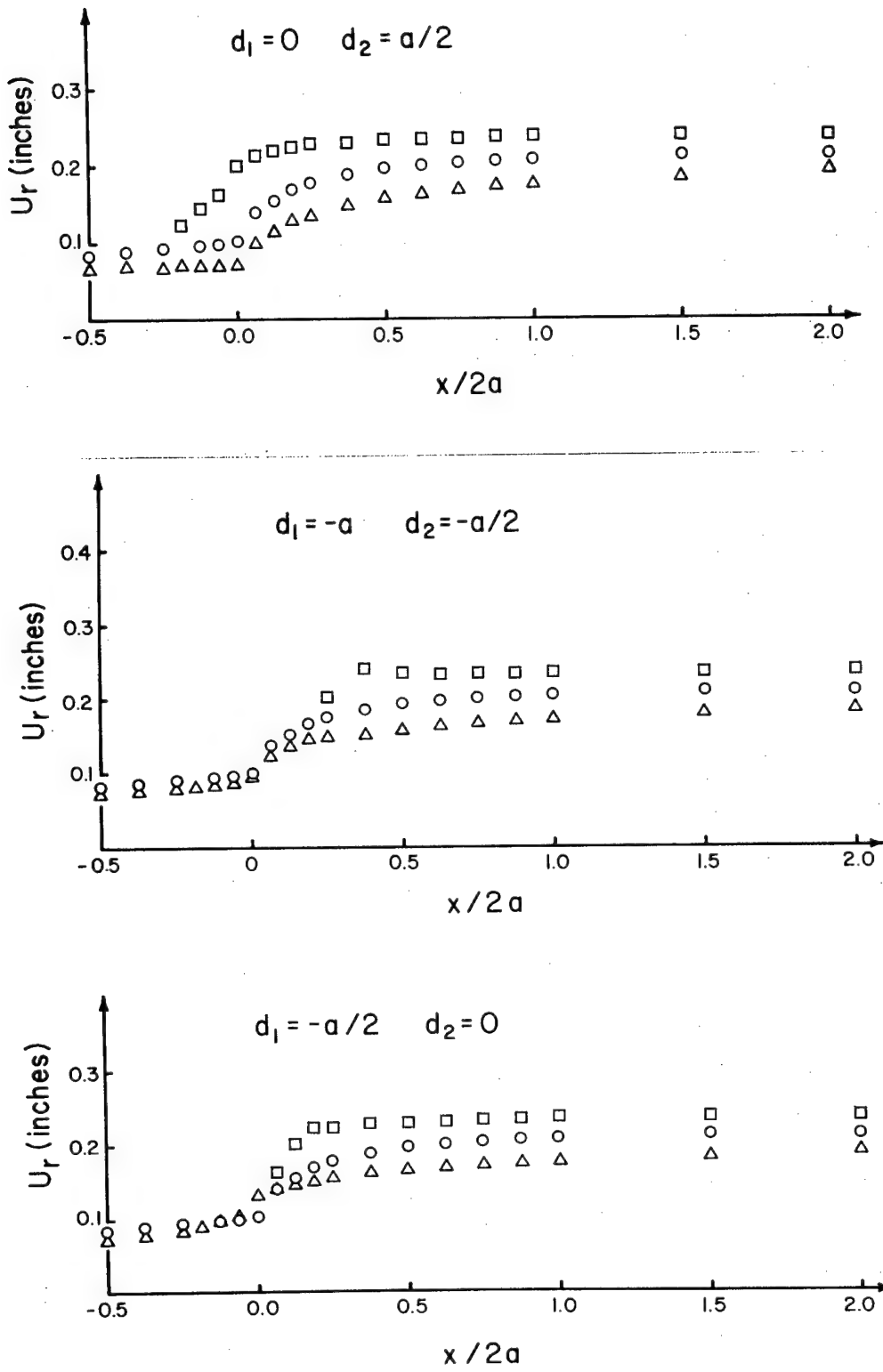


Figure III.23. Radial Displacement Along the Tunnel when the Face is Near a Narrow Rock Zone with Different Stiffness. Geometry as in Figure III.17b. Triangles:  $E_2 = 10 E_1$  Squares:  $E_2 = E_1/10$

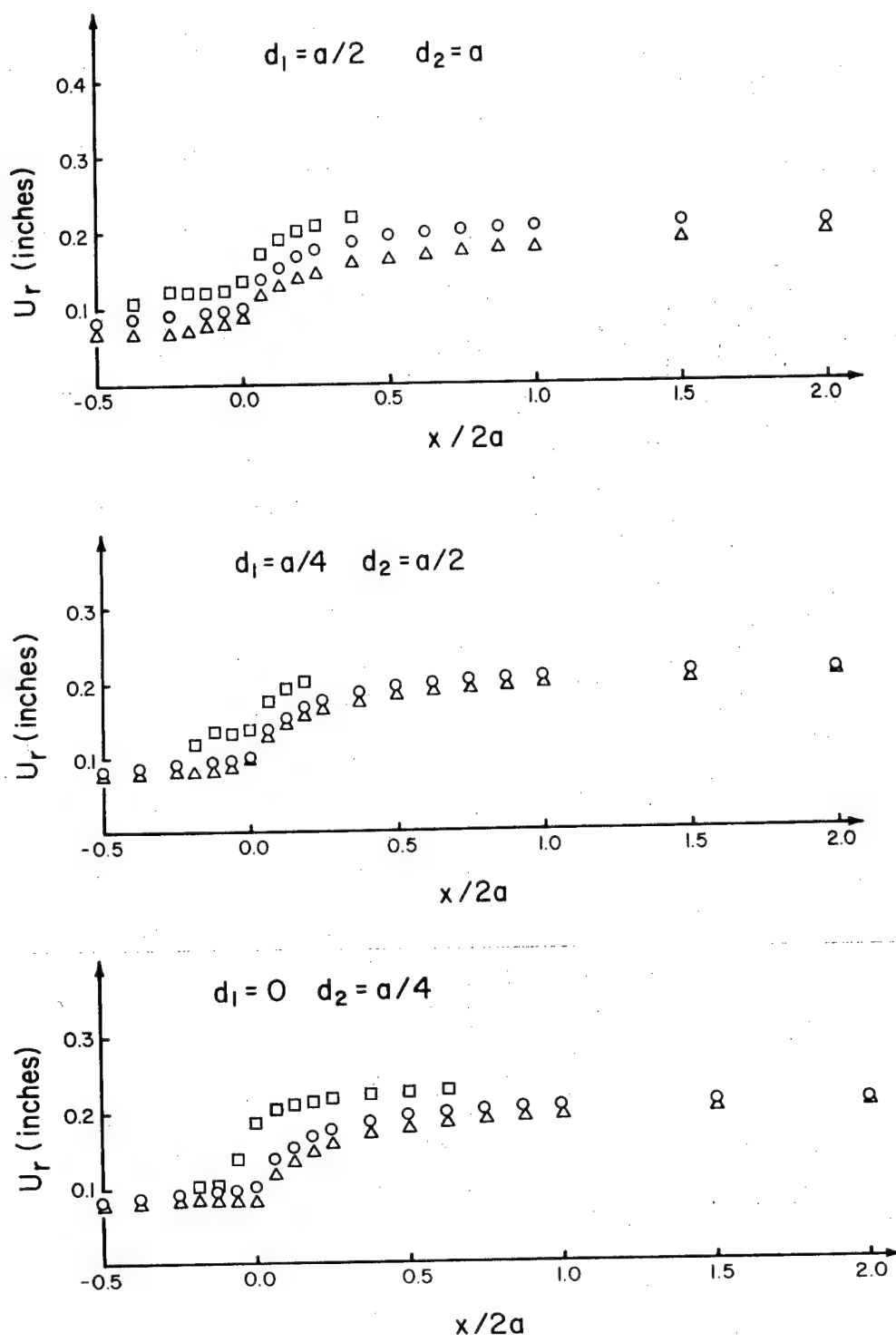


Figure III.23. Radial Displacement Along the Tunnel when the Face is Near a Narrow Rock Zone with Different Stiffness. Geometry as in Figure III.17b. Triangles:  $E_2 = 10 E_1$  Squares:  $E_2 = E_1/10$

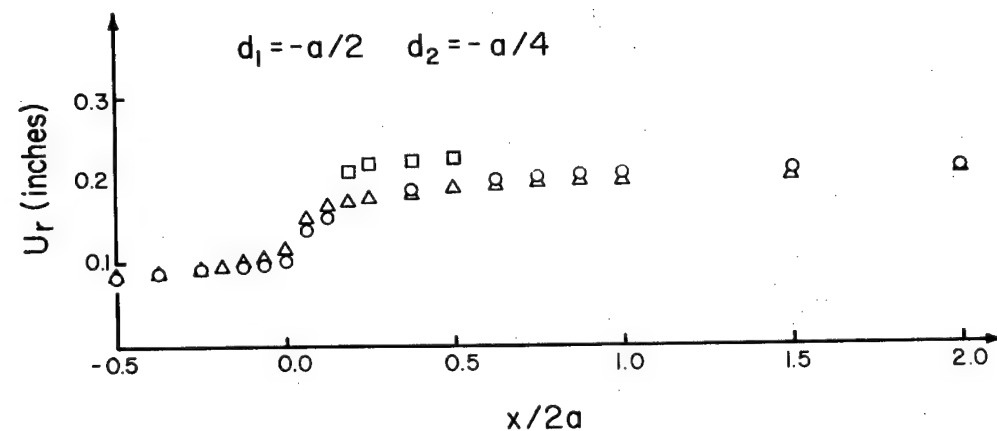
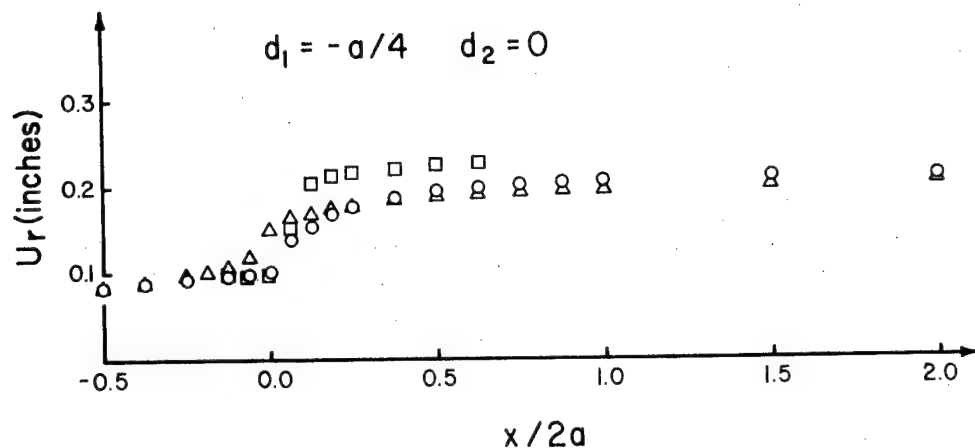


Figure III.23. Radial Displacement  $U_r$  Along the Tunnel when the Face is Near a Narrow Rock Zone with Different Stiffness. Geometry as in Figure III.17b.  
 Triangles:  $E_2 = 10 E_1$    Squares:  $E_2 = E_1/10$   
 Circles:  $E_2 = E_1$

at the time of support erection when the face is very stiff, while it will be rather unsensitive when the face is soft.

III-4.3. Plane Strain Stiffness Analysis of Support Loading Caused by Rock Failure.

III-4.3.1. Introduction. The combination of the finite element rock failure model (III-2) and of the stiffness support model (III-3) with a simulation of the excavation sequence should allow a reasonably accurate analysis of the overall phenomena occurring during support loading caused by rock softening and weakening. It was shown in the preceding section that tunnel support loading near the face, as a general rule, must be treated as a three-dimensional problem. Once the face has advanced up to a few tunnel diameters beyond the point of support erection the problem is more likely to approach a two-dimensional one, at least when the rock behavior is not dominated by a few major discontinuities. If support loading continues once the face has advanced several diameters it indicates a continued (time-dependent) stiffness change of rock, support, or both.

Two methods would seem to be appropriate for

the simulation of the mining sequence, or for taking into account the influence of the face, in a two-dimensional model. Firstly, one can load an unmined mesh, and then sequentially eliminate a series of elements, corresponding more or less precisely to an actual excavation sequence. Secondly, one can apply boundary forces equivalent to the pre-mining stressfield at both the tunnel circumference and the external boundaries. The forces at the tunnel periphery are then gradually reduced to simulate mining. In both methods, at some point in between the pre-mining and the final excavation step the support system stiffness matrix is connected to the rock mass stiffness matrix.

The second method, a gradual reduction of the internal boundary forces, is far less demanding in computer memory requirements. Indeed, when a progressive elimination of elements is used a far greater number of elements is required to model the problem, because the zone of high strain gradients shifts gradually towards the final tunnel periphery. Whether either of these methods is more "accurate" is a somewhat artificial question because of the substantial simplifications already introduced. In the real near-the-face condition

the plane perpendicular to the tunnel axis has only geometrically a somewhat special significance. The displacements, even in a circular tunnel in a homogeneous elastic rock are not radial (or, more generally, in-plane) but have an out-of-plane component. The principal stresses (strains) within the plane perpendicular to the tunnel axis are not truly principal stresses with respect to the complete three-dimensional stress (strain) state. Particularly for a plane very close to the tunnel face the deviations are large. Consequently, the two-dimensional analysis given here can only be considered as a preliminary step in the study of near-face tunnel support loading.

III-4.3.2. Support loading during face advance. The method used for the plane strain calculation of the ground-support interaction during face advance is illustrated on Figure III.24. Applied boundary stresses enforce a stress and displacement distribution corresponding to a pre-mining situation. The nodal point forces at the tunnel periphery are eliminated stepwise, to simulate the progressive reduction of internal pressure associated with face advance. At some

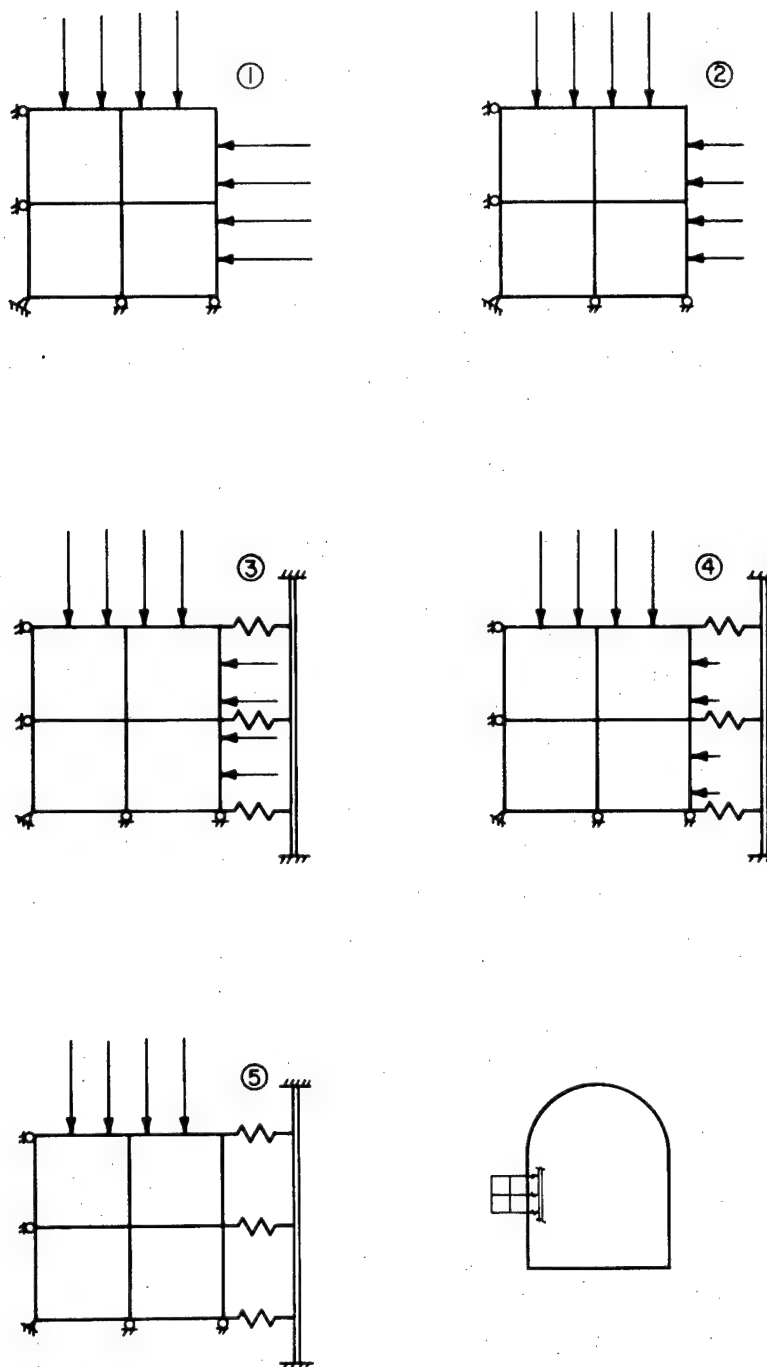


Figure III.24. Graphical Representation of one of the Simple Problems Used for Debugging TUNSUP, and Illustration of the Sequence of Computations. The Four Element Mesh Representing the Ground is Compressed Hydrostatically in step (1). The confining pressure is reduced to simulate face advance, (2), after which the support is connected, (3), and equivalent mining proceeds, (4), until completed (5).

intermediate stage the support is connected to the ground. An estimate of the appropriate moment for starting the interaction can be based upon the results of the axisymmetric analysis discussed in the preceding section. From that discussion it is fairly obvious that it is next to impossible to give any fast and easy rules for making such an estimate. Indeed, the convergence fraction that precedes support interaction with the ground depends on a variety of factors such as face distance, nonlinearity of the rock behavior, face stiffness, heterogeneity of the rock mass, stress state, etc.

It is not sufficient, in a calculation of this type, to combine the ground and support stiffness matrices in order to start the interaction sequence. The problem can be illustrated by considering point A on Figure III.25. The displacement  $u_A$  of this point has a two-fold meaning. When A is considered to be a point on the ground (finite element mesh)  $u_A$  indicates the full displacement that occurs after the initial unloading step. When A is considered to be a point on the support,  $u_A$  denotes the displacement subsequent to support connection only. These two values of the displacements at the rock-support contact points must be

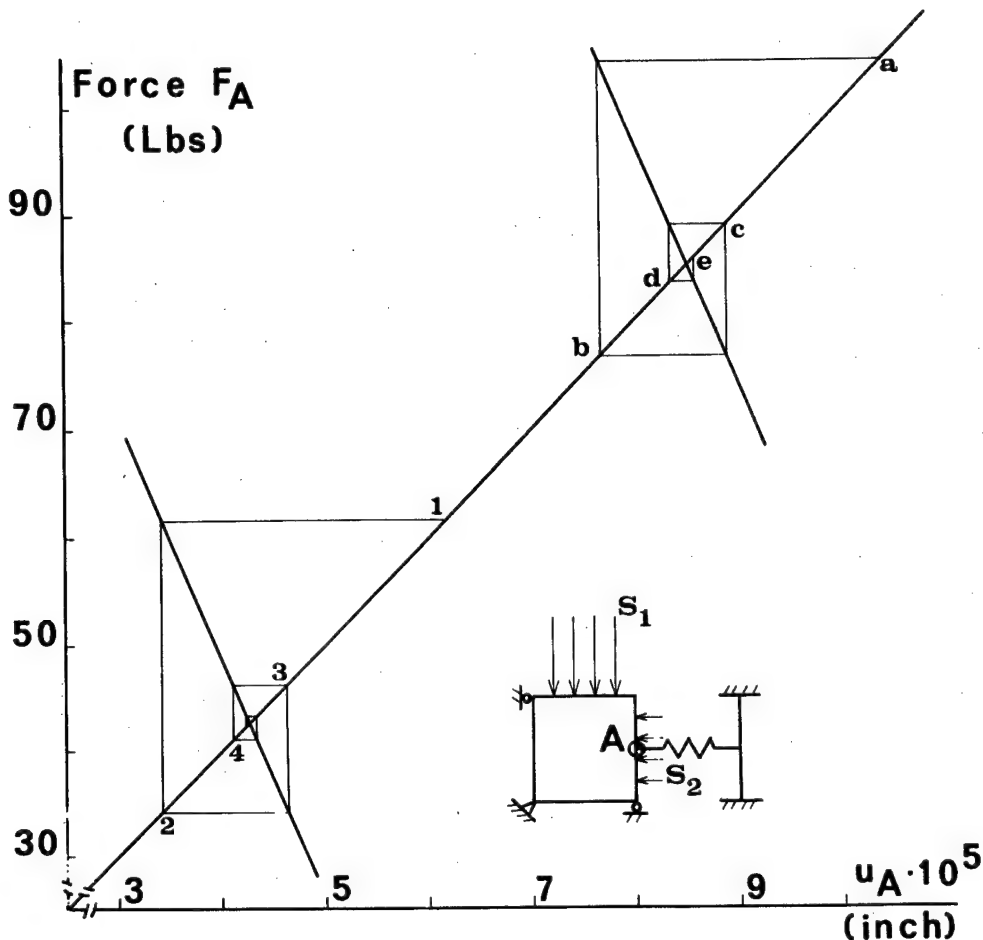


Figure III.25. Numerical Example of Iterative Convergence Towards the Equilibrium Position Between "Ground" and "Support" at each Unloading Step.

$F_A$  is the contact force between "ground" and "support",  $u_A$  is the displacement increment over the displacement that occurred prior to making contact between ground and support.

$S_1$  remains constant. Points 1, 2, 3, ... indicate the iterations after the first reduction in  $S_2$  that follows support installation; points a, b, c ... indicate the iterations after the next reduction in  $S_2$ .

separated explicitly, unless the entire calculation is sequential.<sup>4</sup> If such a distinction is not made, the effective displacements to which the support is subjected are excessive, the support will be loaded much heavier than would result from a correct calculation, and correspondingly the confining pressure exerted on the rock will be too high.

The separation method used here makes it necessary to approach the equilibrium state between ground and support iteratively, as illustrated on Figure III.25. (In many cases the equilibrium will be between nonlinear characteristics, not, as in this example, between straight line loading and unloading characteristics). The iterative approach described here fits in rather well with the iterative sequences already used for solving the finite element stiffness equations and for modifying the element properties. By combining these various iterative schemes a relatively fast approach to the equilibrium position at each step is usually obtained with a decidedly small number of iterations on the finite element equations, by far the major

---

<sup>4</sup>The calculation is then fully self-contained at each step, and cumulative values are obtained through appropriate summation after each step.

contributor to the total number of arithmetic operations.

While the full emphasis in this discussion has been on modeling the support loading due to near-face convergence, an entirely similar method could be used to study the consequences of time-dependent softening of either ground or support.

III-4.3.3. Examples of ground and support behavior analysis performed in plane strain. The examples presented in this section have been calculated with the program TUNSUP, given in Appendix C, in which most of the plane strain finite element techniques discussed in this chapter are incorporated. The examples have been selected to illustrate some points of practical significance in the mechanics of tunnel supports, to point out some of the interesting features of the analysis method, and to illustrate some of the dubious properties of the proposed rock failure model.

The central section of the finite element mesh used for all the examples is shown in Figure III.26, where one of the blocked steel set models is also included. The rock modulus  $E$  has been taken equal to 500,000 psi, the Poisson's ratio  $\nu$  equal to 0.2

and the applied hydrostatic pressure  $P$  equal to 1,000 psi. No weight has been assigned to the elements. The tunnel (rock periphery) is 20 feet wide and high. Unloading of the tunnel boundary from the initial hydrostatic stress is performed in 20 steps.

The first set of examples illustrates failure patterns around unlined tunnels. Figures III.27a, b, c correspond respectively to rock with a uniaxial strength  $\sigma_c$  of 1,000 psi, 500 psi and 250 psi. For each of these the absolute value of the post-peak stress-strain slope equals the pre-peak slope, the angle of internal friction derived from peak strengths equals  $30^\circ$ , the angle of internal friction associated with the residual strengths equals  $15^\circ$ , the residual cohesion is one-tenth of the intact cohesion.

In each case the failure propagates deepest behind the flat sections of the tunnel periphery. While it is true that the maximum stress concentration occurs in the sharp corner at the floor, the build-up in confining pressure is sufficiently fast to prevent failure propagation in this region (see also Figure III.28).

The overall fracture pattern description,

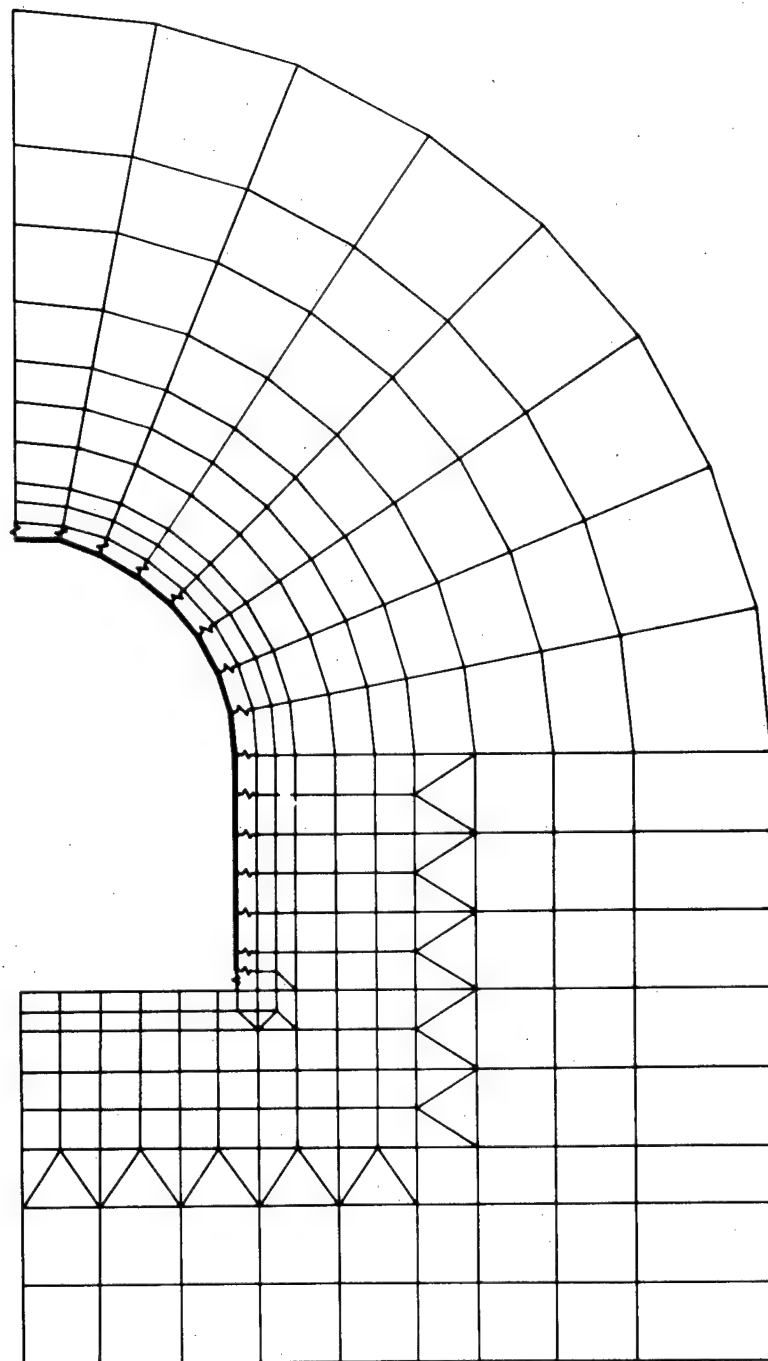


Figure III.26. Central Section of Finite Element Mesh Used for Rock Modeling for Figures III.27 Through III.31. Geometry of blocked steel set used for Figures III.29 and III.30a,b.

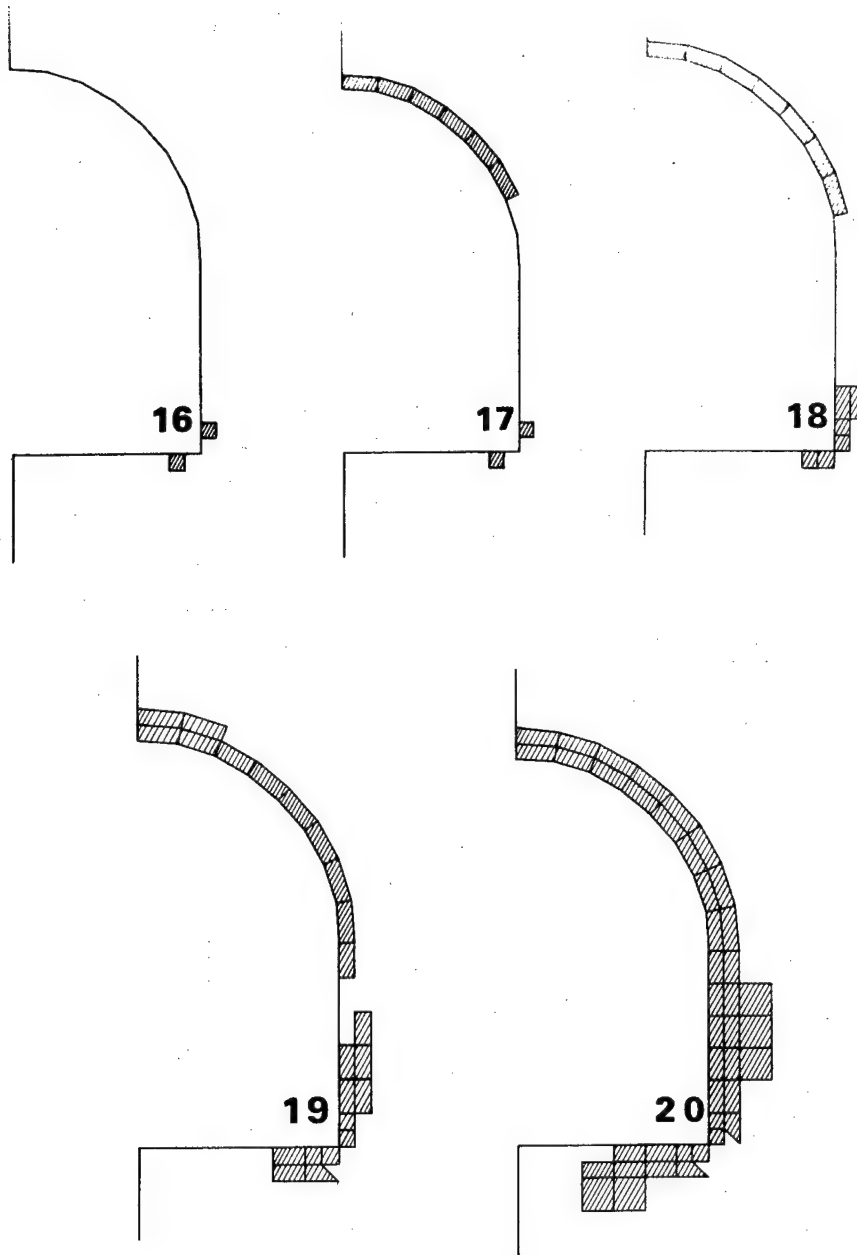


Figure III.27a. Progressive "Failure" Development Around a Tunnel when the Boundary Stresses are Eliminated in 20 "Equivalent Mining" Unloading Steps. Uniaxial Compressive strength  $\sigma_c = 1,000$  psi; hydrostatic stressfield of 1,000 psi.

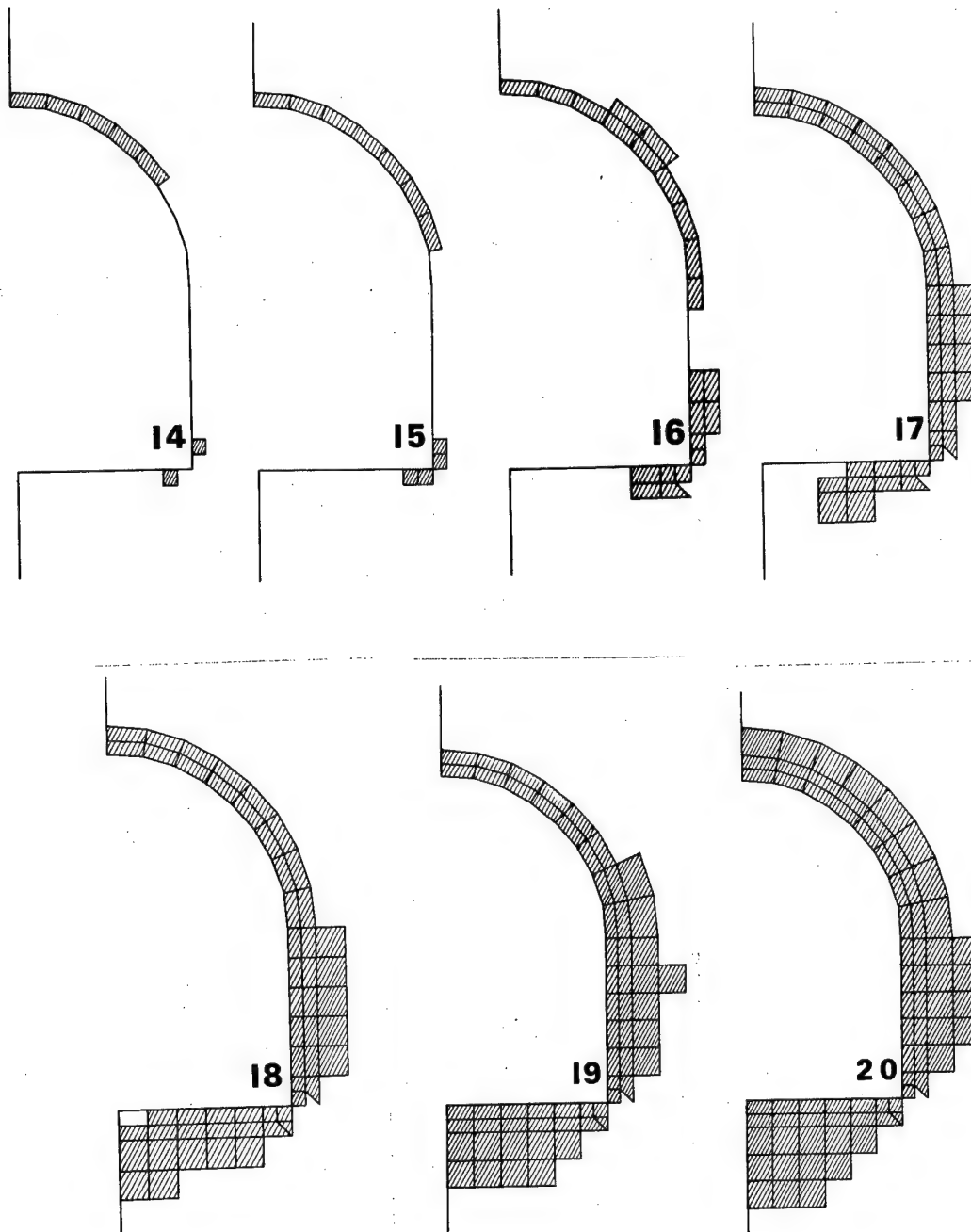


Figure III.27b. Progressive "Failure" Development During the Last Seven Steps of a 20-step "Equivalent Mining" Unloading Sequence. Uniaxial compressive strength  $\sigma_c = 500$  psi; hydrostatic stressfield of 1,000 psi.

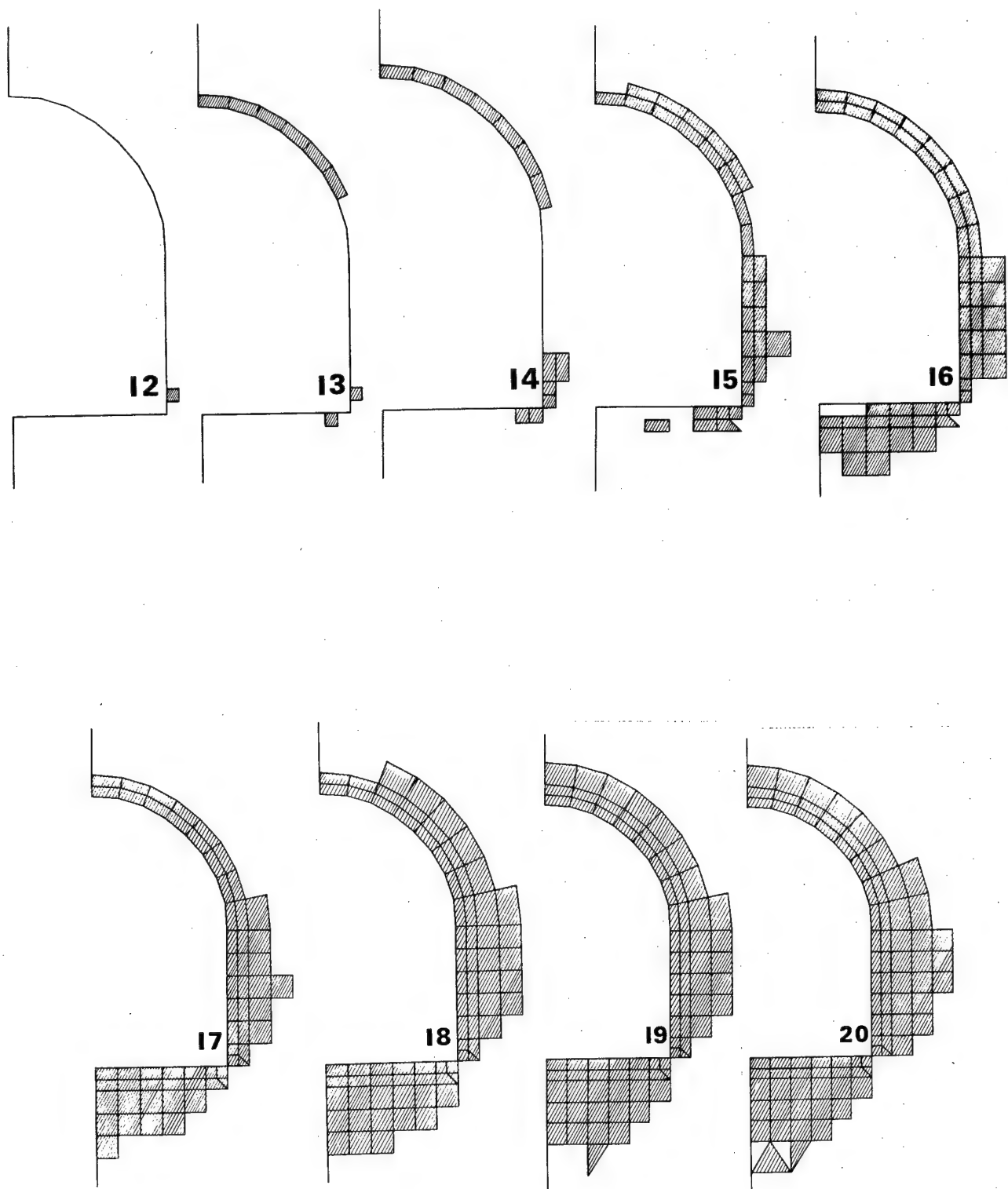


Figure III.27c. Progressive "Failure" Development During a 20-step "Equivalent Mining" Unloading Sequence. Uni-axial Compressive Strength  $\sigma_c = 250$  psi; hydrostatic stressfield of 1,000 psi.

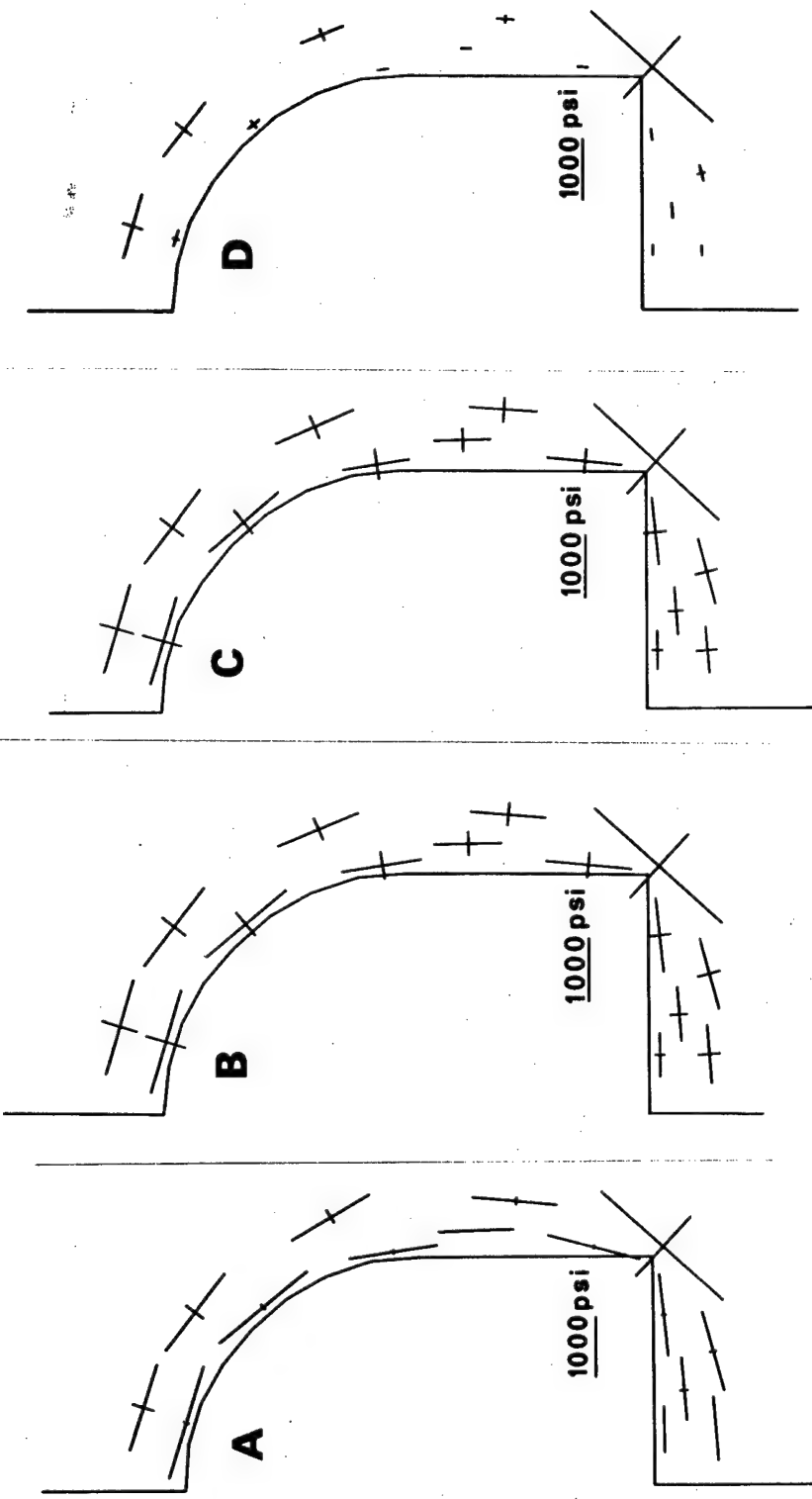


Figure III.28. Stresses at 15 points Around a Tunnel in an Imposed Hydrostatic Stressfield of 1,000 psi After Complete Stress Relief of the Tunnel Periphery and for Different Types of Rock Behavior.

- A: elastic solution
- B, C, D: uniaxial compressive strength  $\sigma_c = 250$  psi, cohesion  $c_i = 72$  psi, angle of internal friction  $\phi_i = 30^\circ$
- B: no strength drop beyond "peak"; residual cohesion  $c_r =$  intact cohesion  $c_i$ ; residual friction  $\phi_r =$  intact friction  $\phi_i$ ; large volume increase beyond "peak"
- C:  $c_r = c_i/10$ ;  $\phi_r = 15^\circ$ ; large volume increase beyond peak; absolute value of post-peak stress-strain slope equals pre-peak slope
- D: same as C, except for volume increase, here very small.

as in Figures III.27, lumping together all the elements in which the properties are modified from the original ones, is not a very sensitive indicator of the changes associated with failure. A more precise comparison is possible on the basis of the state of stress, as shown in Figure III.28. Plotted here are the principal stresses at selected points around the tunnel, after complete unloading, for different rock models: A, elastic; B, no strength drop beyond the peak  $\sigma_c = 250$  psi, large volume increase; C, strength drop and large volume increase, same properties as for Figure III.27c, described in a preceding paragraph; D, same stress-strain curves as for C, but only a small volume increase.

It is clear from the results that the volume increase associated with failure plays a dominant role in the resulting stress distribution and thus upon the degree of instability caused by failure. Whether a large ubiquitous volume increase associated with failure is a reasonable proposition must be questioned, because of the resulting extremely strong stabilizing influence.

It has been pointed out in the discussion on support stiffness models (section III-3.3) that the

interface elements between ground and support must be treated rather carefully. An example of this is illustrated in Figure III.29, where the influence of the stiffness of the footings underneath a steel set on the loading of the set is described. In order to isolate the influence of this element, the ground model was elastic throughout this calculation. The blocking point geometry at initial contact (after unloading step 10 in a 20-step sequence) is shown in Figure III.26. The range of footing stiffness values illustrated here is the one within which the results change most rapidly. Even if the footing is much stiffer than the highest value ( $2.5 \times 10^5$  lbs/in)<sup>5</sup> used here, the resulting blocking point force distribution will not be greatly affected. If the footing stiffness is much softer than  $2.5 \times 10^4$  lbs/in, the contact forces will be concentrated even more in the crown, but the overall picture will not be very different.<sup>6</sup>

---

<sup>5</sup>This specific number would obviously be different for ground, steel sets or blocking points with different stiffnesses. In this particular case the stiffness is about 2@5 times lower than the stiffness of an average double beam wall plate for the support type used in the calculation, and assuming that the wall plate rests on an infinitely stiff floor.

<sup>6</sup>When the footing is very soft a relatively small load suffices to cause a large contraction in

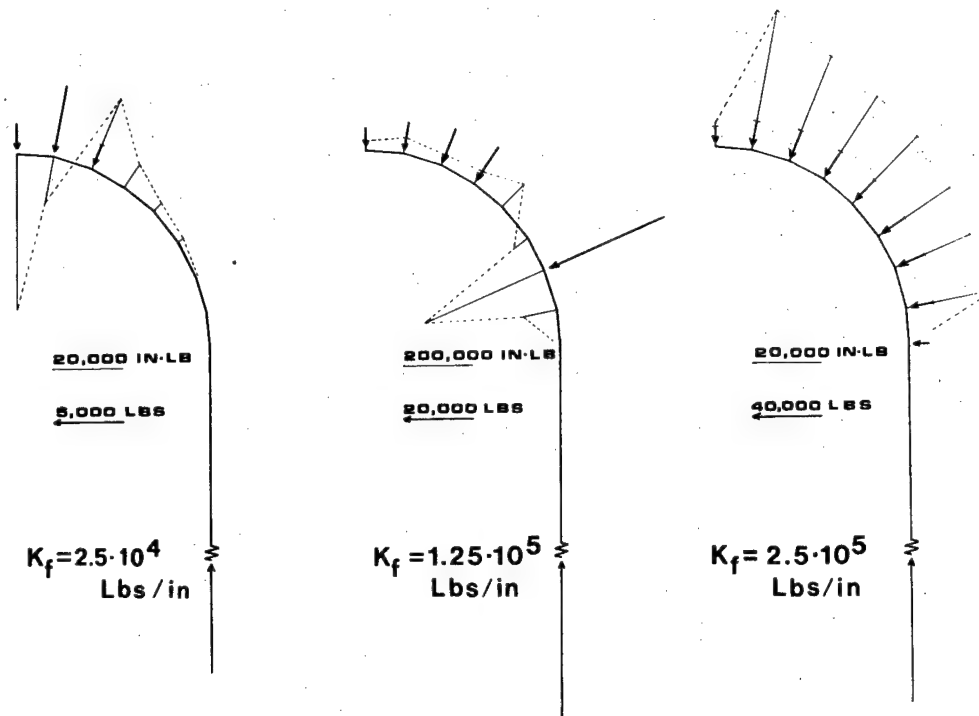


Figure III.29. Influence of Variations in the Footing Stiffness Upon the Contact Forces Between a Steel Set and the Ground and Upon the Bending Moment Distribution in the Steel Set. The plotted results are the values after complete equivalent mining unloading in 20 steps, with the support "connected" after unloading step 10. Tunnel is 20 feet wide, 20 feet high.  $8 \times 5\frac{1}{4}$  WF (17 lbs/ft) steel sets, at 5 ft spacing. Block spacing as in Figure III.26, block stiffness = 2,500,000 lbs/in. The rock is elastic throughout the calculation, with a Young's modulus  $E = 500,000$  psi and a Poisson's ratio  $\nu = 0.2$ .

If the supporting capacity of the steel set is to be fully and efficiently utilized, the footing stiffness must exceed a minimum value. On the other hand, little will be gained by increasing it much beyond the minimum. This minimum value can be estimated (rather roughly) from the requirement that the contraction of the footing (including the influence of excessively blasted rock, muck underneath the wallplate, influence of water on the floor, etc.) should not exceed the contraction of the blocked steel, or the footing stiffness should certainly not be smaller than the combined stiffness of the (roof) blocks.

The next three figures (III.30a, b, c) show three stages in the load development on a steel set installed within a failing rock mass. The properties assigned to the rock are identical to those used for the calculation of Figures III.27c and III.28c. The influence of all three support types upon the extent of the failure zone is small, as this zone is reduced by a few elements only. Similarly, on the scale used in Figure III.28, the

---

the footing and thus settlement of the steel set, with a consequent potential loss of contact at many blocking points.

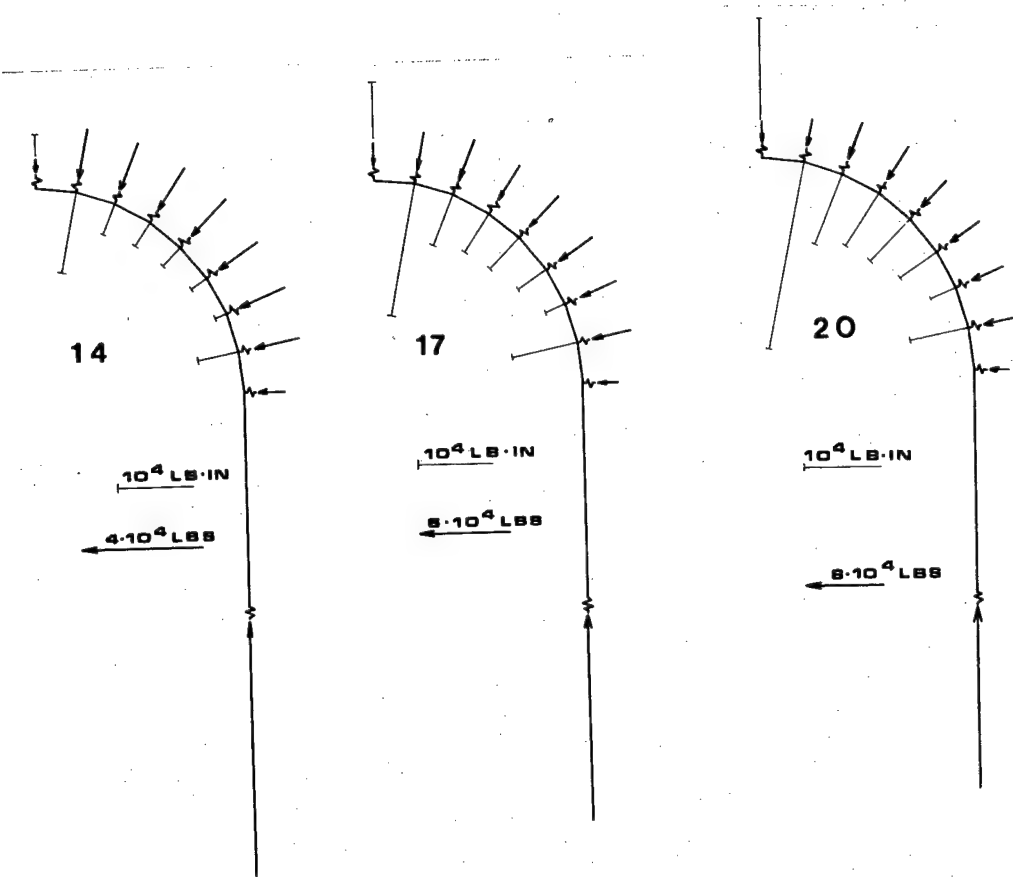


Figure III.30a. Steel Set Blocking Point Forces and Bending Moments at Three Steps in a 20-step Equivalent Mining Unloading Sequence with the Steel Set Connected After Step Ten.  
 All conditions as in Figure III.29, with high footing stiffness, except that ground is failing as in Figure III.28c.

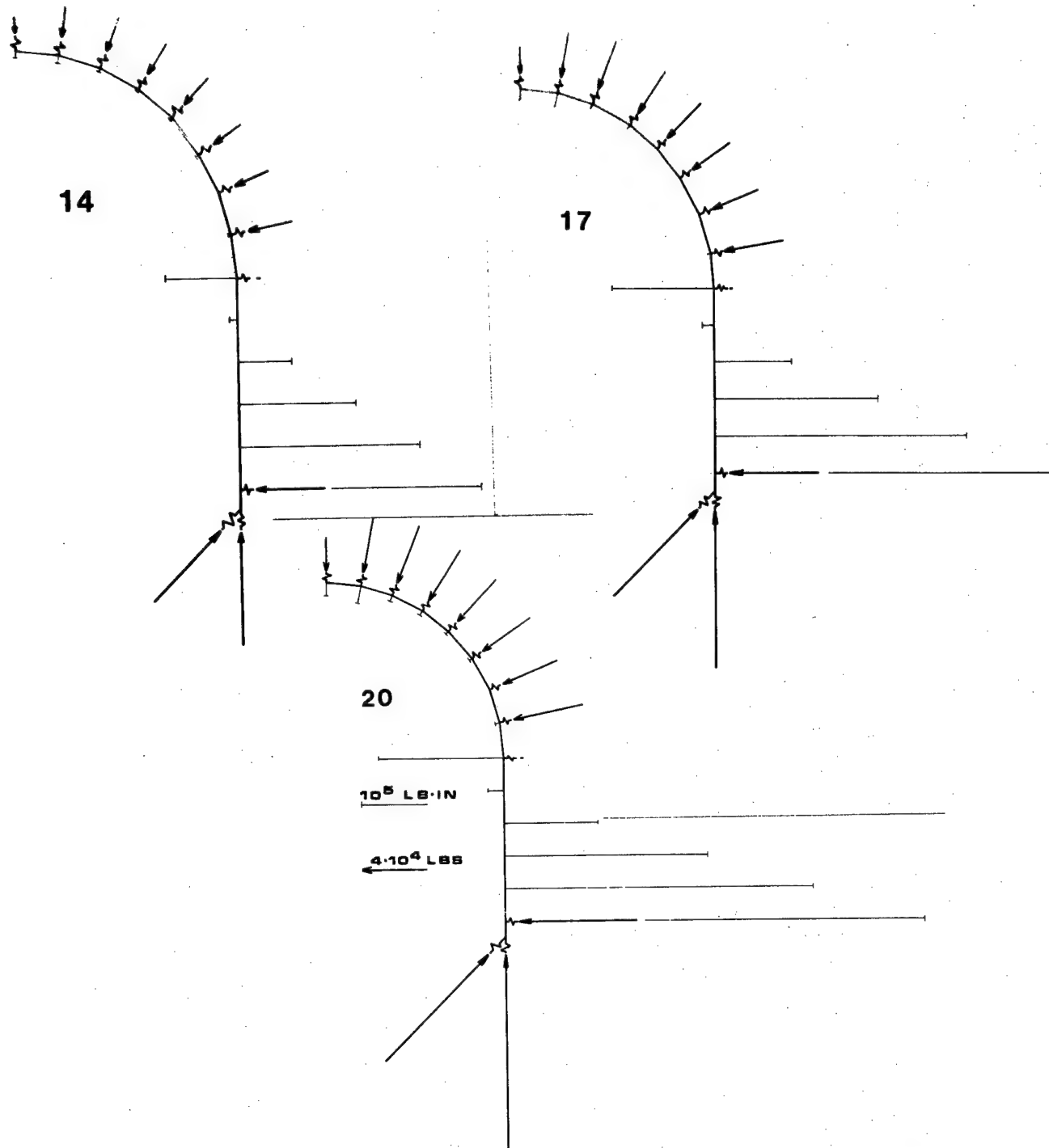
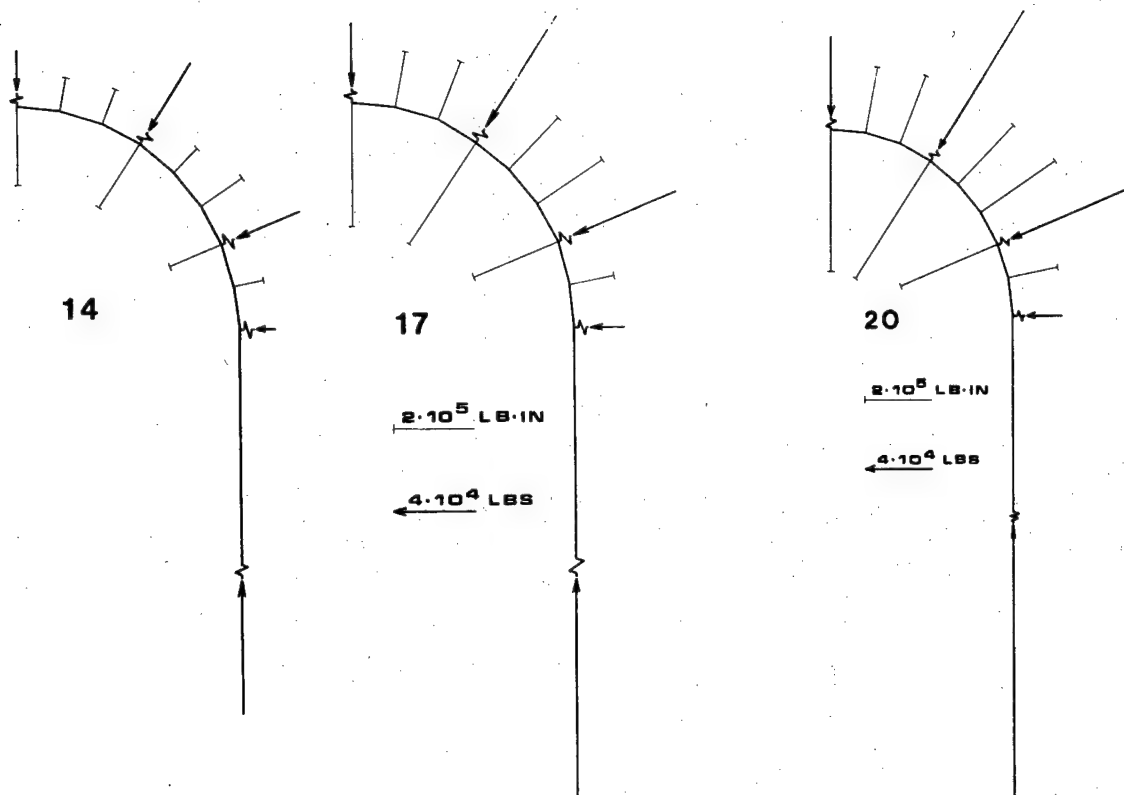


Figure III.30b. Steel Set Blocking Point Forces and Bending Moments at Three Steps of a 20-Step Equivalent Mining Unloading Sequence, with the Steel Set Connected After Step Ten. All conditions as in Figure III.30a, except for the footing stiffness to which a large horizontal component has been added.



**Figure III.30c. Steel Set Blocking Point Forces and Bending Moments at Three Steps of a 20-Step Equivalent Mining Unloading Sequence, with the Steel Set Connected After Step Ten.**  
 All conditions as in Figure III.30a, with the exceptions that only four blocking points are used in the upper steel set section versus nine in the preceding calculations and that the steel set spacing is only three feet.

change in stresses due to the support action would be barely visible, if at all.

In all three examples the stress component due to bending is small compared to the axial force stress component. Although no detailed comparisons have been made, the overall picture is qualitatively not unlike the one that would be obtained from the Proctor and White method. (This is not the case in the first set on Figure III.29, where nearly all blocking points have been inactivated).

The vertical leg of the steel set provides no support to the sidewalls when there is no horizontal footing stiffness, but even with a rather high horizontal stiffness (Figure III.30b) whatever sidewall confinement is provided remains very localized.<sup>7</sup>

---

<sup>7</sup> In this calculation it is implied that the horizontal stiffness is due to shear stiffness between the steel set and the floor. An alternative that could be included with a trivial change in the program would be a spring (allowed to act in tension, which the blocking point springs are not) connecting the steel set footing to a point within the rock mass, thus simulating a point-anchored rock bolt. An invert strut could obviously be included very simply. It would appear that any of these measures would have only a very localized effect as regards the confinement pressure provided on the flat vertical sidewalls.

A somewhat surprising result is the very small force, in all three cases, at the springline. Also rather unexpected was the fact that the blocking point springs that were in compression after the first support contact step remained so during the entire sequence, and that none of the others was ever reactivated.

The last example (Figure III.31) is an attempt at modeling a shotcrete liner. Two extreme models have been used, one with complete displacement continuity between ground and support, one with continuity only in the direction perpendicular to the contact surface. For the fully continuous model (two figures on the left) the support is represented by beam elements and the nodal points are assigned the (post support erection) displacements of the corresponding ground nodal point. At the other extreme, where no shear stiffness is assumed between ground and support (which might correspond more closely to the behavior of a cast-in-place not backgrouted concrete liner) the support is modeled with beam elements and with short, stiff springs (the latter used to preclude mutual penetration of ground and support).

The normal contact force distribution is

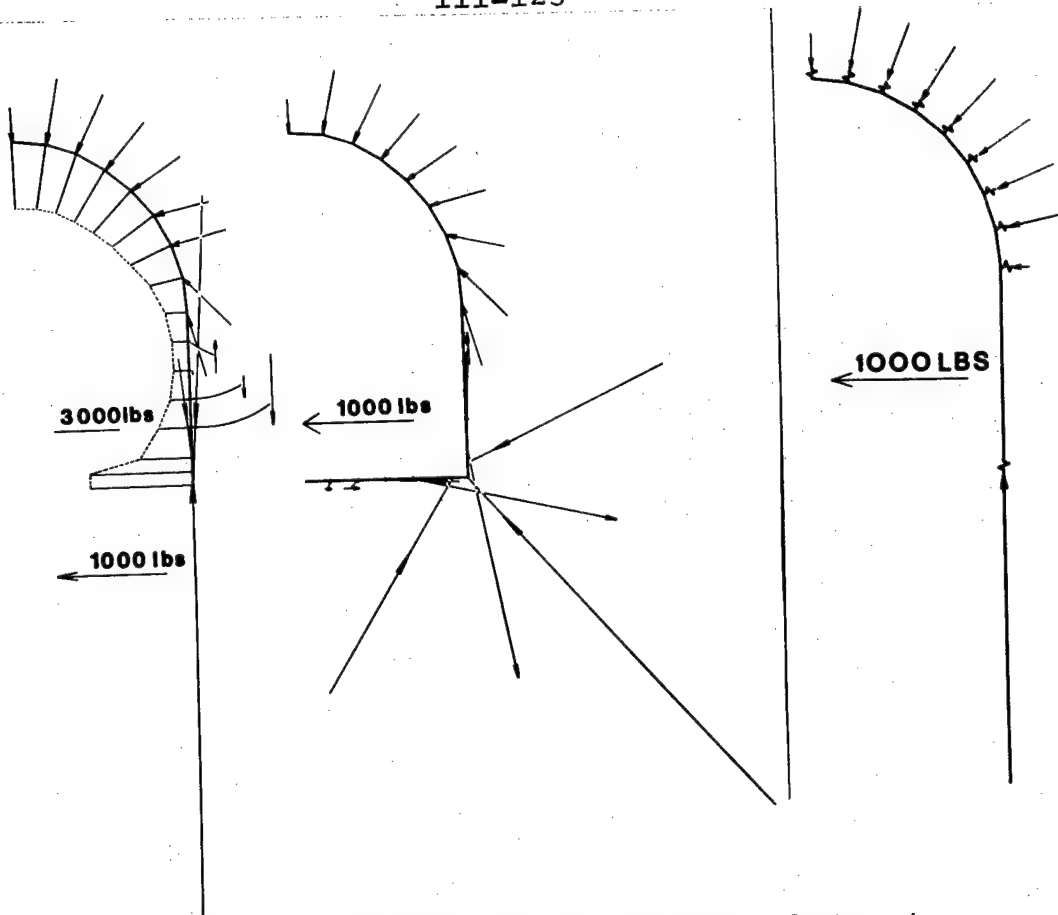


**Figure III.31.** Contact Forces Between Shotcrete Liner and Ground After Equivalent Mining Unloading in 20 Steps and with the Support Activated After Step 10.

Ground modulus  $E = 500,000$  psi,  
Poisson's ratio  $\nu = 0.2$ .  
Pre-mining hydrostatic stressfield of 1,000 psi.  
Shotcrete modulus  $E = 500,000$  psi,  
thickness = 4 inches.

Left: Shotcrete modeled with beam elements; complete displacement continuity at the nodal points, i.e., infinite normal and shear stiffness between ground and support; dotted lines connect points indicating the magnitude of the normal force within the liner.

Middle: Same as above, but with floor beam.

Right: Same shotcrete model as on left, but without shear stiffness, and very high normal stiffness enforced with very short, very stiff springs.

fairly similar for the two extreme models. But in the presence of shear stiffness the shear forces become a significant part of the total contact forces.<sup>8</sup> In both examples of continuous displacement calculations (with and without floor beam) the normal forces within the liner are reduced to very small values at some points around the periphery. This fact, also frequently apparent on diagrams of measured tangential pressures in shotcrete liners (in the references cited in the footnote, for example) would tend to indicate that shotcrete liners do not act as integrated units, but rather as somewhat isolated segments. This is also indicative of the very good interaction between ground and support, as it shows the stabilization mechanism by means of a very local and immediate stress redistribution within the rock mass, a mechanism which is, mutatis mutandis, reminiscent of fully grouted bolt action.

---

<sup>8</sup> This has some obvious implications for the instrumentation of shotcrete liners, and for the interpretation of the measurements. When the normal forces are only one part of the significant contact forces, and that this is probably frequently the case can be seen from the lack of equilibrium in measured radial pressure diagrams, e.g., Golser, 1973, Figure 3; Rabcewicz, et al., 1972, Figure 14, then the measurement of only the normal pressures provides a very incomplete picture of the ground-support interaction.

As previously observed for steel sets, very little confinement is provided on flat surfaces, whether wall or floor. In this case also the horizontal stiffness, provided here through a floor beam, has a very localized effect only. Of interest also is the development of rather high tensile forces between ground and support at some points.

The preceding examples are only preliminary approaches to the analysis of some problems in the mechanics of tunnel supports with finite elements. More comprehensive studies, covering ranges of properties, as well as detailed comparisons with field observations are needed to confirm or to refute any general validity of the results and conclusions.

## Chapter IV

### SUMMARY, CONCLUSIONS AND POSSIBLE FURTHER DEVELOPMENTS

#### IV-1. Summary

Two methods have been used to study the transition from a pre-tunneling to a post-tunneling equilibrium state. In the first part of this thesis closed-form expressions have been obtained for the characteristics that describe the interaction between ground and support. In the second part a strain-softening dilatant finite element continuum was developed to represent the (failing) rock mass. It was used to analyze the face influence in a circular tunnel, and it was combined with a matrix structural stiffness model to study the interaction between support and rock in a two-dimensional simulation of excavation and support loading. In both parts an effort was made to represent the two aspects of the problem, the support system and the ground, to an approximately similar degree of realism, with methods of about equal

simplicity or complexity.

Although the closed-form solutions are based upon highly idealized and simplified assumptions, these were chosen in such a way that the influence of some of the basic characteristics of rock failure upon support loading could be evaluated. This necessitated the use of a strain-softening model with a dilatant volumetric behavior to characterize the failing rock. Because of the large stress relaxations associated with deeply propagating broken or stress-relieved zones it is necessary to consider the potential significance of gravity effects.

The ground-support interaction problem is statically indeterminate, and can therefore only be solved when the displacements are determined. This requires further assumptions about the pre-tunneling stress state and about the stress changes induced by tunneling. It is also at this point that the volumetric rock behavior during failure must be incorporated into the analysis.

The final result of the calculations that represent the rock behavior is the "ground reaction curve" or "ground characteristic." A numerical method is outlined that would permit a relatively simple generalization and extension of the ground

reaction calculations. On the other hand, simple techniques are suggested for including such effects as variations with time and with size.

The study of the ground behavior is complemented by simple structural analysis methods that permit accounting for support behavior. A detailed evaluation of blocked steel set and grouted rock bolt support action is given, while a more general descriptive discussion is presented of other common support methods, together with an outline of the requirements that should be met by more precise and realistic models.

The first part of this thesis, on the continuum analysis of tunnel support loading, is concluded with a discussion of some potential practical applications. The need for a large number of material properties and characteristics severely limits the direct design applicability of such methods. The difficulties are compounded by the uncertainty introduced by the potentially very significant if not dominating influence exerted by construction procedures. It is possible, however, to outline some generally desirable properties of support systems. It nevertheless remains true that refinement and optimization of tunnel supports can only be

accomplished through detailed observation of in-situ installations. But this, in turn, requires a realistic tool for the interpretation and application of the measurement results.

While the first part of this thesis was oriented towards the development of general results with broad implications from a highly idealized situation, the second part was directed towards the development of a "case study" technique that requires far less idealizations and simplifications with respect to geometry, boundary conditions and material characterization. It was nevertheless possible, with this method also, to study some situations that can be considered as archetypical for a variety of real tunneling conditions.

In this second part, a finite element analysis technique is proposed for the study of strain-softening dilatant failing rock. The method is based upon a sequential modification of the elastic constants. Loading or "unloading," the latter corresponding to gradual excavation, progresses stepwise, and after each step the elastic constants are adjusted in each element in which the limiting elastic strain has been exceeded. This adjustment is based upon the largest (compressive) strain and

smallest ( $\sim$  confining) stress, and proceeds to follow a set of input stress-strain data. After each adjustment iterative problem solutions are performed until no more changes occur, and prior to applying the next change in boundary conditions.

The finite element analysis was used by itself to study the influence of the face upon tunnel support loading. The analysis of this strictly three-dimensional problem was limited to the axisymmetric case. Failure and convergence patterns near the face were presented, and a simplified study was made of the consequences for support loading.

A two-dimensional plane strain model was developed in which excavation is simulated through progressive "unloading" of the tunnel periphery. In this analysis the support action is represented through a combination of beam and spring elements. A fairly detailed discussion is presented of the requirements that must be met by stiffness models that are to be used for studying the behavior of common support systems. Because of its relative simplicity, a blocked steel set is considered in some more detail.

IV-2. Conclusions

Two methods have been presented for the analysis of tunnel support loading caused by rock failure. For both of them an attempt was made to model the mechanics of the interaction between ground and support. Because of this interactive nature of the problem, emphasis was put on the development of methods that take into account realistic stiffnesses for the two interacting elements, as well as a realistic sequence for the progressive interaction between them.

In the closed-form solutions it was found that the progressive strength reduction of failing rock has a profound effect upon the requirements for an ideal or optimum support method. As failure develops, a stress-relaxed zone propagates into the rock mass. In the "dynamic" or progressively changing nature of the stress distributions lies a possibility for fundamentally different support requirements or ground reaction characteristics. From a continuum mechanics point of view, one can conclude that the consequences of rock failure can radically change the support requirements that would be postulated upon the basis of conventional plastic analysis. From the latter, one can hardly avoid the

conclusion that supports should be soft, that large displacements are desirable, and that delayed installation of yielding supports should tend to optimize support loads. This conclusion must be qualified somewhat when gravity effects assume a non-negligible role. It was shown that localized loads are likely to become more predominant when the tunnel is at rather shallow depth and when the residual friction of the broken material is very low. The more significant the gravity effects are, the larger the differences should be between roof and floor support requirements. In difficult ground, however, where the use of continuum type analyses has most often been suggested, such differences tend to be minor compared to the overall support requirements.

Although the entire derivation and discussion of the ground reaction was based upon the assumption that the rock was and remained continuous, the general conclusion that the required support pressure decreases rapidly during the initial small convergence but tends to increase once an optimum displacement has been exceeded is likely to have a more general validity. Indeed, the essential factor needed for the development of such a model is a

particular sequence of equilibrium states or stress configurations. There is no a priori reason why an equivalent sequence of equilibrium states should not determine support requirements in real (discontinuous) rock masses, and there is much semi-quantitative information that it does.

The closed-form expressions for the support stiffness calculations have been used to emphasize the need to incorporate into such calculations a realistic rock-support interface element, as well as the dearth of information about such interfaces. It was shown that the support characteristic of a blocked steel set is likely, in many practical situations, to be dominated by the stiffness of the wooden blocks. Similarly, the support action of grouted rock bolts will be significantly affected by the effective in-situ action of the "contact" elements, notably the end forces and the displacement and shear stress distribution along the bolt.

The closed-form solutions presented here involve too many rock and support properties, properties too difficult and expensive to determine not only prior to but even during construction, to be of much value as "cookbook" type design rules. However, they do provide guidelines that can be used

to evaluate the significance of measurements and observations, to compare the influence of varying support systems and to assess the effect and value of narrowing down the range of uncertainty about the rock and support parameters.

From the axisymmetric finite element analysis it follows quite clearly that the distance from the face at which supports are erected can have a dominant effect upon (at least the short-term) support loading and support effectiveness. One cannot give general rules for such effects, unless the degree of homogeneity of the rock mass as well as the failure patterns near the face are established. Indeed, the convergence pattern near the face will be basically different depending upon the relative stiffness of the rock ahead of and behind the face. Whether these stiffness changes existed prior to tunneling or are induced by it might not profoundly affect the (qualitative) convergence sequence, but it is nevertheless likely that the amplification of stiffness differences caused by tunneling will have a strong bearing upon the type of remedial action that can or should be taken.

#### IV-3. Further Development and Research

##### IV-3.1. Introduction. The subject of tunnel

support loading is a rather broad one, involving many aspects of mechanics, geology and construction engineering. As a consequence, research related to it can progress along many paths. In the last decade it has greatly increased, and has taken many directions. Many of these possibilities do not fit directly or obviously within the framework of this thesis, and are therefore not discussed.

Two distinct possibilities exist for continuing the work presented here, and ideally they should progress more or less simultaneously. On the one hand, the analysis techniques that have been presented must be improved, further developed and corrected or refined. On the other hand, their validity and practical significance must be established.

IV-3.2. Further Development of Presented Analyses. Necessary further developments of the presented analysis methods include straightforward extensions and generalizations as well as more profound changes aimed at the development of fundamentally different and more realistic models. While the latter should be the more profitable and basic propositions, they are also the far more

difficult ones to pinpoint, particularly beyond the stage of somewhat nebulous and vague declarations of intent and desirability.

Several "straightforward" type extensions of the closed-form results have already been suggested in Part II. Improvements or generalizations in this area should concern the analysis of both ground and support characteristics. Incorporation into the ground characteristic of (some types of) time-and size-dependency presents no problems. Similarly, a numerical generalization of the calculations, thus allowing an inclusion of a wide range of non-linear effects should not be overly demanding.

A number of potential improvements or refinements of the support characteristic calculations are similarly obvious. This involves notably the non-linear behavior of (crushing) wooden blocks, the development of plastic hinges in the steel rings, the time and face distance effects of shotcrete hardening, the calculation of grouted bolt stress distributions based upon a more comprehensive displacement field calculation, the influence of strain-hardening upon bolt behavior.

A more inherent shortcoming of the closed-form solutions, and one not so easily overcome, is the

assumption of radial symmetry. Indeed, numerous observations in laboratory experiments [Daemen and Fairhurst, 1970; Jamet, 1973; Gay, 1973 (the last two list numerous additional references)] as well as observations and descriptions of fracture patterns around tunnels (Rabczewicz, 1965, 1969; Sperry and Heuer, 1972) clearly indicate that fractured zones do not tend to be axisymmetric. Many convergence and load measurements on tunnel supports tend to confirm the unlikelihood of axisymmetric behavior. This, in fact, is not surprising in view of the frequently non-symmetric appearance of the final collapse shape assumed by a cylindrical rock specimen in triaxial compression. From a general point of view, whether the non-symmetric behavior is due to non-perfect loading, or to frictional end-effects, or to some (minor) variation in rock properties, or to non-perfect grinding of the specimen ends or some similar mechanism is quite immaterial. A relatively minor perturbation seems to, or at least can have a dominating effect, so that a stability problem exists, as is confirmed by the need to reduce the load.

Equivalently, around the opening of a hollow cylinder in a "homogeneous isotropic" rock (or

similar artificial brittle material such as hydro-stone), and, a fortiori, around a tunnel, even assuming perfectly hydrostatic loading, it is not unlikely that some local perturbation will have a dominant effect upon failure initiation, and thus, propagation being considered as an unstable event, upon the ultimate broken zone development.

It is not clear to the writer whether and how the general support design problem could be approached from this point of view. It is not unlikely, however, that an analysis that accounts for the failure mechanism and associated energy changes might lead to some type of stability or ultimate load design criterion (Fairhurst and Cook, 1966; Cook, 1966).

A number of further extensions and developments of the stiffness analysis of tunnel support loading caused by rock failure as presented in Chapter III should not pose serious difficulties. A first and rather obvious extension would be to incorporate the failing rock model into a fully three-dimensional finite element program. Of probably more benefit, cost-effectively and from a tunnel support mechanics viewpoint, would be the inclusion in the analysis of time-dependent decreases in rock strength and stiffness. This could be

accomplished by a step-wise pseudo time-dependent change of the elastic constants in elements in which a certain fraction of the rock strength has been exceeded. The step-wise change could be imposed in a manner that forces the stress-strain state in the element towards the post-peak branch. Substantial laboratory evidence indicates that such a time-dependent path might be quite realistic (Wawersik, 1972; Peng, 1973; Hudson and Brown, 1972). And numerous measurements have shown that tunnel support loading often continues for prolonged periods of time.

It might be worthwhile to include the possibility for entering non-linearized failure description input into the finite element analysis. This could probably most efficiently be accomplished by expressing the stress-strain-volume relations in terms of spline functions (Desai and Abel, 1972, p. 325).

It would be valuable to incorporate a progressive mining and support erection sequence into the axisymmetric finite element model. The support characteristics in this case necessarily being radially symmetric, it would be relatively simple to incorporate the closed-form stiffness results

obtained in Appendix A (eventually in a more general nonlinear form) into such an analysis. This would permit a direct comparison of the behavior and efficiency of various support systems when failure near the face precludes a simple linear analysis.

While it might similarly be interesting to include a mining sequence, i.e., possibility for element removal, into the two-dimensional plane strain program, it is less than obvious that this would greatly improve the realistic nature of the analysis. Probably of more interest here is the development of a truly orthotropic and consistent rock failure model. In connection with this, and although somewhat outside the realm of tunnel support loading, it is clear that a more comprehensive body of experimental evidence about rock failure under polyaxial conditions would be most helpful.

A problem in the finite element rock failure model that certainly remains wide open at this point is the one of stability, uniqueness and convergence. It is very likely that what is desirable in the solution is some form of instability. But this does nothing to alleviate the problem of uniqueness and of convergence, the opposite being more likely.

Besides improvements to the representation of

rock failure, a number of extensions could be made to refine the support modeling. Starting with the simplest case, that of the blocked steel set, it might be necessary first and foremost to include some rotational freedom at beam element nodal points that correspond to connections between steel set segments as well as plastic hinges at sections where the elastic limit has been exceeded. Crushing and nonlinear time-dependent stiffness changes of wooden blocks might be included. For concrete and shotcrete support modeling, but certainly for loose or semi-stiff backfill, it would seem appropriate to include shear elements besides spring elements to study the influence of the interface characteristics. A detailed analysis of the increasingly used combination of steel sets, shotcrete and grouted bolts poses several difficult problems. The first one is the combination of steel sets and shotcrete, and the interaction between them. The second one is the evaluation of the in-situ shear stiffness along grouted bolts.

Because of the long running times of the computer programs, a great deal of work could (and should) justifiably be spent in improving the programming itself, as well as in some other ways that

might substantially reduce the computing cost.

Among the latter two possibilities should certainly be considered. The first one is the use of stiffness coefficients (Crouch, 1970) or, more generally, of substructural analysis methods (Pzremieniecki, 1968), in order to reduce the number of equations. The second one is the possibility of using an alternate equation solver, and it would appear that some of the more sophisticated iterative schemes should be considered first.

Most of the emphasis in this section on further developments has been upon further development of the analysis techniques, and the truism that this is necessary should be obvious. It is nevertheless worthwhile to explore some other potential avenues of further study, and at the same time return somewhat closer to the immediate problem of tunnel support loading.

While admitting the crudity in some approximations of the presented analyses, they nevertheless provide a method for a reasonably efficient comparative study of some support problems. An example of this was given in the study of the face influence upon support loading. An example of a similar parametric analysis that would be of interest and

could be performed without difficulties or changes to the plane program is that of the influence of blocking upon steel set behavior and loading. Factors that could easily be considered are block spacing, and variations thereof around an average; block stiffness, and variations thereof, whether due to block construction or due to overbreak; reblocking, i.e., partial removal, replacement or addition of blocks after some load has come on the set. Obvious examples for possible parametric analyses with regard to ground behavior are the study of lined and unlined openings in rock masses subjected to a variety of stressfields, and with a variety of intact and residual strengths as well as with various rates of progressive change from one to the other.

IV-3.3. Evaluation of the Validity and the Practical Significance of the Presented Analysis Methods. Any analysis of the types presented here needs experimental confirmation or evaluation. While the methods might be rejected upon the basis of fundamental or theoretical considerations, these cannot be used to justify their validity. An experimental program should, therefore, be considered an

integral part or at least a logical extension of the development of the preceding analysis methods, particularly so as the analysis is relatively simplistic compared to the real complexities of the problem.

An experimental program of sufficient amplitude to evaluate the practical validity, shortcomings and needed improvements of the presented analysis techniques should not be outside the realm of present-day engineering and economically justifiable possibilities. It is indeed a well-recognized fact (OECD Conference on Tunnelling, Washington, D.C., 1970) that serious shortcomings exist in the state-of-the-art of tunnel support design, that the support cost is frequently a significant factor of the total tunneling cost, and that the total volume of tunneling will significantly increase in the foreseeable future. Moreover, the geology of the area to be tunneled through is usually only partially known, at best, and the knowledge about the mechanical characteristics of the rock mass tends to be as meager, or worse. In addition comes a significant uncertainty factor introduced by construction influences, notably blasting and support erection.

It would appear that this combination of

factors should lead to a situation where Terzaghi's (1943, p. 2) "learn as we go" or Peck's (1969) "Observational Method" would find an ideal field of application. This has been strongly emphasized by Rabcewicz (1963, 1965, 1968), who has repeatedly stressed the need to consider instrumentation programs as an integral part of tunneling, as it has become in the "New Austrian Tunneling Method."

Assuming that the methods of support action analysis presented here can be considered as a valid "working hypothesis" for tunnel support evaluation, one should, ideally, find testing conditions where simultaneous benefits would be derived for owner and experimenter. This would necessitate an instrumentation and investigation program that is cost-effective in reducing the total tunneling cost while allowing an evaluation of the analysis method.

The cost factor evinces the need to consider each tunneling project on its particular merits, and the unlikelihood that a universally acceptable program can or should be devised. There must exist some correlation between tunneling cost, complexity of design and analysis methods used as a working hypothesis and comprehensiveness of field investigations and support instrumentation used to evaluate

their applicability.

Considering cases of increasing complexity, one might start, for a tunnel of limited overall cost, with the ground reaction as represented in Figures II.11 as a working hypothesis. The purpose of the (low cost) instrumentation program would then be to determine whether an optimum support stiffness exists, and what it is. In order to evaluate the validity of the hypothesis one needs assurance of a sufficient continuity in geological conditions along the tunnel, so that direct comparisons of measurements along different sections are meaningful. By comparing deformations in supports of different but known stiffnesses, one can locate points on the ground reaction curve.

A more complete evaluation would incorporate measurements of stresses, whether in between rock and support or within the support. Although in principle deformation measurements on a liner of known stiffness should be sufficient to allow back-calculation of the loads, this is a rather problematic procedure, because it requires at the least some assumptions about the load or contact distribution. Some redundancy is desirable as well as some specific information about loads.

A far more comprehensive investigation would be required if not only the shape of the ground reaction is postulated as a working hypothesis, or the existence of an optimum convergence for the support equilibrium, but if, moreover, one wishes to determine the ground reaction curve quantitatively and fairly accurately. This necessitates a knowledge of the stress-state and of the mechanical properties of the rock mass. Deformation and pressure measurements on supports of various stiffnesses should be sufficient to allow back-calculations, considering the support as a large-scale inclusion instrument implanted in a rock mass with more or less unknown behavior.

Whether the most elementary closed-form solutions, structural stiffness analysis, or the combination of the latter with finite element analysis constitutes the most appropriate interpretation tool would seem to depend mainly upon economic factors. When rather expensive comprehensive instrumentation programs are implemented there seems little justification for limiting the interpretation to a simplistic minimum. On the other hand, when the information gained is a bare minimum, a comprehensive parametric back-analysis by means of finite

element rock mass modeling and stiffness support modeling would be a laborious large-scale project, justifiable only under special circumstances. In the absence of sufficient information and redundancy, a good deal of judgment is necessary to avoid the danger of replacing analysis by curve fitting and arbitrary parameter adjustments.

## REFERENCES

Abel, John F.: "Tunnel Mechanics." Quarterly of the Colorado School of Mines, Vol. 62, No. 2, April 1967.

Anonymous: "Wood Handbook." U.S. Department of Agriculture, Handbook No. 72, 1955.

Baker, L. E., R. S. Sandhu and W. Y. Shieh. "Application of Elasto-Plastic Analysis of Rock Mechanics by Finite Element Method." Ch. 14, pp. 237-251, Eleventh Symposium on Rock Mechanics, June 1969, Berkeley, California, AIME Publication, 1970.

Barla, G.: "A Method for the Analysis of Stress in Brittle Rock." Int. J. Rock Mech. Min. Sci., pp. 87-102, Vol. 9, No. 1, January 1972.

Baudendistel, M.: "Wechselwirkung von Tunnelauskleidung und Gebirge." Heft 51, Veröffentlichungen des Institutes für Bodenmechanik und Felsmechanik der Universität Fridericiana in Karlsruhe, 1972.

\_\_\_\_\_.: "Zur Bemessung von Tunnelauskleidungen in wenig Festem Gebirge." Rock Mechanics, Supplementum 2, 1973, pp. 279-312.

Bieniawski, Z. T.: "Time-Dependent Behaviour of Fractured Rock." Rock Mechanics, Vol. 2, No. 3, pp. 123-137, September 1970.

Brace, W. F.: "Brittle Fracture of Rocks," pp. 111-174, State of Stress in the Earth's Crust, June 1963, Santa Monica, California; American Elsevier Publishing Company, New York, 1964.

Brace, W. F., B. W. Paulding, Jr. and C. Scholz: "Dilatancy in the Fracture of Crystalline Rocks." Journal of Geophys. Res., pp. 3939-3954, Vol. 71, No. 16, 1966.

Brace, W. F. and J. D. Byerlee: "Recent Experimental Studies of Brittle Fracture of Rocks," Ch. 2, pp. 58-81, Eighth Symposium on Rock Mechanics, University of Minnesota, September 1966; AIME Publication, 1967.

Brady, B. T.: "A Mechanical Equation of State for Brittle Rock--Part I--The Pre-failure Behavior of Brittle Rock." Int. J. Rock Mech. Min. Sci., Vol. 7, pp. 385-421, 1970, Appendix B.

Bray, J. W.: "A Study of Jointed and Fractured Rock --Part II--Theory of Limiting Equilibrium." Felsmechanik und Ingenieurgeologie, Vol. V, No. 4, 1967, pp. 197-216.

Burke, H. H.: "Garrison Dam--Investigation and Construction." ASCE Proceedings, Journal of the Soil Mechanics and Foundations Division, Paper 1438, November 1957.

Cook, N.G.W.: "The Design of Underground Excavations." Ch. 6, pp. 167-193, Eighth Symposium on Rock Mechanics, Minneapolis, 1966; Published by AIME, 1967.

Cording, E. J., A. J. Hendron, Jr. and D. U. Deere: "Rock Engineering for Underground Caverns." Symposium on Underground Chambers, ASCE, Phoenix, Arizona, January 1971, pp. 567-600.

Cornet, F. H.: "Compression Tests on Saturated Porous Rocks," Ph.D. Thesis, University of Minnesota, March 1975.

Cornet, F. H. and C. Fairhurst: "Influence of Pore Pressure on the Deformation Behavior of Saturated Rocks." Third Conference of the International Society for Rock Mechanics, Denver, September 1974.

Crouch, S. L.: "The Influence of Failed Rock on the Mechanical Behavior of Underground Excavations." Ph.D. Thesis, University of Minnesota, December, 1970a.

\_\_\_\_\_.: "Experimental Determination of Volumetric Strains in Failed Rock." Int. J. Rock Mech. Min. Sci., Vol. 7, No. 6, pp. 589-603, 1970b.

\_\_\_\_\_.: "The Post-failure Behavior of Norite in Triaxial Compression." *Engineering Geology*, Vol. 6, pp. 19-30, 1972.

Crouch, S. L. and C. Fairhurst: "Analysis of Rock Mass Deformations Due to Excavations." *Rock Mechanics Symposium, Applied Mechanics Division, ASME*, November 1973, pp. 25-40.

Daemen, J.J.K. and C. Fairhurst: "Influence of Failed Rock Properties on Tunnel Stability." *Twelfth Symposium on Rock Mechanics, Rolla, Missouri*, November 1970, pp. 855-875.

\_\_\_\_\_.: "Rock Failure and Tunnel Support Loading," pp. 356-369, *Proceedings, International Symposium on Underground Openings, Luzern*, September 1972.

\_\_\_\_\_.: "Ground/Support Interaction--Fundamentals and Design Implications." Part 2 of "Tunnels and Shafts in Rock." EM 1110-2-2901, December 1973, Department of the Army, Corps of Engineers, Office of the Chief of Engineers.

Dahl, H. D.: "A Finite Element Model for Anisotropic Yielding in Gravity Loaded Rock." Ph.D. Thesis, The Pennsylvania State University, 1969.

Dahl, D. and B. Voight: "Isotropic and Anisotropic Plastic Yield Associated with Cylindrical Underground Excavations," pp. 105-110, *International Symposium on Large Permanent Underground Openings, Oslo*, September 1969; Universitetsforlaget, Oslo, 1970.

DeBeer, E. E. and E. Buttiens: "Construction de réservoirs pour hydrocarbures liquéfiés dans l'argile de Boom à Anvers. Etude des mouvements du sol provoqués par cette réalisation." *Travaux*, Septembre 1966, N° 379, pp. 1087-1093, Octobre 1966, N° 380, pp. 1167-1174.

Desai, C. S.: "Theory and Applications of the Finite Element Method in Geotechnical Engineering," pp. 3-90, Vol. I, *Applications of the Finite Element Method in Geotechnical Engineering, Vicksburg, Mississippi*, May 1972.

Desai, C. S. and J. F. Abel: "Introduction to the Finite Element Method." Van Nostrand Reinhold Company, 1972.

Desai, C. S. and L. C. Reese: "Stress--Deformation and Stability Analyses of Deep Boreholes," pp. 475-484, Vol. 2, Proceedings of the Second Congress of the International Society for Rock Mechanics, Beograd 1970.

Dixon, J. D.: "Structural Design Data for Unreinforced Concrete Tunnel Linings." U.S. Bureau of Mines, R I 7297, 1969.

\_\_\_\_\_.: "Analysis of Tunnel Support Structure With Consideration of Support-Rock Interaction." U.S. Bureau of Mines, R I 7526, 1971; also in Transactions, Society of Mining Engineers, AIME, Vol. 250, 1971, pp. 304-309.

\_\_\_\_\_.: "Structural Design Data for Concrete Drift Linings in Block Caving Stopes." U.S. Bureau of Mines, R I 7792, 1973.

Drucker, D. C. and W. Prager: "Soil Mechanics and Plastic Analysis or Limit Design." Quart. Appl. Math., Vol. 10, No. 2, 1952, pp. 157-165.

Egger, P.: "Zur Abschaetzung des Gebirgsdrucks aufgrund des Post-failure--Verhaltens." International Symposium on Underground Openings, Luzern, September 1972, pp. 290-295.

\_\_\_\_\_.: "Design of Tunnel Support Based on the Post-failure Behaviour of the Rock." International Congress on Fracture, Muenchen, April 1973, Vol. X, Paper IX-424.

Fairhurst, C. and N.G.W. Cook: "The Phenomenon of Rock Splitting Parallel to the Direction of Maximum Compression in the Neighbourhood of a Surface." Paper 3.75, pp. 687-892, Vol. II, Proceedings of the 1st Congress of the International Society of Rock Mechanics, Lisbon, 1966.

Gates, R. H.: "Slope Analysis for Explosive Excavations." Proceedings of the Thirteenth Symposium on Rock Mechanics, Urbana, Ill., 1971, pp. 243-268, ASCE Publication, 1972.

\_\_\_\_\_. : "Progressive Failure Model for Clay Shale," pp. 327-347, Vol. I, Applications of the Finite Element Method in Geotechnical Engineering, Vicksburg, Mississippi, May, 1972.

Gay, N. C.: "Fracture Growth Around Openings in Thick-Walled Cylinders of Rock Subjected to Hydrostatic Compression." Int. J. Rock Mech. Min. Sci. & Geomech. Abstr., Vol. 10, No. 3, pp. 209-233, May, 1973.

Girija Vallabhan, C. V. and R. K. Jain: "Octahedral Stress Approach to Analysis of Water Resources Structures," pp. 1185-1210, Vol. III, Applications of the Finite Element Method in Geotechnical Engineering, Vicksburg, Mississippi, May, 1972.

Girija Vallabhan, C. V. and L. C. Reese: "Finite-Element Method for Problems in Soil Mechanics." Proceedings of ASCE, Journal of the Soil Mechanics and Foundations Division, Vol. 94, No. SM2, pp. 473-496, March 1968.

Goguel, Jean: "Répartition des Contraintes autour d'un tunnel cylindrique." Annales des Ponts et Chaussées, 117e Année, Mars-Avril 1947, pp. 157-183.

Golser, J.: "Praktische Beispiele empirischer Dimensionierung von Tunneln." Rock Mechanics, Supplementum 2, 1973, pp. 225-241.

Green, A. E. and W. Zerna: "Theoretical Elasticity." Oxford: Clarendon Press, 1968.

Grob, H.: Diskussionsbeitrag, Rock Mechanics, Supplementum 2, 1973, pp. 387-393.

Hayashi, M. and S. Hibino: "Visco-plastic Analysis on Progressive Relaxation of Underground Excavation Works," pp. 565-575, Vol. 2, Proceedings of the Second Congress of the International Society for Rock Mechanics, Beograd, 1970.

Hearmon, R.F.S.: "An Introduction to Applied Anisotropic Elasticity." Oxford University Press, 1961.

Heuzé, F. E. and R. E. Goodman: "Finite Element Studies of 'Pile Driver' Tunnels, Including Considerations of Support Requirements." Technical Report No. 13; Prepared under Contract DACA 45-71-C-0031 by the University of California, Berkeley, for the Omaha District, Corps of Engineers, Omaha, Nebraska, November 1972.

Hobbs, D. W.: "A Study of the Behaviour of a Broken Rock Under Triaxial Compression and its Application to Mine Roadways." Int. J. Rock Mech. Min. Sci., Vol. 3, pp. 11-43, 1966.

Höeg, K.: "Finite Element Analysis of Strain-Softening Clay," pp. 43-58, Journal of the Soil Mechanics and Foundations Division, Proceedings of ASCE, Vol. 98, No. SM1, January 1972; Closure of Discussion, pp. 1167-1168, Vol. 99, No. SM7, July 1973.

Hopper, R. C., T. A. Lang and A. A. Mathews: "Construction of Straight Creek Tunnel, Colorado." North American Rapid Excavation and Tunneling Conference, Chicago, 1972, Vol. 1, Ch. 28, pp. 501-538.

Hoyaux, B. and B. Ladanyi: "Gravitational Stress Field Around a Tunnel in Soft Ground," pp. 54-61; Canadian Geotechnical Journal, Vol. 7, Number 1, February, 1970a.

\_\_\_\_\_. : "Rock Failure Around a Circular Opening in a Gravity Field with Tectonic Forces," Ch. 17, pp. 281-292, Eleventh Symposium on Rock Mechanics, Berkeley, June 1969, AIME Publication, 1970b.

Hudson, J. A. and E. T. Brown: "Studying Time-Dependent Effects in Failed Rock," pp. 25-34, Proceedings, Fourteenth Symposium on Rock Mechanics, Pennsylvania State University, June 1972; Published by ASCE, 1973.

Hudson, J. A., E. T. Brown and C. Fairhurst: "Optimizing the Control of Rock Failure in Servo-Controlled Laboratory Tests." *Rock Mechanics*, Vol. 3, No. 4, pp. 217-224, December 1971.

Isenberg, J.: "Analytic Modeling of Rock-Structure Interaction." Agbabian Associates, Final Technical Report. U.S. Bureau of Mines, Contract Number HO 220035, April 1973.

Isenberg, J. and C. F. Bagge: "Analysis of Steel-lined Penetration Shafts for Deeply Buried Structures," pp. 1145-1164, Vol. III, Applications of the Finite Element Method in Geotechnical Engineering, Vicksburg, Mississippi, May 1972.

Ishijima, Y. and K. Suzuki: "The Simulation Technique to Analyse the Rock Pressure Applied to Tunnel Supports," pp. 583-586, Vol. 2, Proceedings of the Second Congress of the International Society for Rock Mechanics, Beograd, 1970.

Jaeger, J. C.: "Elasticity, Fracture and Flow." Methuen, London, 1964.

Jaeger, J. C. and N.G.W. Cook: "Fundamentals of Rock Mechanics." Methuen & Co., London, 1969.

Jamet, P. : "Compressive Failure of a Hollow Cylinder Subjected to External Loading." Unpublished M. Sc. Thesis, University of Minnesota, March 1973.

Kovári, K.: "Ein Beitrag zum Bemessungsproblem von Untertagbauten." *Schweizerische Bauzeitung*, Vol. 87, No. 37, pp. 687-697, 1969.

Krech, W. W.: "The Determination of the Mechanical Properties of Rock and Soil by Means of a Hollow Cylinder Loaded with External Pressure." Ph.D. Thesis, University of Minnesota, 1966.

Labasse, H.: "Les Pressions de Terrains Autour des Puits." *Revue Universelle des Mines*, pp. 78-88, 92e Année, S.9, V.5., Mars 1949.

Lane, K. S.: "Garrison Dam--Evaluation of Test Results." Proceedings of ASCE, Journal of the Soil Mechanics and Foundations Division, Paper 1439, Vol. 83, No. SM4, November 1957.

Lecian, J.: "Abstimmen von Gebirgsverformung und Ausbauwiderstand in Strecken und Schachten ohne Abbaueinwirkungen." Glueckauf Forschungshefte. Jahrgang 29, H.6., pp. 311-314, Dezember 1968.

Lekhnitskii, S. G.: "Theory of Elasticity of an Anisotropic Elastic Body." Holden-Day, Inc.; San Francisco, 1963.

Lo, K. Y. and C. F. Lee: "Discussion of Paper by Höeg (1972), Proceedings of ASCE," Journal of the Soil Mechanics and Foundations Division, Vol. 98, No. SM9, pp. 981-983, Sept. 1972.

\_\_\_\_\_. : "Stress Analysis and Slope Stability in Strain-softening Materials." Geotechnique, Vol. 23, No. 1, pp. 1-11, March 1973.

Lombardi, G.: Discussion, Theme 7, Vol. III, pp. 525-526, Proceedings of the 1st Congress of the International Society of Rock Mechanics, Lisbon, 1966.

\_\_\_\_\_. : "The Influence of Rock Characteristics on the Stability of Rock Cavities." Tunnels and Tunnelling, Jan.-Feb. 1970, pp. 19-22; March-April 1970, pp. 104-109.

\_\_\_\_\_. : Diskussionsbeitrag zum Thema 2, pp. 370-378, Proceedings of the International Symposium on Underground Openings, Luzern, Sept. 1972.

\_\_\_\_\_. : "Felsmechanische Probleme am Gotthard." Rock Mechanics, Supplementum 3, pp. 113-130, 1974a.

\_\_\_\_\_. : "Tunnel Support." Third Congress of the International Society for Rock Mechanics, Vol. 1, Theme 4, pp. 1518-28, Denver, September 1974b.

Luetgendorf, H. O.: "Der Mindestausbauwiderstand des Grubenausbau in Strecken und Schachten." Glueckauf Forschungshefte, Jahrgang 29, H. 5., pp. 253-261, Oktober 1968.

Mahar, J. W., F. L. Gau and E. J. Cording.: "Observations During Construction of Rock Tunnels for the Washington, D.C., Subway." North American Rapid Excavation and Tunneling Conference, Vol. 1, Ch. 35, pp. 659-681, 1972.

Malina, H.: "The Numerical Determination of Stresses and Deformations in Rock Taking into Account Discontinuities." Rock Mechanics, Vol. 2, No. 1, pp. 1-16, May 1970.

Mandel, J.: "Les calculs en matière de pressions des terrains." Revue de l'Industrie Minérale, Vol. 41; No. 1, Janvier, pp. 78-92, No. 4, Avril, pp. 313-315, 1959. Translation by C. Fairhurst, University of Nottingham Mining Department Magazine, Vol. No. XVI, 1964.

Martin, H. C. and G. F. Carey: "Introduction to Finite Element Analysis." McGraw-Hill Book Company, 1973.

Melosh, R. J.: "Manipulation Errors in Finite Element Analysis," pp. 857-877, Recent Advances in Matrix Methods of Structural Analysis and Design, Tokyo, August 1969; The University of Alabama Press, 1971.

Morrison, R.G.K. and D. F. Coates: "Soil Mechanics Applied to Rock Failure in Mines." The Canadian Mining and Metallurgical Bulletin, Vol. 48, November 1955, No. 523, pp. 701-711; see also Transactions of the Canadian Institute of Mining and Metallurgy, Vol. LVIII, 1955, pp. 401-411.

Mueller, G., Mueller-Salzburg, L. and H. P. Goetz: "Messung der Spannungs- und Materialumlagerungen in gekluftetem Fels." Proceedings of the 2nd Congress of the International Society for Rock Mechanics, Paper 4-46, Vol. 2, pp. 723-729, Beograd, 1970.

Obert, L. A. and W. I. Duvall: "Rock Mechanics and the Design of Structures in Rock." John Wiley, New York, 1967.

Pacher, F.: "Deformationsmessungen im Versuchsstollen als Mittel zur Erforschung des Gebirgsverhaltens und zur Bemessung des Ausbaues." *Felsmechanik und Ingenieurgeologie, Supplementum IV*, 1964, pp. 149-161.

Peck, R. B.: "Deep Excavations and Tunneling in Soft Ground." State-of-the-Art Report, Seventh International Conference on Soil Mechanics and Foundation Engineering, pp. 225-290, Mexico, 1969a.

\_\_\_\_\_.: "Advantages and Limitations of the Observational Method in Applied Soil Mechanics." *Geotechnique*, Vol. 19, No. 2, pp. 171-187, June, 1969b.

Peng, S. S.: "Time-dependent Aspects of Rock Behavior as Measured by a Servo-controlled Hydraulic Testing Machine," pp. 235-246, *Int. J. Rock Mech. Min. Sci. & Geomech. Abstr.*, Vol. 10, No. 3, May 1973.

Perloff, W. H. and L. E. Pombo: "End Restraint Effects in the Triaxial Test." Proceedings of the Seventh International Conference on Soil Mechanics and Foundation Engineering, Vol. 1, pp. 327-333, Mexico, 1969.

Proctor, R. V. and Th. L. White: "Rock Tunneling with Steel Supports." Commercial Shearing and Stamping Company, Youngstown, Ohio, 1968.

Przemieniecki, J. S.: "Theory of Matrix Structural Analysis." McGraw-Hill Book Company, 1968.

Rabcewicz, L. v.: "Die Ankerung im Tunnelbau ersetzt bisher gebrauchliche Einbaumethoden." *Schweiz. Bauztg.*, Jg. 75, March 1957, pp. 123-131.

\_\_\_\_\_.: "Bemessung von Hohlraumbauten." *Felsmechanik und Ingenieurgeologie, Vol. 1/3-4*, pp. 224-244, 1963.

\_\_\_\_\_.: "The New Austrian Tunneling Method." *Water Power*; November, December 1964 and January 1965.

\_\_\_\_\_  
: "Stability of Tunnels Under Rock Load." June, pp. 225-229; July, pp. 266-273; August, pp. 297-302; Water Power, 1969.

Rabcewicz, L. v., J. Golser und E. Hackl.: "Die Bedeutung der Messung im Hohlraumbau." Der Bauingenieur, 1972, 47. Jahrg., Heft 7, S. 225-234 u. H. 8, S. 278-287.

Reyes, S. F.: "Elastic-Plastic Analysis of Underground Openings by the Finite Element Method." Ph.D. Thesis, University of Illinois, 1966.

Reyes, S. F. and D. U. Deere: "Elastic-Plastic Analysis of Underground Openings by the Finite Element Method," pp. 477-483, Vol. II, Proceedings of the First Congress of the International Society of Rock Mechanics, Lisbon, 1966.

Richter, R.: "Das mittelbare Ingleichgewichthalten bei untertägigen Hohlraumen." Proceedings of the First Congress of the International Society of Rock Mechanics, Lisbon, 1966, Vol. II, Paper 7.25, pp. 375-378.

Roark, R. J.: "Formulas for Stress and Strain." Third Edition, McGraw-Hill, 1954.

Rummel, F. and C. Fairhurst: "Determination of the Post-Failure Behavior of Brittle Rock Using a Servo-Controlled Testing Machine." Rock Mechanics, Vol. 2, No. 4, pp. 189-204, December 1970.

Serata, S.: "Theory and Model of Underground Opening and Support System." Proceedings of the Sixth Symposium on Rock Mechanics, University of Missouri at Rolla, 1964, pp. 260-292.

Singh, B.: "Continuum Characterization of Jointed Rock Masses." Int. J. Rock Mech. Min. Sci. and Geomech. Abstr., Vol. 10, No. 4, pp. 311-349, 1973.

Sirieys, P. M.: "Champs de contraintes autour des tunnels circulaires en élastoplastique." Felsmechanik und Ingenieurgeologie. Vol. II/1, pp. 68-75, 1964.

Sperry, P. E. and R. E. Heuer: "Excavation and Support of Navajo Tunnel No. 3." Proceedings North American Rapid Excavation and Tunneling Conference, Vol. 1, Ch. 29, pp. 539-571, AIME Publication, 1972.

Terzaghi, K.: "Die Erddruckerscheinungen." Oesterr. Wochenschr. oeffentl. Baudienst, Heft 17, pp. 194-199; H. 18, pp. 206-210; H. 19, pp. 218-223; Jg. 1919.

\_\_\_\_\_.: "Erdbaumechanik auf bodenphysikalischer Grundlage." Franz Deuticke, Leipzig und Wien, pp. 212-214, 1925.

\_\_\_\_\_.: "Theoretical Soil Mechanics." John Wiley and Sons, Inc., New York, pp. 202-215, 1943.

\_\_\_\_\_.: "Rock Defects and Loads on Tunnel Supports." Section I, pp. 15-99, of reference by Proctor and White, 1946, revised 1968.

Vouille, G.: "Calcul du revêtement des tunnels creusés dans des terrains présentant des déformations différencées." Industrie Minérale, pp. 13-18, Numéro Spécial du 15 Avril 1974.

Wagner, H.: "The New Austrian Tunnelling Method." The Technology and Potential of Tunnelling, The South African Tunnelling Conference, Johannesburg, 1970, Vol. 1, pp. 121-127.

Wawersik, W. R.: "Detailed Analysis of Rock Failure in Laboratory Compression Tests." Ph.D. Thesis, University of Minnesota, July 1968.

\_\_\_\_\_.: "Time-Dependent Rock Behavior in Uniaxial Compression," pp. 85-106, Proceedings, Fourteenth Symposium on Rock Mechanics, Pennsylvania State University, June 1972; Published by ASCE, 1973.

Wawersik, W. R. and C. Fairhurst: "A Study of Brittle Rock Fracture in Laboratory Compression Experiments." Int. J. Rock Mech. Min. Sci., Vol. 7, No. 5, pp. 561-575, 1970.

Wawersik, W. R. and W. F. Brace: "Post-Failure Behavior of a Granite and Diabase." Rock Mechanics, Vol. 3, No. 2, pp. 61-85, June 1971.

Westergaard, H. M.: "Plastic State of Stress Around a Deep Well." Journal of the Boston Society of Civil Engineers, Vol. XXVII, January 1940, No. 1, pp. 1-5.

Wiebols, G. A., et al.: "Rock Property Tests in a Stiff Testing Machine," Ch. 11, pp. 297-329, Tenth Symposium on Rock Mechanics, Austin, Texas, 1968; AIME Publication, New York, 1972.

Wilson, E. L.: "Finite Element Analysis of Two-Dimensional Structures." Doctor of Engineering Dissertation, University of California, Berkeley, 1963.

\_\_\_\_\_.: "SAP, A General Structural Analysis Program." Report No. UCSESM 70-20, University of California, 1970.

Zienkiewicz, O. C.: "The Finite Element Method in Engineering Science." McGraw-Hill, London, 1971.

Zienkiewicz, O. C., S. Valliappan and I. P. King: "Stress Analysis of Rock as a 'no-tension' Material." Geotechnique, Vol. 18, No. 1, pp. 56-66, 1968.

Zienkiewicz, O. C., B. Best, C. Dullage and K. G. Stagg: "Analysis of Non-linear Problems in Rock Mechanics with Particular Reference to Jointed Rock Systems," Vol. 3, 8-14, pp. 501-509, Proceedings of the Second Congress of the International Society for Rock Mechanics, Beograd, 1970.

## APPENDIX A

### DETAILED CALCULATIONS FOR THE CONTINUUM ANALYSIS OF ROCK-SUPPORT INTERACTION

In this appendix a detailed derivation is given of the results presented in Chapter II.

#### A-1. Stress Distribution

The following equations are used in the derivation of the stress distribution:

Equilibrium (Eq. II-3.4):

$$\sigma_e - \sigma_r - r \frac{d\sigma}{dr} \pm rw = 0 \quad (A.1)$$

Failure condition in the broken zone:

$$\sigma_e^{br} (1 - \sin \phi_r) = \sigma_r^{br} (1 + \sin \phi_r) +$$

$$2 c_r \cos \phi_r \quad (A.2)$$

$$a \leq r \leq b$$

Incipient state of failure on the elastic side of the broken zone limit:

$$\sigma_e^{el} (1 - \sin \phi) = \sigma_r^{el} (1 + \sin \phi) + 2 c \cos \phi \quad (A.3)$$

$$\text{at } r = b$$

Stress distribution in elastic region,  
resulting in:

$$\sigma_{\theta}^{\text{el}} + \sigma_r^{\text{el}} = 2P \quad (\text{A.4})$$

Boundary conditions

$$\sigma_r = P_i \quad \text{at } r = a$$

$$\sigma_r^{\text{el}} = \sigma_r^{\text{br}} \quad \text{at } r = b$$

In the above equations

$\sigma_{\theta}$ ,  $\sigma_r$ : tangential and radial stress

$\sigma_{\theta}^{\text{br}}$ ,  $\sigma_r^{\text{br}}$ : tangential and radial stress in broken zone

$\sigma_{\theta}^{\text{el}}$ ,  $\sigma_r^{\text{el}}$ : tangential and radial stress in elastic region

w = specific weight

c,  $\phi$ : cohesion and angle of internal friction of intact rock

$c_r$ ,  $\phi_r$ : (residual) cohesion and internal friction of broken rock

a, b: tunnel radius and radius of broken zone

P: hydrostatic stressfield

$P_i$ : support pressure

Substituting (A.4) into (A.3), one finds

$$\sigma_r^{\text{el}} = P(1 - \sin \phi) - c \cos \phi \quad \text{at } r = b \quad (\text{A.5})$$

The radial stress at  $r = b$  is determined by the stressfield P and the intact rock strength ( $c, \phi$ ), and is independent of b.

Substituting (A.2) into (A.1) one obtains a

differential equation for  $\sigma_r^{br}$ :

$$\frac{\sigma_r^{br}(1 + \sin \phi_r) - \sigma_r^{br}(1 - \sin \phi_r) + 2 c_r \cos \phi_r}{1 - \sin \phi_r} - r \frac{d \sigma_r^{br}}{dr} \pm wr = 0$$

$$\frac{d \sigma_r^{br}}{dr} - \frac{2 \sin \phi_r}{1 - \sin \phi_r} \cdot \frac{\sigma_r^{br}}{r} = \frac{2 c_r \cos \phi_r}{r(1 - \sin \phi_r)} \pm w$$

(A.6)

Integration of (A.6) results in:

a) when  $\sin \phi_r \neq 1/3$  and  $\phi_r \neq 0$

$$\sigma_r^{br} = -c_r \cot \phi_r \pm \frac{rw(1 - \sin \phi_r)}{1 - 3 \sin \phi_r} + Mr \frac{2 \sin \phi_r}{1 - \sin \phi_r}$$

(A.7a)

b) when  $\sin \phi_r = 1/3$

$$\sigma_r^{br} = -3 c_r \cos \phi_r \pm rw \log r + Mr$$

(A.7b)

c) when  $\phi_r = 0$  equation (A.2) reduces to

$$\sigma_\theta^{br} = \sigma_r^{br} + 2 c_r$$

Substituting in (A.1) gives an equivalent  
for the differential equation (A.6):

$$r \frac{d \sigma_r^{br}}{dr} = 2 c_r \pm rw$$

After integration this gives:

$$\sigma_r^{br} = 2 c_r \log r \pm wr + M$$

(A.7c)

In equations (A.7) M is a constant of integration, which is determined from the boundary

condition on the tunnel periphery  $r = a$ , where the radial stress equals the support pressure,  $\sigma_r = P_i$  at  $r = a$ . After substituting the thus determined constant  $M$  in equations (A.7) one obtains the stress distribution in the broken zone:

a)  $\sin \phi_r \neq 1/3, \phi_r \neq 0$

$$\begin{aligned} \sigma_r^{br} = & -c_r \cot \phi_r \pm \frac{rw (1 - \sin \phi_r)}{1 - 3 \sin \phi_r} \\ & + (P_i + c_r \cot \phi_r \mp aw \frac{1 - \sin \phi_r}{1 - 3 \sin \phi_r}) \left(\frac{r}{a}\right)^{\frac{2 \sin \phi_r}{1 - \sin \phi_r}} \end{aligned} \quad (A.8a)$$

b)  $\sin \phi_r = 1/3$

$$\begin{aligned} \sigma_r^{br} = & -3 c_r \cos \phi_r \pm rw \log r \\ & + (P_i + 3 c_r \cos \phi_r \mp aw \log a) \frac{r}{a} \end{aligned} \quad (A.8b)$$

c)  $\sin \phi_r = 0$

$$\sigma_r^{br} = P_i + 2 c_r \log \frac{r}{a} \pm w (r - a) \quad (A.8c)$$

By introducing the continuity in radial stresses across the broken zone boundary  $r = b$ , i.e., by equating (A.5) and (A.8), one obtains a relationship between the depth  $b$  to which the broken zone propagates and the corresponding support pressure  $P_i$ :

a)  $\sin \phi_r \neq 1/3, \phi_r \neq 0$

$$\begin{aligned}
 P(1 - \sin \phi) - c \cos \phi &= c_r \cot \phi_r \pm bw \frac{1 - \sin \phi_r}{1 - 3 \sin \phi_r} \\
 + (P_i + c_r \cot \phi_r \mp aw \frac{1 - \sin \phi_r}{1 - 3 \sin \phi_r}) \frac{(b)}{(a)} \frac{2 \sin \phi_r}{1 - \sin \phi_r} \\
 P_i &= [P(1 - \sin \phi) - c \cos \phi + c_r \cot \phi_r] \frac{(a)}{(b)} \frac{2 \sin \phi_r}{1 - \sin \phi_r} \\
 - c_r \cot \phi_r \pm \frac{aw(1 - \sin \phi_r)}{1 - 3 \sin \phi_r} &[1 - \frac{(a)}{(b)} \frac{3 \sin \phi_r - 1}{1 - \sin \phi_r}]
 \end{aligned}$$

(A.9a)

b)  $\sin \phi_r = 1/3$

$$P_i = \frac{a}{b} [P(1 - \sin \phi) - c \cos \phi + 3 c_r \cos \phi_r]$$

$$\pm w a \log \frac{a}{b} - 3 c_r \cos \phi_r \quad (A.9b)$$

c)  $\sin \phi_r = 0$

$$P_i = P(1 - \sin \phi) - c \cos \phi - 2 c_r \log \frac{b}{a} - w(b-a) \quad (A.9c)$$

Equations (A.9) are given in Chapter II as equations (II-3.5).

Two functions of the stresses are needed in the calculation of the displacements,  $\sigma_\theta^{br} + \sigma_r^{br}$  and  $\sigma_\theta^{br} - \sigma_r^{br}$ . These can be obtained from (A.2):

$$\begin{aligned}
 \sigma_\theta^{br} + \sigma_r^{br} &= \sigma_r^{br} \frac{1 + \sin \phi_r}{1 - \sin \phi_r} + \frac{2 c_r \cos \phi_r}{1 - \sin \phi_r} + \sigma_r^{br} \\
 &= \frac{2 \sigma_r^{br}}{1 - \sin \phi_r} + \frac{2 c_r \cos \phi_r}{1 - \sin \phi_r} \quad (A.10a)
 \end{aligned}$$

$$\sigma_{\theta}^{br} - \sigma_r^{br} = \frac{2 \sigma_r^{br} \sin \phi_r}{1 - \sin \phi_r} + \frac{2 c_r \cos \phi_r}{1 - \sin \phi_r} \quad (A.11a)$$

When  $\sin \phi_r = 1/3$ , this can be written as:

$$\sigma_r^{br} + \sigma_{\theta}^{br} = 3 \sigma_r^{br} + 3 c_r \cos \phi_r \quad (A.10b)$$

$$\sigma_{\theta}^{br} - \sigma_r^{br} = \sigma_r^{br} + 3 c_r \cos \phi_r \quad (A.11b)$$

When  $\sin \phi_r = 0$ ,

$$\sigma_{\theta}^{br} + \sigma_r^{br} = 2(\sigma_r^{br} + c_r) \quad (A.10c)$$

$$\sigma_{\theta}^{br} - \sigma_r^{br} = 2 c_r \quad (A.11c)$$

Substituting equations (A.8) into (A.10) and (A.11), these functions can be written as:

a)  $\sin \phi_r \neq 1/3, \phi_r \neq 0$

$$\begin{aligned} \sigma_{\theta}^{br} + \sigma_r^{br} &= -2 c_r \cot \phi_r \pm \frac{2 r w}{1 - 3 \sin \phi_r} \alpha_r \\ &+ \frac{2}{1 - \sin \phi_r} [P_i + c_r \cot \phi_r \mp \frac{aw (1 - \sin \phi_r)}{1 - 3 \sin \phi_r}] (\frac{r}{a}) \end{aligned} \quad (A.12a)$$

$$\begin{aligned} \sigma_{\theta}^{br} - \sigma_r^{br} &= \frac{2 \sin \phi_r}{1 - \sin \phi_r} [P_i + c_r \cot \phi_r \mp \\ &\pm \frac{1 - \sin \phi_r}{aw \frac{1 - 3 \sin \phi_r}{1 - \sin \phi_r}} (\frac{r}{a}) \mp \frac{2 r w \sin \phi_r}{1 - 3 \sin \phi_r}] \quad (A.13a) \end{aligned}$$

b)  $\sin \phi_r = 1/3$

$$\sigma_{\theta}^{\text{br}} + \sigma_r^{\text{br}} = -6 c_r \cos \phi_r \pm wr \log r$$

$$+ \frac{3r}{a} [P_i + 3 c_r \cos \phi_r \mp wa \log a] \quad (\text{A.12b})$$

$$\sigma_{\theta}^{\text{br}} - \sigma_r^{\text{br}} = (P_i + 3 c_r \cos \phi_r \mp wa \log a) \frac{r}{a} \pm wr \log r$$

$$(\text{A.13b})$$

c)  $\sin \phi_r = 0$

$$\sigma_{\theta}^{\text{br}} + \sigma_r^{\text{br}} = 2(P_i + c_r) + 4 c_r \log \frac{r}{a} \pm 2w(r-a)$$

$$(\text{A.12c})$$

$$\sigma_{\theta}^{\text{br}} - \sigma_r^{\text{br}} = 2 c_r \quad (\text{A.13c})$$

The above sums and differences of principal stresses have to be integrated from a to b, and it is convenient to separate the various functions of r:

a)  $\sin \phi_r \neq 1/3, \sin \phi_r \neq 0$

$$\sigma_{\theta}^{\text{br}} + \sigma_r^{\text{br}} = K + Lr + Mr^{\alpha} \quad (\text{A.15a})$$

b)  $\sin \phi_r = 1/3$

$$\sigma_{\theta}^{\text{br}} + \sigma_r^{\text{br}} = K + Lr \log r + Mr \quad (\text{A.14b})$$

$$\sigma_{\theta}^{\text{br}} - \sigma_r^{\text{br}} = Lr \log r + Mr \quad (\text{A.15b})$$

c)  $\sin \phi_r = 0$

$$\sigma_{\theta}^{\text{br}} + \sigma_r^{\text{br}} = K + L \log r + Mr \quad (\text{A.14c})$$

In the above expressions K, L and M are the appropriate coefficients for each particular case.

The needed integrals are:

$$\int_a^b (\sigma_{\theta}^{br} + \sigma_r^{br}) r dr, \text{ and } \int_a^b (\sigma_{\theta}^{br} - \sigma_r^{br}) r dr$$

After substituting (A.14) and (A.15), the results are:

$$a) \int_a^b (K + Lr + Mr \alpha_r) r dr = K \frac{b^2 - a^2}{2} + L \frac{b^3 - a^3}{3} + M \frac{\frac{\alpha_r + 2}{b} \frac{\alpha_r + 2}{-a}}{\alpha_r + 2} \quad (A.16a)$$

$$\text{where } \alpha_r + 2 = \frac{2}{1 - \sin \phi_r}$$

$$b) \int_a^b (K + L r \log r + Mr) r dr = K \frac{b^2 - a^2}{2} + L \left( \frac{b^3 \log b - a^3 \log a}{3} - \frac{b^3 - a^3}{9} \right) + M \frac{b^3 - a^3}{3} \quad (A.16b)$$

$$c) \int_a^b (K + L \log r + Mr) r dr = K \frac{b^2 - a^2}{2} + L \left( \frac{b^2 \log b - a^2 \log a}{2} - \frac{b^2 - a^2}{4} \right) + M \frac{b^3 - a^3}{3} \quad (A.16c)$$

## A-2. Displacements

### A-2.1. Constant Volume Increase Throughout

the Broken Zone. Prior to failure the volume per unit tunnel length of rock in the broken zone is  $\gamma (b^2 - a^2)$ . During failure this volume increases

to  $\pi(b^2 - a^2)(1 + K)$ . After failure the volume can also be written as  $\pi[(b - u_b)^2 - (a - u_a)^2]$ , where  $u_a$  and  $u_b$  are the radial displacements at the tunnel surface,  $r = a$ , and at the broken zone boundary,  $r = b$ , respectively.  $K$  is the volume expansion factor. Equating the two expressions for the final volume results in:

$$(a - u_a)^2 = (b - u_b)^2 - (1 + K)(b^2 - a^2) \quad (A.17)$$

$$u_a = a - [(b - u_b)^2 - (1 + K)(b^2 - a^2)]^{1/2} \quad (A.18)$$

A simpler expression for  $u_a$  can be derived by rewriting (A.17) as

$$(b^2 - 2bu_b + u_b^2) - (a^2 - 2au_a + u_a^2) = (1 + K)(b^2 - a^2)$$

Iff  $u_a \ll a$  and  $u_b \ll b$ , this reduces to

$$u_a = \frac{b}{a} u_b + \frac{K(b^2 - a^2)}{2a} \quad (A.19)$$

The error introduced by neglecting  $u_a^2 - u_b^2$  increases with increasing  $K$ , with increasing  $b/a$  and with increasing  $u_b/a$ , as can be seen in Figure A.1.

The displacement  $u_b$  is the displacement at  $r = b$  caused by tunneling, or the displacement induced by the stress change in the elastic region.

A = 10

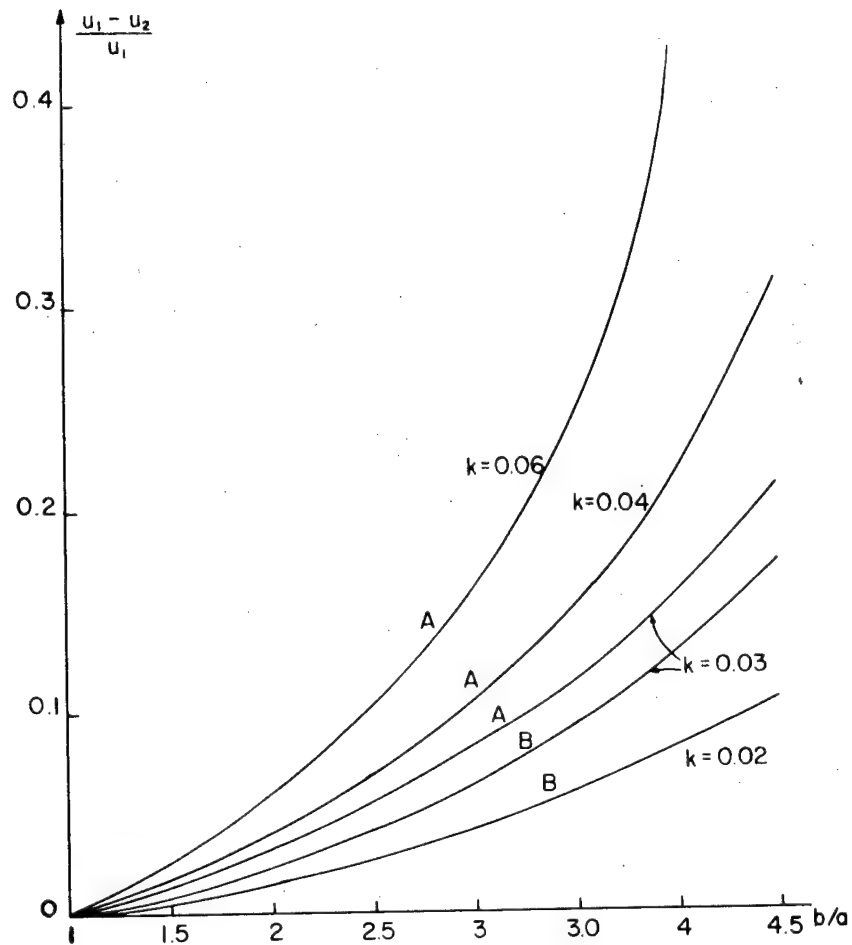


Figure A.1. Relative Error Introduced by Linearizing the "Constant Volume Expansion" Displacement Calculation, i.e., by

neglecting  $u_a^2 - u_b^2$

$u_1$  = exact  $u_a$ , according to equation  
(A.18)

$u_2$  = linearized  $u_a$ , according to equation  
(A.19)

$b, a$  = radius of broken zone and tunnel  
radius

$$A: \frac{u_b}{a} = 0.01 \quad B: \frac{u_b}{a} = 0.0001$$

Prior to tunneling  $\sigma_r = \sigma_\theta = \sigma_z = P$ . After tunneling:

$$\sigma_r^{el} = P - (P - \sigma_{r,r=b}) \frac{b^2}{r^2}$$

$$\sigma_\theta^{el} = P + (P - \sigma_{r,r=b}) \frac{b^2}{r^2}$$

$$\sigma_z^{el} = P$$

The tangential strain change over the pre-tunneling value is:

$$\varepsilon_\theta = \frac{\Delta u}{r} = \frac{\Delta \sigma_\theta - \nu(\Delta \sigma_r + \Delta \sigma_z)}{E}$$

$$\frac{u_b}{b} = \frac{(P - \sigma_{r,r=b})(1 + \nu)}{E} = \frac{(P \sin \phi + c \cos \phi)(1 + \nu)}{E}$$
(A.20)

where  $\sigma_{r,r=b}$  is substituted from (A.5).

A-2.2. Displacements Caused by Elastic Relaxation. Driving a tunnel is equivalent to removing the central core from a loaded very thick cylinder, or to depressurization of the central hole of a hydrostatically loaded thick wall cylinder. During the depressurization, when the stresses reach a critical value (on the hole periphery) failure is initiated. Failure propagates during further depressurization or "unloading." The entire

sequence occurs under constant external pressure.

The lower (radial or confining) principal stress decreases during the process, while the larger (tangential) principal stress increases up to the point of failure and decreases thereafter.

The displacement associated with the propagation of a broken zone will now be considered as an elastic relaxation of the (broken) rock caused by stress relief around the tunnel.

Considering an annulus with volume  $\pi (b^2 - a^2)$  prior to tunneling, its volumetric compression

prior to tunneling can be calculated from

$$\int_a^b \left( \frac{du}{dr} + \frac{u}{r} \right) 2\pi r dr$$
, where the strains are calculated from the hydrostatic stress distribution.

This volumetric compression does not change after tunneling, if the tunnel remains elastic. When the rock surrounding the tunnel has failed up to  $r = b$ , the final compression can be calculated from the same integral, but now using the "broken zone" stress distribution. The difference between the two integrals constitutes the "elastic" volume relaxation.<sup>1</sup> Equating the final volume in this

---

<sup>1</sup>Although it might appear that a more direct solution could be obtained by expressing the volume change in differential form as a function of the stress changes caused by failure, i.e.:

form to the final volume as a function of the displacements, one finds:

$$\pi(b^2 - a^2) + \int_a^b \left( \frac{du^e}{dr} + \frac{u^e}{r} \right) 2\pi r dr - \int_a^b \left( \frac{du^{br}}{dr} + \frac{u^{br}}{r} \right) 2\pi r dr = \pi [(b - u_b)^2 - (a - u_a)^2] \quad (A.21)$$

where:

$$\frac{du^e}{dr} + \frac{u^e}{r} = \frac{2P(1 - 2\nu)}{E}$$

$$\frac{du^{br}}{dr} + \frac{u^{br}}{r} = \frac{(\sigma_\theta^{br} + \sigma_r^{br})(1 - \nu) - 2\nu\sigma_z^{br}}{E}$$

Substituting, and neglecting  $u_a^2 - u_b^2$ , one

obtains for the radial displacement:

$$u_a = \frac{b}{a} u_b + \frac{P(1 - 2\nu)(b^2 - a^2)}{aE} - \frac{(1 - \nu)}{Ea} \int_a^b (\sigma_\theta^{br} + \sigma_r^{br}) r dr + \frac{2\nu}{Ea} \int_a^b \sigma_z^{br} r dr \quad (A.22)$$

The results depend upon  $\sigma_z^{br}$ , and two assumptions for this axial stress will be considered:

i) "Elastic" plane strain, or  $\sigma_z^{br} = P(1 - 2\nu) + \nu(\sigma_\theta^{br} + \sigma_r^{br})$ . Substituting this into (A.22), one finds

$$\frac{d(\Delta u)}{dr} + \frac{\Delta u}{r} = \frac{(\Delta \sigma_r + \Delta \sigma_\theta)(1 - \nu) - 2\nu \Delta \sigma_z}{E}$$

it turns out that the integration of this expression leads to far lengthier computations.

$$u_a = \frac{b}{a} u_b + \frac{(1+\nu)(1-2\nu)}{aE} [P(b^2-a^2) - \int_a^b (\sigma_\theta^{br} + \sigma_r^{br}) r dr]$$

(A.23a)

This equation is given in Chapter II as (III-4.8a). After substituting integrals (A.16) with appropriate coefficients, the radial displacement is given by:

a)  $\sin \phi_r \neq 1/3, \sin \phi_r \neq 0$

$$u_a = \frac{b}{a} u_b + \frac{(1+\nu)(1-2\nu)}{aE} [(P + c_r \cot \phi_r)(b^2-a^2) + \frac{2w(b^3-a^3)}{3(1-3 \sin \phi_r)} - (P_i + c_r \cot \phi_r + \frac{aw(1-\sin \phi_r)}{1-3 \sin \phi_r}) \frac{\alpha_r^2 - a^2}{a \alpha_r}]$$

(A.24a)

b)  $\sin \phi_r = 1/3$

$$u_a = \frac{b}{a} u_b + \frac{(1+\nu)(1-2\nu)}{aE} [P(b^2-a^2) - P_i \frac{b^3-a^3}{a} - 3c_r \cos \phi_r b^2 (\frac{b}{a} - 1) \pm w (\frac{b^3-a^3}{3} - b^3 \log \frac{b}{a})]$$

(A.24b)

c)  $\sin \phi_r = 0$

$$u_a = \frac{b}{a} u_b + \frac{(1+\nu)(1-2\nu)}{aE} [(P - P_i)(b^2-a^2) - 2c_r b^2 \log \frac{b}{a} + \frac{w(b-a)^2(2b+a)}{3}]$$

(A.24c)

ii) "Plastic" plane strain, or

$$\sigma_z^{br} = \frac{\sigma_\theta^{br} + \sigma_r^{br}}{2} - \sin \phi_r \frac{\sigma_\theta^{br} - \sigma_r^{br}}{2}$$

Substituting this into (A.22), one finds

$$u_a = \frac{b}{a} u_b + \frac{P(1-2\nu)(b^2-a^2)}{aE} - \frac{1-2\nu}{aE} \int_a^b (\sigma_\theta^{br} + \sigma_r^{br}) r dr$$

$$- \frac{\nu \sin \phi_r}{aE} \int_a^b (\sigma_\theta^{br} - \sigma_r^{br}) r dr \quad (A.23b)$$

This equation is given in Chapter II as (II-4.8c). After substituting integrals (A.16) with appropriate coefficients, the radial displacement is given by:

a)  $\sin \phi_r \neq 1/3, \sin \phi_r \neq 0$

$$u_a = \frac{b}{a} u_b + \frac{(P + c_r \cot \phi_r)(1-2\nu)(b^2-a^2)}{aE}$$

$$- \frac{(1-2\nu + \nu \sin^2 \phi_r)}{aE} \left( \frac{2w(b^3-a^3)}{3(1-3 \sin \phi_r)} \right)$$

$$+ \frac{b}{a} \left[ \frac{c_r^2 - a^2}{c_r - a} \left[ P_i + c_r \cot \phi_r \mp \frac{aw(1-\sin \phi_r)}{1-3 \sin \phi_r} \right] \right] \quad (A.25a)$$

b)  $\sin \phi_r = 1/3$

$$u_a = \frac{b}{a} u_b + \frac{P(1-2\nu)(b^2-a^2)}{aE} - \frac{3 c_r \cos \phi_r (b-a)}{a^2 E}$$

$$[ (1-2\nu) b^2 + \frac{\nu(b^2+ab+a^2)}{9} ] - \frac{1-2\nu+\nu/9}{aE}$$

$$[ P_i \frac{b^3-a^3}{a} \mp w \left( \frac{b^3-a^3}{3} - b^3 \log \frac{b}{a} \right) ] \quad (A.25b)$$

c)  $\sin \phi_r = 0$

$$u_a = \frac{b}{a} u_b + \frac{1-2\nu}{aE} [(P - P_i) (b^2 - a^2) - 2 c_r b^2 \log \frac{b}{a} + \frac{w(b-a)^2(2b+a)}{3}] \quad (A.25c)$$

After substitution of (A.20), and neglecting the gravity terms, the equations (A.24) and (A.25) for the displacements can be written in dimensionless form, for example (A.25c) as:

$$\frac{u_a}{a} = \left(\frac{b}{a}\right)^2 \frac{(P \sin \phi + c \cos \phi)(1+\nu)}{E} + (1-2\nu) \left[ \frac{P - P_i}{E} \left(\frac{b}{a}\right)^2 - 2 \frac{c_r}{E} \left(\frac{b}{a}\right)^2 \log \frac{b}{a} \right] \quad (A.26c)$$

The displacements have been calculated for two different cases. It is likely that there is a gradual change from an "elastic" plane strain condition during the initial stages of failure, when  $\sigma_\theta$  is the largest principal stress, to a condition where  $\sigma_z$  becomes the largest principal stress as  $\sigma_\theta$  decreases with further propagation of the broken zone. One would then expect the "plastic" plane strain condition to be valid in an annulus immediately surrounding the tunnel, and the "elastic" plane strain condition through the remainder of the broken zone (as well as in the elastic region).

The difference between the displacements calculated for the two cases can be calculated from (A.22), after substitution of the appropriate  $\sigma_z^{br}$ :

$$u_a^{el} - u_a^{pl} = \frac{2 \nu}{a E_r} \int_a^b \left[ \left( P - \frac{\sigma_\theta^{br} + \sigma_r^{br}}{2} \right) (1 - 2 \nu) + \sin \phi_r \frac{\sigma_\theta^{br} - \sigma_r^{br}}{2} \right] r dr \quad (A.27)$$

The integrand is always positive, or  $u_a^{el} > u_a^{pl}$  (equal iff  $a = b$ ). The difference will increase with increasing  $b$ . The difference increases with increasing  $\nu_r$  up to  $1/4$ , beyond that no general statement is possible. This can be seen by rewriting the difference as:

$$f(\nu) = A \nu (1 - 2 \nu) + B \nu$$

$$f'(\nu) = A (1 - 4 \nu) + B$$

$A$  and  $B$  are positive constants. When  $\phi_r = 0$ ,  $B = 0$  and  $f(\nu)$  is symmetric around  $\nu = 1/4$ , and the difference is then a true maximum at  $\nu = 1/4$ . As  $B$  increases with  $\phi_r$  the maximum difference shifts to higher  $\nu$  values with higher  $\phi_r$ .

The difference will increase with increasing  $P$  for constant support pressure  $P_i$  (i.e., constant  $\sigma_\theta^{br}$  and  $\sigma_r^{br}$ ). The difference will decrease for increasing tunnel size ( $a$ ) and will increase for decreasing residual stiffness ( $E_r$ ).

Cumulative effects of the various parameters on the relative difference are shown in Figures A.2 and II.8.

A-3. Computer Programs for the Calculation of the Ground Reaction Curve

A-3.1. Introduction. The following programs calculate the required support pressure and the corresponding displacements for increasing values of the broken zone radius  $b$ . In both programs the support pressure is calculated according to equations (A.25), also given as (II-3.5). In the first program, GRCSZE, the displacement calculation is based upon the assumption that the axial stress  $\sigma_z$  is given by the elastic plane strain assumption, and equations (A.24) are used. In this program, an entirely independent displacement calculation according to (A.18) is also included. In the second program, GRCEXPD, the axial stress  $\sigma_z$  is calculated from the plastic plane strain condition, and equations (A.25) are evaluated. In GRCSZE a set of ground reaction curves is calculated for various values of the residual strength, always taken to be constant for each particular curve (for example, Figures II.8 and II.9). In GRCEXPD the expressions (II-4.16) through (II-4.18) are

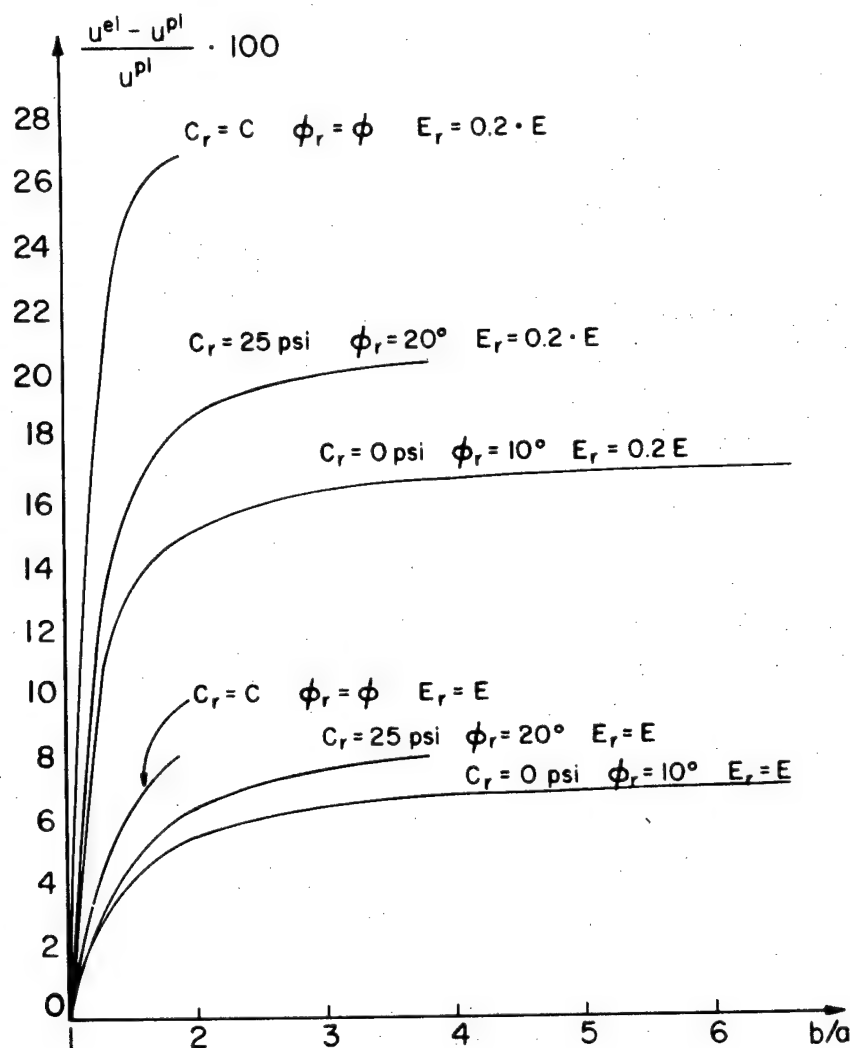


Figure A.2. Relative Difference Between Radial Tunnel Wall Displacements  $u$  Calculated for  $\sigma_z$  Determined from the "Elastic" plane strain Assumption ( $u^{el}$ ) or from the "Plastic" Plane Strain Assumption ( $u^{pl}$ ).

Common data:

$P = 500 \text{ psi}$	$E = 10^6 \text{ psi}$
$\nu = 0.25$	$c = 50 \text{ psi}$
$\phi = 30^\circ$	$w = 0 \text{ lbs/in}^3$

substituted, so that the ground reaction curve can be calculated for a gradual (exponential) strength and stiffness decrease. Only one curve is calculated for an input data card.

#### A-3.2. Input.

A-3.2.1. Program GRCSZE. Input data are submitted with one data card. FORMAT (F.10.1, 5F8.2, 5F6.2) as follows:

Column 1-10: Young's modulus E of the rock, in psi.

11-18: Hydrostatic stressfield P, in psi.

19-26: Tunnel radius A, in feet.

27-34: Poisson's ratio V.

35-42: Residual modulus decrement factor

RK ( $0 \leq RK < 1$ ).

A first calculation is performed with the residual modulus  $E_{res}$  equal to the original modulus E. If RK is different from zero, a series of calculations is initiated during which the residual is decreased by  $RK \times E$  at each step. The series is terminated when a zero or negative modulus results.

43-50: Specific weight of the rock, in  $\text{lbs/in}^3$

51-56: Cohesion of the rock, in psi.

57-62: Angle of internal friction of the rock, in degrees.

63-68: Residual cohesion decrement DELCR,  
in psi.

A first calculation is performed with the residual cohesion equal to the "intact" cohesion. If DELCR differs from zero, a series of calculations is initiated such that at each step the residual cohesion is decreased with the decrement punched here. The series is terminated when a negative residual cohesion results.

69-74: Residual angle of internal friction decrement DELPHIR, in degrees. Used in a similar way as the preceding decrements.

75-80: Constant volume increase increment DXK. An initial calculation of the displacements is based upon the assumption that the broken zone rock undergoes no volume change. Subsequent calculations are performed after adding an increment DXK to the volume expansion factor during each cycle.

A-3.2.2. Program GRCEXP. Input data are submitted with one data card, FØRMAT (2E9.4, 7F6.2, 4F5.1), as follows:

Column 1-9: Initial Young's modulus E of the rock,  
in psi.

10-18: Minimum residual Young's modulus  
 $E_{res}^{\min}$ , in psi.

19-24: Hydrostatic stressfield P, in psi.

25-30: Tunnel radius AF, in feet.

31-36: Poisson's ratio V.

37-42: Specific weight W, in lbs/in<sup>3</sup>.

43-48: Cohesion of the rock C, in psi.

49-54: Angle of internal friction PHID, in degrees.

55-60: Minimum residual cohesion ( $c_r^{\min}$  in (II-4.16)) CRMIN, in psi.

61-65: Minimum residual angle of internal friction ( $\phi_r^{\min}$  in (II-4.17)) PHIRMIN, in degrees.

66-70: Parameter k (II-4.16) determining the rate of decrease in residual cohesion, PARK ( $PARK \geq 0$ ).

71-75: Parameter l (II-4.17) determining the rate of decrease in residual internal friction, PARL.

76-80: Parameter m (II-4.18) determining the rate of decrease in residual modulus, PARM.

A-3.3. Output. All input data are

printed on the first output page, as well as some values calculated directly from the input. This includes the uniaxial compressive rock strength, the equivalent tunnel depth calculated from the (hydrostatic) stress and the rock weight and the bulk modulus. Also printed is the radial displacement that would result if the rock had sufficient strength to remain elastic following tunneling. This value determines the intersection of the elastic ground reaction curve with the (horizontal) displacement axis.

A-3.3.1. Program GRCSZE. Values of the residual cohesion, friction and bulk modulus as well as the broken zone volume increase (in %) are printed as a heading above the calculated data giving the ground characteristics. These data are printed in ten columns. The first one gives the radius  $b$  of the broken zone (in ft), the second one, the value of  $b$  divided by the tunnel radius  $a$ . The next three columns give results when the gravity forces are neglected ( $w = 0$ ), namely, the support pressure, the displacement and the displacement divided by the tunnel radius. The following columns give support pressures and displacements at the

tunnel roof and floor. All displacements are given in inches, all support pressures in psi.

The last column is entirely independent from all preceding ones but the first two. It gives the displacements based upon the assumption of a constant volume increase throughout the broken zone. This calculation is altogether independent from the stress distribution so that the last column from any page of the printout can be combined with the third column of any page in order to obtain the data defining the ground reaction curve for that particular combination of strength and displacement properties.

The support pressures and the displacements are calculated for every combination of the generated values of the residual modulus, cohesion and friction, from  $b/a = 1$  in steps of  $b/a = 0.1$  up to either  $b/a = 6.6$  or the value of  $b/a$  where all support pressure requirements reduce to zero, whichever is smaller.

When all calculations for the first data card input are terminated the next data card will be read. This cycle will continue until all data sets have been processed, following which an error message will be printed. It is thus possible to

run multiple problems with one program compilation.

A-3.3.2. Program GRCEXP. The calculated data determining the ground reaction curve are printed in twelve columns. The first nine columns give the same variables as the corresponding columns of the previous program. The last three columns give respectively the residual angle of internal friction (column headed PHIR), the residual cohesion (CRES) and the residual Young's modulus (ERES) used for the corresponding b/a value. A check on the decline rate of the residual properties is thus provided.

```

PROGRAM GRCSZE(INPUT,OUTPUT)
C THIS PROGRAM CALCULATES A SET OF GROUND REACTION CURVES FOR VARIOUS
C RESIDUAL STRENGTH VALUES AND ELASTIC RELAXATION
C AXIAL STRESS SIGZ FROM ELASTIC PLANE STRAIN
C DIMENSION U(3),PS(3),WU(3)
C Y = ASIN(1./3.)
300 READ 10,E,P,AF,V,RK,w,C,PHID,DELCR,DELPHIR,DXK
10 FORMAT(F10.1*F8.2*F6.2)
IF(DXK) 432,432,433
432 DXK = 0.001
433 XK = - DXK
IF(DELCR) 400,400,410
400 DELCR = C
410 IF(DELPHIR) 420,420,430
420 DELPHIR = PHI
430 WF = 1728.*W
VR = 1.*V
VE = VR/E
VP = 1.-2.*V
OK = E/VP/3.
WU(1) = 0.
WU(2) = - W
WU(3) = W
PHI = PHID/57.2957795131
DEP = P/W/12.
S1 = 1. - SIN(PHI)
PP = P*S1
CC = C*COS(PHI)
PPI = PP - CC
PPA = P - PPI
SIGC = 2.*CC/S1
PRINT 20,P,AF,E,V,OK,C,PHID,SIGC,W,WF,DEP,DELCR,DELPHIR,RK
20 FORMAT(// PRE TUNNELING STRESS = * F7.1* PSI* 5X* TUNNEL RADIUS =
1*F6.2* FEET// ROCK PROPERTIES//5X* YOUNG'S MODULUS = * F10.1 *
2 PSI*5X* POISSON'S RATIO = *F6.3, 5X* ORIGINAL BULK MODULUS = *F11
3.1* PSI * //5X* COHESION = *F7.2* PSI*5X* ANGL
4E OF INTERNAL FRICTION = *F6.1* DEGREES* 5X* UNIAXIAL COMPRESSIVE
5 STRENGTH = *F8.2* PSI//5X* SPECIFIC WEIGHT = *F6.3* LBS/CURIC I
6NCH =*F7.2* LBS/CUBIC FT*5X* CORRESPONDING TUNNEL DEPTH = *F7.1
7* FEET//5X* DECREMENT OF RESIDUAL COHESION = *F8.2*PSI*7X* DECRE
8MENT OF RESIDUAL ANGLE OF INTERNAL FRICTION = *F7.2* DEGREES//5X*
9 FRACTIONAL BULK MODULUS CHANGE =*F6.3//)
A = 12.*AF
UAR = P*VE
UAO = A*UAR
PRINT 50,UAO,UAR
50 FORMAT(//. FINAL RADIAL DISPLACEMENT IF THE TUNNEL WERE TO R
1EMAIN ELASTIC = *E10.4* INCHES// RELATIVE TO TUNNEL RADIUS
2= *E12.4)
IF(SIGC - 2.*P) 22,24,24
24 PRINT 25
25 FORMAT(// UNIAXIAL COMPRESSIVE STRENGTH IS LARGER THAN MAXIMUM ST
1RESS NO FAILURE //)
GO TO 300
22 CONTINUE
VEP = VE*VP/A
A2 = A*A

```

```

A3 = A2*A
DELPHIR = DELPHIR/57.2957795131
CR = C
60 CONTINUE
PHIR = PHI
70 CONTINUE
X = ABS(Y - PHIR)
FK = 1.
PHIRD = PHIR*57.2957795
520 RKR = FK*OK
XK = XK + DXK
XKX = XK*100.
PRINT 180,CR,PHIRD,RKR,XKX
VF = VEP/FK
CP = COS(PHIR)
IF(PHIR) 440,440,450
450 S1R = 1. - SIN(PHIR)
S3R = 1. - 3.*SIN(PHIR)
ALR = 2.*SIN(PHIR)/(1.-SIN(PHIR))
ALR1 = ALR - 1.
ALR2 = ALR + 2.
CCR = CR/TAN(PHIR)
440 A1 = AF/10.
BF = AF - A1
NC = - 1
DO 110 IJ = 1,57
BF = BF + A1
B = 12.*BF
B2 = B*B
B3 = B2*B
BA2 = (B-A)*(B+A)
BA3 = (B-A)*(B*B + A*B + A*A)
AB = A/B
BA = B/A
UB = B*VE*PPA
UA2 = (B-UB)**2 - (1.+XK)*BA2
IF(UA2) 82,83,83
82 UA2 = 0.
83 UAK = A - SQRT(UA2)
UAR = UB*BA
OB = BF
IF(PHIR) 200,200,210
200 CONTINUE
PS(1) = PPI - 2.*CR*ALOG(BA)
IF(PS(1)) 350,360,360
350 IF(NC) 352,354,354
354 PS(2) = PS(1) + W*(B-A)
U(2) = UAR + VF*((P-PS(2))*BA2 - 2.*CR*B2*ALOG(BA) + W*(B-A)*(B-A)
1*(1.*B+A)/3.)
IF(PS(2)) 111,356,356
356 PRINT 358,BF,RA,PS(2),U(2),UAK
358 FORMAT(F9.2,F10.3,37X,F14.3,E14.4,28X,E14.4)
GO TO 110
352 PS(1) = 0.
NC = 1
BA = EXP(PPI/2./CR)
B = BA*A
PS(2) = W*(B-A)

```

```

BF = B/12.
UB = B*VE*PPA
U(1) = BA*UB + VF*(P*(B-A)*(B+A) - 2.*CR*B*B*ALOG(BA))
U(2) = U(1) + VF*W*(B-A)*(B-A)*(A+2.*B)/3. - VF*PS(2)*(B-A)*(B+A)
460 UOA = U(1)/A
PRINT 470,BF,BA,PS(1),U(1),UOA,PS(2),U(2),UAK
470 FORMAT(F9.2,F11.3,F13.3,E14.4,E10.3,F14.3,E14.4,28X,E14.4)
BF = OB - A1
GO TO 110
360 PS(2) = PS(1) + W*(B-A)
PS(3) = PS(1) - W*(B-A)
IF(PS(3)) 370,380,380
370 PS(3) = 0.
DO 372 I = 1,2
372 U(I) = UAR + VE*VP*((P-PS(I))*BA2 - WU(I)*(B-A)*(B-A)*(2.*B+A)/3.
1 - 2.*CR*B*B*ALOG(BA))/A/FK
461 UOA = U(1)/A
PRINT 470,BF,BA,PS(1),U(1),UOA,PS(2),U(2),UAK
GO TO 110
380 DO 220 I = 1,3
220 U(I) = UAR + VE*VP*((P-PS(I))*BA2 - WU(I)*(B-A)*(B-A)*(2.*B+A)/3.
1 - 2.*CR*B*B*ALOG(BA))/A/FK
GO TO 240
210 IF(X=0.001) 250,250,260
250 GR = W*A*ALOG(BA)
CCR = 2.*SQRT(2.)*CR
PS(1) = (PPI + CCR)*AB - CCR
IF(PS(1)) 270,280,280
270 IF(NC) 272,274,274
274 PS(2) = PS(1) + GR
U(2) = UAR + VF*(P*BA2 + 3.*CR*CP*B2*(A-B)/A - PS(2)*BA3/A -
1 W*(BA3 - 3.*B3*ALOG(BA))/3.)
IF(PS(2)) 111,356,356
272 PS(1) = 0.
NC = 1
BA = PPI/2./SQRT(2.)/CR + 1.
B = BA*A
BF = B/12.
UB = B*VE*PPA
PS(2) = W*A*ALOG(BA)
U(1) = UB*BA + VF*(P*(B-A)*(B+A) - 3.*CR*CP*(B-A)*B*B/A)
U(2) = U(1) - VF*(W*((B-A)*(B*B*B*A+A*A)/3. - B*B*B*ALOG(BA)) +
1 PS(2)*(B-A)*(B*B*B*A+A*A)/A)
GO TO 460
280 PS(2) = PS(1) + GR
PS(3) = PS(1) - GR
IF(PS(3)) 290,310,310
290 PS(3) = 0.
DO 292 I = 1,2
292 U(I) = UAR + VF*(P*BA2 - 3.*CR*CP*(B-A)*B*B/A - PS(I)*BA3/A +
1 WU(I)*(BA3/3. - B*B*B*ALOG(BA)))
GO TO 461
310 DO 320 I = 1,3
320 U(I) = UAR + VF*(P*BA2 - 3.*CR*CP*(B-A)*B*B/A - PS(I)*BA3/A +
1 WU(I)*(BA3/3. - B*B*B*ALOG(BA)))
GO TO 240
260 PS(1) = (PPI + CCR)*AB**ALR - CCR
GR = A*W*(AB**ALR1 - 1.)/(1.-ALR)

```

```

120 IF(PS(1)) 120,130,130
120 IF(NC) 122,124,124
124 PS(2) = PS(1) + GR
  U(2) = UAR + VF*((P+CCR)*BA2 + 2.*W*BA3/3./S3R - (PS(2) + CCR +
  1 A*W*S1R/S3R)*(B***(ALR+2.0) - A***(ALR+2.0))/A**ALR)
  IF(PS(2)) 111,356,356
122 PS(1) = 0.
  NC = 1
  BA = (PPI/CCR + 1.)**(1./ALR)
  B = A*BA
  BF = B/12.
  UB = B*VE*PPA
  PS(2) = A*W*((A/B)**ALR1 - 1.)/(1.-ALR)
  U(1) = UB*BA + VF*((P+CCR)*(B-A)*(B+A) - CCR*(B***(ALR+2.0) - A***(AL
  1R + 2.0))/A**ALR)
  U(2) = U(1) + VF*(2.*W*(B-A)*(H*B + B*A + A*A)/3./S3R - (PS(2) +
  1 A*W*S1R/S3R)*(B***(ALR2) - A***(ALR2))/A**ALR)
  GO TO 460
130 PS(2) = PS(1) + GR
  PS(3) = PS(1) - GR
  IF(PS(3)) 140,150,150
140 DO 142 I = 1,2
142 U(I) = UAR + VF*((P+CCR)*BA2 - 2.*WU(I)*BA3/S3R/3. - (PS(I) + CCR
  1 - A*WU(I)*S1R/S3R)*(B**ALR2 - A**ALR2)/A**ALR)
  GO TO 461
150 DO 230 I = 1,3
230 U(I) = UAR + VF*((P+CCR)*BA2 - 2.*WU(I)*BA3/S3R/3. - (PS(I) + CCR
  1 - A*WU(I)*S1R/S3R)*(B**ALR2 - A**ALR2)/A**ALR)
240 UOA = U(1)/A
  PRINT 100,BF,HA,PS(1),U(1),UOA,PS(2),U(2),PS(3),U(3),UAK
100 FORMAT(F9.2,F10.3,F13.3,E14.4,E10.3,F14.3,E14.4,F14.3,2E14.4)
110 CONTINUE
111 IF(FK - RK) 500,510,500
500 IF(RK) 501,510,501
501 FK = FK - RK
  IF(FK) 510,510,520
510 IF(DELPHIR) 160,160,171
171 PHIR = PHIR - DELPHIR
  IF(ABS(PHIR) - 0.0001) 172,173,173
172 PHIR = 0.
173 IF(PHIR) 160,70,70
160 IF(DELCR) 170,170,161
161 CR = CR - DELCR
  IF(CR) 170,60,60
170 CONTINUE
180 FORMAT(1H1,/* RESIDUAL COHESION = * F7.2* PSI * 5X * RESIDUAL ANG
  1LE OF INTERNAL FRICTION =*F6.2* DEGREES* 5X * RESIDUAL BULK MODULU
  2S = *F11.1* PSI /* BROKEN ZONE VOLUME INCREASE = *F8.3* PER CEN
  3T/*/* RADIUS B B/A SUPPORT PRESS DISPLACEMENT DISPLMNT R00
  4F SUPPORT ROOF FLOOR SUPPORT FLOOR CONST VOL INCR
  5EASE*/20X* NO GRAVITY NO GRAVITY OVER RAD DISP
  6LACEMENT DISPLACEMENT DISPLACEMENT DISPLACEMENT*/)
  PRINT 2
2 FORMAT(1H1)
  GO TO 300
  END

```

```

PROGRAM GRCEXP0(INPUT,OUTPUT)
  THIS PROGRAM CALCULATES THE GROUND REACTION CURVE FOR A GRADUAL
  EXPONENTIAL DECREASE IN THE RESIDUAL PROPERTIES
  AXIAL STRESS SIGZ ACCORDING TO DRUCKER PRAGER      PLANE STRAIN
  DIMENSION U(3),PS(3),WU(3)
  Y = ASIN(1./3.)
300 READ 10,E,EM,P,AF,V,W,C,PHID,CRMIN,PHIRMIN,PARK,PARL,PARM
10 FORMAT(2E9.4,7F6.2,4F5.1)
430 WF = 1728.*W
  VR = 1.*V
  VE = VR/E
  VP = 1.-2.*V
  OK = E/VP/3.
  WU(1) = 0.
  WU(2) = - W
  WU(3) = W
  PHI = PHID/57.2957795131
  DEP = P/W/12.
  S1 = 1. - SIN(PHI)
  PP = P*S1
  CC = C*COS(PHI)
  PPI = PP - CC
  PPA = P - PPI
  SIGC = 2.*CC/S1
  PRINT 20,P,AF,E,V,OK,C,PHID,SIGC,W,WF,DEP,CRMIN,PHIRMIN,EM
20 FORMAT(// PRE TUNNELING STRESS = * F7.1* PSI* 5X* TUNNEL RADIUS =
1*F6.2* FEET///* ROCK PROPERTIES//5X* YOUNG'S MODULUS = * F10.1 *
2 PSI*5X* POISSON'S RATIO = *F6.3, 5X* ORIGINAL BULK MODULUS = *F11
3.1* PSI * //5X* COHESION = *F7.2* PSI*5X* ANGL
4E OF INTERNAL FRICTION = *F6.1* DEGREES* 5X* UNIAXIAL COMPRESSIVE
5 STRENGTH = *F8.2* PSI//5X* SPECIFIC WEIGHT = *F6.3* LBS/CUBIC I
6NCH = *F7.2* LBS/CUBIC FT*5X* CORRESPONDING TUNNEL DEPTH = *F7.1
7* FEET//5X* MINIMUM RESIDUAL COHESION = *F8.2* PSI*7X* MINIMUM
8RESIDUAL ANGLE OF INTERNAL FRICTION = *F8.2* DEGREES//5X* MINIMUM
9 ELASTIC MODULUS = * F11.2* PSI *)
  PRINT 21,PARK,PARL,PARM
21 FORMAT(///* PARAMETERS DETERMINING THE DECREASE IN THE RESIDUAL PRO
1PERTIES//5X* COHESION K = *F10.3,5X* INTERNAL FRICTION L
2= *F10.3/ 5X* YOUNG'S MODULUS M = *F10.3//)
  PHIRMIN = PHIRMIN/57.2957795131
  A = 12.*AF
  UAR = P*VE
  UAO = A*UAR
  PRINT 50,UAO,UAR
50 FORMAT(// FINAL RADIAL DISPLACEMENT IF THE TUNNEL WERE TO R
1EMAIN ELASTIC = *E10.4* INCHES///* RELATIVE TO TUNNEL RADIUS
2= *E12.4)
  IF(SIGC = 2.*P) 22,24,24
24 PRINT 25
25 FORMAT(///* UNIAXIAL COMPRESSIVE STRENGTH IS LARGER THAN MAXIMUM ST
1RESS NO FAILURE //)
  GO TO 300
22 CONTINUE
  A2 = A*A
  A3 = A2*A
  VRES = V
  PRINT 180

```

```

A1 = AF/10.
BF = AF - A1
NC = - 1
DO 110 IJ = 1,57
BF = BF + A1
B = 12.*BF
B2 = B*B
B3 = B2*B
BA2 = (B-A)*(B+A)
BA3 = (B-A)*(B*B + A*B + A*A)
AB = A/B
BA = B/A
CR = CCRMIN + (C-CCRMIN)*EXP(-PARM*(BA*BA-1.))
PHIR = PHIRMIN + (PHI - PHIRMIN)*EXP(-PARL*(BA*BA - 1.))
X = ABS(Y-PHIR)
PHIRD = PHIR*57.2957795
CP = COS(PHIR)
IF(PHIR) 440,440,450
450 S1R = 1. - SIN(PHIR)
S3R = 1. - 3.*SIN(PHIR)
ALR = 2.*SIN(PHIR)/(1.-SIN(PHIR))
ALR1 = ALR - 1.
ALR2 = ALR + 2.
CCR = CR/TAN(PHIR)
440 ERES = EM + (E-EM)*EXP(-PARM*(BA*BA-1.))
UB = B*VE*PPA
UAR = UB*BA
OB = BF
IF(PHIR) 200,200,210
200 CONTINUE
PS(1) = PPI - 2.*CR*ALOG(BA)
IF(PS(1)) 350,360,360
350 IF(NC) 352,354,354
354 PS(2) = PS(1) + W*(B-A)
U(2) = UAR + (1.-2.*VRES)*( (P-PS(2))*BA2 - 2.*CR*B2*ALOG(BA) + W*
1 (B-A)*(B-A)*(2.*B+A)/3.)/A/ERES
IF(PS(2)) 111,356,356
356 PRINT 358,BF,BA,PS(2),U(2),PHIRD,CR,ERES
358 FORMAT(F9.2,F10.3,37X,F14.3,E14.4,28X,F6.2,F7.3,F10.1)
      GO TO 110
352 PS(1) = 0.
      NC = 1
      BA = EXP(PPI/2./CR)
      B = BA*A
      PS(2) = W*(B-A)
      BF = B/12.
      UB = B*VE*PPA
      U(1) = BA*UB + (1.-2.*VRES)*(P*(B-A)*(B+A) - 2.*CR*B*B*ALOG(BA))/A
      1 /ERES
      U(2) = U(1) + (1.-2.*VRES)*(B-A)*((B-A)*(A+2.*B)*W/3. - PS(2)*
      1 (B+A))/A/ERES
      460 UOA = U(1)/A
      PRINT 470,BF,BA,PS(1),U(1),UOA,PS(2),U(2),PHIRD,CR,ERES
      470 FORMAT(F9.2,F10.3,F13.3,E14.4,E10.3,F14.3,E14.4,28X,F6.2,F7.3,F10.
      11)
      BF = OB - A1
      GO TO 110
360 PS(2) = PS(1) + W*(B-A)

```

```

PS(3) = PS(1) - W*(B-A)
IF(PS(3)) 370,380,380
370 PS(3) = 0.
DO 372 I = 1,2
372 U(I) = UAR + (1.-2.*VRES)*((P-PS(I))*BA2 - WU(I)*(B-A)*(B-A)*
1 (2.*B*A)/3. - 2.*CR*B*B*ALOG(BA))/A/ERES
461 UOA = U(1)/A
PRINT 470,BF,BA,PS(1),U(1),UOA,PS(2),U(2),PHIRD,CR,ERES
GO TO 110
380 DO 220 I = 1,3
220 U(I) = UAR + (1.-2.*VRES)*((P-PS(I))*BA2 - WU(I)*(B-A)*(B-A)*
1 (2.*B*A)/3. - 2.*CR*B*B*ALOG(BA))/A/ERES
GO TO 240
210 IF(X=0.001) 250,250,260
250 GR = W*A*ALOG(BA)
CCR = 2.*SQRT(2.)*CR
PS(1) = (PPI + CCR)*AB - CCR
IF(PS(1)) 270,280,280
270 IF(NC) 272,274,274
274 PS(2) = PS(1) + GR
U(2) = UAR + P*(1.-2.*VRES)*BA2/A/ERES - 3.*CR*CP*(B-A)*((1.-2.*VR
1 ES)*B2 + VRES*(B2+A2+A*B)/9.)/A2/ERES - (1.-(2.-1./9.)*VRES)*(PS(2
2)*BA3/A + W*(BA3/3.-B3*ALOG(BA)))/A/ERES
IF(PS(2)) 111,356,356
272 PS(1) = 0.
NC = 1
BA = PPI/2./SQRT(2.)/CR + 1.
B = BA*A
BF = B/12.
UB = B*V*PPA
PS(2) = W*A*ALOG(BA)
U(1) = UB*BA + P*(1.-2.*VRES)*(B-A)*(B+A)/A/ERES - 3.*CR*CP*(B-A)*
1((1.-2.*VRES)*B*B + VRES*(B*B + A*B + A*A)/9.)/A2/ERES
U(2) = U(1) - (1.-2.*VRES + VRES/9.)*(PS(2)*(B-A)*(B*B+B*A*A)/A
1 + W*((B-A)*(B*B + B*A + A*A)/3. - B*B*B*ALOG(BA)))/A/ERES
GO TO 460
280 PS(2) = PS(1) + GR
PS(3) = PS(1) - GR
IF(PS(3)) 290,310,310
290 PS(3) = 0.
DO 292 I = 1,2
292 U(I) = UAR + P*(1.-2.*VRES)*BA2/A/ERES - 3.*CR*CP*(B-A)*((1.-2.*V
1 RES)*B2 + VRES*(B2+A2+A*B)/9.)/A2/ERES - (1.-2.*VRES + VRES/9.)*
2 (PS(2)*BA3/A - WU(I)*(BA3/3. - B3*ALOG(BA)))/A/ERES
GO TO 461
310 DO 320 I = 1,3
320 U(I) = UAR + P*(1.-2.*VRES)*BA2/A/ERES - 3.*CR*CP*(B-A)*((1.-2.*V
1 RES)*B2 + VRES*(B2+A2+A*B)/9.)/A2/ERES - (1.-2.*VRES + VRES/9.)*
2 (PS(2)*BA3/A - WU(I)*(BA3/3. - B3*ALOG(BA)))/A/ERES
GO TO 240
260 PS(1) = (PPI + CCR)*AB**ALR - CCR
GR = A*W*(AB**ALR1 - 1.)/(1.-ALR)
IF(PS(1)) 120,130,130
120 IF(NC) 122,124,124
124 PS(2) = PS(1) + GR
U(2) = UAR + (P+CCR)*(1.-2.*VRES)*(B-A)*(B+A)/A/ERES - (1.-2.*VRES
1 + VRES*(SIN(PHIR))**2)*(-2.*W*BA3/3./S3R + (B**ALR2 - A**ALR2)
2 *(PS(2)*CCR + A*W*S1R/S3R)/A**ALR)/A/ERES

```

```

122 IF(PS(2)) 111,356,356
122 PS(1) = 0.
      NC = 1
      BA = (PPI/CCR + 1.)**(1./ALR)
      B = A*BA
      BF = B/12.
      UB = B*VE*PPA
      PS(2) = A*W*((A/B)**ALR1 - 1.)/(1.-ALR)
      U(1) = UB*BA + (P+CCR)*(1.-2.*VRES)*(B-A)*(B+A)/A/ERES - (1.-2.*VRES*
      1 + VRES*(SIN(PHIR))**2)*(B**ALR2 - A**ALR2)*CCR/ERES/A**ALR/A
      U(2) = U(1) - (1.-2.*VRES + VRES*(SIN(PHIR))**2)*(-2.*W*(B-A)*(B+B*
      1 + B*A+A*A)/3./S3R + (B**ALR2-A**ALR2)*(PS(2) + A*W*S1R/S3R)/A**ALR
      2)/A/ERES
      GO TO 460
130 PS(2) = PS(1) + GR
      PS(3) = PS(1) - GR
      IF(PS(3)) 140,150,150
140 DO 142 I = 1,2
142 U(I) = UAR + (P+CCR)*(1.-2.*VRES)*BA2/A/ERES - (1.-2.*VRES + VRES*
      1*(SIN(PHIR))**2)*(WU(I)*2.*BA3/3./S3R + (B**ALR2 - A**ALR2)*(PS(I)
      2 + CCR - WU(I)*A*S1R/S3R)/A**ALR)/A/ERES
      GO TO 461
150 DO 230 I = 1,3
230 U(I) = UAR + (P+CCR)*(1.-2.*VRES)*BA2/A/ERES - (1.-2.*VRES + VRES*
      1*(SIN(PHIR))**2)*(WU(I)*2.*BA3/3./S3R + (B**ALR2 - A**ALR2)*(PS(I)
      2 + CCR - WU(I)*A*S1R/S3R)/A**ALR)/A/ERES
240 UOA = U(1)/A
      PRINT 100,BF,BA,PS(1),U(1),UOA,PS(2),U(2),PS(3),U(3),PHIRD,CR,ERES
100 FORMAT(F9.2,F10.3,F13.3,E14.4,E10.3,F14.3,E14.4,F14.3,E14.4,F6.2,
      1F7.3,F10.1)
110 CONTINUE
111 CONTINUE
180 FORMAT(/////* RADIUS B B/A SUPPORT PRESS DISPLACEMENT DISPL
      1MNT ROOF SUPPORT ROOF FLOOR SUPPORT FLOOR PHIR
      2 CRES ERES * / 20X* NO GRAVITY NO GRAVITY OVER RAD
      3 DISPLACEMENT DISPLACEMENT * / )
      PRINT 2
2 FORMAT(1H1)
      GO TO 300
      END

```

A-4. Support Stiffness Calculation

The support stiffness as defined in II.6 and as calculated here is equal to the average support pressure developed on the tunnel walls for a unit convergence of the support system. It is assumed that the convergence and the support reaction pressure are radially symmetric.

A-4.1. Shotcrete Cylinder. The stiffness of a shotcrete liner is assumed to be that of a hollow cylinder of the thickness  $t$  and external radius  $a$ . For a thick wall cylinder in plane strain the expression for the stiffness is:

$$K_{ss} = \frac{P_i}{u_a} = \frac{E (2a-t)t}{(1+\nu) a [(1-2\nu) a^2 + (a-t)^2]} \quad (A.28a)$$

For a thin wall cylinder ( $t \leq 0.04 a$ ) this can be reduced to:

$$K_{ss} = \frac{Et}{2a} \quad (A.28b)$$

A-4.2. Blocked Steel Set. Determining the stiffness of a blocked steel set requires the determination of the steel set stiffness and of the stiffness of the wooden block. In a simplified form the stiffness of the steel set can be assumed to consist of the "ring stiffness," or stiffness

under an evenly distributed (external) pressure and of the "bending stiffness," or stiffness under a number of evenly spaced radial forces (Roark, 1954, p. 158). The stiffness of a wooden blocking point is assumed to equal that of a linear spring. The resultant steel set stiffness can then be written as:

$$\frac{1}{K_{ss}} = \frac{u_a}{P_i} = \frac{Sa^2}{EA} + \frac{Sa^4}{EI} \left( \frac{\theta(\theta+sc)}{2s^2} - 1 \right) + \frac{2Sa\theta t_B}{A_B E_B} \quad (A.29)$$

where:

$K_{ss}$  = stiffness of blocked steel set  
 $a, u_a$  = tunnel radius and radial displacement  
 $P_i$  = support pressure  
 $A, E, I$  = steel cross-sectional area, elastic modulus and moment of inertia  
 $s$  = steel set spacing

$2\theta$  = angle between blocking points

$n = \pi/\theta$  = number of blocking points

$s = \sin \theta, c = \cos \theta$

$E_B, t_B$  = elastic modulus and thickness of blocks

$A_B$  = cross-sectional area of blocks,

in all calculations for Figures II.12, II.13 and A.3 assumed equal to the square of the steel set flange width.

Figure A.3 illustrates the effect of block

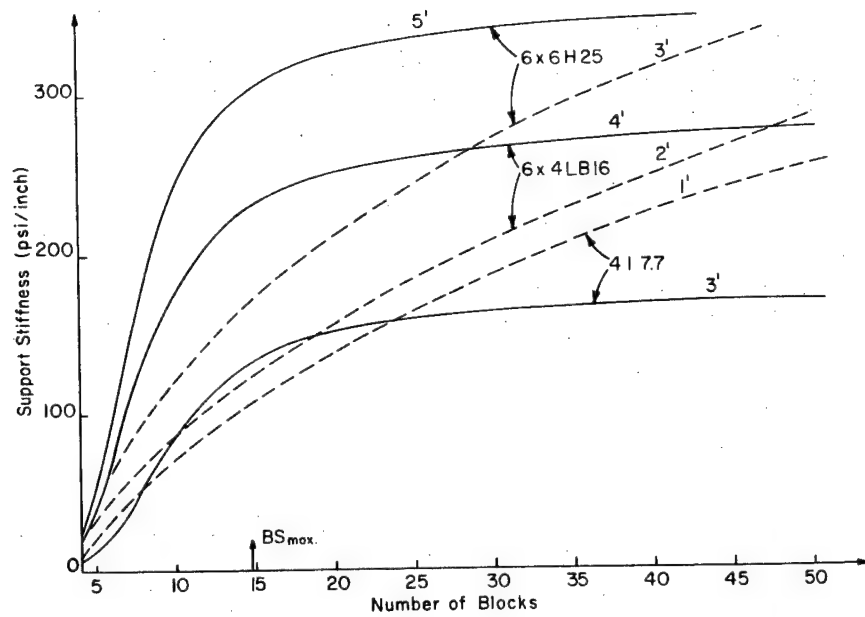


Figure A.3. Support Stiffness of Light (4I 7.7), Intermediate (6x4 LB 16), and Heavy (6x6 H 25) Steel Sets at the Indicated Spacings (1 ft, 2 ft, ... 5 ft) in a 16.7 ft Diameter Tunnel. Block thickness is 8 inches, block modulus is either  $1.4 \times 10^6$  psi (full lines) or  $8 \times 10^4$  psi (dotted lines). The number of (evenly spaced) blocks corresponding to the maximum recommended block spacing (from Proctor and White, 1968) is indicated ( $BS_{max}$ ).

spacing (or number of blocks) upon the support stiffness of a light, intermediate and heavy steel set in a 16.7 ft diameter tunnel for stiff and soft blocks. For stiff blocks the total stiffness will not increase significantly when the number of blocking points is increased much beyond the minimum recommended number. For soft blocking points the total stiffness will continue to increase well beyond that point.

A-4.3. Rock Bolts. Two types of rock bolts are considered. In point anchored bolts the interaction between bolt and rock is limited to rather short lengths at the ends of the bolt. It will be assumed that for such cases the bolt action can be replaced by a force applied on the tunnel surface (through the bearing plate) and that this force can be replaced by a pressure distributed evenly over the rock surface. The anchor force is assumed to be exerted well within the elastic region, and the anchor is assumed to be sufficiently stiff and strong to guarantee that no relative displacement between bolt end and hole bottom can occur. There is substantial empirical and experimental evidence that the latter condition, in most rock types, can

only be met by bolts grouted over some length, particularly when the bolts are to be effective over extended periods of time. The second bolt type is the one where friction can develop along the entire bolt length, either because the bolt was grouted or because it was driven in place.

The stress induced in the rock by bolt action is determined by the bolt tension generated by the relative displacement between bolt anchor and bolt bearing plate (an installation tension does not affect the stiffness if the yield limit is not exceeded, although it does correspond to an initial induced stress). The relative displacement between the bolt ends can be calculated from the expression for the radial displacement  $u_r$  at radius  $r$  as a function of the radial displacement  $u_a$  on the tunnel periphery ( $r = a$ ):

$$u_r = \frac{a}{r} u_a \quad (A.30)$$

This expression is correct in the elastic domain, but assumes that no volume change occurs in the broken rock (compare with equation A.19). When failure does occur, the strain calculated from A.30 will be an underestimate, and therefore the bolt stiffness as calculated here will be too low.

A-4.3.1. Point anchored bolts. The change in length  $\Delta l$  of a bolt of length  $l$  induced by a tunnel wall displacement  $u_a$  that occurs after bolt installation is given by:

$$\Delta l = u_a - u_l = u_a - \frac{a}{a+l} u_a = \frac{1}{a+l} u_a \quad (A.31)$$

The forces developed at the bolt ends are then:

$$A \cdot E_b \cdot \frac{\Delta l}{l} = \frac{\pi d_b^2 E_b}{4(a+l)} u_a \quad (A.32)$$

where  $A$  is the bolt cross-sectional area,  $E_b$  is the elastic modulus of the bolt and  $d_b$  is the bolt diameter.

Assuming that this force corresponds to a distributed support pressure  $P_i$  and that the bolts are at distances  $s_p$  along the tunnel and  $s_a$  across the tunnel, the equality of two expressions of the bolt forces gives:

$$P_i s_a s_p = \frac{\pi d_b^2 E_b}{4(a+l)} u_a \quad (A.33)$$

The stiffness of the bolt system is then given by:

$$K_b = \frac{P_i}{u_a} = \frac{\pi d_b^2 E_b}{4s_a s_p (a+l)} \quad (A.34)$$

A-4.3.2. Full friction bolts. The stress distribution induced by a bolt that can generate friction along its entire length is not as easily calculated as that resulting from the preceding bolt type. For that reason, the stiffness concept as used here is not directly applicable to this type of bolt. The interaction between rock and bolt will depend upon the boundary conditions, specifically upon the degree of displacement continuity between rock and bolt ends (stiffness and strength of anchor and bearing plate) and between hole walls and bolt circumference (shear stiffness and strength of grout, rock-grout and bolt-grout contact). Four possible assumptions regarding the interaction are discussed, representing extreme cases of boundary conditions. In all these cases the induced stress distribution will approach that of point anchored bolts when plastic yield progresses in the bolt. As long as the bolt remains elastic the induced stresses can be markedly different.

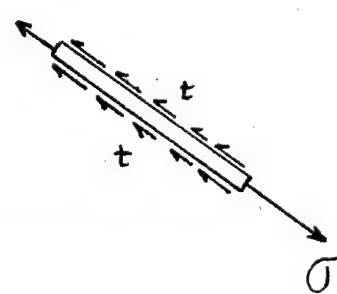
Basic equations common to all cases are:

$$\sigma + \frac{d\sigma}{dr} dr$$

i. Equilibrium

Writing the conditions

for equilibrium of a bolt



segment of length  $dr$  results in:

$$\frac{\pi d_b^2}{4} \left( \sigma + \frac{d\sigma}{dr} - \sigma \right) - \pi d_b t dr = 0$$

$$t = \frac{d_b}{4} \frac{d\sigma}{dr} \quad (A.35)$$

$\sigma$  is the bolt tension,  $t$  is the shear stress between bolt and rock.

ii. Relation between bolt stress, strain and displacement.

$$\sigma = E_b \frac{du}{dr} \quad (A.36)$$

ASSUMPTION A: Complete displacement continuity

From equations (A.30,35,36) one can derive the boundary conditions required to assure complete displacement continuity between bolt and rock. Writing the displacement relative to the bolt anchor (which adds a rigid body displacement only), the results can be written as:

$$u = \left( \frac{a}{r} - \frac{a}{a+1} \right) u_a \quad (A.37a)$$

$$\sigma = E_b \frac{du}{dr} = - E_b \frac{a}{r^2} u_a \quad (A.37b)$$

$$t = \frac{d_b}{4} \frac{d\sigma}{dr} = \frac{E_b d_b a}{2r^3} u_a \quad (A.37c)$$

The stress distribution along the bolt is illustrated in Figure A.4a. In order to have a complete displacement continuity a sufficiently

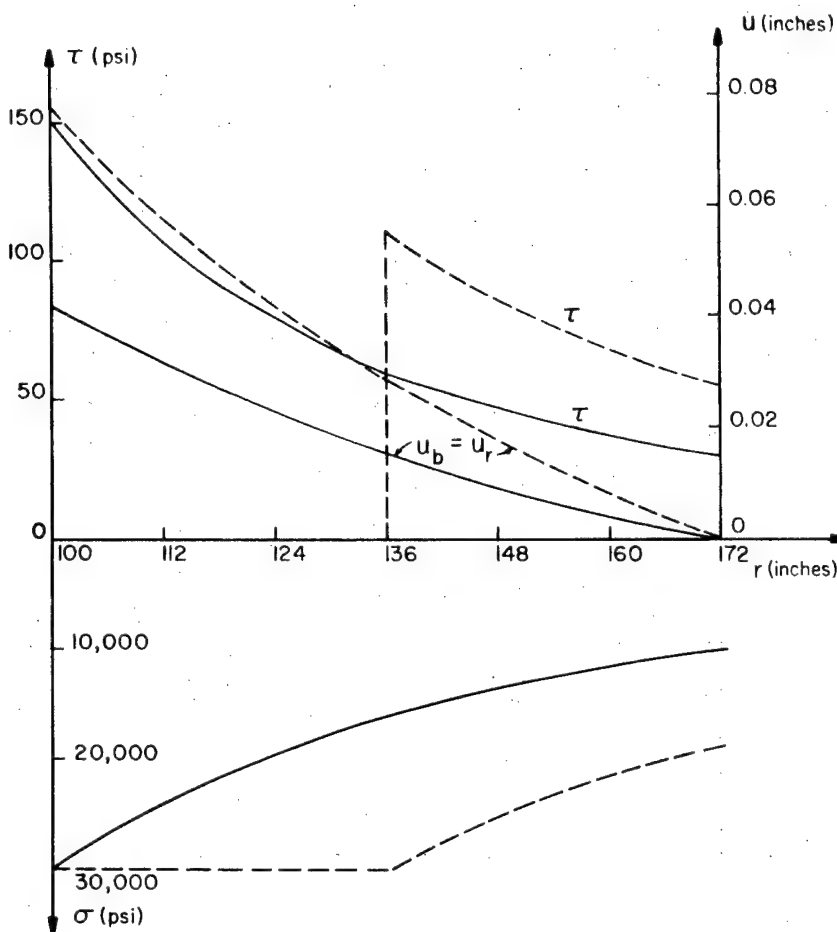


**Figure A.4a.** Stresses and Displacements Along a Fully Grouted Bolt with Complete Displacement Continuity Between Bolt and Rock. Full lines: elastic bolt; dotted lines: one-half of the bolt is plastic.

$r$  = radial distance along bolt ( $r = 100"$  =  $a$ , tunnel periphery)

$u_b$ ,  $u_r$  = bolt and rock displacement

$\sigma$  = bolt tension  $\tau$  = shear stress between bolt and rock

Bolt length = 72 inches, bolt diameter = 1 inch

stiff and strong bond has to exist across the bolt ends (bearing plate and anchor).

The resultant forces at the bolt ends ( $F_a$  at  $r = a$ ,  $F_{a+1}$  at  $r = a + 1$ ) and the total shear force  $F_t$  along the bolt are given by:

$$F_a = \frac{\pi d_b^2 E_b}{4a} u_a \quad (A.38a)$$

$$F_{a+1} = \frac{\pi d_b^2 E_b a}{4(a+1)^2} u_a \quad (A.38b)$$

$$F_t = \int_a^{a+1} \pi d_b t dr = \frac{\pi d_b^2 E_b 1(2a+1)}{4 a (a+1)^2} u_a \quad (A.38c)$$

The direct equivalent of the stiffness calculation for the point anchored bolt could now be performed by assuming that the bearing plate force  $F_a$  is distributed evenly over the rock. A calculation entirely parallel to the one producing (A.34) yields

$$K_b = \frac{\pi d_b^2 E_b}{4(a+1)} u_a \quad (A.34a)$$

This might be interpreted as a higher stiffness for the continuous displacement bolt. However, the entire bolt now acts as an anchor, and forces of opposite sign are induced all along the bolt, in particular, starting directly behind the bearing plate. Therefore, the stress distribution at some

depth will not correspond to the one induced by a point force on the surface. For this reason it is doubtful that a direct stiffness calculation as above is very meaningful.

The maximum bolt tension is reached at the tunnel periphery so that plastic yield will be initiated at that point and will progress towards the anchor with increasing tunnel convergence. When strain hardening is neglected, it follows from (A.35) that the shear stress along the plastic bolt section is nullified. The tunnel wall displacement at which a bolt length  $l_p$  has yielded results from (A.37b):

$$u_a^{y, a+l_p} = \frac{\sigma_y (a+l_p)^2}{a E_b}$$

where  $\sigma_y$  is the yield stress of the bolt steel.

In a continuous displacement bolt yield is initiated when:

$$u_a^{y, i} = \frac{\sigma_y^a}{E_b} \quad (A.40)$$

The entire bolt yields when

$$u_a^{y, f} = \frac{\sigma_y^{(a+1)}^2}{a E_b} = \frac{\sigma_y^{(a+1)}}{E_b} \cdot \frac{a+1}{a} \quad (A.41)$$

These results can be compared with the displacement at which a point anchored bolt yields:

$$u_a^y = \frac{\sigma_y^{(a+1)}}{E_b} \quad (A.42)$$

At this displacement the entire bolt yields.

For a continuous displacement bolt yield will be initiated for a smaller displacement and will be complete for a larger displacement.

The stress distribution along the bolt induced by a displacement that causes yield of half the bolt ( $l_p = 1/2$ ) is shown in Figure A.4a. Equilibrium is now maintained by the end forces and by the shear stress block along the anchor half of the bolt. The required anchor end force increases with progressing yield. As yield progresses the stress induced in the rock approaches that of a (yielding) point anchored bolt.

**ASSUMPTION B:** No end forces, friction along the bolt.

The actual shear force distribution generated along the bolt will depend upon the developing relative displacements between the rock and the bolt, and in particular, upon the shear stiffness of the contact area along the bolt. A condition that must be satisfied is that the resulting shear force is zero, because the shear stresses are self-equilibrating. The simplest assumption is that of

a linear shear stress distribution. Imposing the condition of zero end forces and of equal rock and bolt displacements at the point of zero shear stress, the results, obtained by integrating (A.35) and (A.36) can be written as:

$$t = A \left(1 - \frac{2r}{2a + 1}\right) \quad (A.43a)$$

$$\delta = \frac{4A (r - a) (1 + a - r)}{(2a + 1) d_b} \quad (A.43b)$$

$$u_b = \frac{4A}{E_b d_b} \left[ \frac{r^2}{2} - \frac{r^3}{3(2a+1)} - \frac{a(a+1)}{2a+1} r + \frac{a(a+1)}{2} - \frac{(2a+1)^2}{12} \right] + \frac{a l u_a}{(a+1)(2a+1)} \quad (A.43c)$$

The factor A could be considered as an "empirical" factor, dependent upon the properties of the rock-steel interface. However, some conditions must necessarily be satisfied in order that the solution be consistent. In particular, it is necessary that the relative displacement between bolt and rock be oriented in a direction conforming with the direction of the induced shear stresses. In this solution the bolt half close to the tunnel ( $r < a + 1/2$ ) tends to be pulled out by the rock, while the other half ( $r > a + 1/2$ ) anchors the bolt. This argument permits the derivation of some necessary conditions that have to be imposed upon the constant A:

i. at  $r = a + 1/2$ ,  $\frac{du_b}{dr} \geq \frac{du_r}{dr}$ , or

$$A \geq - \frac{4a u_a E_b d_b}{l^2 (2a + 1)}$$

ii. at  $r = a + 1$ ,  $u_b \geq 0$ , or

$$A \geq - \frac{3a E_b d_b u_a}{l^2 (a + 1)}$$

In these conditions  $u_b$  is the bolt displacement and  $u_r$  is the rock displacement, both with respect to  $u = 0$  at  $r = a + 1$ . When  $l \leq 2a$  condition i is more stringent, whereas condition ii is to be used when  $l \geq 2a$ . In the former case the constant A can be written as:

$$A = -k \frac{4a u_a E_b d_b}{l^2 (2a + 1)} \quad (A.44)$$

where  $0 < k < 1$

Displacements and stresses along the bolt for this solution are plotted in Figure A.4b. The maximum bolt tension is generated in the middle of the bolt. The displacement at which plastic yield is initiated can be calculated from (A.43b) after substitution of (A.44). For  $k = 1$  this results in

$$u_a^{y,i} = \frac{\sigma_y (2a+1)^2}{4 E_b a} = \frac{\sigma_y a}{E_b} \left( \frac{2a+1}{2a} \right)^2 = \frac{\sigma_y (a+1)}{E_b} \cdot \frac{(2a+1)^2}{4a(a+1)}$$

(A.45)

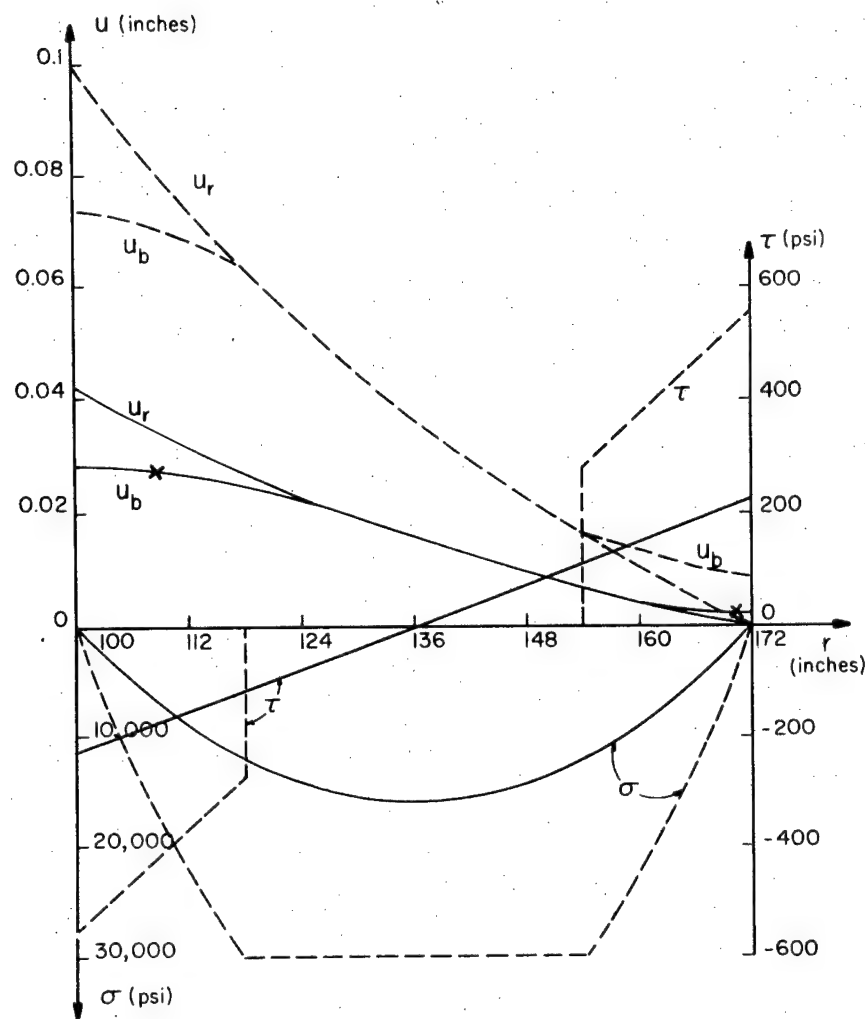


**Figure A.4b.** Stresses and Displacements Along a Fully Grouted Bolt Without End Forces

Same symbols as on Figure A.4a.

Yield will be initiated for a larger displacement than for either a continuous displacement or a point anchored bolt. To calculate the effects associated with progressive yield it will be assumed that yield progresses symmetrically about the middle of the bolt. This assumption is consistent with the calculated bolt tension distribution, but not with the (more fundamental) relative displacements. Assuming that the bolt has yielded from  $a + l_p$  up to  $a + l - l_p$ , the preceding calculation can be repeated for those  $r$ -values where the bolt remains elastic. The complete solution can then be written as:

for  $a + l_p \leq r \leq a + l - l_p$ :

$$u_b = u_r \quad \sigma = \sigma_y \quad t = 0$$

for  $a \leq r \leq a + l_p$ :

$$u = \frac{4A(r-a-1_p)}{E_b d_b} \left[ \frac{r+a+1_p}{2} - \frac{r^2 + (a+1_p)r + (a+1_p)^2}{3(2a+1)} \right] - \frac{a(a+1)}{2a+1} + \frac{(1-1_p)a u_a}{(a+1_p)(a+1)} \quad (A.46a)$$

for  $a + l - l_p \leq r \leq a + l$

$$u = \frac{4A(r-a-1+1_p)}{E_b d_b} \left[ \frac{r+a+1-1_p}{2} - \frac{r^2 + (a+1-1_p)r + (a+1-1_p)^2}{3(2a+1)} \right] - \frac{a(a+1)}{2a+1} + \frac{a l_p u_a}{(a+1)(a+1-1_p)} \quad (A.46b)$$

similar necessary conditions as above can be imposed to guarantee consistent relative displacements and shear stresses, and, for  $l \leq 2a$ , this results in

$$A = -k \frac{(2a+1) E_b d_b a u_a}{4(l-1_p) l_p (a+1-1_p)}^2 \quad (A.47)$$

From this

$$\delta = -k \frac{E_b a u_a (r-a) (a+1-r)}{(l-1_p) l_p (a+1-1_p)}^2 \quad (A.48)$$

$$t = -k \frac{E_b d_b a u_a (2a+1-r)}{4(l-1_p) l_p (a+1-1_p)}^2 \quad (A.49)$$

The preceding results are illustrated in Figure A.4b for the case where half the bolt has yielded ( $l_p = 1/4$ ). Equilibrium is maintained by the blocks of shear stress near the ends of the bolt. As yield progresses the induced stress distribution approaches that of a point anchored bolt. The limit displacement that causes yield of the entire bolt can be deduced from (A.48) and is identical to that at complete yield of a continuous displacement bolt (A.41).

ASSUMPTION C: Friction along bolt compensates anchor end force

With this assumption, the compressive force

exerted on the rock by the shear stresses along the bolt is in equilibrium with the anchor force at the bolt end, while no force is exerted at the tunnel periphery (no bearing plate). Assuming that the displacement continuity at the anchor end is assured by the end force, i.e.,  $u_b = 0$  at  $r = a + 1$ , and that therefore  $t = 0$  at  $r = a + 1$ , one can proceed from:

$$t = A(r - a - 1) \quad (A.50)$$

Integrating (A.35) after substitution of (A.50), and imposing the equilibrium condition

$$\pi d_b \int_a^{a+1} t dr = \frac{\pi d_b^2}{4} \sigma_{r=a+1}$$

results in:

$$\sigma = \frac{2A(r-a)(r-a-21)}{d_b} \quad (A.51)$$

Integrating (A.36) and imposing  $u_b = 0$  at  $r = a + 1$  results in:

$$u_b = \frac{2A(r-a-1)((r-(a+1))^2 - 31^2)}{3E_b d_b} \quad (A.52)$$

In order to assure that the relative displacements be consistent with the developed shear stresses it is necessary that  $u_b \leq u_r$ . A necessary condition is that at  $r = a + 1$ :

$$\frac{du_b}{dr} \geq \frac{du_r}{dr}$$

$$\text{or } A = k \frac{E_b d_b a u_a}{2 l^2 (a+1)^2}$$

with  $0 \leq k \leq 1$

Stresses and displacements along an elastic bolt tensioned according to this assumption are shown in Figure A.4c. The maximum bolt tension occurs at the bolt anchor. Yield is initiated there when:

$$u_a^{y,i} = \frac{\sigma_y (a+1)^2}{E_b a} \quad (\text{A.53})$$

This is the same displacement that causes complete yield of the continuous displacement bolt (Assumption A), the friction only bolt (Assumption B) and the bearing plate bolt (Assumption D).

One can proceed by assuming that the bolt has yielded from  $a + l_p$  up to  $a + l$ , and impose the proper conditions at the elastic-plastic boundary point and along the elastic and plastic bolt sections. The results from such a calculation indicate that the displacement required to propagate yield decreases with increasing length of the yielded section, pointing out an instability (this is associated with the equality of bolt and rock

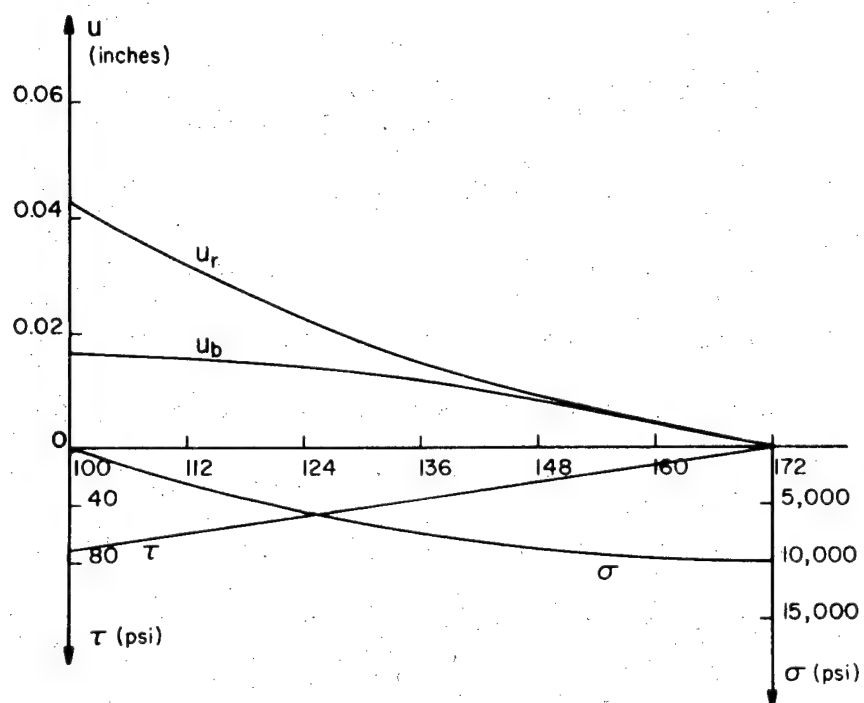


Figure A.4c. Stresses and Displacements Along a Fully Grouted Bolt When Friction Along the Bolt Compensates an Anchor End Force (Elastic Solution Only).

Symbols as in Figure A.4a.

displacements along the plastic bolt section.

Postulating that the effective bolt length is equal to the true bolt length minus the yielded bolt length it can be seen that the above conclusion follows directly from A.52 .

**ASSUMPTION D: Friction along bolt compensates bearing plate force**

This assumption can be regarded as the reversal of the preceding one. It is assumed that the bearing plate assures displacement continuity between rock and bolt on the tunnel periphery ( $u_b = u_r$  at  $r = a$ ). Friction along the bolt anchors the bolt and equilibrates the pull-out force at the bearing plate. Proceeding as before one finds:

$$t = A (r - a) \quad (A.54a)$$

$$\sigma = \frac{2A (r - a - 1)(r - a + 1)}{d_b} \quad (A.54b)$$

$$u_b = \frac{2A (r - a) ((r - a)^2 - 3l^2)}{3E_b d_b} + \frac{l u_a}{a+1} \quad (A.54c)$$

A necessary condition is that the bolt displacement  $u_b$  must be larger than the rock displacement  $u_r$ , and in particular:

$$\text{at } r = a \quad \frac{du_b}{dr} \geq \frac{du_r}{dr} \quad \text{or } A \leq \frac{E_b d_b u_a}{2a l^2}$$

$$\text{at } r = a + l \quad u_b \geq 0 \quad \text{or } A \leq \frac{3E_b d_b u_a}{4(a+l) l^2}$$

$$\text{for } l \geq a/2 \quad A = k \frac{E_b d_b u_a}{2 a l^2}$$

$$l \leq a/2 \quad A = k \frac{3E_b d_b u_a}{4(a+l) l^2}$$

For the results plotted in Figure A.4d this necessary condition was not sufficient, and  $k$  was arbitrarily taken equal to 0.9. Plastic yield is initiated at the bearing plate,

$$\text{for } l \geq a/2 \quad \text{when } u_a^{y,i} = \frac{a \sigma_y}{k E_b}$$

$$\text{for } l \leq a/2 \quad \text{when } u_a^{y,i} = \frac{\sigma_y a}{k E_b} \cdot \frac{2(a+1)}{3a}$$

In the first case, assuming  $k = 1$ , yield is initiated for the same displacement that initiates yield in a continuous displacement bolt. When the bolt is shorter than half the tunnel radius, yield is initiated for a smaller displacement. When yield has progressed along a bolt section of length  $l_p$  the bolt displacement in the elastic section can be written as:

$$u_b = \frac{2A(r-a-l_p)}{3E_b d_b} [r^2 + (a+l_p) r + (a+l_p)^2 - 3a(r+a+l_p) + 3(a^2 - l_p^2)] + \frac{(1-l_p) a u_a}{(a+l_p)(a+l_p)} \quad (\text{A.55})$$

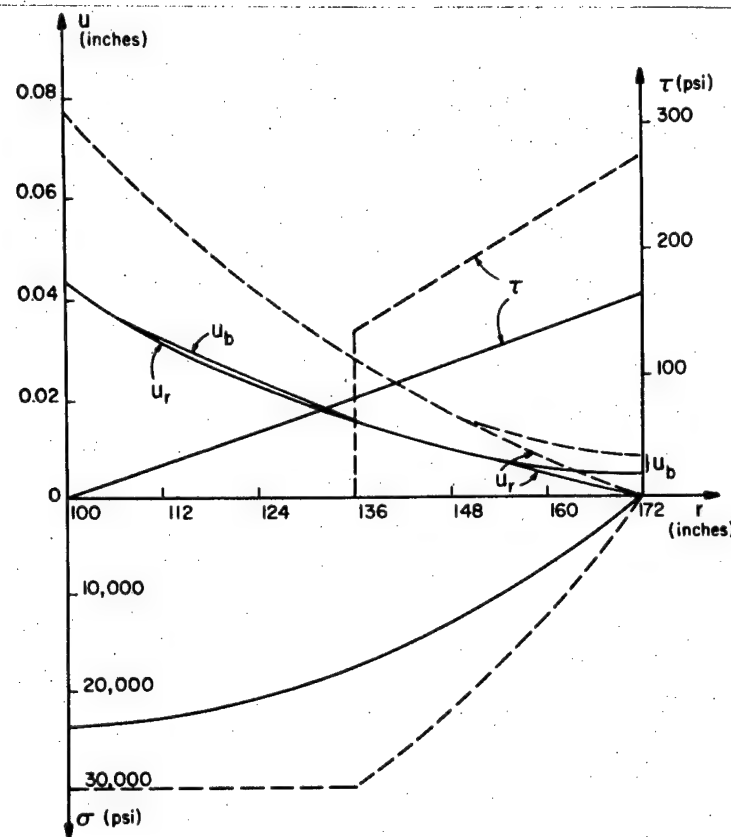


Figure A.4d. Stresses and Displacements Along a Fully Grouted Bolt When Friction Along the Bolt Equilibrates a Bearing Plate End Force.

Symbols as in Figure A.4a.

The stress and displacement results along a bolt that has yielded up to the middle ( $l_p = 1/2$ ) are plotted in Figure A.4d. Equilibrium is maintained between the bearing plate force (constant once yield is initiated) and the shear stress block near the anchor. As before, the induced stress will approach that of a point anchored bolt with progressive yielding. The entire bolt will have yielded for the same displacement that causes complete yielding in the preceding cases (A.41 and A.53).

Because a rock bolt does not exert a net force on the rock around a tunnel the concept of support stiffness as defined in II.6 is not directly applicable to a bolt support. For bolts with the entire anchor section well within a zone that remains elastic, this problem is not too serious. In that case, the assumption of a fairly homogeneous distribution throughout the broken zone of the stresses induced by bolt tensioning appears to be a reasonable one. For bolts that are in intimate contact with the rock along their entire length forces of opposite direction can be generated within very short distances. In that case, it is more difficult to justify the assumption of a homogeneous

stress distribution in the rock. Therefore, the applicability of this method of support action analysis is questionable, certainly during the initial stages of deformation.

It has been shown in the preceding analysis that for all assumptions, whether yield progresses from the bearing plate, from the middle of the bolt, or from the anchor end, the forces applied to the rock by the bolt tend towards a configuration equivalent to that developed by a point anchored bolt. Therefore, the concept of stiffness can be used in a "limit" sense, i.e., with regard to the maximum support pressure corresponding to (perfect) plastic yield of the bolts, the characteristic of a full-friction bolt system will approach the characteristic of a point anchored bolt system.

Comparing the net-force in one direction<sup>2</sup> exerted by bolts on the rock (Figure A.5) it can be seen that this force increases more rapidly for full-friction bolts with bearing plates (Assumptions A and D) than for point anchored bolts (PA), and

---

<sup>2</sup> Equal to the bearing plate force for Assumptions A and D and for a point anchored bolt, equal to the total shear force for Assumption C and to the positive shear force for Assumption B.

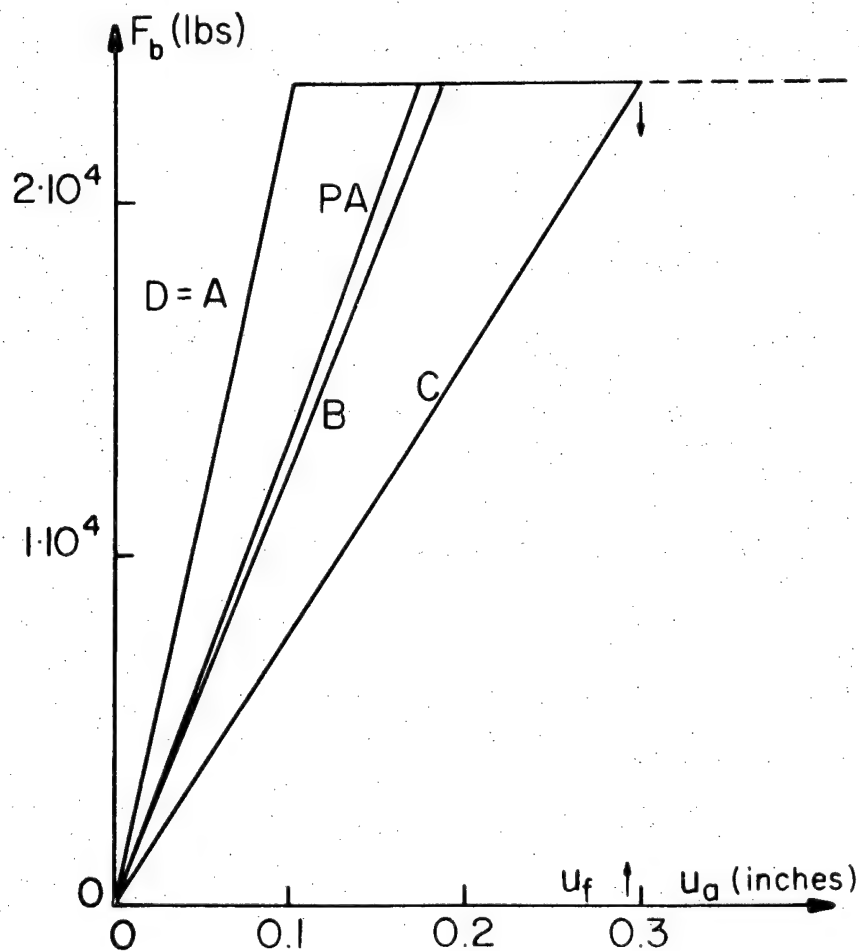


Figure A.5. Net Force  $F_b$  in One Direction Applied to the Rock by bolts of Different Types for Increasing Tunnel Convergence ( $= 2u_a$ ).

Tunnel diameter is 16.7 ft, bolt length 6 ft, bolt diameter 1 inch, bolt steel modulus  $3 \times 10^7$  psi

PA: Point Anchored Bolt

A, B, C, D: Fully grouted bolts with boundary end conditions as in Figures A.4a, b, c, d.

$u_f^y$ : tunnel wall displacement at complete yield of all grouted bolt types.

less rapidly for full-friction bolts without bearing plates. For this reason the support characteristics given in Figure II.14 for various systems of point anchored bolts can be considered as reasonable approximations for fully grouted bolts, provided the latter are equipped with bearing plates. If no or only very small forces can be exerted at the tunnel periphery (Assumptions B and C) the stiffness of friction bolts will be smaller than that of point anchored bolts. In all cases it would appear that the stiffness and the strength of the bond between rock and bolt ends are essential parameters.

The preceding derivations were made to discuss the bolting support action in terms of support stiffness, and do not represent a comprehensive analysis of bolt support action. Even within those limitations some of the assumptions made are debatable. Some specific examples are the assumptions regarding the shear stress distribution. For Assumptions B through D it might be justified to accept a slope of opposite sign for the shear distribution, or to assume that no jump occurs across the elastic-plastic boundary. As regards the generated forces, a comprehensive bolt action

analysis might have to include the compression on the bolt induced by closure of the borehole during tunnel convergence. The shear stress distribution will undoubtedly be influenced by rugosities in the borehole wall, irregularities in grout thickness, opening of cracks, etc. An analysis such as the preceding one should be complemented by field observations. Critical unknowns are the end and shear stresses. Information about these could be obtained from strain gaged bolts (Equations A.35 and A.36 relate strain gradient to shear stress).

Pull-out tests can give an indication of the anchor strength. But the interpretation of such tests with regard to support efficiency is not a trivial one, because the relative displacements between bolt and rock (and therefore, the developed shear stress distribution) are entirely different in the two configurations. The configuration considered here that comes closest to that of a pull-out test is the one of Assumption D, where the bolt displacement  $u_b$  is larger than or equal to the rock displacement along the entire bolt length. In a pull-out test the bolt displacement is larger everywhere, and the largest displacement difference occurs at the hole collar.

## APPENDIX B

### DETERMINATION OF THE PSEUDO-ELASTIC CONSTANTS IN THE FINITE ELEMENT ROCK FAILURE MODEL

#### B-1. Introduction

In this appendix a more detailed derivation is given of the methods used for the determination of the elastic constants in the finite element simulation of rock failure. This presentation is organized according to the various elastic models.

#### B-2. Plane Strain Isotropic Model

For a homogeneous linearly elastic isotropic material under plane strain conditions the stress-strain relations can be written as:

$$\epsilon_x = \frac{\sigma_x (1-\nu^2) - \nu (1+\nu) \sigma_z}{E} \quad (B.1)$$

$$\epsilon_z = \frac{\sigma_z (1-\nu^2) - \nu (1+\nu) \sigma_x}{E} \quad (B.2)$$

Dividing (B.1) by (B.2) and solving the result for  $\nu$  gives the first of expressions (III-2.6) and back substitution of  $\nu$  into (B.2) provides the

second of those expressions used in the plane strain program.

### B-3. Transversely Isotropic Model

While in principle the (physical) attractiveness and justification improve as an equivalent elastic model more closely approximates the three-dimensional physical aspects of rock failure, the number of necessary assumptions increases and the mathematical derivations become more strenuous. These factors, added to the lack of available experimental data, make the character of these more complex models also more hypothetical. Nevertheless, given the established inadequacy of the isotropic model, and the significant amount of information that is available about rock fracture in triaxial tests, it seems necessary and possible to establish some progress towards the development of a more comprehensive rock failure model.

The transversely isotropic model would appear to be an appropriate extension of the isotropic model for the case of a triaxial test, certainly during the initial stages of failure, i.e., as long as radial symmetry is maintained and as long as the radial and tangential directions are fully equivalent.

The determination of the elastic constants derived from an (idealized) triaxial test can proceed directly from the stress-strain relations:

$$\begin{aligned}\varepsilon_r + \varepsilon_\theta &= \frac{2(1-\nu_1) \sigma_{\text{con}}}{E_1} - \frac{2\nu_2 \sigma_z}{E_2} \\ \varepsilon_z &= -\frac{2\nu_2 \sigma_{\text{con}}}{E_2} + \frac{\sigma_z}{E_2}\end{aligned}\quad (\text{B.3})$$

Although this model is derived specifically for the triaxial test, and although it is less apt to give a realistic description of rock failure in a less homogeneous stressfield, it is an appropriate basis for a more generalized model. In order to derive the sequence of pseudo-elastic constants by means of equations (B.3) it is necessary that a continuous record be available of the axial stress  $\sigma_z$ , the (usually constant) confining pressure  $\sigma_{\text{con}}$ , the axial strain  $\varepsilon_z$  and the lateral volume expansion  $\varepsilon_r + \varepsilon_\theta$ . To reduce the number of unknown material properties in equations (B.3) from four to two it will be assumed that the following relations (Crouch, 1970, p. 90) hold:

$$\begin{aligned}E_1 &= \frac{E_0}{1 + \alpha(\frac{\nu_2}{\nu_0} - 1)} & \nu_1 &= \frac{\nu_0}{1 + \alpha(\frac{\nu_2}{\nu_0} - 1)}\end{aligned}\quad (\text{B.4})$$

$E_0$  and  $\nu_0$  are the initial elastic modulus and Poisson's ratio of the unfailed (isotropic) rock,  $\alpha$  is an as yet undetermined (positive) parameter. These relations were based upon the postulate that the stiffness perpendicular to the largest principal stress decreases with increasing (inelastic) lateral expansion.

From the second of equations (B.3) one finds:

$$E_2 = \frac{\sigma_z - 2\nu_2 \sigma_{\text{con}}}{\epsilon_z} \quad (\text{B.5})$$

Substitution of (B.4) and (B.5) into the first of equations (B.3) results in a quadratic equation for  $\nu_2$ :

$$\begin{aligned} & - \frac{4\alpha \sigma_{\text{con}}^2}{E_0 \nu_0} \nu_2^2 + \nu_2 [2\alpha \frac{\sigma_{\text{con}} \sigma_z}{E_0 \nu_0} - \frac{4\sigma_{\text{con}}^2}{E_0} (1-\alpha-\nu_0)] \\ & - 2\sigma_z \epsilon_z + 2\sigma_{\text{con}} (\epsilon_r + \epsilon_\theta) ] + (1-\alpha-\nu_0) \frac{2\sigma_{\text{con}} \sigma_z}{E_0} \\ & - \sigma_z (\epsilon_r + \epsilon_\theta) = 0 \quad (\text{B.6a}) \end{aligned}$$

In order to simplify the manipulations one can rewrite this equation as:

$$a \nu_2^2 + b \nu_2 + c = 0 \quad (\text{B.6b})$$

where  $a$ ,  $b$  and  $c$  are the appropriate coefficients corresponding to the ones in (B.6a).

In order to determine the correct branch of the solution that should be used, one can consider the equivalent problem for an isotropic material. After substitution of the stress-strain relations (III-2.3) for an isotropic model, equation (B.6a) reduces to:

$$-\frac{4\alpha\sigma_{\text{con}}^2}{E\nu}\nu_2^2 + [2\alpha\frac{\sigma_{\text{con}}\sigma_z}{\nu} + 4\alpha\sigma_{\text{con}}^2 - 2\sigma_z^2]\nu_2 - 2\alpha\sigma_{\text{con}}\sigma_z + 2\nu\sigma_z^2 = 0 \quad (\text{B.7})$$

For this equation  $(b^2 - 4ac)$  can be written as:

$$\begin{aligned} b^2 - 4ac &= (2\alpha\frac{\sigma_z\sigma_{\text{con}}}{\nu} - 4\alpha\sigma_{\text{con}}^2 - 2\sigma_z^2)^2 = \\ (\nu a - \frac{c}{\nu})^2 &= (2\sigma_z^2 + 4\alpha\sigma_{\text{con}}^2 - 2\alpha\frac{\sigma_{\text{con}}\sigma_z}{\nu})^2 = \\ (\frac{c}{\nu} - a\nu)^2 & \end{aligned} \quad (\text{B.8})$$

when  $\frac{c}{\nu} - a\nu > 0$

$$\begin{aligned} \sqrt{b^2 - 4ac} &= 2\sigma_z^2 + 4\alpha\sigma_{\text{con}}^2 - 2\alpha\frac{\sigma_{\text{con}}\sigma_z}{\nu} = \frac{c}{\nu} - a\nu \\ \text{and } \nu_2 &= \frac{-b - \sqrt{b^2 - 4ac}}{2a} = \nu \end{aligned} \quad (\text{B.9a})$$

when  $\nu a - \frac{c}{\nu} > 0$

$$\nu_2 = \frac{-b + \sqrt{b^2 - 4ac}}{2a} = \nu \quad (\text{B.9b})$$

It will be assumed that the criterion  $\nu a - \frac{c}{\nu} > 0$ , easily calculated from the coefficients of the quadratic equation, can be used to determine

the appropriate branch of the anisotropic solution.

Once the  $\nu_2$  Poisson's ratio has been determined, the other elastic constants follow from back substitution into equations (B.4) and (B.5). The last step in the derivation of the equivalent anisotropic constants is a check that positive definiteness is satisfied. With stress-strain relations (B.3) a necessary and sufficient condition is that

$$1 - \nu_1 - 2 \nu_2^2 \frac{E_1}{E_2} > 0 \quad (B.10)$$

with  $\nu_1, \nu_2, E_1$  and  $E_2 > 0$

By extensive numerical checking of the preceding derivations, i.e., by assuming a wide range of stress-lateral volume change-axial strain relations it was found that the determination of the elastic constants from the above expressions frequently leads to an acceptable result (in that the positive definiteness is satisfied). However, this is far from always true, for either of two reasons. The first problem is that the quadratic equation (B.6) occasionally has imaginary roots. The second problem is that positive definiteness is not always satisfied.<sup>1</sup> The latter difficulty can always be

---

<sup>1</sup>It should not be surprising that these problems

circumvented by increasing the value of the up to now arbitrary parameter  $\alpha$ . It is not as simple to eliminate the former difficulty, and it appears that the best solution at this time is to limit the input to sets of values where the problem does not arise. This necessitates that the combined changes in stiffness and volume should not be too large, or that a simultaneous very steep post-peak strength drop and very steep lateral volume increase cannot be modeled in terms of the preceding anisotropic model. Under all circumstances, a very careful analysis of the input data, prior to their use in the finite element calculations is a strict necessity if unpleasant surprises are to be avoided.

Figures B.1 and B.2 illustrate some results from (closed-form) calculations according to the methods outlined above. The solid lines represent "experimental input" from an idealized triaxial "test." The points are calculated values based

---

do arise. There is indeed no a priori justification for the assumption that any fairly arbitrarily selected relation between lateral volume changes and axial stresses and strains can be fitted within a framework of transversally anisotropic elasticity. In fact, limitations similar to the ones for isotropic elasticity discussed in III-2.3.3 do exist, but have not been investigated.

B = 8

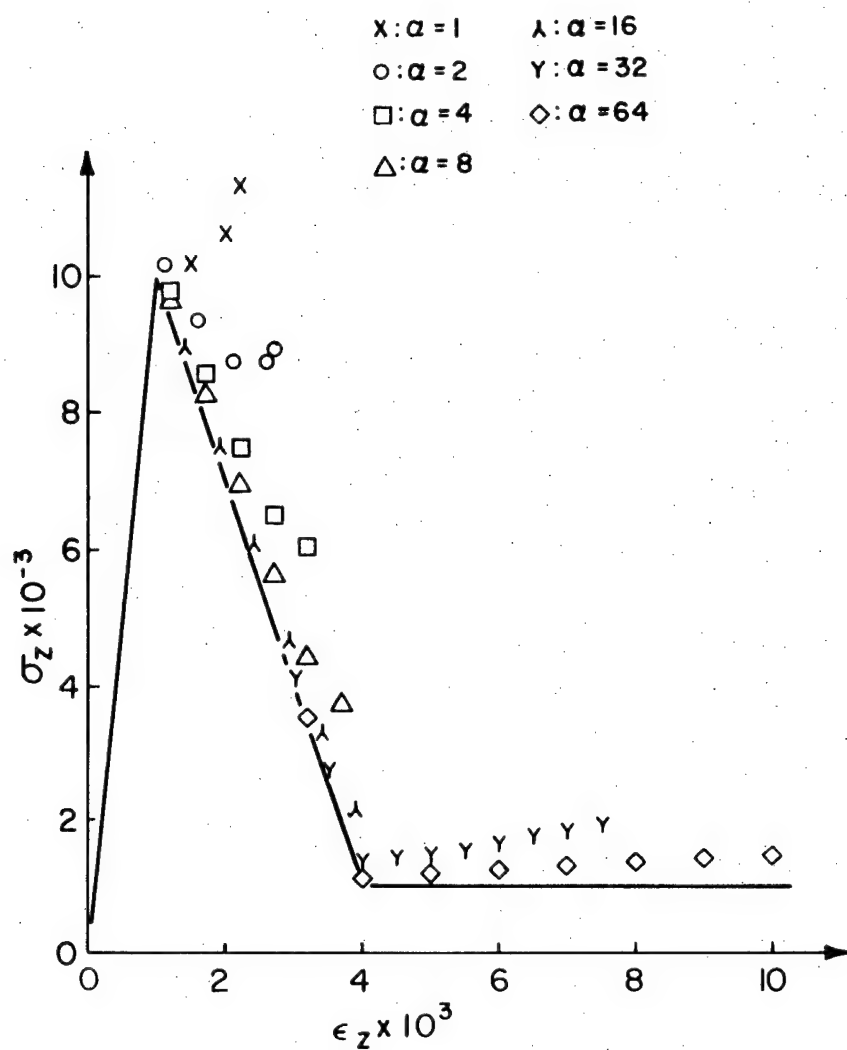


Figure B.1. Uniaxial Stress-Strain Curve and Calculated Plane Strain Behavior for Different  $\alpha$ -values when Elastic Constants are Calculated According to Equation (B.6).

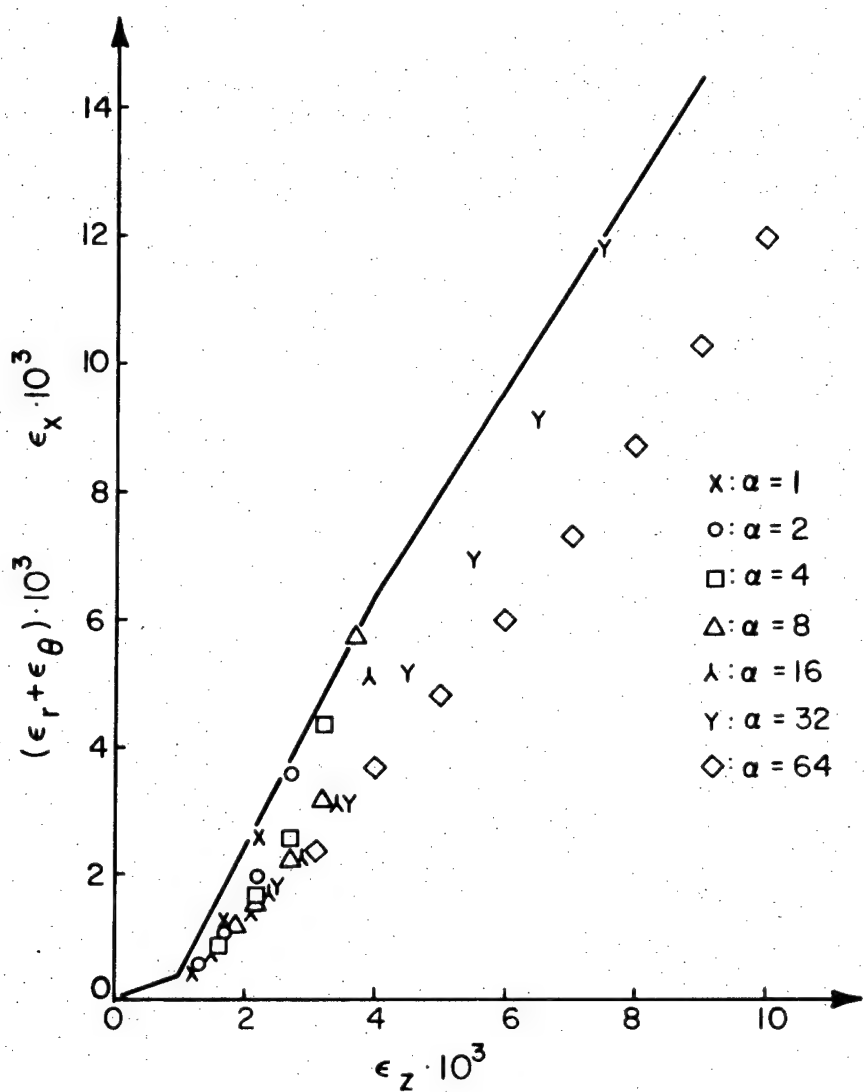


Figure B.2. Lateral Volume Change  $\epsilon_r + \epsilon_\theta$  Associated with Uniaxial Stress-Strain Curve of Figure B.1 for Calculation of Elastic Constants from (B.6). Points  $\epsilon_x$  are corresponding plane strain results for various  $\alpha$ -values.

upon substitution of pseudo-elastic constants calculated from quadratic equation (B.6) with conditions (B.9) and for  $\alpha$ -values ranging from (the minimum value) 1 up to 64. The last point for each  $\alpha$ -value, the plotted point for the largest axial strain, was the last point for which positive definiteness was satisfied.<sup>2</sup> Figure B.1 shows an input uniaxial stress-strain curve and back-calculated corresponding axial stress versus axial strain values for a plane strain condition in which the minor principal stress equals zero. Figure B.2 shows the assumed input lateral strain under uniaxial conditions (solid line) and the calculated minor principal strain points for plane strain conditions. For this example, unless  $\alpha$  is very large, and this implies an extremely rapid decrease in  $\nu_1$  and  $E_1$  (equations B.4), positive definiteness cannot be satisfied shortly after the peak strength has been exceeded. Whether results of this type are qualitatively correct (and results obtained from problems with smaller volume increase so that

---

<sup>2</sup> It might be pointed out that the volume increase, Figure B.2, is very large as can be seen from a comparison with Figure III.3b illustrating the limits for an isotropic calculation.

the positive definiteness problem is eliminated are qualitatively similar) can only be evaluated from experimental comparisons of triaxial and plane strain tests.

An alternate relation between the elastic constants can be defined so that only linear equations result for the elastic constants, replacing (B.4) by:

$$E_1 = \frac{E_2}{1 + \alpha \left( \frac{\nu_2}{\nu_0} - 1 \right)} \quad \nu_1 = \frac{\nu_2}{1 + \alpha \left( \frac{\nu_2}{\nu_0} - 1 \right)} \quad (B.11)$$

and substituting these equations into (B.3) results in:

$$\nu_2 = \frac{\frac{(\varepsilon_r + \varepsilon_\theta) \sigma_z}{\varepsilon_z} + 2(\alpha - 1) \sigma_{con}}{2 \left[ \frac{(\varepsilon_r + \varepsilon_\theta) \sigma_{con}}{\varepsilon_z} + \left( \frac{\alpha}{\nu_0} - 1 \right) \sigma_{con} - \sigma_z \right]} \quad (B.12)$$

$$E_2 = \frac{\sigma_z - 2 \nu_2 \sigma_{con}}{\varepsilon_z} \quad (B.12)$$

These relations imply that  $\nu_1 / E_1 = \nu_2 / E_2$ , and that  $E_1$  is smaller than  $E_2$  for positive  $\alpha$  and increasing  $\nu_2$ . The physical or experimental justification for (B.11) is thus far less evident than for (B.4).

When it is assumed that relations (B.11) exist

between elastic constants the criterion for positive definiteness reduces to:

$$1 + \alpha \left( \frac{\nu_2}{\nu_0} - 1 \right) - \nu_2 - 2 \nu_2^2 > 0 \quad (B.13)$$

This in itself is easily satisfied by adjusting  $\alpha$ , but that does not imply that all problems are eliminated. It is indeed not impossible that, because of the fairly complicated dependency of  $\nu_2$  upon  $\alpha$ ,  $\delta_{\text{con}}$ ,  $\varepsilon_r + \varepsilon_\theta$ , etc. situations might arise where unacceptable values for  $\nu_2$  (e.g.,  $\nu_2 < 0$  or  $\nu_2 > 1$ ) or for  $E_2$  ( $< 0$ ) are calculated. It remains therefore necessary, in every case where a particular configuration of stress-strain-volume changes is to be represented by a transversally isotropic elastic material, to check the input data over the entire stress-strain domain that might occur in the finite element calculations, in order to ascertain the internal consistency of the equivalent elastic parameters. As could be expected, it is frequently difficult to guarantee this internal consistency, unless the descending slope of the axial stress-axial strain curve is not too steep and the associated inelastic volume increase is not too large.

Results based upon assumption (B.11) and

corresponding to Figures B.1 and 2 are shown in Figures B.3 and B.4. The solid lines are uni-axial input data, the points are calculated for plane strain conditions.

As was pointed out in the introduction to this section, the determination of the multiple elastic constants invokes many hypotheses. The following diagrammatic representation illustrates the relative position of the two previously discussed assumptions within the more general framework of eight reasonable options that have been considered during this investigation.

One can start from two basic alternatives: the information about the rock behavior is given either in the form of plane strain data or in the form of triaxial data. In the latter case there is little doubt but that the radial and tangential directions are equivalent, so that the anisotropy axis coincides with the axial loading direction. In the former case, if the (probably fictional) assumption of anisotropy is to be maintained, one can assume that the material properties in the plane strain direction are equal either to those in the principal loading direction or to those in the minimum principal stress direction. It is then

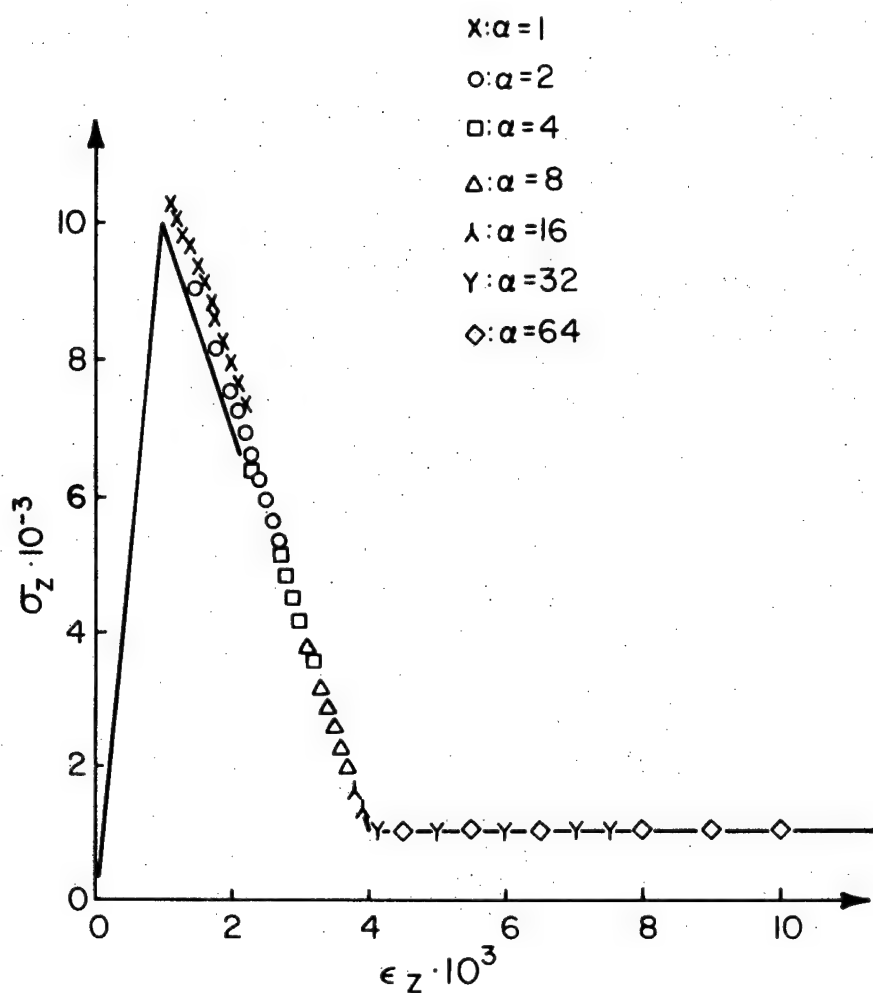


Figure B.3. Uniaxial Stress-Strain Curve and Calculated Plane Strain Points for Various  $\alpha$ -values when the Elastic Constants are Calculated According to Equations (B.12).

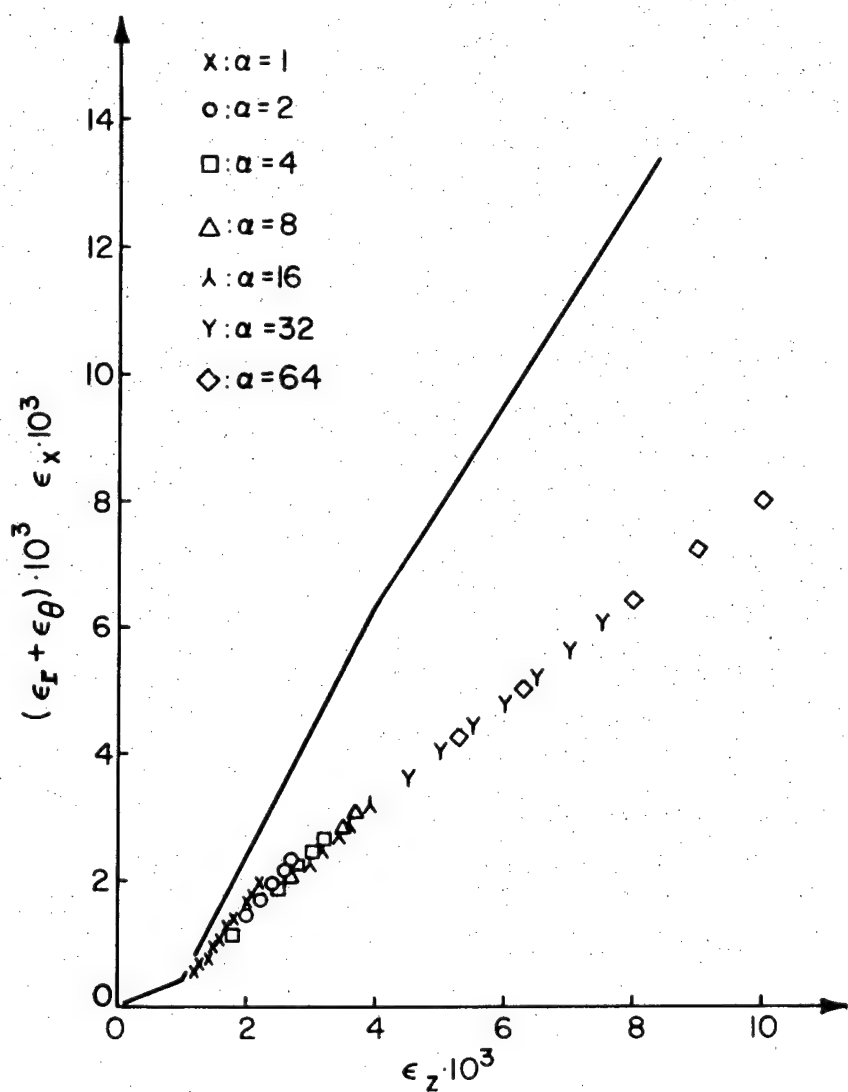


Figure B.4. Lateral Volume Change  $\epsilon_r + \epsilon_\theta$  Associated with Uniaxial Stress-Strain Curve of Figure B.3 for Calculation of Elastic Constants from (B.12). Points ( $\epsilon_x$ ) are corresponding plane strain results for various  $\alpha$ -values.

necessary to make assumptions about acceptable relations between various elastic constants.

Finally, when the constants have been derived from the triaxial assumption, it still must be decided what type of anisotropy will be used in the stiffness matrix formulation.

Two of the options have already been discussed in some detail. A short survey of the options, their applicability and related problems follows.

Option 1

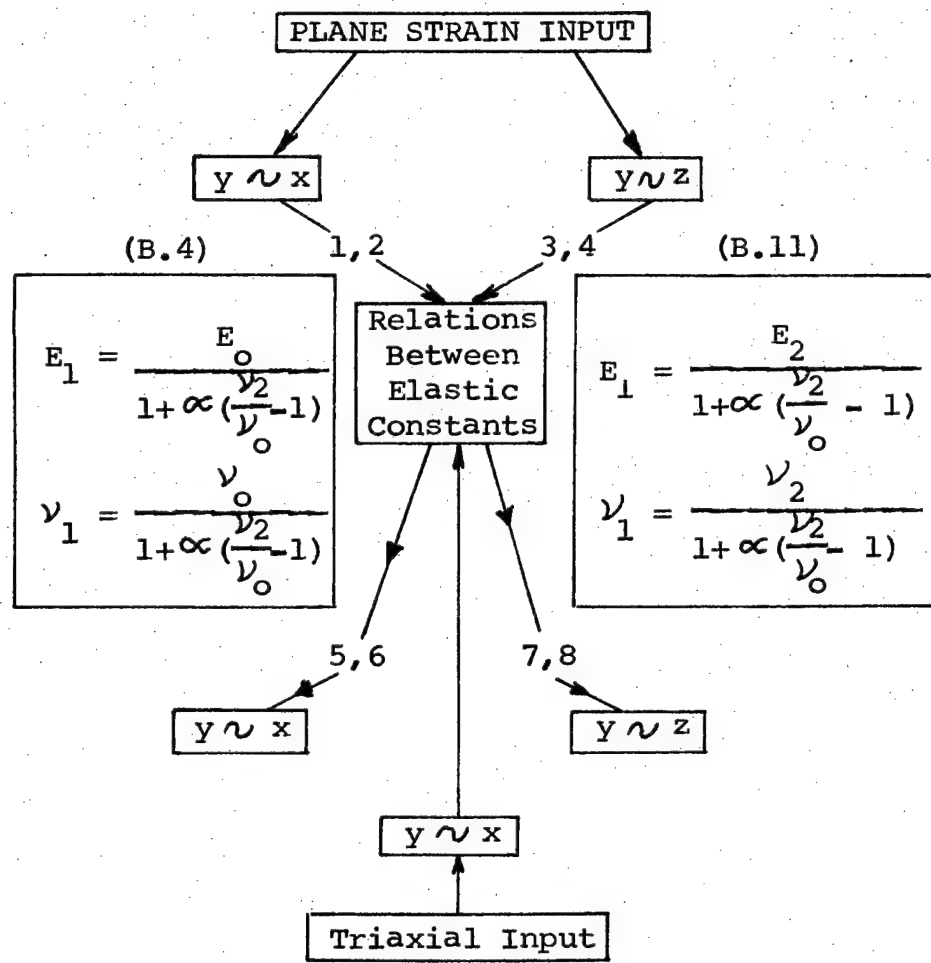
Plane strain input; plane strain direction assigned same constants as minimum principal stress direction, relations (B.4) between elastic constants. This option leads to a fourth order equation for  $\nu_2$ , and has not been considered in any more detail.

Option 2

Plane strain input; plane strain direction assigned same constants as minimum principal stress directions; relations (B.11) between elastic constants. This option leads to a quadratic equation for  $\nu_2$  with long complicated coefficients, and results in the same condition (B.9,16) as for options 4,5 and 7.

Option 3

Plane strain input; plane strain direction



Diagrammatic Representation of the Eight Options Considered for the Definition of Equivalent Transversally Isotropic Pseudo-elastic Constants

assigned same constants as largest principal stress direction; relations (B.4) between elastic constants. This option leads to a fourth order equation for  $\nu_2$ , and has not been considered in any more detail.

Option 4

Plane strain input; plane strain direction assigned same constants as largest principal stress direction; relations (B.11) between elastic constants. This option leads to the following quadratic equation for  $\nu_2$ :

$$\nu_2^2 (\varepsilon_z - \varepsilon_x) (\sigma_x + \sigma_z) - \nu_2 [\sigma_x \varepsilon_x + \varepsilon_z (\sigma_x \frac{\alpha}{\nu_0} - \sigma_z)] + \varepsilon_x \sigma_z - \varepsilon_z \sigma_x (1 - \alpha) = 0 \quad (B.14)$$

In order to define the appropriate branch of the solution, one can proceed in a similar way as in the discussion following quadratic equation (B.6). After substitution of the isotropic plane strain stress-strain relations equation (B.14) becomes:

$$\nu_2^2 (\sigma_z^2 - \sigma_x^2) - \nu_2 [(1-\nu) (\sigma_x^2 - \sigma_z^2) + \sigma_x \frac{\alpha}{\nu_0} < (1-\nu) \sigma_z - \nu \sigma_x] - \nu (\sigma_z^2 - \sigma_x^2) + \sigma_x \alpha [-\nu \sigma_x + (1-\nu) \sigma_z] = 0 \quad (B.15)$$

The discriminant of this quadratic equation can be written as:

$$b^2 - 4ac = [(1+\nu)(\sigma_z^2 - \sigma_x^2) - \sigma_x \frac{\infty}{\nu} \times (1-\nu) \sigma_z - \nu \sigma_x]^2$$

$$= (\nu a - \frac{c}{\nu})^2 = (\frac{c}{\nu} - \nu a)^2 \quad (B.16)$$

$$\text{When } (1+\nu)(\sigma_z^2 - \sigma_x^2) - \sigma_x \frac{\infty}{\nu} [(1-\nu) \sigma_z - \nu \sigma_x] = \nu a - \frac{c}{\nu} > 0$$

$$\nu = \frac{-b + \sqrt{b^2 - 4ac}}{2a}$$

$$\text{When } \nu a - \frac{c}{\nu} < 0$$

$$\nu = \frac{-b - \sqrt{b^2 - 4ac}}{2a}$$

By continuity it will be assumed that the same relation between the coefficients of the quadratic equation for  $\nu_2$  can be used to select the correct branch for the solution of that equation.

#### Options 5, 6, 7 and 8

When the input is considered as results from triaxial tests, the equivalent elastic constants are calculated from (B.6a) for options 5 and 7, and from (B.12) for options 6 and 8. The determination of the selected option must then be completed by inserting the desired elastic properties corresponding to the plane strain direction into the stiffness matrix. This can be done most efficiently directly in the computer program, by inserting the desired replacement statements after the computation of the

first elastic constants. The form of the stress-strain relations used in the computer program is given in the next section.

The principal advantage of using triaxial data input is that enough experimental data is available to make a good estimate of the qualitative behavior of rock under such conditions. In addition, a straightforward evaluation of all elastic constants is possible, whether assumptions (B.4) or (B.11) are used.

The principal advantage of using plane strain input data is that a direct verification of the degree of approximation induced by the finite element calculations is possible. A simple determination of the elastic constants is not possible when relations (B.4) are assumed to exist.

#### B-4. Orthotropic Rock Failure Model

The three principal stresses will be different under all but the most simplistic boundary conditions. As a consequence, the likelihood of the transversally isotropic model being truly equivalent to the deformational characteristic of failed rock is small. This problem is easily illustrated for the anisotropic derivation presented in the previous

section. It was necessary there to assume that the plane strain direction was equivalent, with regard to change in stiffness, to either the largest or the smallest principal stress direction. While no experimental evidence is available, neither of these two alterations is particularly attractive.

In principle, it would therefore seem reasonable to generalize the failed rock equivalent to a fully orthotropic material. The difficulties encountered in the derivation of the anisotropic constants give a fair warning of the problems and hypotheses that will be involved in a similar derivation for a far more complicated symmetry class.

The orthotropic stress-strain relations, as used (Lekhnitskii, pp. 20-21) for the formulation of the plane strain stiffness matrix, are given by:

$$\begin{aligned}\varepsilon_x &= \frac{\sigma_x}{E_1} - \frac{\nu_{21}}{E_2} \sigma_y - \frac{\nu_{31}}{E_3} \sigma_z \\ \varepsilon_y &= -\frac{\nu_{12}}{E_1} \sigma_x + \frac{\sigma_y}{E_2} - \frac{\nu_{32}}{E_3} \sigma_z \\ \varepsilon_z &= -\frac{\nu_{13}}{E_1} \sigma_x - \frac{\nu_{23}}{E_3} \sigma_y + \frac{\sigma_z}{E_3}\end{aligned}\quad (B.17)$$

$$\gamma_{xy} = \frac{t_{xy}}{G_{12}} \quad \gamma_{xz} = \frac{t_{xz}}{G_{13}} \quad \gamma_{yz} = \frac{t_{yz}}{G_{23}}$$

Taking the z-direction as plane strain ( $\varepsilon_z = 0$ ),

and eliminating  $\epsilon_z$ , one finds:

$$\begin{aligned}\epsilon_x &= \left(\frac{1}{E_1} - \frac{\nu_{31}^2}{E_3}\right) \sigma_x - \left(\frac{\nu_{21}}{E_2} + \frac{\nu_{31} \nu_{32}}{E_3}\right) \sigma_y \\ \epsilon_y &= -\left(\frac{\nu_{21}}{E_2} + \frac{\nu_{31} \nu_{32}}{E_3}\right) \sigma_x + \left(\frac{1}{E_2} - \frac{\nu_{32}^2}{E_3}\right) \sigma_y \\ \gamma_{xy} &= \frac{t_{xy}}{G_{12}}\end{aligned}\quad (B.18)$$

These equations suffice to solve the plane problem and to formulate the plane stiffness matrix. They are formally identical to the plane strain relations for an anisotropic material (Crouch, 1970, p. 82; Green and Zerna, p. 207). Therefore, at this stage equations (B.18) could be rewritten in terms of four independent constants, the stiffness matrix in turn could be formulated in terms of these constants, and after reducing the number of independent constants by assuming some relations between "elastic" constants the problem could be solved. Such a course, although potentially very fruitful, has not been pursued here.

An assumption that is incorporated in all numerical calculations in order to eliminate the shear moduli is that:

$$\frac{1}{G_{ij}} = \frac{1 + \nu_{ij}}{E_i} + \frac{1 + \nu_{ji}}{E_j} = \frac{1}{E_i} + \frac{1}{E_j} + \frac{2 \nu_{ij}}{E_i} =$$

$$\frac{1}{E_i} + \frac{1}{E_j} + \frac{2\nu_{ji}}{E_j} \quad (B.19)$$

where  $i, j = 1, 2, 3$  and  $i \neq j$

It can be shown that these expressions lead to the correct relations for the shear moduli when any one of three principal axes is taken as an axis of symmetry, i.e., when the material is transversely isotropic. This relation reduces to (III-2.8) when the z-axis is taken as the axis of isotropy.

#### B-5. Orthotropic Cylinder with Cylindrical Anisotropy

This model might be of value for a study of the triaxial test, but here it was considered especially for incorporation into the axisymmetric program that was used to study the influence of the face stiffness on failure development and on the progressive support loading. In principle nine independent elastic constants are included in the model. The shear moduli are eliminated by the same assumption as before (equation B.19). As can be expected from the preceding discussion two basic alternatives can be considered: the elastic constants are derived either from idealized triaxial tests or from idealized assumed results corresponding directly to the geometry and boundary conditions of

the problem to be solved. A combination of the two approaches, with heavy emphasis on the second one, has been used here.

The axi-symmetric finite element with rectangular cross-section and sides parallel and perpendicular to the axis of symmetry is an orthotropic cylinder. It is then desired to change the properties of this cylinder as it is strained into the failing region, in such a way that the cylinder softens, i.e., a larger convergence of the external boundary is caused by a decreasing external pressure, and increases in volume, i.e., a larger internal convergence results from a constant external convergence. The conditions these requirements impose upon the sequence of elastic constants can be derived by considering the analytical solution for the stress and displacement fields in an orthotropic cylinder pressurized internally and externally.

Following Lekhnitskii (1963, p. 65) the stress-strain relations can be written as:

$$\varepsilon_r = a_{11} \sigma_r + a_{12} \sigma_\theta + a_{13} \sigma_z$$

$$\varepsilon_\theta = a_{12} \sigma_r + a_{22} \sigma_\theta + a_{23} \sigma_z \quad (B.20)$$

$$\varepsilon_z = a_{13} \sigma_r + a_{23} \sigma_\theta + a_{33} \sigma_z$$

The stress distribution for the general orthotropic case of a cylinder in plane strain with external pressure  $q$  and internal pressure  $p$  is given by Lekhnitskii (1963, pp. 249-250). These expressions can be substituted in the differential stress-strain relations (Lekhnitskii, pp. 237-239), and after integration one obtains:

$$u_r = (\beta_{12} \sigma_r + \beta_{22} \sigma_\theta) r \quad (B.21)$$

where

$$\beta_{ij} = a_{ij} - \frac{a_{i3} a_{j3}}{a_{33}} \quad (B.22)$$

From (B.21) it is possible to derive  $u_b / u_a$ , the ratio of the external to the internal displacement. The condition can then be imposed that this ratio must increase monotonically for increasing external displacement beyond the point of failure initiation. In order to facilitate computation of this condition it is advantageous to eliminate the transcendental factors from the expressions for the stress distributions. This can be achieved by letting:

$$\beta_{11} = \frac{1}{E_1} - \frac{\nu_{31}^2}{E_3} = \frac{1}{E_2} - \frac{\nu_{32}^2}{E_3} = \beta_{22} \quad (B.23)$$

The determination of the sequence of elastic

constants will then be completed by imposing, at each stress and strain level, a volume increase beyond the homogeneous isotropic elastic one for equal boundary conditions. This requirement is met directly from the ratios between external and internal displacements:

$$\left( \frac{u_a}{u_b \text{ ortho}} \right) = x \left( \frac{u_a}{u_b \text{ iso}} \right) \quad (B.24)$$

where  $x$  is a proportionality factor,  $> 1$ .

After independent definition of some elastic constants, and substitution of assumed relations between additional ones, this equation can be solved. Independently defined first of all is the modulus  $E_2$  in the tangential direction, calculated as secant from a set of axial stress-axial strain curves.

In order to eliminate additional unknowns the following assumptions are introduced:

$$E_3 = E_2 + (E_0 - E_2) \alpha$$

$$E_1 = E_3, \quad \nu_{31} = \nu_{32} \quad (B.25)$$

$$\nu_{31}^2 = \frac{\nu_0^2}{1 + \gamma (1 - \frac{\nu_0}{\nu_{21}})}$$

where  $\alpha$  and  $\gamma$  are positive constants,  $\alpha < 1$ .

The qualitative similarity of the assumptions

(B.25) to (B.3) and (B.11) is easily recognized.

Substitution of (B.25) into (B.24) leads to a quadratic equation for  $\nu_{21}$ . The sign of the selected branch is defined by the assumption of continuity in the sequence starting from the isotropic case, for which the selection of the sign is obvious.

Several implications from these calculations, used for the generation of the data in Section III-4.2.2, should be pointed out:

- the equivalent elastic constants are calculated for the radial and the tangential directions, not for the principal directions.
- every element is considered to be in plane strain.
- every (failing) element is assumed to be a cylinder with rectangular cross section.
- at every confining pressure the modulus  $E_2$  in the tangential direction is calculated as the secant of an axial stress-axial strain curve.

## Appendix C

### COMPUTER PROGRAM TUNSUP FOR THE PLANE STRAIN ANALYSIS OF TUNNEL SUPPORT LOADING CAUSED BY ROCK FAILURE

#### C-1. Introduction

The program included in this appendix has been used to calculate the results discussed in section III-4.3.3. Options are included for plane strain or plane stress elastic analysis, with or without gravity loading, for a variety of imposed boundary conditions, for isotropic rock failure as described in B-2, incremental loading or unloading (equivalent mining), with a support model as discussed in III-3.2 and with a ground-support interaction sequence as described in III-4.3.2.

The program is based on a finite element program written by Crouch (1970a) who used the first program published by Wilson (1963) as a starting point. The program as presented here is not as fully debugged nor as comprehensive as would be desirable. This is due, in part, to severe operational problems at the University of Minnesota

Computer Center during the latter part of 1974, when this program was completed.<sup>1</sup> One example of such a problem is reflected directly in the following program. The tape option is incomplete because the extremely long turn-around times for programs that used tapes and the frequent changes in tape labeling requirements made the use of tapes very inefficient. This is unfortunate because the tape use option is very valuable in several respects. The finite element equations are solved by successive over relaxation, and for such an iterative method it is good practice to reduce the required computation time by using a good initial displacement approximation. For most problems an approximate closed form solution can easily be programmed, and the displacements thus calculated can be written on tape and used as input for the finite element program. This procedure was used with very good results for the axisymmetric calculations discussed in III-4.2, where a large number of problems were presented with a relatively small number of elements

---

<sup>1</sup> The combination of the two main problems, the instability of the operating system and the frequent errors in the card reading equipment resulted in a situation where, for a long program, not more than a few runs a week could be made.

with different properties from one problem to the next one. Such a procedure could not be used for the plane calculations because of the current difficulties with the tape handling system. A second very useful feature of data storage on tape is that it permits easy transfer to various plotting routines, after inspection of the output. Finally, with temporary storage of all data it becomes easy to interrupt the calculations in order to check intermediate results, while the calculations can be restarted with a minimum loss in computer time. This method was used repeatedly in the axisymmetric problems, for example to refine the mesh when it appeared that the failure zone, and thus the region of high strain gradients, approached a mesh section with triangular elements.

An option that can be included rather easily, by assigning different values to the NFE control parameter and by including the calculations given in Appendix B is the use of a variety of failure models. Minor additions would be sufficient to include boundary shear stresses (variable ELT), to include orthotropic elastic materials (variables E1, E2, E3, V1, V2, V3, G1) and to include point anchored rock bolts (by eliminating the check on

the spring tension now imposed for "blocking point" spring elements).

Program TUNSUP is written in FORTRAN IV, and for the version included here 135,000 central memory words are required on a Control Data Corporation CYBER 74 computer with KRONOS operating system and RUN compiler. Running times vary greatly with problem type, notably with the degree of non-linearity, with the number of ground-support interaction steps, with the over relaxation factor, with the degree of approximation of the input displacements, and so on. Computing times for the examples given in III-4 ranged from 2 up to 18 minutes.

### C-2. Input

Card 1: FORMAT (I5)

Cols. 1-5: TAPECOD: Tape selection parameter.

TAPECOD = -3: Input read from tape 2,  
input and output stored  
on tape 1.

-1: Input read from tape 2.

1: Input and output stored  
on tape 1.

0: No tape used.

Card 2: FORMAT (8A10)

cols. 2-80: Identification to be printed with output.

Card 3: FORMAT (6I4,2F4.0,F10.4,3I4,F8.0,I4)

cols. 1-4: NUMEL: Number of plate elements, Maximum  
310.

5-8: NUMNP: Number of nodal points, maximum  
320.

9-12: NCYCM: Maximum number of iterations for  
one solution of the finite ele-  
ment stiffness equations.

13-16: NUMIN: Number of loading or unloading  
(equivalent mining) steps.

17-20: INBEG: First of the steps at which an  
explicit solution is calculated.

21-24: ICOOR: Coordinate system selection.

ICOOR = 0: Cartesian.

1: Polar, nodal point inter-  
polation along circles  
centered at origin.

-1: Polar, nodal point inter-  
polation along radii through  
the origin.

25-28: CODPL: Plane strain (=0) or plane stress  
( $\neq 0$ ).

29-32: CHECK: If different from zero all nodal  
points will be printed out with

all adjacent nodal points.

33-42: DENS: Specific weight (identical for all elements).

43-46: NUMBEAM: Number of (beam plus spring) elements in support model, maximum 32.

47-50: NUMJOI: Number of nodal points in support model, maximum 32.

51-54: NUMSUP: Step in the unloading sequence after which the support is activated.

55-62: SETS: Steel set spacing along the tunnel.

63-66: ITSUP: Number of iterations between ground and support, as discussed in section III-4.3.2. and as illustrated on Figure III.25.

Card 4: FORMAT (4E13.6,4F7.4)

Cols. 1-13: TOLER: Displacement unbalance tolerance after which iterations on stiffness equations will be terminated (the unbalance is equal to the sum of the absolute values of the displacement changes calculated in one iteration).

14-26: ER: Young's modulus of material with code o.

27-39: EP: Young's modulus of material with  
code 1.

40-52: ES: Young's modulus of material with  
code -1.

53-59: VR: Poisson's ratio of material with  
code 0.

60-66: VP: Poisson's ratio of material with  
code 1.

67-73: VS: Poisson's ratio of material with  
code -1.

74-80: BETA: Successive over relaxation factor.

Element cards: FORMAT (7I4, F12.4)

Cols. 1-4: NUME: Element number.

5-8: NPI: Nodal point I.

9-12: NPJ: Nodal point J.

13-16: NPK: Nodal point K.

17-20: NPL: Nodal point L (blank for a tri-  
angular element).

21-24: MAT: Material code (0, 1 or -1).

29-40: E2T: Boundary pressure applied per-  
pendicular to side IK of a tri-  
angular element, to side JK of a  
quadrilateral element.

Element cards can be omitted when the number-  
ing of elements and nodal points is such that the

following interpolation can be used: nodal point numbers I,J,K and L (for quadrilaterals) will be incremented by one for each missing element card, the other element parameters will be assigned equal to those of the first element in the sequence.

Element nodal point numbering must be counter-clockwise in a right-handed coordinate system.

Nodal point cards: FORMAT (I4,2F9.3,2F12.3,2F12.8,  
F10.6)

Cols. 1-4: NPNUM: Nodal point number.

5-13: R: x or r coordinate.

14-22: Z: y or θ coordinate.

23-34: FORR: Horizontal or radial force.

35-46: FORZ: Vertical or tangential force.

47-58: U: Horizontal or radial displacement.

59-70: W: Vertical or tangential displacement.

71-80: BDISC: Boundary displacement code determining restrictions on the displacements.

BDISC = -1: Vertical and horizontal displacements are imposed.

-2: Vertical displacement is imposed.

-3: Horizontal displacement is imposed.

$0 < \text{BDISC} < 360$ : angle (in degrees) with  
the x-axis of the line  
along which the point  
must move.

$360 < \text{BDISC} < 720$ : an input displacement  
along this line is  
imposed and listed in  
the input table as X -  
DISP. (U).

$720 < \text{BDISC}$ : listed displacement is imposed  
but the point is free to move  
perpendicular to the given  
direction.

Nodal point cards can be omitted when the nodal  
point numbering is such that the following inter-  
polation can be used: nodal points are equally spaced  
along a straight line (or along a circle) and all  
variables except the coordinates are identical to  
those of the first nodal point in the sequence.

Support element cards: FORMAT (3I4,4E12.4)

Cols. 1-4: K: Element number.

5-8: NPIB: Nodal point I.

9-12: NPJB: Nodal point J.

13-24: EB: Elastic modulus.

25-36: AB: Cross-sectional area.

37-48: XIB: Modulus of inertia.

49-60: PHIB: Shear deformation coefficient.

Support nodal point cards: FORMAT (5F10.5,2I5)

Cols. 1-10: XB: x-coordinate.

11-20: YB: y-coordinate.

21-30: UB: Horizontal displacement.

31-40: WB: Vertical displacement.

41-50: ROT: Rotation.

51-55: NPBFE: Nodal point of the finite element

mesh associated with the support  
nodal point. The component of  
this finite element nodal point  
displacement that occurs after  
support erection is an imposed  
displacement for this support  
nodal point.

56-60: NP: Conditions imposed on the dis-

placements (applicable only if

NPBFE = 0).

NP: -1: rotation is imposed.

-2: vertical displacement is

imposed.

-3: vertical displacement and

rotation are imposed.

1: horizontal displacement is

imposed.

2: horizontal displacement and rotation are imposed.

3: horizontal and vertical displacement are imposed.

4: all three displacements are fixed.

Card with basic rock failure and ground-support interaction parameters: FORMAT (5I4,7X,F7.1,E13.6, 18X,3I5).

Cols. 1-4: NFE: Failure parameter; when blank, elastic solution only.

5-8: NCON: Number of confining pressure levels for which stress-strain curves are given, maximum 40.

17-20: NFEMX: Maximum number of iterations allowed at any loading or unloading step for changes in the elastic constants.

28-35: SIZC: Difference in confining pressure between two subsequent levels of stress-strain input.

36-48: SIZE: Minimum strain difference in any element between two different subsequent failure states. If the change in the largest principal strain between two iterations is

smaller than this parameter no  
change in elastic constants will  
be made.

66-70: LOAD: If positive, incremental loading;  
if negative, incremental unloading.

71-75: INITUNL: First nodal point at which force  
will be reduced (stepwise)  
during unloading.

76-80: LASTUNL: Last of the finite element  
nodal points at which the force  
will be reduced during unloading.

All nodal points from INITUNL up to LASTUNL  
will be unloaded. The difference between LASTUNL  
and INITUNL should not exceed 32.

Axial stress versus axial strain rock failure model  
cards: FORMAT (4E16.9).

Cols. 1-16: EM: Strain at peak stress.

17-32: ERE: Strain where residual stress is  
reached.

33-48: SM: Peak stress.

49-64: SR: Residual stress.

Lateral strain (volume increase) versus axial strain  
failure cards: FORMAT (5E16.9).

Cols. 1-16: EML: Axial strain at end of first straight  
line section of lateral strain  
graph (elastic limit).

17-32: ERL: Axial strain at end of second straight line section of lateral strain graph.

33-48: PHIR: Lateral strain at end of first straight line section of lateral strain graph.

49-64: PHII: Intersection of line for third segment with vertical axis, i.e., for axial strain equal to zero.

65-80: PHIM: Lateral strain at end of second straight line segment.

### C-3. Output

All basic information punched on the first four cards is printed on the first output page. On the following pages appears all finite element nodal point information input, support system element input, support system nodal point input and failed rock description.

The tables with the element information for the finite element mesh show, in addition to the input, the centroid coordinates and the area of each element. Also printed is the total area covered by the mesh. This frequently facilitates the detection of errors in the mesh.

The step number is printed at each loading or unloading (equivalent mining) step. The iteration number is printed for each iteration needed for additional changes in elastic properties and for each iteration between ground and support. The total number of iterations for each solution of the finite element equations is printed as well as the initial and the final displacement unbalance.

For each unloading step the displacements and forces at all support nodal points are printed, as well as the internal forces. Similarly, for each finite element nodal point the displacements and forces are printed, and for each element the principal stresses, the angle of the largest principal stress with the horizontal axis and the three Young's moduli, the three Poisson's ratios and one shear modulus. The last output information is the strain energy stored in the finite element mesh.

#### C-4. Computational Scheme

The flow chart of Figure C.1 illustrates the basic functions of the main program TUNSUP and of the subroutines, FORM, SSMAT, FORMQ, MODST, SOL and FORMB. The main program performs a significant fraction of all calculations, controls the overall

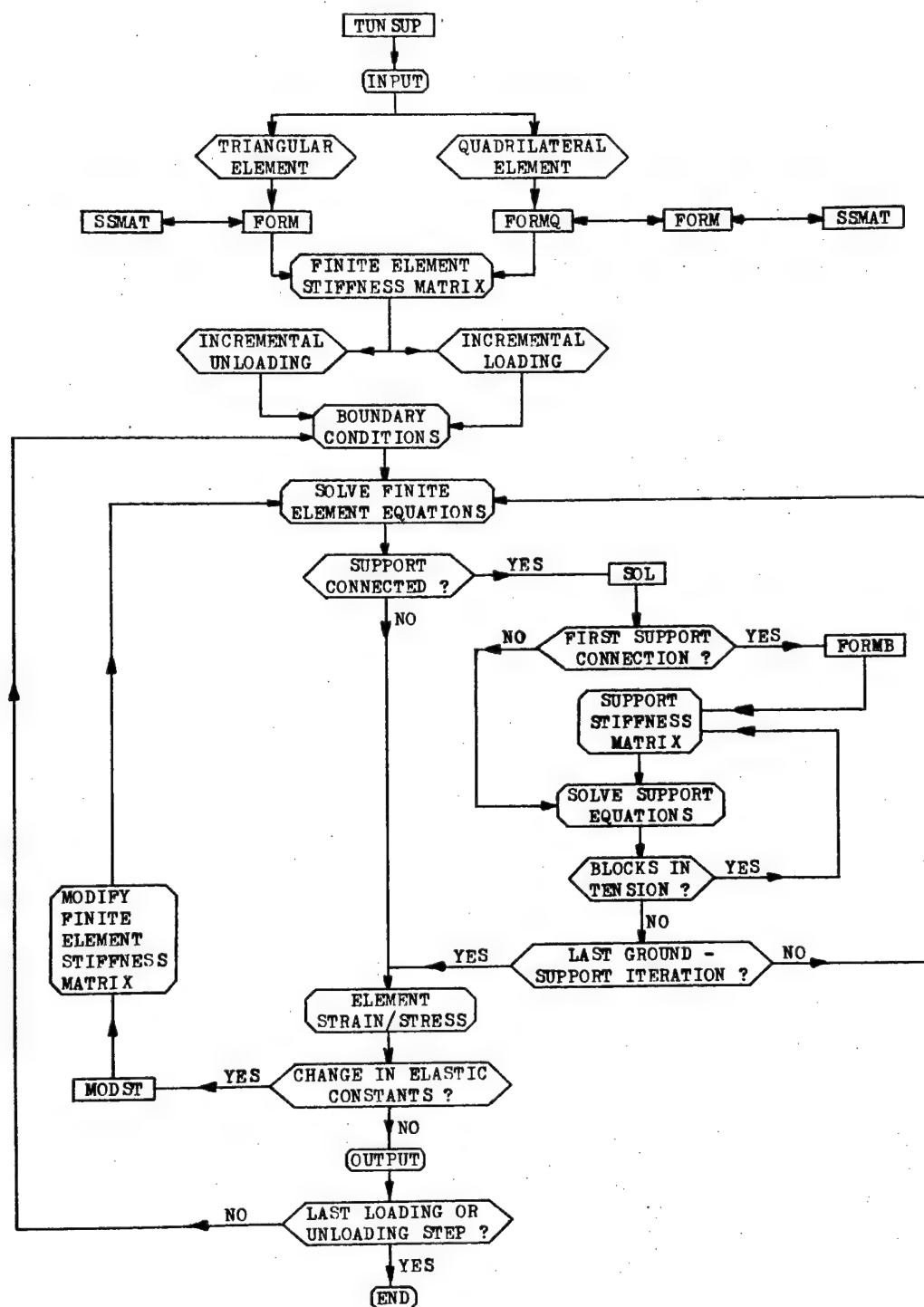


Figure C.1. Simplified Flow Chart For the Principal Operations of Program TUNSUP.

sequence of the calculations and handles the input as well as most of the output. The principal steps in the program are:

1. Input, generation of interpolated elements and nodal points.
2. Calculation of nodal point forces due to gravity and boundary pressures.
3. Stiffness matrix assembly; element stiffness calculation in FORM and FORMQ, including rotations for inclined boundary conditions, with stress-strain relation matrix from SSMAT.
4. Initialization of the boundary conditions for stepwise loading or unloading. Skipped for one-step problems.
5. Solution of finite element equilibrium by successive over relaxation.
6. If no support will be connected, control goes to step 12.
7. If the support will be connected in the next unloading step, the total tunnel periphery displacements up to that step are stored.
8. The support stiffness matrix is assembled in subroutine SOL during the first support connection, with beam stiffnesses calculated in FORMB.
9. The tunnel periphery displacements that

occur after support installation are imposed on the support. The support stiffness equations are solved in subroutine SOL by Gaussian elimination (for a very narrowly banded matrix--no nodal point can be adjacent to more than three nodal points).

10. Tensioned blocking springs are eliminated and step 9 is repeated for the new support geometry.

11. If the maximum number of iterations between ground and support is not exceeded the program returns to step 5, with boundary conditions modified by the support reactions.

12. Stresses and strains are calculated in each element.

13. Stresses and strains are compared with the rock failure model input. New element stiffnesses, when needed, are calculated in subroutine MODST, and control returns to step 5, with unchanged boundary conditions but with a modified stiffness matrix.

14. When no more changes occur, or when the imposed maximum number of iterations is exceeded, an output of nodal point and element results is prepared.

15. If loading or unloading is not yet terminated the boundary conditions are incremented

C-18

or decremented for the next step and computations  
continue at 5.

```

PROGRAM TUNSUP(INPUT,OUTPUT,PUNCH,TAPE1,TAPE2)
COMMON NPI(310),NPJ(310),NPK(310),R(320),Z(320),KOD(320),NAP(320),
1      NP(320,11),S11(320,10),S12(320,10),S21(320,10),S22(320,10),
2      C(3,3),EP,VP,RI,RJ,RK,ZI,ZJ,ZK,S(8,8),MAT(310),NPL(310),ES,
3      VS,CODPL,RL,ZL,BDISC(320)
4      ,NPRE(32),UB(32),WB(32),ROT(32),TEM(32,3),NPIB(32),NPJB(32),
5      XB(32),YB(32),EH(32),AB(32),XIB(32),PHIB(32),NUMBEAM,
6      NUMJOI,SNN(6,6),NPBFEM(32),SUPST
DIMENSION EM(40),ERE(40),SM(40),SR(40),EM1(40),ER1(40),PHIR(40),
1      PHII(40),PHIM(40)
DIMENSION NUME(310),NPNUM(320),FORR(320),FORZ(320),U(320),W(320),
1      LM(4),H(3,8),DIS(8),EPS(3)
DIMENSION SIGR(310),SIG1(310),SIG2(310),SIGT(310),EPM(310),EPMT(31
10),AN(320),E1T(310),E2T(310),E3T(310),G1T(310),V21T(310),V31T(310
2      ,V32T(310),PSIT(310),E1(310),E2(310),E3(310),G1(310),V21(310
3      ,V31(310),V32(310),PSI(310)
DIMENSION FORREX(32),FORZEX(32),UPM(32),WPM(32),FORRB(32),FORZB(32)
100 READ 6,TAPECOD
IF(TAPECOD) 106,104,106
104 READ 1,T1,T2,T3,T4,T5,T6,T7,T8
READ 3,NUMEL,NUMNP,NCYCM,NUMIN,INBEG,ICOOR,CODPL,CHECK,DENS,NUMBEA
1M,NUMJOI,NUMSUP,SETS,ITSUP
IF(NUMEL) 230,230,231
231 READ 4,TOLER,ER,EP,ES,VR,VP,VS,BETA
PRINT 2
PRINT 1,T1,T2,T3,T4,T5,T6,T7,T8
PRINT 17,TAPECOD
PRINT 5,NUMEL,NUMNP,BETA,TOLER,NCYCM,NUMIN,INBEG,NUMBEAM,NUMJOI,SE
1TS,NUMSUP,ITSUP
PRINT 14,ER,VR,EP,VP,ES,VS,DENS
C
PRINT 7,ICOOR,CODPL
PRINT 29
PRINT 2
N = 0
DO 310 K = 1,NUMEL
N = N + 1
READ 10,NUME(N),NPI(N),NPJ(N),NPK(N),NPL(N),MAT(N),E1T(N),E2T(N)
NPC = N - 1
IF(NUMEL-1) 370,370,371
371 NDIF = NUME(N) - NUME(NPC)
NNDIF = NDIF - 1
IF(NDIF - 1) 320,330,340
340 L = NUME(N)
NUME(L) = L
NPI(L) = NPI(N)
NPJ(L) = NPJ(N)
NPK(L) = NPK(N)
NPL(L) = NPL(N)
MAT(L) = MAT(N)
E1T(L) = E1T(N)
E2T(L) = E2T(N)
DO 350 KK = 1,NNDIF
NUME(N) = NUME(NPC) + 1
NPI(N) = NPI(NPC) + 1
NPJ(N) = NPJ(NPC) + 1
NPK(N) = NPK(NPC) + 1

```

```

150 IF(NPL(NPC)) 140,150,140
150 NPL(N) = NPL(NPC)
      GO TO 160
140 NPL(N) = NPL(NPC) + 1
160 CONTINUE
      MAT(N) = MAT(NPC)
      E1T(N) = E1T(NPC)
      E2T(N) = E2T(NPC)
      N = N + 1
350 NPC = NPC + 1
330 IF(N = NUMEL) 310,370,320
310 CONTINUE
370 M = 1
      READ 11,NPNUM(M),R(M),Z(M),FORR(M),FORZ(M),U(M),W(M),BDISC(M)
      DO 500 K = 1,NUMNP
      M = M + 1
      READ 11,NPNUM(M),R(M),Z(M),FORR(M),FORZ(M),U(M),W(M),BDISC(M)
      MPC = M - 1
      MDIF = NPNUM(M) - NPNUM(MPC)
      IF(MDIF = 1) 520,530,540
540 RDIF = R(M) - R(MPC)
      ZDIF = Z(M) - Z(MPC)
      XDIF = MDIF
      DELR = 0.
      IF(ICOOR) 1310,1310,1320
1310 DELR = RDIF/XDIF
1320 DELZ = ZDIF/XDIF
      DO 550 KK = 1,MDIF
      NPNUM(M) = NPNUM(MPC) + 1
      FORR(M) = FORR(MPC)
      FORZ(M) = FORZ(MPC)
      U(M) = U(MPC)
      W(M) = W(MPC)
      R(M) = DELR + R(MPC)
      Z(M) = DELZ + Z(MPC)
      BDISC(M) = BDISC(MPC)
      M = M + 1
550 MPC = MPC + 1
      M = M + 1
530 IF(M=NUMNP) 500,560,520
500 CONTINUE
560 PRINT 13
      PRINT 28,(NPNUM(M),R(M),Z(M),FORR(M),FORZ(M),U(M),W(M),BDISC(M),
1      M = 1,NUMNP)
      IF(ICOOR) 175,174,175
175 DO 176 M=1,NUMNP
      ANGLE = 0.0174532925*Z(M)
      AN(M) = ANGLE
      ANCOS = COS(ANGLE)
      ANSIN = SIN(ANGLE)
      X = R(M)*ANCOS
      Z(M) = R(M)*ANSIN
      R(M) = X
      UX = U(M)*ANCOS - W(M)*ANSIN
      W(M) = U(M)*ANSIN + W(M)*ANCOS
      U(M) = UX
      FX = FORR(M)*ANCOS - FORZ(M)*ANSIN
      FORZ(M) = FORR(M)*ANSIN + FORZ(M)*ANCOS

```

```

176 FORR(M) = RX
174 CONTINUE
175 IF (NUMBEAM) 2000,2080,2070
2070 PRINT 55
DO 2050 N = 1,NUMBEAM
READ 2011,K,NPIB(K),NPJB(K),FB(K),AB(K),XIB(K),PHIB(K)
2011 FORMAT(3I4,4E12.4)
IF (XIB(K)) 2020,5000,2020
2020 PRINT 2010,K,NPIB(K),NPJB(K),EB(K),AB(K),XIB(K),PHIB(K)
2010 FORMAT(I8,11H BEAM ,I12,I16,E14.5,2E12.5,E20.5)
GO TO 2050
5000 PRINT 2060,K,NPIB(K),NPJB(K),ER(K),AR(K)
2060 FORMAT(I8,11H SPRING,I12,I16,E14.5,2E12.5,E20.5)
2050 CONTINUE
2080 IF (NUMJOI) 2090,166,2100
2100 PRINT 56
DO 2030 N=1,NUMJOI
READ 63,XB(N),YB(N),UB(N),WB(N),ROT(N),NPBFEM(N),NPRE(N)
PRINT 64,N,XB(N),YB(N),UB(N),WB(N),ROT(N),NPBFEM(N),NPRE(N)
2030 CONTINUE
166 READ 40,NFE,NCON,NFEMX,ALPHA,SIZC,SIZE,GAMMA,LOAD,INITUNL,LASTUNL
IF (NCON) 240,260,200
200 READ 43,(EM(N),ERE(N),SM(N),SR(N),N=1,NCON)
READ 44,(EM1(N),ER1(N),PHJR(N),PHII(N),PHIM(N),N=1,NCON)
PRINT 16,NCON,SIZC,SIZE,NFEMX
PRINT 83,NFE,ALPHA,GAMMA
252 PRINT 46
PRINT 45,(EM(N),ERE(N),SM(N),SR(N),EM1(N),ER1(N),PHJR(N),PHII(N),
1 PHIM(N),N=1,NCON)
GO TO 261
261 PRINT 15
262 PRINT 19,LOAD,INITUNL,LASTUNL
DO 300 N = 1,NUMEL
EPM(N)=0
EPMT(N) = 0.
E1(N)=ER
E2(N)=ER
E3(N) = ER
G1(N) = ER/(2.0*(1.+VR))
V21(N) = VR
V31(N) = VR
V32(N) = VR
300 PSI(N)=0.0
DO 410 L = 1,NUMNP
DO 400 M = 1,10
S11(L,M)=0.0
S12(L,M)=0.0
S21(L,M)=0.0
S22(L,M)=0.0
400 NP(L,M)=0
NP(L,11) = 0
410 NP(L,1) = L
C
DO 1650 I = INITUNL,LASTUNL
FORREX(I) = 0.
1650 FORZEX(I) = 0.
IF (SETS) 1710,1720,1730
1720 SETS = 1.

```

```

PRINT 49
1730 CONTINUE
PRINT 2
PRINT 12
ARTOT = 0.0
ARCHECK = 0.0
DO 700 N = 1,NUMEL
  I = NPI(N)
  J = NPJ(N)
  K = NPK(N)
  L = NPL(N)
  RI = R(I)
  RJ = R(J)
  RK = R(K)
  RL = R(L)
  ZI = Z(I)
  ZJ = Z(J)
  ZK = Z(K)
  ZL = Z(L)
  IF(E2T(N)) 1605,1620,1605
1605 IF(L) 1600,1600,1610
1600 RD = RK - RI
  ZD = ZI - ZK
  HS = (E2T(N)*ZD/2. - E1T(N)*RD/2.)*SETS
  VS = (E2T(N)*RD/2. + E1T(N)*ZD/2.)*SETS
  FORR(I) = FORR(I) + HS
  FORZ(I) = FORZ(I) + VS
  FORR(K) = FORR(K) + HS
  FORZ(K) = FORZ(K) + VS
  IF(I.LT.INITUNL.OR.I.GT.LASTUNL) GO TO 1630
  FORREX(I) = FORREX(I) + HS
  FORZEX(I) = FORZEX(I) + VS
1630 IF(K.LT.INITUNL.OR.K.GT.LASTUNL) GO TO 1620
  FORREX(K) = FORREX(K) + HS
  FORZEX(K) = FORZEX(K) + VS
  GO TO 1620
1610 RD = RJ - RK
  ZD = ZK - ZJ
  VS = (E2T(N)*RD/2. + E1T(N)*ZD/2.)*SETS
  HS = (E2T(N)*ZD/2. - E1T(N)*RD/2.)*SETS
  FORR(J) = FORR(J) + HS
  FORZ(J) = FORZ(J) + VS
  FORR(K) = FORR(K) + HS
  FORZ(K) = FORZ(K) + VS
  IF(J.LT.INITUNL.OR.J.GT.LASTUNL) GO TO 1640
  FORREX(J) = FORREX(J) + HS
  FORZEX(J) = FORZEX(J) + VS
1640 IF(K.LT.INITUNL.OR.K.GT.LASTUNL) GO TO 1620
  FORREX(K) = FORREX(K) + HS
  FORZEX(K) = FORZEX(K) + VS
1620 CONTINUE
  AREA = 0.5*((RJ-RI)*(ZK-ZI)-(RK-RI)*(ZJ-ZI))
  AR = AREA
  IF(NPL(N)) 120,130,120
130  RC = (PI+RJ+RK)/3.
  ZC = (ZI+ZJ+ZK)/3.
  PRINT 77,NUME(N),NPI(N),NPJ(N),NPK(N),MAT(F),RC,ZC,AREA,E1T(N),
  1 E2T(N)

```

```

CALL FORM(N,AREA,E1,E2,E3,G1,V21,V31,V32,PS1)
ARTOT = ARTOT + AREA
IF(DENS) 403,403,111
111 WEI = - DENS*AREA/3.*SETS
FORZ(I) = FORZ(I) + WEI
FORZ(J) = FORZ(J) + WEI
FORZ(K) = FORZ(K) + WEI
GO TO 403
120 CALL FORMQ(N,AREA,E1,E2,E3,G1,V21,V31,V32,PS1)
RC = (R(I) + R(J) + R(K) + R(L))/4.
ZC = (Z(I) + Z(J) + Z(K) + Z(L))/4.
PRINT 27,NUME(N),NPI(N),NPJ(N),NPK(N),NPL(N),MAT(N),RC,ZC,AREA,
1 E1T(N),E2T(N)
ARTOT = ARTOT + AREA
IF(DENS) 403,403,110
110 CONTINUE
WEI = - DENS*AR/6.*SETS
FORZ(I) = FORZ(I) + WEI
FORZ(J) = FORZ(J) + WEI
FORZ(K) = FORZ(K) + WEI
AR = AREA - AR
WEI = - DENS*AR/6.*SETS
FORZ(I) = FORZ(I) + WEI
FORZ(K) = FORZ(K) + WEI
FORZ(L) = FORZ(L) + WEI
AR = 0.5*((R(J)-R(I))*(Z(L)-Z(I)) - (R(L)-R(I))*(Z(J) - Z(I)))
WET = - DENS*AR/6.*SETS
FORZ(I) = FORZ(I) + WET
FORZ(J) = FORZ(J) + WET
FORZ(L) = FORZ(L) + WET
AR = AREA - AR
WEI = - DENS*AR/6.*SETS
FORZ(J) = FORZ(J) + WET
FORZ(K) = FORZ(K) + WET
FORZ(L) = FORZ(L) + WET
403 IF(AREA) 1300,1300,420
1300 PRINT 21,N
ARCHECK = - 1.
420 LM(1) = NPI(N)
LM(2) = NPJ(N)
LM(3) = NPK(N)
MM = 3
IF(NPL(N)) 450,460,450
450 LM(4) = NPL(N)
MM = 4
460 DO 700 L = 1,MM
LX = LM(L)
DO 700 M = 1,MM
MX = 0
660 MX = MX + 1
IF(NP(LX,MX)-LM(M)) 670,680,670
670 IF(NP(LX,MX)) 660,680,660
680 NP(LX,MX)=LM(M)
IF(MX-10) 690,690,1400
690 S11(LX,MX)=S11(LX,MX)+S(2*L-1,2*M-1)*SETS
S12(LX,MX)=S12(LX,MX) +S(2*L-1,2*M)*SETS
S21(LX,MX)=S21(LX,MX)+S(2*L,2*M-1)*SETS
700 S22(LX,MX)=S22(LX,MX)+S(2*L,2*M)*SETS

```

```

PRINT 31,ARTOT
IF(ARCHECK) 100,106,106
106 IF(TAPECOD) 4228,4229,4227
4227 WRITE(1,1) T1,T2,T3,T4,T5,T6,T7,T8
  WRITE(1,3) NUMEL,NUMNP,NCYCM,NUMIN,INBEG,POOR,CODPL,CHECK,DENS,
  1      NUMBEAM,NUMJOI,NUMSUP,SETS,ITSUP
  WRITE(1,4) TOLER,ER,EP,ES,VR,VP,VS,RETA
  WRITE(1,10) (NUME(N),NPI(N),NPJ(N),NPK(N),NPL(N),MAT(N),EIT(N),EPT
  1      (N),N=1,NUMEL)
  WRITE(1,11) (NPNUM(M),R(M),Z(M),FORR(M),FORZ(M),U(M),W(M),RDISC(M)
  1      ,M=1,NUMNP)
  IF(NUMBEAM) 2000,2200,2210
221 DO 2220 N = 1,NUMBEAM
2220 WRITE(1,2011) N,NPIB(N),NPJB(N),EB(N),AH(N),XIB(N),PHIB(N)
  WRITE(1,63) (XB(N),YB(N),UB(N),WB(N),ROT(N),NPBFEM(N),NPRE(N),
  1      N = 1,NUMJOI)
2200 WRITE(1,40) NFE,NCON,NFEMX,ALPHA,SIZC,SIZE,GAMMA,LOAD,INITUNL, LAST
  1UNL
  IF(NCON) 4230,4229,4230
4230 WRITE(1,43) (EM(N),ERE(N),SM(N),SR(N),N=1,NCON)
  WRITE(1,44) (EM1(N),ER1(N),PHIB(N),PHII(N),PHIM(N),N=1,NCON)
  GO TO 4229
4228 READ (2,1) T1,T2,T3,T4,T5,T6,T7,T8
  READ(2,3) NUMEL,NUMNP,NCYCM,NUMIN,INBEG,POOR,CODPL,CHECK,DENS,
  1      NUMBEAM,NUMJOI,NUMSUP,SETS,ITSUP
  READ (2,4) TOLER,ER,EP,ES,VR,VP,VS,RETA
  READ(2,10) (NUME(N),NPI(N),NPJ(N),NPK(N),NPL(N),MAT(N),EIT(N),EPT
  1      (N),N=1,NUMEL)
  READ(2,11) (NPNUM(M),R(M),Z(M),FORR(M),FORZ(M),U(M),W(M),RDISC(M)
  1      ,M=1,NUMNP)
  IF(NUMBEAM) 2000,2300,2310
2310 DO 2320 N = 1,NUMBEAM
2320 READ(2,2011) K,NPIB(N),NPJB(N),EB(N),AH(N),XIB(N),PHIB(N)
  READ(2,63) (XB(N),YB(N),UB(N),WB(N),ROT(N),NPBFEM(N),NPRE(N),
  1      N = 1,NUMJOI)
2300 READ(2,40) NFE,NCON,NFEMX,ALPHA,SIZC,SIZE,GAMMA,LOAD,INITUNL, LAST
  1UNL
  IF(NCON) 4231,4232,4231
4231 READ(2,43) (EM(N),ERE(N),SM(N),SR(N),N=1,NCON)
  READ(2,44) (EM1(N),ER1(N),PHIB(N),PHII(N),PHIM(N),N=1,NCON)
4232 IF(TAPECOD + 2) 4227,4229,4229
4229 IF(CHECK) 406,407,406
406 PRINT 411
  DO 408 M = 1,NUMNP
408 PRINT 409,M,(NP(M,MX),MX=1,11)
407 DO 720 M = 1,NUMNP
  MX = 1
  IF(BDISC(M)) 710,710,8200
8200 IF(BDISC(M) - 360.) 8201,710,8202
8202 IF(BDISC(M) - 720.) 710,8201,8201
8201 ALP = BDISC(M)/57.29577951
  CA = COS(ALP)
  SA = SIN(ALP)
  FO = FORR(M)*CA + FORZ(M)*SA
  FORZ(M) = -FORR(M)*SA + FORZ(M)*CA
  FORR(M) = FO
  IF(M.LT.INITUNL.OR.M.GT.LASTUNL) GO TO 710
  FO = FORREX(M)*CA + FORZEX(M)*SA

```

```

FORZEX(M) = - FORREX(M)*SA + FORZEX(M)*CA
FORREX(M) = FO
710 MX=MX+1
IF(NP(M,MX)) 720,720,710
720 NAP(M)=MX-1
SUPST = 0,
FINBEG = INBEG
FNUMIN = NUMIN
DO 8000 INNUM = INBEG,NUMIN
ITERS = 0
FINNUM = INNUM
PRINT 2
IF(LOAD) 949,950,951
951 FAC = FINBEG/FNUMIN
IF(INNUM = INBEG) 931,910,931
931 FAC = FINNUM/(FINNUM - 1.)
910 DO 940 M = 1,NUMNP
U(M) = FAC*U(M)
W(M) = FAC*W(M)
FORR(M) = FAC*FORR(M)
940 FORZ(M) = FAC*FORZ(M)
PRINT 81,INNUM
GO TO 950
949 IF(NUMIN = 1) 950,950,936
936 FAC = 1. - 1. / (FNUMIN - FINNUM + 1.)
IF(INNUM = INBEG) 933,933,932
933 FAC = 1. - (FINBEG - 1.) / (FNUMIN - 1.)
932 DO 920 M = INITUNL, LASTUNL
FORZ(M) = FORZ(M) - FORZEX(M)
FORR(M) = FORR(M) - FORREX(M)
FORREX(M) = FAC*FORREX(M)
FORZEX(M) = FAC*FORZEX(M)
FORR(M) = FORR(M) + FORREX(M)
920 FORZ(M) = FORZ(M) + FORZEX(M)
PRINT 82,INNUM
IF(INNUM = NUMSUP) 950,1800,1810
1800 DO 1820 NB = 1,NUMJ0I
DO 1821 M = 1,3
1821 TEM(NB,M) = 0.
IF(NPBFEM(NB)) 1820,1820,1830
1830 NN = NPBFEM(NB)
IF(BDISC(NN)) 1831,1831,1832
1832 ALP = BDISC(NN) / 57.29577951
CA = COS(ALP)
SA = SIN(ALP)
UPM(NB) = U(NN)*CA - W(NN)*SA
WPM(NB) = U(NN)*SA + W(NN)*CA
GO TO 1833
1831 UPM(NB) = U(NN)
WPM(NB) = W(NN)
1833 FORRB(NB) = .
FORZB(NB) = 0.
1820 CONTINUE
GO TO 950
1810 DO 1840 NB = 1,NUMJ0I
IF(NPBFEM(NB)) 1840,1840,1850
1850 NN = NPBFEM(NB)
IF(BDISC(NN)) 1851,1851,1852

```

```

1852 ALP = BDISC(NN)/57.29577951
  CA = COS(ALP)
  SA = SIN(ALP)
  UB(NB) = U(NN)*CA - W(NN)*SA = UPM(NB)
  WB(NB) = U(NN)*SA + W(NN)*CA = WPM(NB)
  GO TO 1853
1851 UB(NB) = U(NN) = UPM(NB)
  WB(NB) = W(NN) = WPM(NB)
1853 NPRE(NB) = 3
1840 CONTINUE
  CALL SOL
  IF(SUPST) 100,1915,1915
1915 DO 1860 NR = 1,NUMJOI
  IF(.NPFEM(NB)) 1860,1860,1870
1870 NN = NPFEM(NR)
  IF(BDISC(NN)) 1873,1873,1875
1875 ALP = BDISC(NN)/57.29577951
  CA = COS(ALP)
  SA = SIN(ALP)
  TEMPOR = TEM(NB,1)*CA + TEM(NB,2)*SA
  TEM(NB,2) = -TEM(NB,1)*SA + TEM(NB,2)*CA
  TEM(NB,1) = TEMPOR
1873 FORR(NN) = FORR(NN) - TEM(NB,1) + FORRA(NB)
  FORZ(NN) = FORZ(NN) - TEM(NB,2) + FORZA(NB)
1874 FORRB(NB) = TEM(NB,1)
  FORZB(NB) = TEM(NB,2)
1860 CONTINUE
  950 KOUNT = 0
  960 NCYC = 0
C
  TOTEN = 0.
  TOTW = 0.
  TOTSE = 0.
  730 SUM = 0.0
  NCYC = NCYC +1
  DO 860 M = 1,NUMNP
    NUM = NAP(M)
    TEMPU = FORR(M)
    TEMPW = FORZ(M)
C
  IF(BDISC(M)) 741,790,770
  741 IF(BDISC(M) + 2.) 760,770,860
  760 DU = 0.0
  GO TO 830
  770 DW = 0.0
  IF(BDISC(M) = 360.) 810,812,812
  812 IF(BDISC(M) = 720.) 860,760,760
C
  790 DO 800 L = 1,NUM
    N = NP(M,L)
    TEMPUE=TEMPU-S11(M,L)*U(N)-S12(M,L)*W(N)
    800 TEMPW=TEMPW-S21(M,L)*U(N)-S22(M,L)*W(N)
    DU = TEMPU/S11(M,1)
    DW = TEMPW/S22(M,1)
    GO TO 850
C
  810 DO 820 L = 1,NUM

```

```

N = NP(M,L)
820 TEMP0=TEMP0-S11(M,L)*U(N)-S12(M,L)*W(N)
DU = TEMP0/S11(M,1)
GO TO 850
C
830 DO 840 L = 1,NUM
N = NP(M,L)
840 TEMPW=TEMPW-S21(M,L)*U(N)-S22(M,L)*W(N)
DW = TEMPW/S22(M,1)
C
850 U(M)=U(M)+BETA*DU
W(M)=W(M)+BETA*DW
851 SUM=SUM+ABS(DU)+ABS(DW)
C
860 CONTINUE
C
IF(NCYC = 1) 862,862,864
862 SUMIN = SUM
864 CONTINUE
C
IF(SUM-TOLER)1010,1010,1000
1000 IF(NCYCM = NCYC) 1010,1010,730
C
1010 PRINT 18,SUMIN,NCYC,SUM
IF(INNUM = NUMSUP) 1880,1890,1K90
1890 IF(ITER = ITSUP) 1910,1880,1880
1910 ITER = ITER + 1
PRINT 88,ITER
GO TO 1810
1880 CONTINUE
C
WRITE(1,18) SUMIN,NCYC,SUM
DO 8300 M = 1,NUMNP
IF(BDISC(M)) 8300,8300,8310
8310 ALP = BDISC(M)/57.29577951
CA = COS(ALP)
SA = SIN(ALP)
U0 = U(M)*CA - W(M)*SA
W(M) = U(M)*SA + W(M)*CA
U(M) = U0
8300 CONTINUE
DO 7060 N = 1,NUMEL
I = NPI(N)
J = NPJ(N)
K = NPK(N)
RI = R(I)
RJ = R(J)
RK = R(K)
ZI = Z(I)
ZJ = Z(J)
ZK = Z(K)
C
DO 1030 L = 1,3
DO 1030 M = 1,8
S(L,M)=0.0
1030 B(L,M)=0.0

```

```

C
DIS(1)=U(I)
DIS(2) = W(I)
DIS(3) = U(J)
DIS(4) = W(J)
DIS(5)=U(K)
DIS(6)=W(K)
IF(NPL(N)) 1031,1032,1031

C
1032 DEL = (RJ-RI)*(ZK-ZI) - (RK-RI)*(ZJ-ZI)
DELT = DEL
S(1,1) = ZJ - ZK
S(1,3) = ZK - ZI
S(1,5) = ZI - ZJ
S(2,2) = RK - RJ
S(2,4) = RI - RK
S(2,6) = RJ - RI
S(3,1) = S(2,2)
S(3,2) = S(1,1)
S(3,3) = S(2,4)
S(3,4) = S(1,3)
S(3,5) = S(2,6)
S(3,6) = S(1,5)

C
DO 1050 L = 1,3
EPS(L) = 0.0
DO 1050 M = 1,6
1050 EPS(L) = EPS(L) - S(L,M)*DIS(M)

C
GO TO 1033
1031 L = NPL(N)
RL = R(L)
ZL = Z(L)
UC = (U(I)+U(J)+U(K)+U(L))/4.
WC = (W(I)+W(J)+W(K)+W(L))/4.
RC = (RI+RJ+RK+RL)/4.
ZC = (ZI+ZJ+ZK+ZL)/4.
DELT = 0.
DEL = (RJ-RI)*(ZC-ZI) - (RC-RI)*(ZJ-ZI)
DELT = DELT + DEL
S(1,1) = ZJ - ZC
S(1,3) = ZC - ZI
S(1,5) = ZI - ZJ
S(2,2) = RC - RJ
S(2,4) = RI - RC
S(2,6) = RJ - RI
S(3,1) = S(2,2)
S(3,2) = S(1,1)
S(3,3) = S(2,4)
S(3,4) = S(1,3)
S(3,5) = S(2,6)
S(3,6) = S(1,5)
DIS(5) = UC
DIS(6) = WC
DO 1051 ML = 1,3
EPS(ML) = 0.0
DO 1051 M = 1,6
1051 EPS(ML) = EPS(ML) - S(ML,M)*DIS(M)

```

```

DEL = (RK-RJ)*(ZC-ZJ) - (RC-RJ)*(ZK-ZJ)
DELT = DELT + DEL
S(1,1) = ZK - ZC
S(1,3) = ZC - ZJ
S(1,5) = ZJ - ZK
S(2,2) = RC - RK
S(2,4) = RJ - RC
S(2,6) = RK - RJ
S(3,1) = S(2,2)
S(3,2) = S(1,1)
S(3,3) = S(2,4)
S(3,4) = S(1,3)
S(3,5) = S(2,6)
S(3,6) = S(1,5)
DIS(1) = U(J)
DIS(2) = W(J)
DIS(3) = U(K)
DIS(4) = W(K)
DO 1052 ML = 1,3
DO 1052 M = 1,6
1052 EPS(ML) = EPS(ML) - S(ML,M)*DIS(M)
DEL = (RL-RK)*(ZC-ZK) - (RC-RK)*(ZL-ZK)
DELT = DELT + DEL
S(1,1) = ZL - ZC
S(1,3) = ZC - ZK
S(1,5) = ZK - ZL
S(2,2) = RC - RL
S(2,4) = RK - RC
S(2,6) = RL - RK
S(3,1) = S(2,2)
S(3,2) = S(1,1)
S(3,3) = S(2,4)
S(3,4) = S(1,3)
S(3,5) = S(2,6)
S(3,6) = S(1,5)
DIS(1) = U(K)
DIS(2) = W(K)
DIS(3) = U(L)
DIS(4) = W(L)
DO 1053 ML = 1,3
DO 1053 M = 1,6
1053 EPS(ML) = EPS(ML) - S(ML,M)*DIS(M)
DEL = (RI-RL)*(ZC-ZL) - (RC-RL)*(ZI-ZL)
DELT = DELT + DEL
S(1,1) = ZI - ZC
S(1,3) = ZC - ZL
S(1,5) = ZL - ZI
S(2,2) = RC - RI
S(2,4) = RL - RC
S(2,6) = RI - RL
S(3,1) = S(2,2)
S(3,2) = S(1,1)
S(3,3) = S(2,4)
S(3,4) = S(1,3)
S(3,5) = S(2,6)
S(3,6) = S(1,5)
DIS(1) = U(L)
DIS(2) = W(L)

```

```

DIS(3) = U(I)
DIS(4) = W(I)
DO 1054 ML = 1,3
DO 1054 M = 1,6
1054 EPS(ML) = EPS(ML) - S(ML,M)*DIS(M)
L = NPL(N)
DIS(7) = U(L)
DIS(8) = W(L)
1033 CONTINUE
DO 1055 M = 1,3
1055 EPS(M) = EPS(M)/DELT

C
      DELT = DELT/2.

C
      CALL SSMAT(N,E1,E2,E3,G1,V21,V31,V32,PSI)

C
      SIGXX = C(1,1)*EPS(1)+C(1,2)*EPS(2)+C(1,3)*EPS(3)
      SIGYY = C(2,1)*EPS(1)+C(2,2)*EPS(2)+C(2,3)*EPS(3)
      TAUXY = C(3,1)*EPS(1) + C(3,2)*EPS(2) + C(3,3)*EPS(3)
      TOTSE = TOTSE + DELT*(SIGXX*EPS(1)+SIGYY*EPS(2)+TAUXY*EPS(3))/2.
      SIGR(N) = SIGYY
      CC = (SIGXX + SIGYY)/2.
      A = SQRT(((SIGYY - SIGXX)/2.)*#2 + TAUXY*#2)
      SIG1(N) = CC + A
      SIG2(N) = CC - A
      PAS = 0.
      SIGT(N) = V31(N)*SIGXX+V32(N)*SIGYY
      IF(CODPL) 8851,8852,8851
8851 SIGT(N) = 0.
8852 IF(A=.0000001) 8855,8855,8854
8854 PAS = - 28.64789*ATAN(2.*TAUXY/(SIGYY-SIGXX))
      IF(2.*SIGXX - SIG1(N) - SIG2(N)) 8850,8865,8865
8850 IF(PAS) 8855,8855,8860
8855 PAS = PAS + 90.
      GO TO 8865
8860 PAS = PAS - 90.
8865 CONTINUE

C
      IF(NCON) 240,7058,7001
7001 ANG = 3.14159253*PAS/180.
      CO2 = COS(ANG)*COS(ANG)
      SI2 = SIN(ANG)*SIN(ANG)
      SICO = SIN(ANG)*COS(ANG)
      SICO2 = SICO*#2
      EPM(N) = EPS(1)*CO2 + EPS(2)*SI2 + SICO*EPS(3)
      IF(MAT(N)) 7058,7005,7058
7005 E1T(N)=E1(N)
      E2T(N)=E2(N)
      E3T(N) = E3(N)
      G1T(N)=G1(N)
      V21T(N) = V21(N)
      V31T(N) = V31(N)
      V32T(N) = V32(N)
      PSIT(N)=PSI(N)
      IF(EPM(N)) 7058,7058,7010
7010 IF(EPM(N) - EPMT(N) - SIZE/2.) 7058,7015,7015

```

```

7015 SIT = SIG2(N)
7020 IF(SIT) 7025,7035,7035
7025 SIT=0
7030 SI = SIT/SIZC
    SCI = INT(SI + 0.5)
    I = SCI + 1.
7205 ST = EPM(N)/SIZE
    STI = INT(ST + 0.5)
7210 SC = SCI*SIZC
    STR = STI*SIZE
7030 IF(SIT - (NCON-1)*SIZC) 7055,7055,7059
7059 PRINT 78,N,I,SIT
    I = NCON
7055 CONTINUE
    STRMIN = AMIN1(EM(I),EM1(I))
    IF(STRMIN-STR) 7057,7058,7058
7057 EPMT(N) = STR
    IF(STR - EM(I)) 7100,7100,7105
7100 SZ = (E1T(N)*STR+V21T(N)*SC*(1.+V21T(N)))/(1.-V21T(N))/((1.+V21T(N))
    1)
    GO TO 7130
7105 IF(STR-ERE(I)) 7115,7120,7120
7120 SZ = SR(I)
    GO TO 7130
7115 SZ = SM(I) + (SM(I)-SR(I))*(STR-EM(I))/(EM(I)-ERE(I))
7130 IF(STR-EM1(I)) 7135,7135,7140
7135 VL = (SC*(1.-V21T(N)) - V21T(N)*SZ)*(1.+V21T(N))/E1T(N)
    GO TO 7160
7140 IF(STR-ER1(I)) 7145,7150,7150
7150 VL = PHII(I) + (PHIR(I) - PHII(I))*STR/ERT(I)
    GO TO 7160
7145 VL = PHIR(I) + (PHIM(I) - PHIR(I))*(STR-ERT(I))/(EM(I)-ER1(I))
7160 IF(STR - VL - VL/100.) 7058,7058,7161
7161 IF(NFE) 9500,7162,9000
7162 V21(N) = (STR*SC - VL*SZ)/(SZ+SC)/(STR-VL)
    V31(N) = V21(N)
    V32(N) = V21(N)
    E1(N) = (1.+V21(N))*((1.-V21(N))*SZ - V21(N)*SC)/STR
    E2(N) = E1(1)
    E3(N) = E1(2)
    GO TO 7200

```

C            CALCULATION OF NON-ISOTROPIC PSEUDO-ELASTIC CONSTANTS  
C            SEE APPENDIX B

THIS SECTION IS INCOMPLETE AND NEEDS DEBUGGING  
IT IS NOT IMPLIED THAT THE OTHERS DO NOT

```

9540 CONTINUE
    GO TO 241
9000 IF(NFE - 5) 9100,9010,9020
9100 IF(NFE-4) 9530,9110,9000
9110 AVAR = (STR-VL)*(SC + SZ)
    BVAR = -(SC*VL + STR*(SC*ALPHA/VR - SZ))
    CVAR = VL*SZ - STR*SC*(1. - ALPHA)
    DVAR = BVAR*BVAR - 4.*AVAR*CVAR
    IF(DVAR) 243,9210,9210
9210 DVA = SQRT(DVAR)
    IF(VR*AVAR - CVAR/VR) 9220,9220,9230
9220 V21(N) = (-BVAR - DVA)/2.*AVAR

```

GO TO 9240  
 9230  $V21(N) = (-BVAR + DVA)/2. / AVAR$   
 9240  $E1(N) = (1. + V21(N)) * (-V21(N) * SC + (1. - V21(N)) * SZ) / STR$   
 $E2(N) = E1(N) / (1. + ALPHA * (V21(N) / VR - 1.))$   
 $V31(N) = V21(N) / (1. + ALPHA * (V21(N) / VR - 1.))$   
 IF(NFE-3) 9510,241,9520  
 9010 CONTINUE  
 $AVAR = -4. * ALPHA * SC * SC / ER / VR$   
 $BVAR = 2. * ALPHA * SC * SZ / ER / VR = 4. * SC * SC * (1. - ALPHA - VR) / ER$   
 1  $- 2. * SZ * STR + 2. * SC * VL$   
 $CVAR = (1. - ALPHA - VR) * 2. * SC * SZ / ER - SZ * VL$   
 IF(ALPHA) 242,7163,7164  
 7164 IF(SC) 7163,7163,7165  
 7163  $V21(N) = - CVAR / BVAR$   
 GO TO 7169  
 7165  $DVAR = BVAR * BVAR = 4. * AVAR * CVAR$   
 IF(DVAR) 243,7166,7167  
 7167  $DVA = SQRT(DVAR)$   
 $IF(VR * AVAR - CVAR / VR) 7166,7166,7168$   
 7168  $V21(N) = (-BVAR + DVA) / 2. / AVAR$   
 7169  $E1(N) = (SZ - 2. * SC * V21(N)) / STR$   
 $E2(N) = ER / (1. + ALPHA * (V21(N) / VR - 1.))$   
 $V31(N) = VR / (1. + ALPHA * (V21(N) / VR - 1.))$   
 IF(NFE = 6) 9510,9030,9520  
 7166  $V21(N) = (-BVAR - DVA) / 2. / AVAR$   
 GO TO 7169  
 9020 IF(NFE = 7) 9030,9010,9030  
 9030 CONTINUE  
 $V21(N) = (VL * SZ / STR + 2. * (ALPHA - 1.) * SC) / 2. / (VL * SC / STR + (ALPHA / VR$   
 1  $- 1.) * SC - SZ)$   
 $E1(N) = (SZ - 2. * V21(N) * SC) / STR$   
 $E2(N) = E1(N) / (1. + ALPHA * (V21(N) / VR - 1.))$   
 $V31(N) = V21(N) / (1. + ALPHA * (V21(N) / VR - 1.))$   
 IF(NFE = 7) 9510,9010,9520  
 9510 CONTINUE  
 $E3(N) = E1(N)$   
 $V32(N) = V21(N)$   
 GO TO 7200  
 9520 CONTINUE  
 $E3(N) = E2(N)$   
 $V32(N) = V31(N)$   
 GO TO 7200  
 9530 IF(NFE-2) 241,9531,241  
 9531  $AVAR = STR * (SC * (ALPHA * ALPHA / VR / VR - 1.) - (1. + ALPHA / VR) * SZ) + VL * (SZ * SC +$   
 1  $ALPHA * SC / VR)$   
 $BVAR = STR * (SC * 2. * ALPHA * (1. - ALPHA) / VR - (1. - ALPHA) * SZ) - VL * (ALPHA$   
 1  $* SZ / VR - (1. - ALPHA) * SC)$   
 $CVAR = STR * SC * (1. - 2. * ALPHA + ALPHA * ALPHA) - (1. - ALPHA) * SZ * VL$   
 IF(AVAR) 9540,9550,9540  
 9550  $V21(N) = - CVAR / BVAR$   
 GO TO 9240  
 9540  $DVAR = BVAR * BVAR = 4. * AVAR * CVAR$   
 IF(DVAR) 243,9580,9570  
 9570  $DVA = SQRT(DVAR)$   
 IF(CVAR / VR - AVAR \* VR) 9580,9590,9590  
 9580  $V21(N) = (-BVAR + DVA) / 2. / AVAR$   
 GO TO 9240  
 9590  $V21(N) = (-BVAR - DVA) / 2. / AVAR$

```

GO TO 9240
7200 G1(N) = 1. / (1. / E1(N) + 1. / E2(N) + 2. * V21(N) / E2(N))
7058 PS1(N) = (PAS-90.1) / 57.2957795
7060 CONTINUE
KOUNT = KOUNT + 1
DO 8330 M = 1,NUMNP
IF(BDISC(M)) 8330,8330,8340
8340 ALP = BDISC(M) / 57.29577951
CA = COS(ALP)
SA = SIN(ALP)
UN = U(M)*CA + W(M)*SA
W(N) = - U(M)*SA + W(M)*CA
U(M) = UN
8330 CONTINUE
IF(NCON) 7065,1500,7065
7065 KDFX = 0
PRINT 70,KOUNT,INNUM
PRINT 2
DO 7095 N=1,NUMEL
IF(MAT(N)) 7095,7070,7095
7070 IF(V21(N) = V21T(N) = V21T(N)/10000.) 7075,7075,7080
7075 IF(E2(N) = E2T(N) + E2T(N)/10000.) 7080,7095,7085
7080 KDFX = KDEX + 1
KOD(KDEX) = N
PRINT 61,KDEX,N,E1(N),E1T(N),E2(N),E2T(N),V21(N),V21T(N)
IF(0.92-V21(N)-2.*V31(N)*V31(N)*E2(N)/E1(N)) 7094,7095,7095
C      FOR ORTHOTROPIC FAILURE THIS CHECK SHOULD BE REPLACED BY A MORE
C      GENERAL CHECK ON POSITIVE DEFINITENESS
7094 KDFX = KDEX - 1
7085 E1(N) = E1T(N)
E2(N) = E2T(N)
E3(N) = E3T(N)
G1(N) = G1T(N)
V21(N) = V21T(N)
V31(N) = V31T(N)
V32(N) = V32T(N)
7095 CONTINUE
IF(KDEX) 1500,1500,8010
8010 CALL MODSTM(KDFX,E1,E2,E3,G1,V21,V31,V32,PSI,E1T,E2T,E3T,G1T,
V21T,V31T,V32T,PS1T)
1 IF(KOUNT = NFEMX) 960,960,1500
1500 PRINT 2
IF(IC00R) 1201,1202,1211
1202 PRINT 26
DO 1200 M = 1,NUMNP
FOR = 0
FOZ = 0
NUM = NAP(M)
TOTW = TOTW + FORR(M)*U(M) + FORZ(M)*W(M)
DO 1195 L = 1,NUM
N = NP(M,L)
TOTEN = TOTEN + S11(M,L)*U(M)*U(N) + S12(M,L)*U(M)*W(N) + S21(M,L)
1 *U(N)*W(M) + S22(M,L)*W(M)*W(N)
FOR = FOR + S11(M,L)*U(N) + S12(M,L)*W(N)
1195 FOZ = FOZ + S21(M,L)*U(N) + S22(M,L)*W(N)
IF(BDISC(M)) 8400,8400,8410
8410 ALP = BDISC(M) / 57.29577951
CA = COS(ALP)

```

```

SA = SIN(ALP)
U0 = U(M)*CA - W(M)*SA
W0 = U(M)*SA + W(M)*CA
FO = FOR*CA - FOZ*SA
FOZ = FOR*SA + FOZ*CA
PRINT 25,M,U0,W0,FO,FOZ
WRITE(1,25) M,U(M),W(M),FOR,FOZ
GO TO 1200
8400 PRINT 25,M,U(M),W(M),FOR,FOZ
WRITE(1,25) M,U0,W0,FO,FOZ
1200 CONTINUE
GO TO 8011
1201 PRINT 126
DO 1203 M = 1,NUMNP
TOTW = TOTW + FORR(M)*U(M) + FORZ(M)*W(M)
FOR = 0.
FOZ = 0.
NUM = NAP(M)
DO 1196 L = 1,NUM
N = NP(M,L)
TOTEN = TOTEN + S11(M,L)*U(M)*U(N) + S12(M,L)*U(M)*W(N) + S21(M,L)
] *U(N)*W(M) + S22(M,L)*W(M)*W(N)
FOR = FOR + S11(M,L)*U(N) + S12(M,L)*W(N)
1196 FOZ = FOZ + S21(M,L)*U(N) + S22(M,L)*W(N)
ANGLE = AN(M)
ANCOS = COS(ANGLE)
ANSIN = SIN(ANGLE)
IF(BDISC(M) .LT. 8500,8500,8510
8510 ALP = BDISC(M)/57.29577951
CA = COS(ALP)
SA = SIN(ALP)
U0 = U(M)*CA - W(M)*SA
W0 = U(M)*SA + W(M)*CA
UR = JO*ANCOS + W0*ANSIN
UT = W0*ANCOS - U0*ANSIN
FO = FOR*CA - FOZ*SA
FOZ = FOR*SA + FOZ*CA
FOR = FO
RADFOR = FO*ANCOS + FOZ*ANSIN
TANFOR = FOZ*ANCOS - FOR*ANSIN
PRINT 125,M,U0,W0,FO,FOZ,UR,UT,RADFOR,TANFOR
WRITE(1,125) M,U0,W0,FO,FOZ,UR,UT,RADFOR,TANFOR
GO TO 1203
8500 CONTINUE
UR = U(M)*ANCOS + W(M)*ANSIN
UT = W(M)*ANCOS - U(M)*ANSIN
RADFOR = FOR*ANCOS+FOZ*ANSIN
TANFOR = FOZ*ANCOS - FOR*ANSIN
PRINT 125,M,U(M)*W(M),FOR,FOZ,UR,UT,RADFOR,TANFOR
WRITE(1,125) M,U(M),W(M),FOR,FOZ,UR,UT,RADFOR,TANFOR
1203 CONTINUE
8011 CONTINUE
8320 CONTINUE
PRINT 2
PRINT 23
PRINT 32
DO 1501 N = 1,NUMEL
PAS = 57.295779513*PSI(N)+90.

```

```

IF (MAT(N)) 1057,1060,1057
1057 PRINT 24,N,SIG1(N),SIG2(N),SIGR(N),SIGT(N),PAS
      WRITE(1,24) N,SIG1(N),SIG2(N),SIGT(N),PAS
      GO TO 1501
1060 IF (NCON) 1059,1061,1059
1059 PRINT 60,N,SIG1(N),SIG2(N),SIGR(N),SIGT(N),PAS,E1(N),E2(N),E3(N),
      1 G1(N),V21(N),V31(N),V32(N)
      WRITE(1,60) N,SIG1(N),SIG2(N),SIGT(N),PAS,E1(N),E2(N),E3(N),G1(N),
      1 V21(N),V31(N),V32(N)
      GO TO 1501
1061 PRINT 30,N,SIG1(N),SIG2(N),SIGR(N),SIGT(N),PAS
      WRITE(1,30) N,SIG1(N),SIG2(N),SIGT(N),PAS
1501 CONTINUE
      TOTSE = TOTSE*SETS
      TOTEN = TOTEN/2.
      TOTW = TOTW/2.
      PRINT 33,TOTEN,TOTSE,TOTW
      WRITE(1,33) TOTEN,TOTSE,TOTW
8000 CONTINUE
C
      GO TO 100
C
1400 PRINT 22,LX,(NP(LX,M),M=2,MX)
      PRINT 2
      GO TO 100
C
1710 PRINT 50
      GO TO 100
3200 PRINT 9,N,NUME(N),NUME(NPC)
      GO TO 100
2400 PRINT 84,NCON
      GO TO 100
2410 PRINT 85,NFE
      GO TO 100
2420 PRINT 86,ALPHA
      GO TO 100
2430 PRINT 87,N
      GO TO 100
5200 PRINT 8,M,NPNUM(M),NPNUM(MPC)
      GO TO 100
2000 PRINT 2001
      GO TO 100
2090 PRINT 2091
      GO TO 100
C
1 FORMAT(8A10)
2 FORMAT(////)
3 FORMAT(6I4,2F4.0,F10.4,3I4,F8.0,I4)
4 FORMAT(4E13.6,4F7.4)
5 FORMAT(//22H NUMBER OF ELEMENTS = I5,26H NUMBER OF NODAL POINTS
      1= I5// 26H OVER-RELAXATION FACTOR = F7.3,5X+35H DISPLACEMENT UNRA
      2LANCE TOLERANCE = E10.3 // 33H MAXIMUM NUMBER OF ITERATIONS = I6
      3,5X,27H NUMBER OF LOADING STEPS = I6,5X,3I4H INITIAL LOADING STEP N
      4UMMER = I6 // 18H SUPPORT SYSTEM I10, I3H ELEMENTS I4,
      5 25H JOINTS SET SPACING = F8.2 //47H SUPPORT WILL B
      6E ACTIVATED AT UNLOADING STEP I5 , 23H AT EACH UNLOADING STEP
      7 I6, 56H ITERATIONS BETWEEN GROUND AND SUPPORT WILL BE PERFORMED/)
6 FORMAT(I5)

```

7 FORMAT(//26H COORDINATE SYSTEM CODE = 15,5X,34H CODE = 0 CARTE  
 1SIAN COORDINATES /36X,75H CODE = 1 POLAR COORDINATES, INTERPOLA  
 TION OF NODAL POINTS ALONG CIRCLES / 36X,73H CODE = -1 POLAR COO  
 3RDINATES, INTERPOLATION OF NODAL POINTS ALONG RADII //48H PLANE  
 4STRESS OR PLANE STRAIN SELECTION CODE = 14,44H IF = 0,PLANE STRATN  
 5 OTHERWISE PLANE STRESS / )  
 8 FORMAT(///\* ERROR IN NODAL POINT NUMBERING \*,3I10)  
 9 FORMAT(///\* ERROR IN ELEMENT NUMBERING\*,3I10)  
 10 FORMAT(6I4,2F12.4)  
 11 FORMAT(14,2F9.3,2F12.3,2F12.8,F10.6)  
 12 FORMAT(119H ELEMENT NODAL POINTS MATERIAL CENT  
 1ROID COORDINATES ELEMENT AREA BOUNDARY STRESSES /  
 213X,58HI J K L CODE X Y  
 3 21X\*32H PARALLEL PERPENDICULAR / )  
 13 FORMAT(110H NP X - ORD Y - ORD X-FORCE  
 1 Y-FORCE X - DISPL Y - DISPL BOUND CODE / )  
 14 FORMAT(// 26H MATERIAL CODE 0 E = F15.3,18H POISSON'S RATIO  
 1= F8.3// 26H MATERIAL CODE 1 E = F15.3,18H POISSON'S RATIO  
 2= F8.3// 26H MATERIAL CODE -1 E = F15.3,18H POISSON'S RATIO  
 3= F8.3// 21H MATERIAL DENSITY = E12.4 / )  
 15 FORMAT(//23H ELASTIC SOLUTION ONLY / )  
 16 FORMAT(//25H POCK FAILURE DEFINITION // 39H NUMBER OF CONFINING  
 1PRESSURE LEVELS = 13,32H CONFINING PRESSURE INCREMENT = F9.2 //  
 224H STRAIN INTERVAL SIZE = F10.3,10X,52H MAXIMUM NUMBER OF ITERAT  
 3IONS AT EACH LOADING STEP = 13//28H STRESS-STRAIN-VOLUME INPUT/ )  
 17 FORMAT(13H TAPE CODE = 15,4X,8H IF = -3,37H INPUT FROM TAPE 2  
 1OUTPUT ON TAPE 1 / 22X,27H IF = -1 INPUT FROM TAPE 2 /22X,25H IF  
 2 = 1 OUTPUT ON TAPE 1 )  
 18 FORMAT(//54H DISPLACEMENT UNBALANCE AFTER FIRST OVER RELAXATION =  
 1E13.6 // 7H AFTER 15,34H ITERATIONS THE DISPL. UNBALANCE = E13.6)  
 19 FORMAT(17H LOADING CODE = 13, 61H INCREMENTAL LOADING WHEN PO  
 1SITIVE, UNLOADING WHEN NEGATIVE //56X,22H ALL NP FORCES FROM NP  
 2 15.7H TO NP 15.37H WILL BE DECREMENTED DURING UNLOADING / )  
 21 FORMAT(32H ZERO OR NEGATIVE AREA, EL. NO.,I4)  
 22 FORMAT(\* MORE THAN 9 N.P. ADJACENT TO NODAL POINT \* I4 /  
 1 27H ADJACENT NODAL POINTS ARE 18I6 )  
 23 FORMAT(133H EL SIG1 SIG2 VERT STRES Z-STRES  
 1 ANGLE E1 E2 E3 G1 V21 V  
 231 V32 )  
 24 FORMAT(I4,4E12.4,F10.4)  
 25 FORMAT(I10,4E21.8)  
 26 FORMAT(\* NODAL POINT HORIZ DISPL VERT DISPL  
 1HORIZ FORCE VERT FORCE \*//)  
 27 FORMAT(I8,4I6,I12,5F16.5)  
 28 FORMAT(I4,7F15.6)  
 29 FORMAT(//117H BOUNDARY (DISPLACEMENT) CODE IN NOD POINT INPUT TAB  
 1LE WHEN = -1 VERTICAL AND HORIZONTAL DISPLACEMENT ARE IMPOSED /  
 258X,43H WHEN = -2 VERTICAL DISPLACEMENT IS IMPOSED / 58X,46H WHEN  
 3= -3 HORIZONTAL DISPLACEMENT IS IMPOSED /5X, 97H IF POSITIVE, T  
 4HE ANGLE (IN DEGREES) WITH THE X-AXIS OF THE LINE ALONG WHICH THE  
 5POINT MUST MOVE /5X,115H IF LARGER THAN 360, AN INPUT DISPLACEMEN  
 6T ALONG THIS LINE IS IMPOSED AND LISTED IN THE INPUT TABLE AS X-DI  
 7SP.(U) /5X,123H IF LARGER THAN 720. THE LISTED DISPLACEMENT IS I  
 8MPPOSED BUT THE POINT IS FREE TO MOVE PERPENDICULAR TO THE GIVEN DI  
 9RECTION / )  
 30 FORMAT(I4,4E12.4,F10.4,15H \* \* \* \* )  
 31 FORMAT(//14H TOTAL AREA = F15.5//)  
 32 FORMAT( 65H (X-Y PLANE) (X-Y PLANE)

```

1FROM X           //)
33 FORMAT(//// 85H STRAIN ENERGY CALCULATED FROM TRANSPOSED DISPLACEMENTS X STIFFNESS X DISPLACEMENTS = E15.6//68H STRAIN ENERGY CALCULATED FROM STRESS X STRAIN AT ELEMENT CENTERS = E15.6//33H WORK DONE BY BOUNDARY FORCES = E16.6, 63H MEANINGFUL ONLY WHEN NO NON-ZERO DISPLACEMENTS ARE IMPOSED //)
46 FORMAT(2I4,8X,I4,2F7.1,E13.6,F18.3,3I5)
43 FORMAT(4E16.9)
44 FORMAT(5E16.9)
45 FORMAT(9E15.7)
46 FORMAT(/135H      EM          ERE          PEAK STRESS  RESIDUAL
1  STRESS.  EM1      ERI          PHIR          PHTI
3  PHIM          /)
49 FORMAT(// 55H INPUT SET SPACING WAS ZERO HAS BEEN REPLACED BY 0
1NE //)
50 FORMAT(// 31H INPUT SET SPACING IS NEGATIVE //)
55 FORMAT(//22H SUPPORT SYSTEM INPUT//114H ELEMENT TYPE NOD
1POINT I NOD POINT J E-MODULUS AREA I-MOMENT
2 SHEAR DEF COEFFICIENT //)
56 FORMAT(//134H JOINT      X-COORD      Y-COORD      X-DISPL.
1  Y-DISPL      ROTATION      ASSOCIATED FEM NP      BOUND C
10DE          //)
60 FORMAT(I4,4E12.4,F10.4,4E12.4,3F7.4)
61 FORMAT(2I5,6E17.8)
62 FORMAT(4F10.1)
63 FORMAT(5F10.5,2I5)
64 FORMAT(I6,5E15.5,I25,I15)
70 FORMAT(///*  ITERATION*,I3,* AT LOADING STEP*, I5//)
77 FORMAT(I8,3I6,6X,I12,5F16.5)
78 FORMAT(/ 11H IN ELEMENT I4,32H THE CONFINING PRESSURE LEVEL = I5,
1, 30H AND THE CONFINING PRESSURE = E15.3,27H REPLACED BY (NCON-1)
2*SIZC / )
81 FORMAT(5X,14H LOADING STEP I5//)
82 FORMAT(5X,16H UNLOADING STEP I5//)
83 FORMAT(//37H FAILURE MODEL SELECTION CODE NFE = I5 //94H NFE =
10 ISOTROPIC FAILURE           NEGATIVE NFE ORTHOTROPIC FAILURE
2E (APPENDIX B.4 B.5) //99H POSITIVE NFE TRANSVERSE ISOTROPIC FAILURE
3LURE NFE CODE CORRESPONDS TO OPTION NUMBER IN APPENDIX B.3 //
432H FAILURE PARAMETERS ALPHA = F8.1,10H GAMMA = F8.1 /)
84 FORMAT(// 8H NCON = I6,46H NEGATIVE NUMBER OF CONFINING PRESSURE LEVELS //)
85 FORMAT(// 34H THIS FAILURE MODEL OPTION, NFE = I5,33H IS NOT INCL
1UDFD IN THIS PROGRAM //)
86 FORMAT(// 33H NEGATIVE ALPHA IS NOT PERMITTED //)
87 FORMAT(// 67H NEGATIVE SQUARE ROOT IN FAILURE CONSTANTS CALCULATIONS, ELEMENT I5 //)
88 FORMAT(//13H ITERATION I3,30H BETWEEN GROUND AND SUPPORT //)
125 FORMAT(I10,8E15.6)
126 FORMAT(* NOD POINT  HOR DISPL  VERT DISPL  HOR FORCE
1  VERT FORCE  RAD DISPL  TANG DISPL  RAD FORCE  TAN
2G FORCE  /*)
409 FORMAT(12I6)           ADJACENT NODAL POINTS *//)
411 FORMAT(////////* NP
2001 FORMAT(// 35H NEGATIVE NUMBER OF BEAM ELEMENTS //)
2091 FORMAT(// 39H NEGATIVE NUMBER OF JOINTS IN SUPPORT //)
230 CONTINUE
STOP
END

```

```

SUBROUTINE FORM(N,AREA,E1,E2,E3,G1,V21,V31,V32,PSI)
COMMON NPI(310),NPJ(310),NPK(310),R(320),Z(320),K0D(320),NAP(320),
1      NP(320,11),S11(320,10),S12(320,10),S21(320,10),S22(320,10),
2      C(3,3),EP,VP,RI,RJ,RK,ZI,ZJ,ZK,S(8,8),MAT(310),NPL(310),ES,
3      VS,CODPL,RL,ZL,BDISC(320),
4      ,NPRE(32),UB(32),WB(32),ROT(32),TEM(32,3),NPIB(32),NPJB(32),
5      XB(32),YB(32),EB(32),AB(32),XIB(32),PHIB(32),NUMBEAM,
6      NUMJOI,SNN(6,6),NPBFEM(32),SUPST
DIMENSION SS(6,6),B(6,6)

C
CALL SSMAT(N,E1,E2,E3,G1,V21,V31,V32,PSI)
DO 620 L = 1,6
DO 620 M = 1,6
S(L,M) = 0.
620 B(L,M)=0.0
B(1,1) = ZJ-ZK
B(1,3) = ZK - ZI
B(1,5) = ZI - ZJ
B(2,2) = RK - RJ
B(2,4) = RI - RK
B(2,6) = RJ - RI
B(3,1) = B(2,2)
B(3,2) = B(1,1)
B(3,3) = B(2,4)
B(3,4) = B(1,3)
B(3,5) = B(2,6)
B(3,6) = B(1,5)
DO 10 I = 1,3
DO 10 J = 1,6
SS(I,J) = 0.
DO 10 K = 1,3
10 SS(I,J) = SS(I,J) + C(I,K)*B(K,J)
DO 30 I = 1,6
DO 30 J = 1,6
DO 30 K = 1,3
30 S(I,J) = S(I,J) + B(K,I)*SS(K,J)
DO 40 I = 1,6
DO 40 J = 1,6
40 S(I,J) = S(I,J)/4./AREA
IF(NPL(N)) 712,100,712
100 I = NPI(N)
J = NPJ(N)
K = NPK(N)
IF(BDISC(I)) 110,110,120
110 IF(BDISC(J)) 130,130,120
130 IF(BDISC(K)) 712,712,120
120 DO 140 IK = 1,6
DO 140 JK = 1,6
140 B(IK,JK) = 0.
IF(BDISC(I)) 150,150,160
150 B(1,1) = 1.
B(2,2) = 1.
GO TO 170
160 ALP = BDISC(I)/57.29577951
B(1,1) = COS(ALP)
B(1,2) = - SIN(ALP)
B(2,1) = - B(1,2)

```

B(2,2) = B(1,1)  
170 IF(BDISC(J)) 180,180,190  
180 B(3,3) = 1.  
B(4,4) = 1.  
GO TO 200  
190 ALP = BDISC(J)/57.29577951  
B(3,3) = COS(ALP)  
B(3,4) = - SIN(ALP)  
B(4,3) = - B(3,4)  
B(4,4) = B(3,3)  
200 IF(BDISC(K)) 210,210,220  
210 B(5,5) = 1.  
B(6,6) = 1.  
GO TO 230  
220 ALP = BDISC(K) / 57.29577951  
B(5,5) = COS(ALP)  
B(5,6) = - SIN(ALP)  
B(6,5) = - B(5,6)  
B(6,6) = B(5,5)  
230 DO 240 I = 1,6  
DO 240 J = 1,6  
SS(I,J) = 0.  
DO 240 K = 1,6  
240 SS(I,J) = SS(I,J) + S(I,K)\*B(K,J)  
DO 260 I = 1,6  
DO 260 J = 1,6  
S(I,J) = 0.  
DO 260 K = 1,6  
260 S(I,J) = S(I,J) + B(K,I)\*SS(K,J)  
712 RETURN  
END

```

SUBROUTINE SSMAT(N,E1,E2,E3,G1,V21,V31,V32,PSI)
COMMON NPI(310),NPJ(310),NPK(310),R(320),Z(320),KOD(320),NAP(320),
1      NP(320,11),S11(320,10),S12(320,10),S21(320,10),S22(320,10),
2      C(3,3),EP,VP,RI,RJ,RK,ZI,ZJ,ZK,S(8,8),MAT(310),NPL(310),ES,
3      VS,CODPL,RL,ZL,BDISC(320),
4      ,NPRE(32),UB(32),WB(32),ROT(32),TEM(32,3),NPIB(32),NPJB(32),
5      XB(32),YB(32),EB(32),AB(32),XIB(32),PHIB(32),NUMBEAM,
6      NUMJOI,SNN(6,6),NPBFEM(32),SUPST
DIMENSION E1(310),E2(310),E3(310),G1(310),V21(310),V31(310),
1      V32(310),PSI(310),E1T(310),E2T(310),E3T(310),G1T(310),
2      V21T(310),V31T(310),V32T(310),PSIT(310)
DIMENSION D(3,3),A(3,3)
C
C
C(1,3) = 0.
C(2,3) = 0.
C(3,1) = 0.
C(3,2) = 0.
IF(CODPL) 70,80,70
80 IF(MAT(N)) 55,105
C
55 COMM = ES/(1.+VS)/(1.-2.*VS)
C(1,1) = COMM*(1.-VS)
C(1,2) = COMM*VS
C(2,1) = C(1,2)
C(2,2) = C(1,1)
C(3,3) = .5*ES/(1.+VS)
GO TO 15
5 COMM = EP/(1.+VP)/(1.-2.*VP)
C(1,1) = COMM*(1.-VP)
C(1,2) = COMM *VP
C(2,1) = C(1,2)
C(2,2) = C(1,1)
C(3,3) = .5*EP/(1.+VP)
GO TO 15
C
10 AL1 = 1./E1(N) - V31(N)*V31(N)/E3(N)
AL2 = 1./E2(N) - V32(N)*V32(N)/E3(N)
BE = V21(N)/E2(N) + V31(N)*V32(N) / E3(N)
COMM = 1. / (AL1*AL2 - BE*BE)
C(1,1) = AL2*COMM
C(1,2) = BE*COMM
C(2,1) = C(1,2)
C(2,2) = AL1*COMM
C(3,3) = G1(N)
GO TO 90
70 IF(MAT(N)) 155,110,105
155 COMM = ES/(1.-VS)/(1.+VS)
C(1,1) = COMM
C(1,2) = VS*COMM
C(2,1) = C(1,2)
C(2,2) = C(1,1)
C(3,3) = ES/(1.+VS)/2.
GO TO 15
105 COMM = EP/(1.+VP)/(1.-VP)
C(1,1) = COMM
C(1,2) = VP*COMM
C(2,1) = C(1,2)
C(2,2) = C(1,1)

```

```

C(3,3) = EP/(1.+VP)/2.
GO TO 15
110 COMM = 1. - V21(N)*V21(N)*E1(N)/E2(N)
C(1,1) = E1(N)/COMM
C(1,2) = V21(N)*C(1,1)
C(2,1) = C(1,2)
C(2,2) = E2(N)/COMM
C(3,3) = G1(N)

C
90 TEST = PSI(N)
TEST = SIN(TEST)
IF(ABS(TEST) = 0.0175)15,15,20
20 DO 25 I = 1,3
DO 25 J = 1,3
25 D(I,J)=0.0
D(1,1)=COS(PSI(N))**2
D(1,2)=SIN(PSI(N))**2
D(1,3) = -SIN(2.*PSI(N))
D(2,1)=D(1,2)
D(2,2)=D(1,1)
D(2,3) = - D(1,3)
D(3,1) = D(2,3)/2.
D(3,2) = -D(3,1)
D(3,3) = D(1,1) - D(1,2)
DO 50 I = 1,3
DO 50 J = 1,3
A(I,J) = 0.
DO 50 K = 1,3
50 A(I,J) = A(I,J) + D(I,K)*C(K,J)
DO 60 I = 1,3
DO 60 J = 1,3
C(I,J) = 0.
DO 60 K = 1,3
60 C(I,J) = C(I,J) + A(I,K)*D(J,K)
15 RETURN
END

```

```

SUBROUTINE FORMQ(N,AREA,E1,E2,E3,G1,V21,V31,V32,PSI)
COMMON NPI(310),NPJ(310),NPK(310),R(320),Z(320),KOD(320),NAP(320),
1      NP(320,11),S11(320,10),S12(320,10),S21(320,10),S22(320,10),
2      C(3,3),EP,VP,RI,RJ,RK,ZI,ZJ,ZK,S(8,8),MAT(310),NPL(310),ES,
3      VS,CODPL,RL,ZL,HDISC(320)
4      *NPRE(32),UB(32),WB(32),ROT(32),TEM(32,3),NPIB(32),NPJB(32),
5      XB(32),YB(32),EB(32),AB(32),XIB(32),PHIB(32),NUMBEAM,
6      NUMJOI,SNN(6,6),NPBFEM(32),SUPST
DIMENSION SA(2,2),SS(8,8),SN(10,10)
ARQUAD = 0.
DO 620 L = 1,10
DO 620 M = 1,10
620 SN(L,M) = 0.0
RIO = RI
ZIO = ZI
RJO = RJ
ZJO = ZJ
RKO = RK
ZKO = ZK
RL0 = RL
ZL0 = ZL
RK = (RI+RJ+RK+RL)/4.
ZK = (ZI+ZJ+ZK+ZL)/4.
AREA = 0.5*((RJ-RI)*(ZK-ZI) - (RK-RI)*(ZJ-ZI))
ARQUAD= ARQUAD + AREA
CALL FORM(N,AREA,E1,E2,E3,G1,V21,V31,V32,PSI)
DO 10 I = 1,4
DO 10 J = 1,4
10 SN(I,J) = S(I,J)
DO 20 I = 1,4
SN(I,9) = S(I,5)
20 SN(I,10) = S(I,6)
DO 30 I = 5,6
J = I + 4
SN(J,9) = S(I,5)
30 SN(J,10) = S(I,6)
RI = RJO
ZI = ZJO
RJ = RKO
ZJ = ZKO
AREA = 0.5*((RJ-RI)*(ZK-ZI) - (RK-RI)*(ZJ-ZI))
CALL FORM(N,AREA,E1,E2,E3,G1,V21,V31,V32,PSI)
ARQUAD= ARQUAD + AREA
DO 40 I = 1,4
K = I + 2
DO 40 J = 1,4
L = J + 2
40 SN(K,L) = SN(K,L) + S(I,J)
DO 50 I = 1,4
K = I + 2
SN(K,9) = S(I,5) + SN(K,9)
50 SN(K,10) = S(I,6) + SN(K,10)
DO 60 I = 5,6
J = I + 4
SN(J,9) = SN(J,9) + S(I,5)
60 SN(J,10) = SN(J,10) + S(I,6)
RI = RKO

```

```

ZI = ZKO
RJ = RLO
ZJ = ZLO
AREA = 0.5*((RJ-RI)*(ZK-ZI) - (RK-RI)*(ZJ-ZI))
ARQUAD= ARQUAD + AREA
CALL FORM(N,AREA,E1,E2,E3,G1,V21,V31,V32,PSI)
DO 70 I = 1,6
J = I + 4
DO 70 K = 1,6
L = K + 4
70 SN(J,L) = SN(J,L) + S(I,K)
RI = RLO
ZI = ZLO
RJ = RIO
ZJ = ZIO
AREA = 0.5*((RJ-RI)*(ZK-ZI) - (RK-RI)*(ZJ-ZI))
ARQUAD= ARQUAD + AREA
CALL FORM(N,AREA,E1,E2,E3,G1,V21,V31,V32,PSI)
DO 80 I = 1,2
K = I + 6
DO 80 J = 1,2
L = J + 6
80 SN(K,L) = SN(K,L) + S(I,J)
DO 90 I = 3,4
L = I - 2
DO 90 J = 1,2
K = J + 6
90 SN(L,K) = SN(L,K) + S(I,J)
DO 100 I = 3,4
K = I - 2
DO 100 J = 3,4
L = J - 2
100 SN(K,L) = SN(K,L) + S(I,J)
DO 110 I = 5,6
K = I + 4
DO 110 J = 5,6
L = J + 4
110 SN(K,L) = SN(K,L) + S(I,J)
DO 120 I = 1,2
K = I + 6
DO 120 J = 5,6
L = J + 4
120 SN(K,L) = SN(K,L) + S(I,J)
DO 140 I = 3,4
L = I - 2
DO 140 J = 5,6
K = J + 4
140 SN(L,K) = SN(L,K) + S(I,J)
DO 150 I = 1,10
DO 150 J = 1,10
130 SN(J,I) = SN(I,J)
D = SN(9,9)*SN(10,10) - SN(9,10)*SN(10,9)
SA(1,1) = SN(10,10)/D
SA(1,2) = - SN(10,9)/D
SA(2,1) = SA(1,2)
SA(2,2) = SN(9,9)/D
DO 200 I = 1,8
DO 200 J = 1,2

```

```

S(I,J) = 0.
DO 200 K = 1,2
L = K + 8
200 S(I,J) = S(I,J) + SN(I,L)*SA(K,J)
DO 210 I = 1,8
DO 210 J = 1,8
SS(I,J) = 0.0
DO 210 K = 1,2
L = K + 8
210 SS(I,J) = SS(I,J) + S(I,K)*SN(L,J)
DO 220 I = 1,8
DO 220 J = 1,8
220 S(I,J) = SN(I,J) - SS(I,J)
AREA = ARQUAD
I = NPI(N)
J = NPJ(N)
K = NPK(N)
L = NPL(N)
IF(BDISC(I)) 300,300,310
300 IF(BDISC(J)) 320,320,310
320 IF(BDISC(K)) 330,330,310
330 IF(BDISC(L)) 712,712,310
310 DO 340 M = 1,8
DO 340 MM = 1,8
340 SS(M,MM) = 0.
IF(BDISC(I)) 350,350,360
350 SS(1,1) = 1.
SS(2,2) = 1.
GO TO 370
360 ALP = BDISC(I)/57.29577951
SS(1,1) = COS(ALP)
SS(1,2) = - SIN(ALP)
SS(2,1) = - SS(1,2)
SS(2,2) = SS(1,1)
370 IF(BDISC(J)) 380,380,390
380 SS(3,3) = 1.
SS(4,4) = 1.
GO TO 400
390 ALP = BDISC(J)/57.29577951
SS(3,3) = COS(ALP)
SS(3,4) = - SIN(ALP)
SS(4,3) = - SS(3,4)
SS(4,4) = SS(3,3)
400 IF(BDISC(K)) 410,410,420
410 SS(5,5) = 1.
SS(6,6) = 1.
GO TO 430
420 ALP = BDISC(K)/57.29577951
SS(5,5) = COS(ALP)
SS(6,6) = SS(5,5)
SS(5,6) = - SIN(ALP)
SS(6,5) = - SS(5,6)
430 IF(BDISC(L)) 440,440,450
440 SS(7,7) = 1.
SS(8,8) = 1.
GO TO 460
450 ALP = BDISC(L)/57.29577951
SS(7,7) = COS(ALP)

```

```
SS(7,8) = - SIN(ALP)
SS(8,7) = - SS(7,8)
SS(8,8) = SS(7,7)
460 DO 470 I = 1,8
      DO 470 J = 1,8
      SN(I,J) = 0.
      DO 470 K = 1,8
470 SN(I,J) = SN(I,J) + S(I,K)*SS(K,J)
      DO 480 I = 1,8
      DO 480 J = 1,8
      S(I,J) = 0.
      DO 480 K = 1,8
480 S(I,J) = S(I,J) + SS(K,I) *SN(K,J)
712 RETURN
END
```

```

SUBROUTINE MODSTM(KDEX,E1,E2,E3,G1,V21,V31,V32,PSI,E1T,E2T,E3T,G1T
1 ,V21T,V31T,V32T,PSIT)
COMMON NPI(310),NPJ(310),NPK(310),R(320),Z(320),KOD(320),NAP(320),
1 NP(320,11),S11(320,10),S12(320,10),S21(320,10),S22(320,10),
2 C(3,3),EP,VP,R1,RJ,RK,ZI,ZJ,ZK,S(8,8),MAT(310),NPL(310),ES,
3 VS,CODPL,RL,ZL,BDISC(320)
4 ,NPRE(32),UB(32),WB(32),ROT(32),TEM(32,3),NPIB(32),NPJB(32),
5 XB(32),YB(32),EB(32),AB(32),XIB(32),PHIB(32),NUMBEAM,
6 NUMJOI,SNN(6,6),NPBFEM(32),SUPST
DIMENSION E1(310),E2(310),E3(310),G1(310),V21(310),V31(310),
1 V32(310),PSI(310),E1T(310),E2T(310),E3T(310),G1T(310),
2 V21T(310),V31T(310),V32T(310),PSIT(310)
DIMENSION LM(4),T(8,8)
DO 15 KT = 1,KDEX
N = KOD(KT)
I = NPI(N)
J = NPJ(N)
K = NPK(N)
RI = R(I)
RJ = R(J)
RK = R(K)
ZI = Z(I)
ZJ = Z(J)
ZK = Z(K)
AREA = 0.5*((RJ-RI)*(ZK-ZI)-(RK-RI)*(ZJ-ZI))
LL = NPL(N)
RL = R(LL)
ZL = Z(LL)
IF(LL) 30,30,40
30 CALL FORM(N,AREA,E1T,E2T,E3T,G1T,V21T,V31T,V32T,PSIT)
GO TO 50
40 CALL FORMQ(N,AREA,E1T,E2T,E3T,G1T,V21T,V31T,V32T,PSIT)
50 DO 20 L = 1,8
DO 20 M = 1,8
20 T(L,M) = S(L,M)
RI = R(I)
RJ = R(J)
RK = R(K)
RL = R(LL)
ZI = Z(I)
ZJ = Z(J)
ZK = Z(K)
ZL = Z(LL)
IF(LL) 70,70,80
70 CALL FORM(N,AREA,E1,E2,E3,G1,V21,V31,V32,PSI)
GO TO 90
80 CALL FORMQ(N,AREA,E1,E2,E3,G1,V21,V31,V32,PSI)

90 LM(1) = NPI(N)
LM(2) = NPJ(N)
LM(3) = NPK(N)
MM = 3
IF(NPL(N)) 450,460,450
450 LM(4) = NPL(N)
MM = 4
460 DO 15 L = 1,MM
LX=LM(L)

```

```
NUM=NAP(LX)
DO 15 M = 1,MM
C
DO 5 I = 1,NUM
IF(NP(LX,I)-LM(M)) 5,10,5
5 CONTINUE
C
10 S11(LX,I) = S11(LX,I)+S(2*L-1,2*M-1) - T(2*L-1,2*M-1)
S12(LX,I) = S12(LX,I) + S(2*L-1,2*M) - T(2*L-1,2*M)
S21(LX,I) = S21(LX,I) + S(2*L,2*M-1) - T(2*L,2*M-1)
15 S22(LX,I) = S22(LX,I) + S(2*L,2*M) - T(2*L,2*M)
C
RETURN
END
```

```

SUBROUTINE SOL
COMMON NPI(310),NPJ(310),NPK(310),R(320),Z(320),KOD(320),NAP(320),
1      NP(320,11),S11(320,10),S12(320,10),S21(320,10),S22(320,10),
2      C(3,3),EP,VP,RI,RJ,RK,ZI,ZJ,ZK,S(8,8),MAT(310),NPL(310),ES,
3      VS,CODPL,RL,ZL,HDISC(320)
4      ,NPRE(32),UB(32),WH(32),ROT(32),TEM(32,3),NPIB(32),NPJB(32),
5      XB(32),YB(32),EB(32),AB(32),XIB(32),PHIB(32),NUMBEAM,
6      NUMJOI,SNN(6,6),NPBFEM(32),SUPST
DIMENSION BS1(3,32,5),BS2(3,32,5),BS3(3,32,5),SPRC(32)
DIMENSION BS11(32,5),BS12(32,5),BS13(32,5),BS21(32,5),BS22(32,5),
1      BS23(32,5),BS31(32,5),BS32(32,5),BS33(32,5),NPB(32,5),
2      NPB(32),F(3),DIS(6),ELFOR(6),TEM0(32,3),XYZ(3),LM(2)
2222 FORMAT(////////)
NCYCS = 50
NCYCS = 9
IF(SUPST) 2731,200,2731
200 SLTOT = 0.
SUPST = 1.
DO 2030 N = 1,NUMJOI
DO 2031 M = 1,5
BS11(N,M) = 0.
BS12(N,M) = 0.
BS13(N,M) = 0.
BS21(N,M) = 0.
BS22(N,M) = 0.
BS23(N,M) = 0.
BS31(N,M) = 0.
BS32(N,M) = 0.
BS33(N,M) = 0.
2031 NPB(N,M) = 0
NPB(N,5) = 0
DO 2030 J = 1,3
TEM(N,J) = 0.
TEM0(N,J) = TEM(N,J)
2030 NPB(N,1) = N
PRINT 2222
NCYS = 0
3004 CONTINUE
DO 2050 N = 1,NUMBEAM
SPRC(N) = 1.
I = NPIB(N)
J = NPJB(N)
RI = XB(I)
ZI = YB(I)
RJ = XB(J)
ZJ = YB(J)
SL = SQRT((ZJ-ZI)*(ZJ-ZI) + (RJ-RI)*(RJ-RI))
SLTOT = SLTOT + SL
IF(XIB(N)) 6200,6300,6200
6300 C = (RJ - RI)/SL
S = (ZJ-ZI)/SL
DO 6310 L = 1,6
DO 6310 M = 1,6
6310 SNN(L,M) = 0.
STIF = EB(N)*AB(N)/SL
SNN(1,1) = C*C*STIF
SNN(1,2) = C*S*STIF

```

```

SNN(1,4) = - SNN(1,1)
SNN(1,5) = - SNN(1,2)
SNN(2,1) = SNN(1,2)
SNN(2,2) = S*S*STIF
SNN(2,4) = SNN(1,5)
SNN(2,5) = -SNN(2,2)
SNN(4,1) = SNN(1,4)
SNN(4,2) = SNN(2,4)
SNN(4,4) = SNN(1,1)
SNN(4,5) = SNN(1,2)
SNN(5,1) = SNN(1,5)
SNN(5,2) = SNN(2,5)
SNN(5,4) = SNN(4,5)
SNN(5,5) = SNN(2,2)
GO TO 6220
6200 CALL FORMB(N)
6220 MMM = 2
LM(1) = NPIB(N)
LM(2) = NPJB(N)
DO 250 L = 1,MMM
LX = LM(L)
DO 2050 M = 1,MMM
MX = 0
2660 MX = MX + 1
IF(NPB(LX,MX) = LM(M)) 2670,2680,2670
2670 IF(NPB(LX,MX)) 2660,2680,2660
2680 NPB(LX,MX) = LM(M)
IF(MX = 5) 2690,2400,2400
2690 LL = 3*L
L1 = LL - 1
L2 = L1 - 1
MM = 3*M
M1 = MM - 1
M2 = MM - 2
BS11(LX,MX) = BS11(LX,MX) + SNN(L2,M2)
BS12(LX,MX) = BS12(LX,MX) + SNN(L2,M1)
BS13(LX,MX) = BS13(LX,MX) + SNN(L2,MM)
BS21(LX,MX) = BS21(LX,MX) + SNN(L1,M2)
BS22(LX,MX) = BS22(LX,MX) + SNN(L1,M1)
BS23(LX,MX) = BS23(LX,MX) + SNN(L1,MM)
BS31(LX,MX) = BS31(LX,MX) + SNN(LL,M2)
BS32(LX,MX) = BS32(LX,MX) + SNN(LL,M1)
2050 BS33(LX,MX) = BS33(LX,MX) + SNN(LL,MM)
PRINT 6431,SLTOT
6431 FORMAT(/// 24H TOTAL SUPPORT LENGTH = F10.3 //)
DO 2720 M=1,NUMJ0I
MX = 1
2710 MX = MX + 1
IF(NPB(M,MX)) 2720,2720,2710
2720 NAPB(M) = MX - 1
2731 NCYS = 0
2732 DO 300 N = 1,NUMJ0I
DO 300 J = 1,3
300 TEM(N,J) = TEM0(N,J)
DO 6001 M = 1,NUMJ0I
DO 6001 I = 1,5
BS1(1,M,I) = BS11(M,I)
BS1(2,M,I) = BS21(M,I)

```

```

BS1(3,M,I) = RS31(M,I)
BS2(1,M,I) = BS12(M,I)
BS2(2,M,I) = BS22(M,I)
BS2(3,M,I) = BS32(M,I)
BS3(1,M,I) = BS13(M,I)
BS3(2,M,I) = BS23(M,I)
6001 BS3(3,M,I) = BS33(M,I)
8001 DO 6004 M = 1,NUMJOI
      IF(NPRE(M)) 2746,2744,2745
2746 IF(NPRE(M) + 2) 2740,2741,2742
2740 BS2(2,M,1) = BS2(2,M,1)*1.E+08
      BS3(3,M,1) = BS3(3,M,1)*1.E+08
      TEM(M,2) = BS2(2,M,1)*WB(M)
      TEM(M,3) = BS3(3,M,1)*ROT(M)
      GO TO 2744
2741 BS2(2,M,1) = BS2(2,M,1)*1.E+08
      TEM(M,2) = BS2(2,M,1)*WB(M)
      GO TO 2744
2742 BS3(3,M,1) = BS3(3,M,1)*1.E+08
      TEM(M,3) = BS3(3,M,1)*ROT(M)
      GO TO 2744
2745 BS1(1,M,1) = BS1(1,M,1)*1.E+08
      TEM(M,1) = BS1(1,M,1)*UB(M)
      IF(NPRE(M) - 2) 2744,2747,2748
2747 BS3(3,M,1) = BS3(3,M,1)*1.E+08
      TEM(M,3) = BS3(3,M,1)*ROT(M)
      GO TO 2744
2748 BS2(2,M,1) = BS2(2,M,1)*1.E+08
      TEM(M,2) = BS2(2,M,1)*WB(M)
      IF(NPRE(M) - 3) 2744,2744,2751
2751 BS3(3,M,1) = BS3(3,M,1)*1.E+08
      TEM(M,3) = BS3(3,M,1)*ROT(M)
2744 CONTINUE
6004 CONTINUE
      JOI = NUMJOI - 1
1031 FORMAT(I5,10E12.5/)
      DO 2860 M = 1,JOI
      NAPM = NAPB(M)
      IF(.0000001 - RS1(1,M,1)) 5330,5335,5335
5330 DO 5002 J = 2,3
      IF(BS1(J,M,1)) 5201,5002,5201
5201 F(J) = BS1(J,M,1)/BS1(1,M,1)
      TEM(M,J) = TEM(M,J) - TEM(M,1)*F(J)
      BS2(J,M,1) = BS2(J,M,1) - BS2(1,M,1)*F(J)
      BS3(J,M,1) = BS3(J,M,1) - BS3(1,M,1)*F(J)
      DO 5222 N = 2,NAPM
      NN = NPB(M,N)
      IF(NN - M) 5222,5222,5401
5401 BS1(J,M,N) = BS1(J,M,N) - BS1(1,M,N)*F(J)
      BS2(J,M,N) = BS2(J,M,N) - BS2(1,M,N)*F(J)
      BS3(J,M,N) = BS3(J,M,N) - BS3(1,M,N)*F(J)
5222 CONTINUE
5002 CONTINUE
      DO 5432 N = 2,NAPM
      NN = NPB(M,N)
      IF(NN - M) 5432,5432,5403
5403 NAPN = NAPB(NN)
      DO 5433 K = 2,NAPN

```

```

KK = NPB(NN,K)
IF(KK - M) 5433,5404,5433
5404 DO 5434 I = 1,3
IF(BS1(I,NN,K)) 5405,5434,5405
5405 F(I) = BS1(I,NN,K)/BS1(1,M,1)
TEM(NN,I) = TEM(NN,I) - TEM(M,1)*F(I)
BS2(I,NN,K) = BS2(I,NN,K) - BS2(1,M,1)*F(I)
BS3(I,NN,K) = BS3(I,NN,K) - BS3(1,M,1)*F(I)
DO 5402 L = 2,NAPM
KM = NPB(M,L)
IF(KM - M) 5402,5402,5406
5406 DO 5422 LL = 1,NAPN
LNN = NPB(NN,LL)
IF(LNN - KM) 5409,5408,5409
5408 BS1(I,NN,LL) = BS1(I,NN,LL) - BS1(1,M,L)*F(I)
BS2(I,NN,LL) = BS2(I,NN,LL) - BS2(1,M,L)*F(I)
BS3(I,NN,LL) = BS3(I,NN,LL) - BS3(1,M,L)*F(I)
GO TO 5402
5409 IF(LL - NAPN) 5422,5421,5422
5421 NAPNB = NAPB(NN)
IF(NAPNB - NAPN - 1) 5426,5427,5427
5426 NAPB(NN) = NAPB(NN) + 1
KX = NAPB(NN)
NPB(NN,KX) = KM
5427 CONTINUE
BS1(I,NN,KX) = - BS1(1,M,L)*F(I)
BS2(I,NN,KX) = - BS2(1,M,L)*F(I)
BS3(I,NN,KX) = - BS3(1,M,L)*F(I)
5422 CONTINUE
5402 CONTINUE
5434 CONTINUE
5433 CONTINUE
5432 CONTINUE
5335 IF(.000001 - BS2(2,M,1)) 5340,5345,5345
5340 IF(BS2(3,M,1)) 5410,5415,5410
5410 F(1) = BS2(3,M,1)/BS2(2,M,1)
BS3(3,M,1) = BS3(3,M,1) - BS3(2,M,1)*F(1)
TEM(M,3) = TEM(M,3) - TEM(M,2)*F(1)
DO 5420 N = 2,NAPM
NN = NPB(M,N)
IF(NN - M) 5420,5420,5430
5430 BS1(3,M,N) = BS1(3,M,N) - BS1(2,M,N) * F(1)
BS2(3,M,N) = BS2(3,M,N) - BS2(2,M,N) * F(1)
BS3(3,M,N) = BS3(3,M,N) - BS3(2,M,N) * F(1)
5420 CONTINUE
5415 DO 5532 N = 2,NAPM
NN = NPB(M,N)
IF(NN-M) 5532,5532,5503
5503 NAPN = NAPB(NN)
DO 5533 K = 2,NAPN
KK = NPB(NN,K)
IF(KK - M) 5533,5504,5533
5504 DO 5534 I = 1,3
IF(BS2(I,NN,K)) 5505,5534,5505
5505 F(I) = BS2(I,NN,K)/BS2(2,M,1)
TEM(NN,I) = TEM(NN,I) - TEM(M,2)*F(I)
BS3(I,NN,K) = BS3(I,NN,K) - BS3(2,M,1) * F(I)
DO 5502 L = 2,NAPM

```

```

KM = NPB(M,L)
IF(KM = M) 5502,5502,5506
5506 DO 5522 LL = 1,NAPN
LNN = NPB(NN,LL)
IF(LNN = KM) 5509,5508,5509
5508 BS1(I,NN,LL) = BS1(I,NN,LL) - BS1(2,M,L) * F(I)
BS2(I,NN,LL) = BS2(I,NN,LL) - BS2(2,M,L) * F(I)
BS3(I,NN,LL) = BS3(I,NN,LL) - BS3(2,M,L) * F(I)
GO TO 5502
5509 IF(LL = NAPN) 5522,5521,5522
5521 NAPNB = NAPB(NN)
IF(NAPNB = NAPN - 1) 5526,5527,5527
5526 NAPB(NN) = NAPB(NN) + 1
KX = NAPB(NN)
NPB(NN,KX) = KM
5527 CONTINUE
BS1(I,NN,KX) = - BS1(2,M,L)*F(I)
BS2(I,NN,KX) = - BS2(2,M,L)*F(I)
BS3(I,NN,KX) = - BS3(2,M,L)*F(I)
5522 CONTINUE
5502 CONTINUE
5534 CONTINUE
5533 CONTINUE
5532 CONTINUE
5345 IF(.000001 = BS3(3,M,1)) 5351,2860,2860
5351 DO 5632 N = 2,NAPM
NN = NPB(M,N)
IF(NN = M) 5632,5632,5603
5603 NAPN = NAPB(NN)
DO 5633 K = 2,NAPN
KK = NPB(NN,K)
IF(KK = M) 5633,5604,5633
5604 DO 5634 I = 1,3
IF(BS3(I,NN,K)) 5605,5634,5605
5605 F(I) = BS3(I,NN,K)/BS3(3,M,1)
TEM(NN,I) = TEM(NN,I) - TEM(M,3)*F(I)
DO 5602 L = 2,NAPM
KM = NPB(M,L)
IF(KM = M) 5602,5602,5606
5606 DO 5622 LL = 1,NAPN
LNN = NPB(NN,LL)
IF(LNN = KM) 5609,5608,5609
5608 BS1(I,NN,LL) = BS1(I,NN,LL) - BS1(3,M,L) * F(I)
BS2(I,NN,LL) = BS2(I,NN,LL) - BS2(3,M,L) * F(I)
BS3(I,NN,LL) = BS3(I,NN,LL) - BS3(3,M,L) * F(I)
GO TO 5602
5609 IF(LL = NAPN) 5622,5621,5602
5621 NAPNB = NAPB(NN)
IF(NAPNB = NAPN - 1) 5626,5627,5627
5626 NAPB(NN) = NAPB(NN) + 1
KX = NAPB(NN)
NPB(NN,KX) = KM
5627 CONTINUE
BS1(I,NN,KX) = - BS1(3,M,L)*F(I)
BS2(I,NN,KX) = - BS2(3,M,L)*F(I)
BS3(I,NN,KX) = - BS3(3,M,L)*F(I)
5622 CONTINUE
5602 CONTINUE

```

```

5634 CONTINUE
5633 CONTINUE
5632 CONTINUE
2860 CONTINUE
M = NUMJOI
IF(.000001 - BS1(1,M,1)) 5208,5350,5350
5208 DO 5007 I = 2,3
IF(BS1(I,M,1)) 5717,5007,5717
5717 CONTINUE
F(I) = BS1(I,M,1)/BS1(1,M,1)
BS2(I,M,1) = BS2(I,M,1) - BS2(1,M,1)*F(I)
BS3(I,M,1) = BS3(I,M,1) - BS3(1,M,1)*F(I)
TEM(M,I) = TEM(M+I) - TEM(M+1)*F(I)
5007 CONTINUE
5350 IF(.000001 - BS2(2,M,1)) 5355,5360,5360
5355 F(1) = BS2(3,M,1)/BS2(2,M,1)
BS3(3,M,1) = BS3(3,M,1) - BS3(2,M,1)*F(1)
TEM(M,3) = TEM(M,3) - TEM(M,2)*F(1)
5360 IF(BS3(3,M,1)) 5305,5306,5305
5306 ROT(M) = ROT(M)
GO TO 5308
5305 CONTINUE
ROT(M) = TEM(M,3)/BS3(3,M,1)
5308 CONTINUE
WB(M) = WB(M)
IF(BS2(2,M,1)) 5365,5370,5365
5365 WB(M) = (TEM(M,2) - BS3(2,M,1)*ROT(M))/BS2(2,M,1)
5370 UB(M) = UB(M)
IF(BS1(1,M,1)) 5375,5380,5375
5375 UB(M) = (TEM(M,1) - BS3(1,M,1)*ROT(M) - BS2(1,M,1)*WB(M))/BS1(1,M,1)
1 / 1
5380 DO 5100 K = 1,JOI
M = NUMJOI - K
XYZ(1) = 0.
XYZ(2) = 0.
XYZ(3) = 0.
NAPM = NAPB(M)
DO 5110 N = 1,NAPM
NN = NPB(M,N)
IF(M>NN) 5115,5110,5110
5115 DO 5116 L = 1,3
5116 XYZ(L) = XYZ(L) + BS1(L,M,N)*UB(NN) + BS2(L,M,N)*WB(NN) +
1 BS3(L,M,N)*ROT(NN)
5116 CONTINUE
ROT(M) = ROT(M)
IF(.000001 - BS3(3,M,1)) 5315,5316,5316
5315 CONTINUE
ROT(M) = (TEM(M,3) - XYZ(3))/BS3(3,M,1)
5316 WB(M) = WB(M)
IF(.000001 - BS2(2,M,1)) 5320,5385,5385
5320 WB(M) = (TEM(M,2) - XYZ(2) - BS3(2,M,1)*ROT(M))/BS2(2,M,1)
5385 UB(M) = UB(M)
IF(.000001 - BS1(1,M,1)) 5390,5100,5100
5390 UB(M) = (TEM(M,1) - XYZ(1) - BS3(1,M,1)*ROT(M) - BS2(1,M,1)*WB(M))
1 / BS1(1,M,1)
5100 CONTINUE
PRINT 11
11 FORMAT(///*           JOINT      U           W           ROT

```

```

1      HOR FORCE      VERT FORCE      MOMENT *//)
DO 2200 M = 1,NUMJOI
FO = 0.0
FOZ = 0.0
FMOM = 0.0
NUM = NAPB(M)
DO 2195 L = 1,NUM
N = NPB(M,L)
FO = FO + BS11(M,L)*UB(N)*BS12(M,L)*WB(N)*BS13(M,L)*ROT(N)
FOZ = FOZ + BS21(M,L)*UB(N) + BS22(M,L)*WB(N) + BS23(M,L)*ROT(N)
2195 FMOM = FMOM + BS31(M,L)*UB(N) + BS32(M,L)*WB(N) + BS33(M,L)*ROT(N)
IF(NPBFEM(M)) 2200,2200,2210
2210 TEM(M,1) = FO
TEM(M,2) = FOZ
2200 PRINT 2025,M,IJB(M),WB(M),ROT(M),FO,FOZ,FMOM
2025 FORMAT(110,6E15.5)
PRINT 12
12 FORMAT(///* ELEMENT          JOINT 1
1      JOINT 2      */ *      AXIAL FORCE      PERPE
2ND FORCE      MOMENT      AXIAL FORCE      PERPEND FORCE      MO
3MENT *//)
MODIF = 0
NCYS = NCYS + 1
DO 3055 N = 1,NUMBEAM
I = NPIB(N)
J = NPJB(N)
RI = XB(I)
ZI = YB(I)
RJ = XB(J)
ZJ = YB(J)
DIS(1) = UB(I)
DIS(2) = WB(I)
DIS(3) = ROT(I)
DIS(4) = UB(J)
DIS(5) = WB(J)
DIS(6) = ROT(J)
XLB = SQRT((ZJ-ZI)*(ZJ-ZI) + (RJ-RI)*(RJ-RI))
C = (RJ-RI)/XLB
S = (ZJ-ZI)/XLB
DI2 = UB(J)*C + WB(J)*S
DI1 = UB(I)*C + WB(I)*S
XLN = XLB + DI2 - DI1
IF(XIB(N)) 7200,7300,7200
7300 STIF = EB(N)*AB(N)/XLB
DO 7310 L = 1,6
DO 7310 M = 1,6
7310 SNN(L,M) = 0.
SNN(1,1) = C*C*STIF
SNN(1,2) = C*S*STIF
SNN(1,4) = - SNN(1,1)
SNN(1,5) = - SNN(1,2)
SNN(2,1) = SNN(1,2)
SNN(2,2) = S*S*STIF
SNN(2,4) = SNN(1,5)
SNN(2,5) = -SNN(2,2)
SNN(4,1) = SNN(1,4)
SNN(4,2) = SNN(2,4)
SNN(4,4) = SNN(1,1)

```

```

SNN(4,5) = SNN(1,2)
SNN(5,1) = SNN(1,5)
SNN(5,2) = SNN(2,5)
SNN(5,4) = SNN(4,5)
SNN(5,5) = SNN(2,2)
IF(XLN = XLB) 7430,7220,7400
7400 IF(SPRC(N)) 7220,7422,7420
7420 LM(1) = I
PRINT 4,N
4 FORMAT(/* SPRING# I4 * IS IN TENSION *)
LM(2) = J
DO 7451 L = 1,2
LX = LM(L)
DO 7451 M = 1,2
MX = 0
7660 MX = MX + 1
IF(NPB(LX,MX) = LM(M)) 7660,7680,7660
7680 CONTINUE
LL = 3*L
L1 = LL - 1
L2 = L1 - 1
MM = 3*M
M1 = MM - 1
M2 = MM - 2
BS11(LX,MX) = BS11(LX,MX) - SNN(L2,M2)
BS12(LX,MX) = BS12(LX,MX) - SNN(L2,M1)
BS13(LX,MX) = BS13(LX,MX) - SNN(L2,MM)
BS21(LX,MX) = BS21(LX,MX) - SNN(L1,M2)
BS22(LX,MX) = BS22(LX,MX) - SNN(L1,M1)
BS23(LX,MX) = BS23(LX,MX) - SNN(L1,MM)
BS31(LX,MX) = BS31(LX,MX) - SNN(LL,M2)
BS32(LX,MX) = BS32(LX,MX) - SNN(LL,M1)
7451 BS33(LX,MX) = BS33(LX,MX) - SNN(LL,MM)
SPRC(N) = 0.
MODIF = MODIF + 1
GO TO 7220
7430 IF(SPRC(N)) 7220,7440,7220
7440 LM(1) = I
LM(2) = J
DO 7551 L = 1,2
LX = LM(L)
DO 7551 M = 1,2
MX = 0
7760 MX = MX + 1
IF(NPB(LX,MX) = LM(M)) 7760,7780,7760
7780 CONTINUE
LL = 3*L
L1 = LL - 1
L2 = L1 - 1
MM = 3*M
M1 = MM - 1
M2 = MM - 2
BS11(LX,MX) = BS11(LX,MX) + SNN(L2,M2)
BS12(LX,MX) = BS12(LX,MX) + SNN(L2,M1)
BS13(LX,MX) = BS13(LX,MX) + SNN(L2,MM)
BS21(LX,MX) = BS21(LX,MX) + SNN(L1,M2)
BS22(LX,MX) = BS22(LX,MX) + SNN(L1,M1)
BS23(LX,MX) = BS23(LX,MX) + SNN(L1,MM)

```

```

BS31(LX,MX) = BS31(LX,MX) + SNN(LL,M2)
BS32(LX,MX) = BS32(LX,MX) + SNN(LL,M1)
7551 BS33(LX,MX) = BS33(LX,MX) + SNN(LL,MM)
SPRC(N) = 1.
MODIF = MODIF + 1
7422 DO 7421 L = 1,6
7421 ELFOR(L) = 0.
PRINT 5,N
5 FORMAT(105X *SPRING * I4 * IS ELIMINATED * )
GO TO 3055
7200 CALL FORMB(N)
7220 DO 3060 J = 1,6
ELFOR(J) = 0.
DO 3060 I = 1,6
3060 ELFOR(J) = ELFOR(J) + SNN(J,I)*DIS(I)
XF1 = ELFOR(1)
XF4 = ELFOR(4)
ELFOR(1) = XF1*C + ELFOR(2)*S
ELFOR(2) = ELFOR(2)*C - XF1*S
ELFOR(4) = XF4*C + ELFOR(5)*S
ELFOR(5) = ELFOR(5)*C - XF4*S
3055 PRINT 3070,N,(ELFOR(J),J=1,6),XLB,XLN
3070 FORMAT(15,3E15.5,5X,3E15.5,2F15.7)
IF(MODIF) 7450,3001,7450
7450 PRINT 3,NCYS
3 FORMAT(///* ITERATION * I4///)
IF(NCYCS - NCYS) 7460,2732,2732
7460 PRINT 7
7 FORMAT(///* MAXIMUM NUMBER OF ITERATIONS IS EXCEEDED SUPPORT IS
1 JUMPING AROUND *//)
SUPST = - 1.
GO TO 3001
2400 PRINT 2401,N
2401 FORMAT(///I5,* MORE THAN 3 ADJACENT NODAL POINTS *///)
3000 CONTINUE
3001 D= 0.
RETURN
END

```

```

SUBROUTINE FORMB(N)
COMMON NPI(310),NPJ(310),NPK(310),R(320),Z(320),KOD(320),NAP(320),
1      NP(320,11),S11(320,10),S12(320,10),S21(320,10),S22(320,10),
2      C(3,3),EP,VP,RI,RJ,RK,ZI,ZJ,ZK,S(8,8),MAT(310),NPL(310),ES,
3      VS,CODPL,RL,ZL,BDISC(320)
4      *NPRE(32),UB(32),WB(32),ROT(32),TEM(32,3),NPIB(32),NPJB(32),
5      XB(32),YB(32),EB(32),AB(32),XIB(32),PHIB(32),NUMBEAM,
6      NUMJOI,SNN(6,6),NPBFEM(32),SUPST
DIMENSION Q(6,6),SB(6,6),SI(6,6)
DO 10 I = 1,6
DO 10 J = 1,6
Q(I,J) = 0.
10 SB(I,J) = 0.
21 FORMAT(I10,4E18.8/)
XLB = SQRT((ZJ-ZI)*(ZJ-ZI)+(RJ-RI)*(RJ-RI))
SB(1,1) = EB(N)*AB(N)/XLB
SB(1,4) = -SB(1,1)
SB(4,4) = SB(1,1)
SB(4,1) = SB(1,4)
SBPR = EB(N)*XIB(N)/XLB/(1.+PHIB(N))
SB(2,3) = 6.*SBPR/XLB
SB(3,2) = SB(2,3)
SB(2,6) = SB(2,3)
SB(6,2) = SB(2,6)
SB(3,5) = -SB(2,3)
SB(5,3) = SB(3,5)
SB(5,6) = SB(3,5)
SB(6,5) = SB(5,6)
SB(2,2) = 2.*SB(2,3)/XLB
SB(2,5) = -SB(2,2)
SB(5,2) = SB(2,5)
SB(5,5) = SB(2,2)
SB(3,3) = (4.+PHIB(N))*SBPR
SB(6,6) = SB(3,3)
SB(3,6) = (2.-PHIB(N))*SBPR
SB(6,3) = SB(3,6)
Q(1,1) = (RJ-RI)/XLB
Q(1,2) = (ZJ-ZI)/XLB
60 Q(2,1) = -Q(1,2)
Q(2,2) = Q(1,1)
Q(3,3) = 1.
Q(4,4) = Q(1,1)
Q(5,5) = Q(1,1)
Q(6,6) = 1.
Q(4,5) = Q(1,2)
Q(5,4) = Q(2,1)
DO 20 I = 1,6
DO 20 J = 1,6
SI(I,J) = 0.
DO 20 K = 1,6
20 SI(I,J) = SI(I,J) + SB(I,K)*Q(K,J)
DO 30 I = 1,6
DO 30 J = 1,6
SNN(I,J) = 0.
DO 30 K = 1,6
30 SNN(I,J) = SNN(I,J) + Q(K,I)*SI(K,J)
RETURN
END

```

DISTRIBUTION LIST

HQDA (DARD-ZA) WASH DC 20310 (2)

HQDA (DAEN-ZA)	(1), (DAEN-ASI-L)	(2), (DAEN-CWE)	(2),
(DAEN-CWE-C)	(1), (DAEN-CWE-D)	(1), (DAEN-CWE-G)	(1),
(DAEN-CWE-S)	(1), (DAEN-CWR-R)	(1), (DAEN-CWZ-R)	(1),
(DAEN-MCD)	(1), (DAEN-MCE)	(1), (DAEN-MCE-A)	(1),
(DAEN-MCE-D)	(1), (DAEN-MCE-P)	(1), (DAEN-MCZ-S)	(1);

WASH DC 20314

Division Engineers, U. S. Army Engineer Divisions

Huntsville	(2)	North Pacific	(2)
Lower Mississippi Valley	(2)	Ohio River	(2)
Missouri River	(2)	South Atlantic	(2)
New England	(2)	South Pacific	(2)
North Atlantic	(2)	Southwestern	(2)
North Central	(2)		

Directors, U. S. Army Engineer Division Laboratories

New England	(2)	South Atlantic	(2)
North Atlantic	(2)	South Pacific	(2)
North Pacific	(2)	Southwestern	(2)
North Central	(2)	Ohio River	(2)

District Engineers, U. S. Army Engineer Districts

Alaska	(2)	New Orleans	(2)
Albuquerque	(2)	New York	(2)
Baltimore	(2)	Norfolk	(2)
Buffalo	(2)	Omaha	(2)
Charleston	(2)	Philadelphia	(2)
Chicago	(2)	Pittsburgh	(2)
Detroit	(2)	Portland	(2)
Fort Worth	(2)	Rock Island	(2)
Galveston	(2)	Sacramento	(2)
Huntington	(2)	St. Louis	(2)
Jacksonville	(2)	St. Paul	(2)
Kansas City	(2)	San Francisco	(2)
Little Rock	(2)	Savannah	(2)
Los Angeles	(2)	Seattle	(2)
Louisville	(2)	Tulsa	(2)
Memphis	(2)	Vicksburg	(2)
Mobile	(2)	Walla Walla	(2)
Nashville	(2)	Wilmington	(2)

	<u>No. of Copies</u>
President, Mississippi River Commission, CE, P. O. Box 80, Vicksburg, Mississippi 39180	1
Research Center Library, U. S. Army Engineer Waterways Experiment Station, P. O. Box 631, Vicksburg, Mississippi 39180	10
U. S. Army Cold Regions, Research and Engineering Laboratory, (USA CRREL), Hanover, New Hampshire 03755	1
U. S. Army Engineer School Library, Thayer Hall (Bldg. 270), Fort Belvoir, Virginia 22060	1

DEPARTMENT OF THE NAVY

Naval Civil Engineering Laboratory, ATTN: Technical Library L31, Port Hueneme, California 93041	1
--	---

OTHER DOD AGENCIES

Administrator, Defense Documentation Center, Cameron Station, Building 5, Alexandria, Virginia 22314	12
---	----

OTHER GOVERNMENT AGENCIES

Federal Highway Administration, Office of Research, ATTN: Chief, Materials Division, Washington, D. C. 20591	1
--	---

Highway Research Board, ATTN: Librarian, 2101 Constitution Ave., N.W., Washington, D. C. 20418	1
---	---

Tennessee Valley Authority, ATTN: J. H. Coulson, 415 Union Building, Knoxville, Tennessee 37902	1
--	---

U. S. Bureau of Mines, Spokane Mining Research Center, ATTN: George B. Wallace, N. 1430 Washington Street, Spokane, Washington 99201	1
--	---

UNIVERSITY

University of Illinois, Department of Civil Engineering, ATTN: A. J. Hendron, Jr., Civil Engineering Building, Urbana, Illinois 61801	1
---	---

Massachusetts Institute of Technology, Cambridge, Massachusetts 02139	1
--	---

No. of Copies

UNIVERSITY (Cont'd)

University of California, Berkeley, Department of Civil Engineering, ATTN: Tor L. Brekke, Geotechnical Engineering, Davis Hall, Berkeley, California 94720	2
University of Minnesota, Department of Mining and Civil Engineering, ATTN: Charles Fairhurst, 112 Mines and Metallurgy Bldg., Minneapolis, Minn. 55455	2
University of Missouri at Rolla, ATTN: Dr. N. B. Aughenbaugh, Chairman, Department of Mining, Petr., & Geol. Engineering, Rolla, Missouri 65401	1
South Dakota School of Mines and Technology, Department of Mining Engineering, ATTN: Dr. E. Hoskins, Rapid City, South Dakota 57701	1
University of Purdue, Department of Civil Engineering, ATTN: William R. Judd, West Lafayette, Indiana 47907	1
University of Toronto, Department of Civil Engineering ATTN: Jean-Claude Roegiers, Rock Mechanics, Toronto, Ontario, M5, S1A1	1

INDUSTRY and INDIVIDUALS

Hirschfeld, R. C., Geotechnical Engineers, Inc. 934 Main Street, Winchester, Massachusetts 01890	1
Lane, K. S., 10014 Kingswood Circle, Sun City, Arizona 85351	1
Patton, F. D., Consulting Engineering Geologist, 1775 Bellevue Ave., Apt. 1504, West Vancouver, B.C.	1
Shannon & Wilson, Inc., ATTN: S. D. Wilson; 1105 N. 38th Street, Seattle, Washington 98103	1
Stone & Webster Engineering Corp., ATTN: Dr. J. L. Rosenblad, P. O. Box 2325, Boston, Massachusetts 02107	1
Woodward-Lundgren & Associates, ATTN: Librarian, P. O. Box 24075, Oakland, California 94623	1
Woodward-Clyde, ATTN: D. J. Lachell, <del>1425</del> <sup>1373</sup> Broad Street Clifton, New Jersey 07012	1
General Analytics, Inc., ATTN: Richard E. Gray, 580 Beatty Road, Monroeville, Pennsylvania 15146	1

## UNCLASSIFIED

SECURITY CLASSIFICATION OF THIS PAGE (When Data Entered)

REPORT DOCUMENTATION PAGE		READ INSTRUCTIONS BEFORE COMPLETING FORM
1. REPORT NUMBER Technical Report MRD-3-75	2. GOVT ACCESSION NO.	3. RECIPIENT'S CATALOG NUMBER
4. TITLE (and Subtitle) RATIONAL DESIGN OF TUNNEL SUPPORTS Subtitle: Tunnel Support Loading Caused by Rock Failure		5. TYPE OF REPORT & PERIOD COVERED
7. AUTHOR(s) Jaak Joseph K. Daemen		6. PERFORMING ORG. REPORT NUMBER MRD-3-75
9. PERFORMING ORGANIZATION NAME AND ADDRESS Department of Civil & Mining Engineering University of Minnesota Minneapolis, Minnesota		8. CONTRACT OR GRANT NUMBER(s) DACP 45-74-C-0066
11. CONTROLLING OFFICE NAME AND ADDRESS Department of the Army Office, Chief of Engineers Washington, D. C.		10. PROGRAM ELEMENT, PROJECT, TASK AREA & WORK UNIT NUMBERS DD Form 1498
14. MONITORING AGENCY NAME & ADDRESS (if different from Controlling Office) Department of the Army Missouri River Division, Corps of Engineers P. O. Box 103, Downtown Station Omaha, Nebraska 68101		12. REPORT DATE May 1975
16. DISTRIBUTION STATEMENT (of this Report) This document has been approved for public release and sale; its distribution is unlimited.		13. NUMBER OF PAGES 445
17. DISTRIBUTION STATEMENT (of the abstract entered in Block 20, if different from Report)		15. SECURITY CLASS. (of this report) Unclassified
18. SUPPLEMENTARY NOTES		15a. DECLASSIFICATION/DOWNGRADING SCHEDULE
19. KEY WORDS (Continue on reverse side if necessary and identify by block number)		<i>Tunnel - supports</i>
20. ABSTRACT (Continue on reverse side if necessary and identify by block number) Two methods are presented for the analysis of tunnel support loading caused by rock failure. In the first part of this thesis closed-form solutions are used, in the second part numerical techniques. Emphasis is put upon the statical indeterminacy of the problem and upon the necessity for considering the relative displacements between ground and support. From this follows the need for a realistic calculation of the stiffness of ground and support, as well as the		

Block 20 - Cont'd.

need to consider the sequential development of the interaction between these two elements. It is assumed that the rock mass behavior during failure is softening and dilatant. Interface problems between ground and support that can strongly influence the effective support stiffness are discussed.

The closed-form solutions obtained in the first part are expressed in terms of ground and support characteristics. The derivations are based upon the assumption that the problem is radially symmetric. Bounds for the ground reaction can be derived by accounting for the intact and the residual rock strength. Within the thus defined domain the ground behavior is determined by the rate of strength loss with increasing strain. The ground reaction curve can have fundamentally different shapes depending upon the post-failure rock behavior. Corresponding to failing or yielding sections of the ground reaction will be the desirability of stiff or soft supporting methods. The increased trend towards the use of stiffer supports as well as the emphasis on the need for early installation manifested by the combined use of reinforced shotcrete, grouted bolts and steel sets confirms the likelihood that optimum support conditions can be approached when only limited convergence is allowed. The optimum equilibrium state depends on the brittleness or the relative instability of the failing rock. The optimum displacement will be affected by rock loosening, but loosening will have a dominant effect only when the tunnel is shallow, the residual friction very low and when pronounced differences exist between support pressures required on the roof and on the floor.

Strength of material formulas are used to calculate the support stiffness or characteristic. The significance of the ground-support interface is illustrated with examples of the influence of wood blocking on steel set characteristics and of the influence of end bonds and longitudinal shear bonds on the behavior of grouted bolts. The wide range of theoretically possible behavior modes indicates the need for pertinent field evaluation of the true support action provided by such systems. The sensitivity of some support system characteristics to ostensibly secondary structural elements suggests that practical problems must exist in obtaining a consistent utilization of the full support capacity of such systems. It also indicates the serious difficulties likely to be encountered in the design and implementation of representative in-situ observation programs.

In the second part of this thesis the ground behavior is modeled by the finite element method. The elastic parameters that determine the rock behavior are changed progressively in order to simulate softening and volume increase of the failing rock mass.

This method is used in an axisymmetric analysis of failure patterns near the face and to study the influence of face behavior on support loading. Initial support loading strongly depends on the stiffness of the rock ahead of the face relative to the rock stiffness behind the face, and can depend strongly on the face distance at the time of support erection.

A simple equivalent mining method is used to simulate progressive excavation in a plane strain analysis. The support model consists of beam and spring elements. At least for some support systems the latter must be chosen with care if the model is to be realistic.